IRF5 in defining inflammatory macrophages: studies *in vitro* and *in vivo*

Miriam Weiss,
St Cross College

A thesis submitted for the degree Doctor of Philosophy at the
Kennedy Institute of Rheumatology
Nuffield Department of Orthopaedics, Rheumatology and Musculoskeletal Sciences
University of Oxford

Supervisor: Prof. Irina Udalova

October 2015

Abstract

Macrophages are an integral part of the innate immune system and key players in pathogen clearance and tissue remodelling. Both functions are accomplished by a heterogeneous network of diverse macrophage populations that display pro- and anti-inflammatory properties. Understanding the molecular pathways that control this heterogeneity should provide abundant scope for the generation of more specific and effective therapeutics.

Previously, our laboratory identified the transcription factor interferon regulatory factor 5 (IRF5) as the master regulator of the pro-inflammatory phenotype in human *in vitro* differentiated macrophages. Here, we show that murine macrophages with pro-inflammatory capacities *in vitro* and *in vivo* are also characterised by high levels of IRF5. IRF5 is upregulated *in vitro* in response to inflammatory stimuli such as GM-CSF and IFN-γ and in a subset of *in vivo* macrophages in the arthritic knee joint during the model of antigen-induced arthritis (AIA). IRF5 is also expressed in other myeloid cells *in vivo*, especially in $Ly6C^{hi}$ monocytes and to a lesser extent in dendritic cells and neutrophils.

We furthermore explored the role of IRF5 and IRF5-expressing macrophages in acute inflammation using two different models, AIA and acute lung injury, which are characterised by an extensive initial influx of neutrophils. Mice lacking IRF5 display reduced disease severity and decreased signs of inflammation in both models. Specifically, far fewer neutrophils accumulate at the site of inflammation. We investigated the molecular mechanisms underlying this phenomenon and discovered that $IRF5^{-/-}$ mice produced reduced levels of chemokines important for neutrophil recruitment, such as CXCL1. These studies extend our knowledge of the IRF5 expression pattern *in vivo* and suggest that in addition to the previously proposed role of IRF5 in chronic inflammation, it also has an important function in orchestrating initial acute responses. Thus, IRF5 blockade may be beneficial for both acute and chronic inflammation.

Declaration

The copyright of this thesis rests with the author and is made available under a Creative Commons Attribution Non-Commercial No Derivatives licence. Researchers are free to copy, distribute or transmit the thesis on the condition that they attribute it, that they do not use it for commercial purposes and that they do not alter, transform or build upon it. For any reuse or distribution, researchers must make it clear to others the licence terms of this work.

I declare that the present thesis is the result of my own work. All experimental data described in this thesis are original and have been performed by myself, unless stated below or indicated in the text. Experiments described below were performed by or with help from others.

Katrina Blazek (Kennedy Institute of Rheumatology) performed initial AIA experiments on IRF5 WT and KO animals from which isolated RNA as well as some data on neutrophils and B-cells in blood and spleen were used (Chapters 4 and 5, Figure 4.3, Figure 4.8, Figure 5.3, Figure 5.4, Figure 5.10, Figure 5.11). Dr. Adam J. Byrne (Kennedy Institute of Rheumatology) was largely involved in conducting AIA experiments with me on IRF5 WT and KO animals used in chapter 5. Measurements of IgG serum levels, histological analyses and parts of the acute lung injury model were contributed by him (Figure 5.1, Figure 5.10 and Figure 5.16). Neutrophil migration experiments were performed and analysed by Dr. Adam J Byrne in collaboration with Dr. James E. Pease (Imperial College London) who provided advice and operated the Taxiscan (Figure 5.12). Dr. David G. Saliba (Kennedy Institute of Rheumatology)

performed and analysed ChIP-Seq experiments used in section 5.2.10 (Figure 5.17, Figure 5.18). RNA derived from IRF5 WT and KO *in vitro* differentiated macrophages stimulated with LPS used in the same section was also provided by Dr. David G. Saliba (Figure 5.19). I am appreciative of the help from the aforementioned.

Parts of this thesis have been published in research articles as detailed below. Some data described in chapter 3 and 4 have been published with me as a first author in a research article entitled “IRF5 is a specific marker of inflammatory macrophages *in vivo*”, Mediators of Inflammation, (Weiss et al., 2013). Parts of chapter 4 and 5 have also been published with me as a first author as “IRF5 controls both acute and chronic inflammation”, Proceedings of the National Academy of Sciences of the United States of America (PNAS) (Weiss et al., 2015). Both articles can be found at the end of this thesis in the supplement. The ChIP-Seq data set used in chapter 5 was released as part of a larger study in Cell Reports, “IRF5:RelA Interaction Targets Inflammatory Genes in Macrophages”, (Saliba et al., 2014), with Dr. David G. Saliba as a first author and myself as one of the co-authors.

This work has been carried out at the Kennedy Institute of Rheumatology and was funded by the Kennedy Institute trustees, the American Asthma Foundation and the Medical Research Council.

Miriam Weiss

(October 2015)

Acknowledgments

First and foremost, I would like to thank my supervisor Irina Udalova for giving me the opportunity to work on this project that allowed me to be involved in truly interesting research. I am very grateful for her support, guidance and knowing both when to push me but also giving me the freedom to explore my own ideas. Furthermore, I would also like to thank my previous academic supervisors Matthias Dobbelstein and Halyna Schcherbata for encouraging me to pursue a PhD and teaching me critical thinking and love for science from the beginning.

I am in debt to all the members of the Udalova lab, past and present, for their help both in the lab and outside of work. Thanks to everyone for putting up with me and all my talk about bread and macrophages and showing me the good sides of life in the UK. Especially, I would like to thank Adam Byrne for discussion, motivation and teaching me all I needed to know about mouse work. Also thanks for making long lab hours more enjoyable with science songs and swearing, even before 9am. I am grateful to Katrina for teaching me basic FACS and other lab skills, like avoiding waste at all cost, but also for organising many social events. I would also like to thank Hayley for her advice on anything PhD related, taking over all mouse and organisational tasks in Oxford but in particular for all the baked goods brought in over the years. Thank you David, for critical comments in lab meetings but also for nerdy jokes and stories about butterflies. I am grateful to Grisha for sharing his endless knowledge about cloning, and many other unrelated topics, with me. I would also like to thank Thomas for supervising me in the first months. I am grateful to Tariq for enduring my complaining and constant teasing but also for introducing me to a

variety of wines (good wines can only be dry though!). I would also like to thank Alastair for enlightening me about the true and varied meanings of the word ‘fine’.

I am truly grateful to all members of the Kennedy Institute for advice on any issue and willingness to help with new techniques. I have really enjoyed working here throughout. Specifically, I would like to thank the previous ground floor members Kay, Fiona, Andy, Anne-Marie, Anna and Raquel for always being up for a coffee or tea break. Kay and Fiona, thank you especially for helping and teaching me a lot about mice and specifically about AIA. Andy, thank you for introducing me to surfing, always being up for fun and helping me. I am also grateful to all the people in the snacking bay, especially Emily for baking and positive reinforcement, and other members of the Powrie group.

I would like to say a special thank you to my friends in the UK and everywhere else, without your support and distraction, when needed, I would have never made it. I am in debt to Richard for his continuous support at any time of the day regarding any issue whatsoever. Thank you so much for helping me through the harder times and almost never getting tired of my complaining. Also thank you for your honesty and for pushing me to keep going. I literally would not be here without you. I am grateful for the close friends that know me since school and will never stop teasing me. Thank you Frunz and Maggie, I am glad it still feels like we see each other every day. I would also like to thank my London friends who made me enjoy this city even more. Thank you Janni, Cat, Rob, Filipa, Rui, Anne, Christian, Vickel and Karli. Danke Susi, dass du seit des

Bachelors für mich da bist und mich zur Patentante gemacht hast. Beziehungsweise, dafür danke ich auch Marcel und Marius, ich bin froh zu wissen, dass immer bei euch willkommen bin. I am also grateful to the Göttingen bunch even though it took me a while to appreciate the benefits of all of it. Especially thank you Paula for enjoying art as much as I do and for support via flux or messages, I am truly grateful to have you as a friend. Also thank you Rafik, Lena and Hale for fun times and nerdy jokes. Especially Lena for always welcoming me in New York! Thank you to Antje und Uli for keeping in touch and coming to visit me whenever possible!
Thank you F. for motivation, advice, sharing plane love and all other offerings.

Ich möchte diese Arbeit auch und besonders meiner Familie widmen. Ohne euch, wäre ich nicht hier und hätte all das nicht schaffen können. Ganz besonders möchte ich meinem Vater Thomi danken für seine ausnahmslose Unterstützung in jeder Situation und seine stoische Ruhe in stressigen Situationen. Ebenso möchte ich meiner Mutter Caroline danken für ihre bedingungslose Liebe, ihren Stolz egal wie klein der Anlass und die jährlichen Adventspakete auf die ich mich immer freue. Meinem Bruder Aron für alles, immer und sowieso, weil er der beste Bruder ist, den ich mir vorstellen kann. Du kannst mich von jetzt an deinen Freunden als Dr. Weiss vorstellen! Weiterhin möchte ich meinen Großeltern danken, besonders meinen Großmüttern, für ihre Anerkennung und Unterstützung, obwohl sie mich lieber in Deutschland sehen würden. Ausserdem bedanken möchte ich mich bei Maike und Wieland. Dem Rest der Familie, auch wenn nicht namentlich erwähnt, bin ich dankbar dafür, dass sie immer für mich da waren.

Table of contents

List of figures

List of tables

List of abbreviations

AIA	Antigen-induced arthritis
ANA	Antinuclear antibody
APC	Antigen presenting cell
AU	Arbitrary units
BCR	B-cell receptor
BM	Bone marrow
BMDM	Bone marrow-derived macrophages
bp	base pairs
BSA	Bovine serum albumin
CCL	Chemokine (C-C motif) ligand
CCR	Chemokine (C-C motif) receptor
CD	Cluster of differentiation
cDC	Classical or conventional DC
CDP	Common DC progenitor
CFA	Complete Freund's adjuvant
ChIP	Chromatin immunoprecipitation
CIA	Collagen-induced arthritis
CLP	Common lymphoid progenitor
CLR	C-type lectin receptor
CMP	Common myeloid progenitor
cMoP	Common monocyte progenitor
CXCL	Chemokine (C-X-C motif) ligand
CXCR	Chemokine (C-X-C motif) receptor
DAMP	Damage-associated molecular pattern

DBD	DNA-binding domain
DC	Dendritic cell
DNA	Deoxyribonucleic acid
ELISA	Enzyme linked immunosorbent assay
EMP	Erythro-myeloid progenitor
FACS	Fluorescence-activated cell sorting
FL	Fetal liver
GAS	Gamma-activated sequence
GM-CSF	Granulocyte macrophage colony-stimulating factor
GMP	Granulocyte macrophage progenitor
GWAS	Genome-wide association study
HRP	Horseradish peroxidase
HSC	Haematopoietic stem cell
IAD	IRF association domain
IBD	Inflammatory bowel disease
IFN	Interferon
Ig	Immunoglobulin
IL	Interleukin
ILC	Innate lymphoid cell
IRF	IFN regulatory factor
ISRE	Interferon stimulated response element
kb	kilo base
LN	Lymph node
LPS	Lipopolysaccharide
mBSA	Methylated BSA

M-CSF	Macrophage colony-stimulating factor
MDP	Monocyte/macrophage and DC progenitor
MFI	Mean fluorescence intensity
MHC	Major histocompatibility complex
MPS	Mononuclear phagocyte system
mRNA	messenger RNA
NET	Neutrophil extracellular traps
NF-κB	Nuclear factor κB
NK	Natural killer
PAMP	Pathogen-associated molecular pattern
PBMC	Peripheral blood mononuclear cell
pDC	Plasmacytoid dendritic cell
PRR	Pathogen recognition receptor
RA	Rheumatoid arthritis
RF	Rheumatoid factor
RNAP II	RNA Polymerase II
RLR	RIG-like receptor
RNA	Ribonucleic acid
rpm	Revolutions per minute
SEM	Standard error of the mean
SLE	Systemic lupus erythematosus
SNP	Single nucleotide polymorphism
STAT	Signal transducer and activator of transcription
TCR	T-cell receptor
TF	Transcription factor

TLR	Toll-like receptor
TNF	Tumour necrosis factor
V(D)J	Variable (diverse) joining
YS	Yolk sac

1. General introduction

1.1. The immune system

The immune system has evolved to maintain host health as the body faces different threats and challenges. These threats consist of external pathogens such as bacteria, viruses and parasites, which can cause infection but can also include internal tissue injury. To mount an appropriate response to these challenges, it is crucial that the immune system is able to distinguish between self and non-self or healthy and damaged tissue. In vertebrates, there are two arms of immunity: the innate and the adaptive immune system. Successful defence relies on a well-coordinated interplay of these two arms. Innate immunity is responsible for initiating a rapid but nonspecific response to external and internal danger whilst adaptive immunity is able to mount a long-lasting and specific immune response.

Innate immune cells can recognise evolutionary conserved structures on pathogens, so called PAMPs (pathogen-associated molecular pattern) but also DAMPs (danger-associated molecular pattern), which are released by injured cells. Pathogens have however adapted by constantly evolving to evade the immune system's recognition. Innate immune cells are unable to induce a tailored response to a specific pathogen or generate immunological memory. In contrast, lymphocytes of the adaptive immune system, consisting of B-cells and T-cells, are able to fill this gap. Lymphocytes express antigen specific receptors, B- and T-cell receptors (BCR and TCR, respectively), which evolve constantly and can adapt as they undergo re-arrangement, clonal selection and expansion processes. However, this dynamic adaptation requires strict 'quality control' to prevent the occurrence of lymphocytes reacting to self-antigens. Defects in this

system can lead to autoimmunity where the immune system attacks host tissue and causes its destruction. One such example is rheumatoid arthritis (RA), an autoimmune disease affecting the joints, which will be discussed in detail later (see 1.5 Rheumatoid arthritis).

1.1.1. Innate immunity

The innate immune system is the first line of defence when dealing with infections. It non-specifically recognises foreign elements and rapidly induces a response to prevent spreading of the infection. Inflammation is characterised locally by five cardinal signs: *calor* (heat), *rubor* (redness), *dolor* (pain), *tumor* (swelling) and *functio laesa* (loss of function). These are caused by increased blood flow and permeability of vessels at the site of inflammation. In vertebrates, the innate arm also leads to activation of the adaptive immunity, which is absent in non-vertebrates (Pancer and Cooper 2006).

Cellular innate immunity

Cellular components of the innate immune system are monocytes, macrophages, dendritic cells (DCs), granulocytes, mast cells, natural killer (NK) cells and the recently discovered ILCs (innate lymphoid cells).

Neutrophils, the most abundant type of granulocytes, along with macrophages and DCs are all phagocytes. Phagocytes represent the largest fraction of the innate immune system and are characterised by their ability to digest microorganisms and particles. They are responsible for clearance of bacteria and other pathogens but they can also remove damaged tissue or dying cells

(Matzinger 2002). Macrophages and DCs express pattern recognition receptors (PRRs) to detect PAMPs and DAMPs such as LPS (lipopolysaccharide) and tenascin C, respectively (Medzhitov and Janeway 2002). The activation of PRRs leads to downstream signalling that induces production of inflammatory cytokines and chemokines, which ultimately shapes the nature and polarisation of adaptive immunity (Brubaker et al. 2015). Macrophages, DCs and neutrophils belong to the myeloid lineage whose development and functions will be discussed in more detail in section 1.2 of the general introduction.

Mast cells are most commonly found at mucosal sites and mostly known for their contribution to allergy by Immunoglobulin (Ig) E mediated release of histamine (Moon et al. 2010). However, they also participate in the host defence against pathogens and display more heterogonous phenotypes than previously appreciated (Abraham and St John 2010). They are functionally similar to basophil granulocytes (see below).

NK cells and ILCs derive from a common lymphoid progenitor (CLP) but lack expression of antigen specific receptors and are thus considered to be 'innate' T-cell equivalents. NK cells are specifically efficient at killing virus infected cells whereas ILCs produce high amounts of effector cytokines, such as Interferon (IFN) γ, Interleukin (IL) 4 or GM-CSF (granulocyte macrophage colony-stimulating factor, CSF-2), in response to the surrounding cytokine milieu (Eberl et al. 2015).

NK cells express an array of receptors to detect stress signals and the absence or presence of MHC (major histocompatibility complex) I, which is expressed by

all healthy cells but lost by infected or transformed cells (Lanier 2005). NK cell receptors are germline encoded, like PRRs, and thus cannot adapt to provide antigen specificity. However, NK cells can express different combinations of these receptors and thereby confer a certain degree of specificity. Once activated, NK cells produce cytokines, granzymes and perforin to kill the infected or transformed cell. NK cells can be considered part of the ILC family and are then referred to as EOMES $^{+}$ ILC1s. However, the exact relationship and nomenclature of NK cells as ILCs is still under debate (Eberl et al. 2015).

There are three types of ILCs: ILC1, ILC2 and ILC3. Each type expresses master regulator transcription factors (TF) analogous to T-cell subsets (see 1.1.2 Adaptive immunity, T-cells), T-bet (Th1), Gata-3 (Th2) and RORγt (Th17), respectively (Serafini et al. 2015). This is mirrored by the key effector cytokines expressed by each subset. ILC1s secrete IFN-γ and Tumour necrosis factor (TNF) α, ILC2s produce IL-4, IL-5 and IL-13 while ILC3s are characterised by IL-17, IL-22 and GM-CSF expression (Spits and Di Santo 2011). ILCs are activated by cytokines in their environment, which are produced by myeloid cells or epithelial cells. They express cytokine receptors to sense these cues but do not possess antigen specific receptors, and thus belong to the innate immune system (Artis and Spits 2015). Their expansion in inflamed tissues however can provide some kind of tissue memory of infection (Artis and Spits 2015).

Humoral innate immunity

Innate immunity also has a non-cellular arm consisting of anti-microbial peptides produced by cells of the innate immune system. These secreted

factors include a variety of proteins such as components of the complement system or acute-phase reactants such as C-reactive protein (Turvey and Broide 2010). Functionally, humoral immunity is important for opsonisation where proteins recognise and bind to antigen and lead to its enhanced phagocytosis. However, innate humoral proteins can also cause cell lysis, such as the membrane attacking complexed formed by active factors of the complement system (Sarma and Ward 2011). Chemotaxis can also be initiated leading to attraction of additional players of the immune system, both innate and adaptive, and thereby promoting an inflammatory response. Components of humoral innate immunity thus also contribute to linking the two arms of immunity (Dunkelberger and Song 2010).

1.1.2. Adaptive immunity

Cells of the adaptive immune system are T- and B-lymphocytes, T-cells and B-cells respectively. Both cell types express variable receptors recognising specific antigens and undergo a selection process to prevent recognition of self-antigens. The adaptive immune system differs from innate immunity by being able to generate memory cells, which ensure long-lasting protection from recurring infections. Memory cells can respond faster and thereby prevent disease establishment. Vaccinations rely on this principle and take advantage of the adaptive immunity's ability to 'learn'.

T-cells

T-cell development takes place in the bone marrow where they originate from the CLP (Koch and Radtke 2011). T-cell precursors then migrate to the thymus

where they mature and undergo positive and negative selection (Klein et al. 2009). The TCR gene fragments are subjected to random V(D)J recombination that results in expression of different and unique TCRs thus recognising a variety of epitopes (Gellert 2002). Successful TCR assembly as such however is insufficient for T-cell differentiation. Thymocytes only survive if they express a TCR with intermediate affinity to MHC presented self-peptides (Daniels et al. 2006) but are not autoreactive following lineage commitment ($CD4^+$ $CD8^-$ or $CD4^-$ $CD8^+$) (Starr et al. 2003). The remaining T-cells egress from the thymus and enter circulation as naïve T-cells. T-cells can be divided into helper ($CD4^+$) and cytotoxic ($CD8^+$) T-cells that fulfil different functions during the immune response.

T helper cells (Th) are crucial for adaptive immune responses to a range of stimuli by both producing large amounts of cytokines that act on innate immune cells but also provide help to B-cells (see Figure 1.1). For naïve T-cells to become activated and differentiate into Th cells, they need to receive three stimulatory signals (Kapsenberg 2003): 1) TCR stimulation by MHC II mediated antigen presentation on antigen-presenting cells (APCs) such as DCs, macrophages or B-cells ensures antigen specificity of the response (Zinkernagel 1974). MHC II molecules display foreign extra-cellular antigens that have been taken up by phagocytosis (Vyas et al. 2008). MHC II expression is restricted to APCs that present exogenous 'non-self' to adaptive immune cells. 2) Co-stimulation of CD28 on T-cells by CD80 or CD86 is essential for activation (Linsley et al. 1990). Co-stimulatory molecules are highly expressed on steady state DCs but can also be upregulated by stimulated APCs (Reis e

Sousa 2006). 3) Presence of cytokines derived from innate immune cells drive the expression of master regulator TFs that polarise T-cells (see below). Polarising cytokines are secreted by activated cells, ensuring that T-cell activation only occurs in the context of infection. Ultimately, these master regulators drive different effector phenotypes, which are characterised by distinct cytokine profiles specific to the environmental stimuli received and shape the immune response accordingly (Kapsenberg 2003).

There are different subsets of Th cells, including Th1, Th2 and Th17 that are characterised by differential TF and cytokine expression (O'Shea and Paul 2010, Zhu et al. 2010). T-bet drives Th1 differentiation and is induced in response to IL-12 and TNF-α (Szabo et al. 2000). Th1 cells secrete IFN-γ and participate in a pro-inflammatory response to intracellular microbes (Mosmann and Coffman 1989). Th2 cells are characterised by expression of Gata3, which is induced in response to cytokines like IL-4 (Zheng and Flavell 1997). Th2 cells are involved in allergic immunity and are important for clearance of parasite infections (Abbas et al. 1996). IL-23, IL-6 and others lead to a Th17 phenotype by activating RORγt, which in turn causes IL-17 production (Harrington et al. 2005, Ivanov et al. 2006). Th17 cells are associated with autoimmunity and clearance of specific extracellular pathogens (Bettelli et al. 2008). Naïve $CD4^+$ T-cells can also become regulatory T-cells (Tregs), which are controlled by the transcriptional repressor Foxp3 (Brunkow et al. 2001, Josefowicz and Rudensky 2009). Tregs are important for suppressing immune responses, in contrast to the aforementioned Th cell subsets, and maintaining self-tolerance (Sakaguchi et al. 2008).

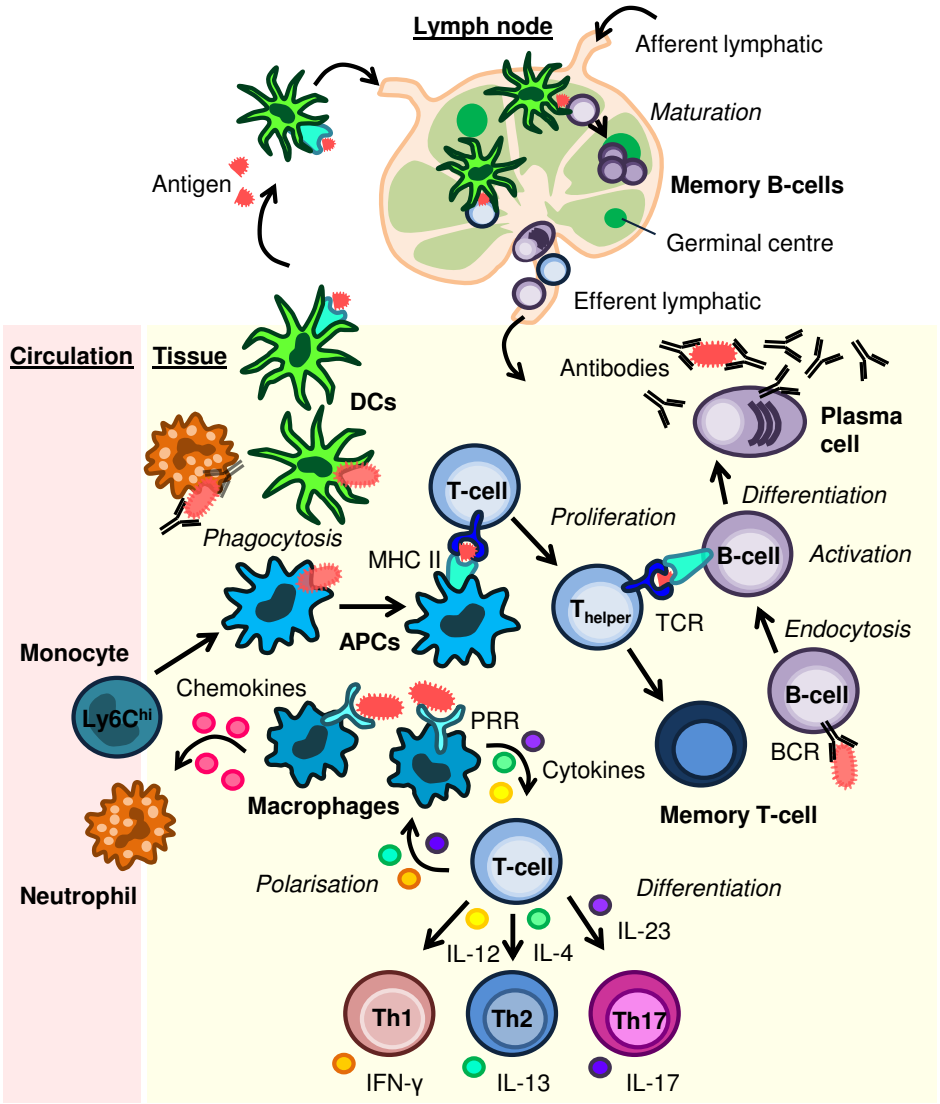

Figure 1.1. Simplified overview of the immune system's response to pathogens.

Upon infection, pathogens are recognised by cells expressing PRRs, such as macrophages. Receptor stimulation induces cytokine expression in turn providing a polarisation signal to T-cells which differentiate into Th1, Th2 or Th17 cells depending on the stimuli. Another signal contributing to T-cell activation is antigen presentation by APCs that phagocytose bacteria to display antigen on surface MHC II molecules that interact with the TCR. Full T-cell activation requires additional stimulation by co-stimulatory molecules (not depicted). Activated T-cells shape the inflammatory environment by secreting cytokines which influence macrophage polarisation. Macrophages can produce chemokines attracting neutrophils and monocytes and thus perpetuating the immune response. Upon tissue entry, monocytes differentiate into macrophages or DCs (depicted as APC). Infiltrating neutrophils take part in pathogen clearance by phagocytosis. Phagocytosis of bacteria is enhanced when those are bound by antibodies which are secreted by mature activated B-cells. B-cells themselves can take up bacteria and present them on MHC II molecules. Co-help provided by T-cells that bind to these MHC II presented antigens leads to B-cell activation and antibody production. B-cells can also be activated in the lymph node by DCs. DCs are professional APCs and present antigens via MHC II following

phagocytosis. They are highly motile and migrate to the lymph node where they can stimulate both naïve T- and B-cells. Activated cells of the adaptive immune system can leave the lymph node via efferent lymph vessels and enter the site of inflammation. Immunological memory is created by either B-cells or T-cells following activation. Memory B-cells are associated with germinal centres while memory T-cells are found throughout the body.

$CD8^+$ effector T-cells are involved in the immune system's responses to viruses, similarly to NK cells (see above). Cytotoxic T-cells recognise antigens presented by MHC I molecules (Harty et al. 2000). In contrast to MHC II molecules, MHC I is present on almost all cells and displays cytosolic antigens. Thereby MHC I presentation provides a self-signal on healthy cells or presents viral antigens in infected cells ('altered self') (Jensen 2007). These signals are detected by $CD8^+$ T-cells that then kill the infected cell (Cui and Kaech 2010).

Both $CD4^+$ and $CD8^+$ T-cells can differentiate into memory T-cells, which are resting until they are activated by exposure to antigen in case of re-infection (Dutton et al. 1998). Memory T-cells remain distributed throughout the body after clearance of infection to provide immune surveillance (Mueller et al. 2013).

γδ T-cells are a subset of T-cells whose TCR is composed of γδ chains rather than αβ chains, which are utilised by $CD4^+$ or $CD8^+$ T-cells. Diversity of the γδ TCR is limited, compared to αβ TCRs, thus restricting the antigen repertoire recognised by γδ T-cells (Vantourout and Hayday 2013). In contrast to αβ T-cells however, they do not rely on antigen presentation in the context of MHC molecules. Moreover, γδ T-cells appear early on in disease and have been shown to be the major initial IL-17 producers in murine disease models of infection or autoimmunity (Chien et al. 2014). Due to their limited variety in

antigen recognition and their rapid response, they have been referred to as 'innate-like' T-cells.

B-cells

B-cells derive from the CLP in the BM and immature B-cells are subjected to two checkpoints before they migrate to B-cell follicles in lymphoid organs (Wardemann et al. 2003). This process is analogous to positive and negative selection of T-cells in the thymus; B-cells that react to self-antigen will die, become anergic or undergo receptor editing (Gonzalez et al. 2011). When mature B-cells encounter antigen, BCR engagement ultimately leads to MHC II mediated presentation of internalised antigen on the B-cell surface (Harwood and Batista 2010). Antigen recognition by Th cells enhances both B- and T-cell activation (see Figure 1.1). Depending on their location, B-cells then become either short-lived antibody secreting plasmablasts or long-term memory B-cells within germinal centres (see Figure 1.1) (McHeyzer-Williams and McHeyzer-Williams 2005).

BCR variety is also achieved by V(D)J recombination of gene fragments, as is the case for the TCR (see above). The BCR itself consists of a membrane bound antibody and a signal transduction moiety (Reth and Wienands 1997). Before the production of antibodies occurs, B-cells undergo class-switch recombination and, in the case of memory cells, somatic hypermutation leading to higher affinity antibodies (Nutt et al. 2015). Secreted antibodies bind to their target antigen causing its neutralisation and facilitating opsonisation (see 1.1.1

Innate immunity, Humoral innate immunity). Antibodies represent the main part of humoral adaptive immunity.

1.2. The myeloid lineage

The myeloid lineage consists of macrophages, DCs and granulocytes, which develop from a shared precursor, the granulocyte macrophage progenitor (GMP). Macrophages were first described by Ilya Metchnikoff in 1892 who described them as ‘large eaters’ (macrophages, derived from Greek ‘macro’ and ‘phago’) (Gordon 2008). He further described other smaller phagocytes as microphages (‘small eaters’), now known as granulocytes. The term mononuclear phagocyte system (MPS) was introduced in 1969 by van Furth and Cohn and used to group all highly phagocytic cells and their precursors, namely macrophages and monocytes (van Furth and Cohn 1968, van Furth et al. 1972). Around the same time Steinmann discovered another cell type and called them dendritic cells because of their morphology (from ‘dendron’, Greek for tree) (Steinman and Cohn 1973). In addition to the initially defined members of the MPS, DCs are usually also considered part of the MPS (Yona and Gordon 2015). Polymorphonuclear granulocytes are part of the myeloid lineage but do not belong to the MPS. Myeloid cells constitute a large proportion of the innate immune system and are thus involved in nonspecific immune defence. The functional diversity and ontogeny of the myeloid cell lineage will be discussed in this chapter.

1.2.1. Development of monocytes, macrophages and DCs

Embryonic origins

During the development of mammalian embryos, haematopoiesis consists of a tightly regulated stepwise process involving several progenitor cell types, which begins in the yolk sac (YS) and ultimately ends up in the bone marrow (BM) (De Kleer et al. 2014). Myelopoiesis starts as early as embryonic age 7.0 (E7.0) of the 20 days of mouse development (Moore and Metcalf 1970). First, the so called 'primitive' haematopoiesis occurs in the ectoderm of the YS, which is replaced by HSC (haematopoietic stem cell) dependent 'definitive' haematopoiesis at E11.0 in the fetal liver (FL) (see Figure 1.2) (Kumaravelu et al. 2002, Kieusseian et al. 2012). The FL is the main haematopoietic organ until the BM becomes the predominant site at birth (Christensen et al. 2004). BM haematopoiesis is discussed in detail in the next section. During intra-uterine development of the embryo, the YS gives rise to macrophages that can seed tissues as early as E9.0 (Takahashi et al. 1989, Ginhoux and Jung 2014). Most of these embryonic tissue macrophages are however replaced by FL monocyte-derived macrophages at a later stage of embryonic development (starting E12.5) (Hoeffel et al. 2015, Sheng et al. 2015). FL haematopoiesis starts on E11 and is dependent on the TF c-Myb (Mucenski et al. 1991). Some have argued that all true tissue-resident macrophages are YS derived due to the presence of primitive F4/80^{hi} CD11b^{lo} macrophages in c-Myb deficient embryos (Schulz et al. 2012). Recently published data however indicate that most tissue-resident macrophages are in fact FL monocyte-derived and that the FL is seeded by a transient wave of YS-derived EMPs (erythro-myeloid progenitors) prior to definitive haematopoiesis (Gomez Perdiguero et al. 2015, Hoeffel et al.

2015). The only tissue-resident macrophages exclusively derived from YS primitive macrophages are microglia in the brain (Ginhoux et al. 2010). This is likely due to establishment of the blood brain barrier at E13.5 preventing FL monocyte-derived macrophages from entering the brain (Daneman et al. 2010). Some populations of tissue-resident macrophages such as Langerhans cells in the skin and cardiac macrophages display a dual origin (Hoeffel et al. 2012, Epelman et al. 2014). Development of these is dependent on M-CSF (CSF-1) receptor (M-CSFR/CD115/CSF1R) signalling, which has been suggested to be used as a defining feature for macrophages (see Nomenclature and identification below and (Guilliams et al. 2014)). Recently, IL-34 has been described as an alternative ligand for the M-CSFR (Lin et al. 2008), explaining the incomplete deletion of macrophages in M-CSF deficient mice (*Csf1*$^{op/op}$/*Csf1*$^{-/-}$) (Yoshida et al. 1990). Specifically, microglia and Langerhans cells are dependent on IL-34 in their development (Greter et al. 2012, Wang et al. 2012).

Myeloid development in human and murine embryos follows the same relative kinetics. However, exact time points differ due to the longer gestation period of 38 weeks in humans. In human embryos, definitive haematopoiesis also begins in the fetal liver, followed by HSCs colonising the thymus and spleen before ultimately shifting to the BM prior to birth at 20-24 weeks (Tavian and Peault 2005).

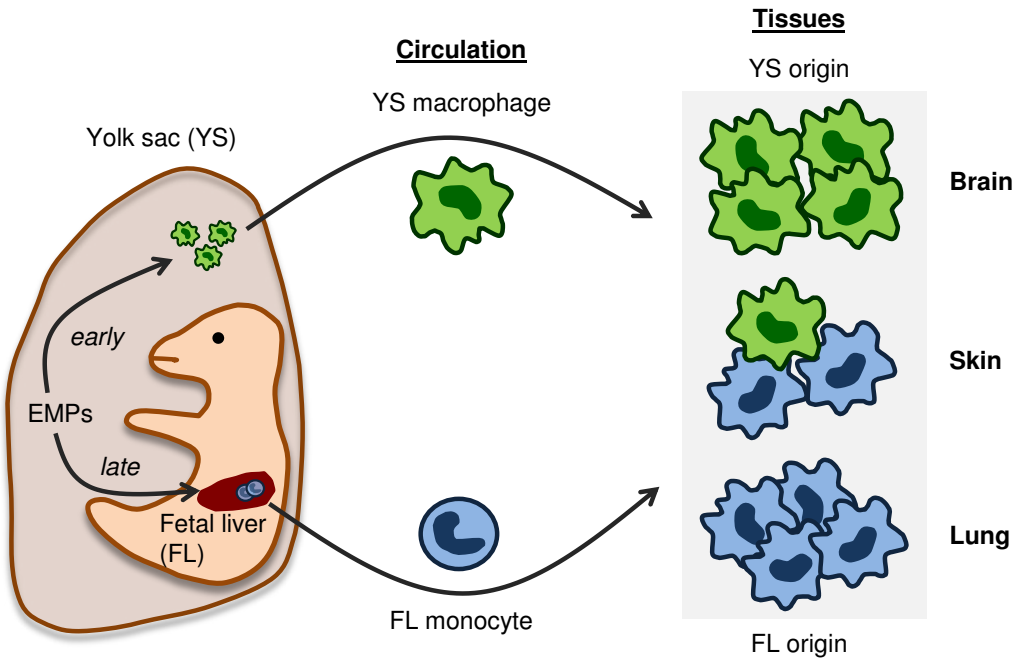

Figure 1.2. Embryonic origins of tissue-resident macrophages.

The majority of tissue-resident macrophages is seeded during embryonic development. YS macrophages arise first from primitive haematopoiesis and seed the embryonic tissues including the brain as early as E9.0. A wave of YS derived EMPs seeds the FL where definitive haematopoiesis is established on E11.0. The FL is the main site of haematopoiesis until birth. On E12.5, FL derived monocytes populate the embryo and dilute the YS derived populations However, YS macrophages remain the sole source of microglia, the brain's resident macrophages, likely due to prior establishment of the blood brain barrier. In other tissues, such as the skin, macrophages display a dual origin with some YS macrophages remaining while in the lung and other organs, resident macrophages are exclusively derived from FL monocytes.

Haematopoiesis in the adult

After birth, the BM becomes the main site of haematopoiesis (see Figure 1.3). HSCs are maintained in their perivascular niche partly consisting of mesenchymal stromal cells and endothelial cells (Morrison and Scadden 2014). HSC progeny lose developmental potential at every step, for example, the common myeloid progenitor (CMP) can generate all cells of the myeloid lineage but has lost lymphoid potential. Next, CMP-derived GMPs give rise to different granulocyte precursors and the monocyte/macrophage and DC progenitor (MDP), which has lost granulocyte potential. The MDP can develop into the

cMoP (common monocyte progenitor) or into the CDP (common DC progenitor). The cMoP has only recently been identified as the committed monocyte precursor (Hettinger et al. 2013). Both MDPs and cMoPs have been detected in the spleen, a site of extramedullary monocytopoiesis (Leuschner et al. 2012, Hettinger et al. 2013). The spleen contains a large monocyte pool, which can be recruited during acute inflammation (Swirski et al. 2009, Leuschner et al. 2012). Monocytes are derived from the cMoP and two subsets have been identified, Ly6C^{hi} CX$_3$CR1^{int} and Ly6C^{lo} CX$_3$CR1^{hi} (Geissmann et al. 2003). There has been some debate about their developmental relationship but recent evidence suggests that Ly6C^{hi} monocytes give rise to Ly6C^{lo} monocytes, both in the BM and in circulation (Hettinger et al. 2013, Yona et al. 2013). Upon tissue entry, monocytes can give rise to both macrophages and DCs of varying and overlapping phenotypes (Ginhoux and Jung 2014). This process is especially prominent under inflammatory conditions. The influence of the local cytokine environment on macrophage phenotypes and functional consequences will be discussed below (see 1.2.2 Macrophage and DC functions, Inflammation).

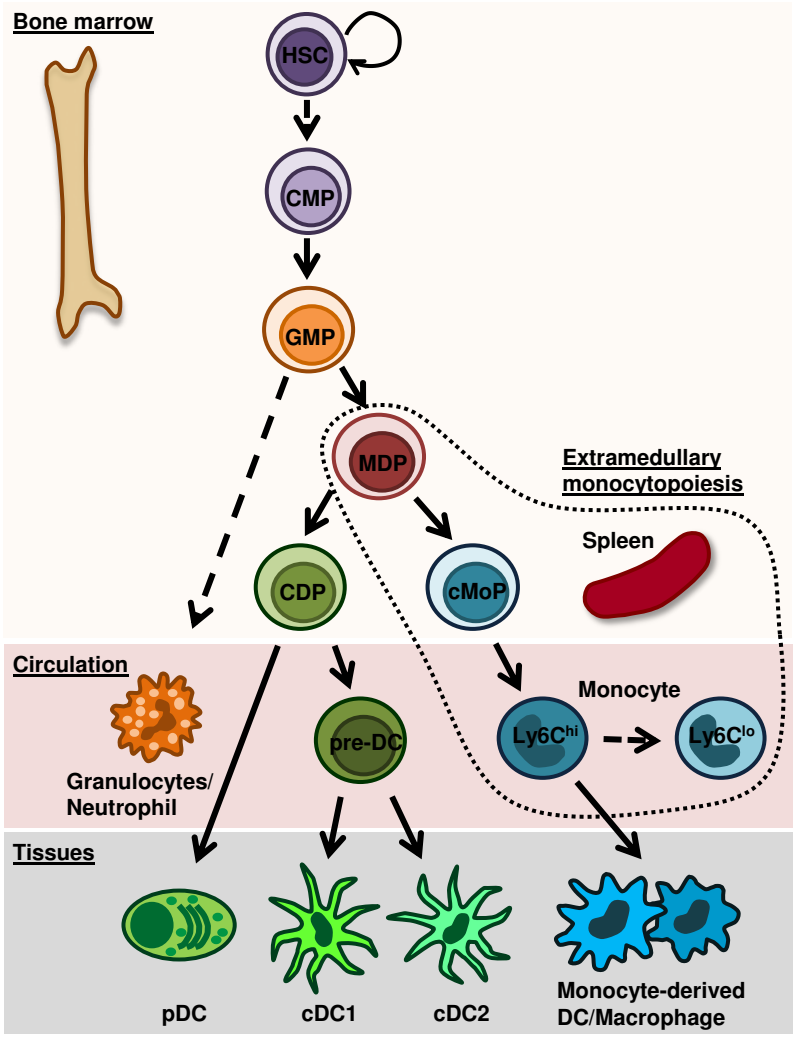

Figure 1.3. Myelopoiesis in the adult in the bone marrow and spleen.

After birth, the BM becomes the predominant site of definitive haematopoiesis which relies on self-renewing HSCs constantly generating progenitors. The myeloid lineage derives from the CMP further giving rise to the GMP. Granulocytes arise from additional precursors (not shown). Neutrophils are the most abundant granulocyte residing in the BM until release into the blood stream. The MDP gives rise to the CDP and cMoP. CDPs develop into pDCs or pre-DCs, the precursors of the cDC1 and cDC2. Two monocyte subsets originate from the cMoP, although recent data suggests that the Ly6C^{hi} subset progresses into Ly6C^{lo} monocytes (indicated by a dotted line). The spleen is a site of extramedullary monocytopoiesis where MDPs, cMoPs and both monocyte subsets have been detected. Monocytes circulate in the blood and upon tissue entry they can differentiate into macrophages and DCs.

During DC development, the CDP first loses its potential to give rise to plasmacytoid dendritic cells (pDCs). pDCs are a specific type of DCs that have a large secretory compartment and are important in viral infections by producing type I IFNs (Reizis et al. 2011). Pre-DCs are CDP-derived and exit the BM

before they give rise to classical DCs (cDCs) in tissues. It has recently been shown that lineage commitment occurs already in the BM at the CDP stage, thus pre-DCs are committed to develop into either DC lineage when entering the circulation (Schlitzer et al. 2015). cDC lineages can be grouped as cDC1 ($CD103^+$ in non-lymphoid organs or $CD8^+$ in lymphoid organs) and cDC2 ($CD11b^+$) (Guilliams et al. 2014). cDC1s are especially efficient at activating $CD8^+$ T-cells while cDC2s are highly efficient at priming $CD4^+$ T-cells (Merad et al. 2013). DC development depends on fms-like tyrosine kinase 3 (Flt3/CD135) signalling, which occurs as part of definitive HSC dependent haematopoiesis (Boyer et al. 2011).

Overall, it is important to keep in mind that although these developmental decisions seem to occur step wise, it is more likely that development occurs as a continuum with transitional cells at any one point (Naik et al. 2013).

Until recently, no equivalents of the murine macrophage/DC progenitors MDP, CDP and pre-DC had been described. Lee et al. however now identified a human granulocyte-monocyte-DC progenitor as well as human MDP and CDP in the BM and cord blood (Lee et al. 2015). Moreover, Breton et al. were able to detect human pre-DCs in BM, cord blood, blood and peripheral lymphoid organs (Breton et al. 2015) . Whether humans possess a cMoP equivalent remains to be determined.

cDCs are constantly replenished from BM precursors due to their short half-life of approximately 3-6 days (McKenna et al. 2000). In contrast, as described earlier, some tissue-resident macrophages such as microglia or alveolar

macrophages are seeded during embryonic development and self-maintain over the course of adult life (Hashimoto et al. 2013, Yona et al. 2013). Tissue-resident macrophages in the intestine however rely on constant monocyte input for their replenishment (Bain et al. 2014). Other tissues contain macrophages seeded during development as well as monocyte dependent populations, such as macrophages and DCs in the skin (Hoeffel et al. 2012, Tamoutounour et al. 2013). Thus, the requirements for monocyte input towards the tissue-resident macrophage pool depend on the tissue analysed.

Nomenclature and identification

There have been many recent attempts to unify the nomenclature of macrophages and DCs. With the discovery that not all macrophages rely on monocyte input throughout life (Hashimoto et al. 2013) also came the realisation that the bidirectional concept of macrophage polarisation *in vitro* may be too unidimensional to do justice to the variety of macrophage phenotypes *in vivo* (Xue et al. 2014) (see 1.2.2 Macrophage and DC functions, Inflammation). Two main approaches of determining cellular identity, based either on ontogeny or function, have been discussed and adopted by various groups. When ontogeny is used as a defining tool, macrophages only consist of tissue-resident macrophages derived from embryonic precursors that rely on M-CSFR signalling during development and are thus absent in *Csf1r*$^{-/-}$ mice (Hashimoto et al. 2011, Guilliams et al. 2014). Flt3 signalling dependent and CDP-derived cells on the other hand will be identified as DCs. All cells derived from monocytes during adulthood are simply called ‘monocyte-derived cell’, which can be further defined using prefixes and suffixes (Guilliams et al. 2014,

Guilliams and van de Laar 2015). In contrast, others have suggested that all monocyte-derived cells are by definition macrophages (Jenkins and Hume 2014).

Historically, however, macrophages and DCs were defined by function according to their ability to present antigens, secrete cytokines and phagocytose. Specifically, macrophages are considered to excel at phagocytosis and cytokine production while DCs are highly migratory 'professional' APCs. However, macrophages are also able to present antigen while DCs can also phagocytose bacteria. This however remains under debate, as some people believe antigen presentation is a unique defining feature of DCs (Geissmann et al. 2010, Jenkins and Hume 2014). The matter is complicated by varying functional capacities and surface marker expression depending on the tissue or inflammatory setting (Guilliams and van de Laar 2015).

Classical surface markers to identify murine DCs are MHC II and CD11c (Steinman et al. 1979, Nussenzweig et al. 1981, Metlay et al. 1990). Macrophages in the mouse on the other hand are mostly identified by expression of F4/80 (Austyn and Gordon 1981). More recently, MerTK and CD64 were identified as supposedly macrophage specific markers (Gautier et al. 2012, Tamoutounour et al. 2012, Schlitzer et al. 2013, Epelman et al. 2014). However, all of the above mentioned markers are in fact not specific for either population causing confusion and difficulties in cell type definition (Geissmann et al. 2010). MHC II and CD11c can be expressed by macrophages, for

example by alveolar macrophages in the lung (Misharin et al. 2013) or synovial macrophages in the joint (Misharin et al. 2014). F4/80 can be found on eosinophils (McGarry and Stewart 1991) and some DC populations (Merad et al. 2013). CD64 has also been described to be expressed on monocyte-derived DCs (Plantinga et al. 2013, Tamoutounour et al. 2013). Specific markers restricted to the DC lineage are DNGR-1 (Clec9a) (Schraml et al. 2013) and Zbtb46 (Satpathy et al. 2012), although they are also not definitive (Schlitzer and Ginhoux 2013). Additional markers used to identify DCs or their subsets are CD135, CD103, SIRPα and others, reviewed in (Merad et al. 2013). To conclude, surface marker based identification of macrophage and DC subsets remains challenging due to the lack of uniquely specific markers. The markers and gating strategy used in this study are described in 4.2.3 Gating strategy of myeloid cell types in the knee.

1.2.2. Macrophage and DC functions

Steady state

In steady state conditions, macrophages are important for tissue homeostasis by acting as sentinels for infectious threats and by participating in tissue repair and remodelling (Wynn et al. 2013). Macrophages are also crucial during development and play a role in branching morphogenesis, angiogenesis and other processes involving phagocytosis of apoptotic cells (Pollard 2009). One of the most well-known developmental functions is those of osteoclasts, the bone's resident macrophages. The absence of bone resorbing osteoclasts in bone morphogenesis leads to osteopetrosis in M-CSF and M-CSFR deficient mice (Yoshida et al. 1990, Cecchini et al. 1994, Dai et al. 2002). Osteopetrosis is

characterised by a lack of bone remodelling and thereby absence of bone cavities such as the marrow cavity, the main site of haematopoiesis (see 1.2.1, section Haematopoiesis in the adult).

The diversity of macrophage phenotypes under homeostatic conditions is huge as macrophages fulfil different tasks depending on the tissue or even the localisation within a specific organ (Gordon et al. 2014). In fact, recent high-dimensional analysis of the murine myeloid system confirmed a clear separation of tissue-resident macrophage subsets (Becher et al. 2014). For example, macrophages in the liver and red pulp of the spleen are involved in iron recycling by phagocytosing senescent or damaged erythrocytes and subsequently releasing haemoglobin and ultimately iron (Ganz 2012). Alveolar macrophages, which reside in the lung airways, are crucial for surfactant clearance as demonstrated by the development of alveolar proteinosis in GM-CSF deficient mice lacking alveolar macrophages (Dranoff et al. 1994, Shibata et al. 2001, Guilliams et al. 2013). Due to the constant exposure to inhaled allergens, alveolar macrophage responsiveness to stimuli is tightly regulated whereas interstitial macrophages can promote inflammation (Kopf et al. 2015). It has been shown recently that the environment not only determines macrophage function but also its transcriptional landscape (Gosselin et al. 2014, Lavin et al. 2014). Interestingly, Lavin et al. showed that terminally differentiated tissue macrophages from the peritoneum can adopt the transcriptional profile of alveolar macrophages when transferred to the lung. These data underline the strong environmental effect on both macrophage phenotype and plasticity. It is thus far unclear how the different origins of tissue-

resident macrophages described above impact on macrophage function, especially compared to the recently described environmental dominance (Gentek et al. 2014).

DCs can be found in lymphoid and non-lymphoid organs and as 'professional' APCs their main function is to instruct the adaptive immune system during infections (see below). DCs are phagocytic and take up antigens in order to present them to T-cells, both in tissues and in the lymph nodes (LNs). In homeostatic conditions, DCs can induce Tregs and mediate both central and peripheral tolerance (Mildner and Jung 2014). Trafficking to LNs also occurs in the steady state in a chemokine (C-C motif) receptor (CCR) 7 dependent manner (Ohl et al. 2004) and has been shown to be necessary for induction of tolerance (Forster et al. 2012).

Inflammation

Macrophages and DCs become activated upon stimulation of PRRs that recognise PAMPs and DAMPs (Medzhitov and Janeway 1997, Matzinger 2002). There are two main classes of PRRs: 1) Membrane-bound receptors including Toll-like receptors (TLRs) and C-type lectin receptors (CLRs) and 2) unbound intracellular receptors such as Retinoic acid-inducible gene (RIG)-I-like receptors (RLRs) and NOD-like receptors (NLRs) (Takeuchi and Akira 2010). Extracellular receptors can bind to bacterial components such as LPS and flagellin while intracellular PRRs can recognise viral RNA. For TLR signalling refer to 1.3.2 Transcriptional mechanisms in activated macrophages, TLR signalling.

Upon activation, mature DCs upregulate CCR7 and migrate to the LN in a CCR7 dependent manner (Yanagihara et al. 1998). DC maturation furthermore leads to upregulation of MHC II and co-stimulatory molecules, thereby priming them for efficient antigen presentation in order to instruct the adaptive immune system (Reis e Sousa 2006) (see Figure 1.1). Macrophages can also present engulfed antigen on MHC II molecules to activate naïve T-cells (Desmedt et al. 1998, Hume 2008). However, DCs are considered to be more efficient at both antigen presentation and migration to the LN (Hashimoto et al. 2011).

During inflammation, macrophages secrete cytokines that shape the inflammatory environment and attract additional immune cells, especially high numbers of neutrophils and monocytes (see below, 1.2.4 Granulocytes, Neutrophils). Many acute infections are characterised by a massive monocyte influx to the site of inflammation (Shi and Pamer 2011). Ly6C^{hi} monocytes are recruited preferentially during infection and can give rise to macrophages/DCs that participate in pathogen clearance (Serbina et al. 2003, Auffray et al. 2009). Monocyte subsets and intrinsic functions are described in the next section 1.2.3. During the resolution stage of inflammation monocyte-derived macrophages can also be involved in tissue repair and wound healing (Gautier et al. 2012).

Cytokines are indispensable to reinforce differentiation or polarisation of all immune cells, as discussed earlier with regards to T-cells. In the case of macrophages, Mills et al. proposed the M1/M2 concept, analogous to T-cells stipulating a dichotomy of macrophage activation based on data mainly derived from *in vitro* cultured cells (Mills et al. 2000). M1 macrophages are considered

pro-inflammatory expressing high levels of IL-12 and IL-23 while M2 macrophages are anti-inflammatory and produce IL-10 (Gordon 2003). However, this concept has proven inadequate to reflect the variety of phenotypes possible, depending on the encountered stimuli and their combination (Xue et al. 2014). Hence, it is more likely that there is wide spectrum of activated macrophage phenotypes, as suggested previously (Mosser and Edwards 2008). Acknowledging the heterogeneity of macrophage phenotypes, a set of standards has recently been proposed by the macrophage community with the goal to unify experimental standards for *in vitro* and *in vivo* studies (Murray et al. 2014).

Macrophages acquire a pro-inflammatory phenotype in response to IFN-γ secreted by T-cells (see Figure 1.1) (Nathan et al. 1983, Dalton et al. 1993). However, macrophages do not necessarily rely on T-cells for activation as PRR stimulation itself or cytokines secreted by activated APCs or fibroblasts, such as TNF-α or GM-CSF respectively, also induce macrophage phenotypic changes (Hamilton 2008, Mosser and Edwards 2008). Macrophages that upregulate the production of reactive oxygen species (ROS) and nitric oxide (NO) via iNOS (inducible NO synthase) contribute to pathogen clearance and host defence (Biswas and Mantovani 2012). Cytokines enhancing the pro-inflammatory environment that are produced in this context are TNF-α, IL-1, IL-6, IL-12 and IL-23 (Arango Duque and Descoteaux 2014). Moreover, pro-inflammatory macrophages express high levels of MHC II and thereby participate in efficient antigen presentation (Biswas and Mantovani 2010). This type of macrophage response is associated with Th1 and Th17 mediated inflammation (Mosser and

Edwards 2008, Krausgruber et al. 2011). Although promotion of inflammation is beneficial when killing of pathogens is critical, the toxic activity of ROS and Th1/Th17 cells themselves can also cause harm by provoking collateral tissue damage (Nathan and Ding 2010). The need for rapid control mechanisms for pro-inflammatory macrophages is evident from the effects of prolonged activity observed in chronic and autoimmune diseases (Murray and Wynn 2011, Sindrilaru et al. 2011). The role of macrophages in the autoimmune disease RA will be discussed in 1.5.2 Macrophages in RA.

In the context of Th2 related inflammation such as parasite infection or allergy, the main cytokines driving macrophage responses are IL-4 and IL-13 (Raes et al. 2005). This enforces an anti-inflammatory or regulatory macrophage phenotype, which is characterised by a reduced responsiveness to TLR ligands as well as IL-10 and arginase 1 (Arg1) production (Biswas and Mantovani 2012). These macrophages can dampen inflammation and are important in tissue remodelling (Gordon 2003). Moreover, they express high levels of scavenging receptors such as the mannose receptor (CD206) (Gordon and Martinez 2010). Tumour associated macrophages display similar properties and their phenotypes are sometimes referred to as ‘M2-like’ (Biswas and Mantovani 2010).

In the resolution phase of inflammation, the cytokine environment changes and macrophages displaying anti-inflammatory phenotypes are more prevalent (Biswas et al. 2012). Whether this is due to actual macrophage plasticity where an individual macrophage changes its phenotype (Stout et al. 2005, Mylonas et

al. 2009, Italiani et al. 2014) or whether this is due to newly infiltrating monocytes being exposed to different signals (Arnold et al. 2007, Crane et al. 2014) is still under debate.

These functions however can also be fulfilled by tissue-resident macrophages, to some extent (Davies et al. 2013). The degree of tissue-resident macrophage participation in inflammation depends on both the type of challenge (Ajuebor et al. 1999) and also its intensity (Rosas et al. 2008). Tissue-resident macrophages self-maintain in the steady state (Sieweke and Allen 2013, Gentek et al. 2014) but have also been shown to proliferate in response to IL-4 in the context of nematode infection (Jenkins et al. 2011). Thus in the context of Th2 driven pathology, macrophages do not necessarily rely on monocyte input. Tissue-resident macrophages may also proliferate when inflammation has subsided to repopulate the tissue (Ajami et al. 2007, Chorro et al. 2009, Davies et al. 2011). Monocyte-derived macrophages have also been demonstrated to actively proliferate during acute inflammation (Davies et al. 2013). Further research will be necessary to determine the exact functional overlap and the differential contributions of tissue-resident macrophages and monocyte-derived cells.

1.2.3. Monocyte subsets and functions

As described earlier, monocytes develop in the BM and spleen and circulate in the blood with a short half-life of 20 hours (Yona et al. 2013). Two subsets of monocytes have been identified in these tissues, 'classical' Ly6C^{hi} CX$_3$CR1^{lo} CCR2^{+} and 'non-classical' Ly6C^{lo} CX$_3$CR1^{hi} CCR2^{-} monocytes (Geissmann et

al. 2003). During inflammation, monocytes exit the blood stream and infiltrate tissues where they can differentiate into macrophages and DCs (Shi and Pamer 2011). Ly6C^{hi} monocytes are also referred to as inflammatory monocytes and rely on CCR2 to egress from the BM (Boring et al. 1997, Serbina and Pamer 2006). However, monocyte effector functions in tissues independent of differentiation into macrophages or DCs have also been described. Ly6C^{+} monocytes have been shown to enter tissues in the steady state for immune surveillance (Jakubzick et al. 2013, Rodero et al. 2015). During infection, monocytes themselves can also actively participate in the inflammatory process by secreting cytokines and producing ROS (Serbina et al. 2008).

Ly6C^{lo} monocytes have been shown to patrol vessels to survey endothelial integrity although they are less prevalent in circulation than the Ly6C^{hi} subset (Auffray et al. 2007). Furthermore, the Ly6C^{lo} subset has been reported to enter tissues in the steady state (Geissmann et al. 2003) although this has recently been challenged by conflicting observations (Jakubzick et al. 2013).

In humans, three subsets of monocytes have been defined: classical CD14^{++} CD16^{-}, intermediate CD14^{++} CD16^{+} and non-classical CD14^{+} CD16^{++} monocytes (Ziegler-Heitbrock et al. 2010). The latter two can collectively be referred to as CD16^{+} monocytes. Non-classical CD14^{+} CD16^{++} monocytes are homologous to the mouse non-classical monocytes while the classical CD14^{++} CD16^{-} subset corresponds to the mouse Ly6C^{hi} subset. Although mouse and human monocyte subsets are similar, they also display species specific differences in their gene expression profiles (Ingersoll et al. 2010).

1.2.4. Granulocytes

Granulocytes are characterised by their polymorphonuclear shaped nucleus and the high abundance of granules in the cytoplasm. They can be subdivided into neutrophils, eosinophils and basophils, which all rapidly undergo degranulation upon activation releasing antimicrobial molecules. Eosinophils are important in Th2 driven inflammation such as parasite infections and allergic diseases including asthma. They produce a large array of cytotoxic materials and cytokines, for example Th2 related IL-4 and IL-13 (Davoine and Lacy 2014). Basophils are the least abundant granulocyte and are involved in parasite clearance and allergy. Despite sharing functional similarities with mast cells, these cell types differ with regards to location and lifespan. Basophils are short-lived and circulating whereas mast cells are long-lived and tissue-resident (Karasuyama et al. 2011).

Neutrophils

Neutrophils are the most abundant of granulocytes and are pivotal for the initial immune response to infection. They belong to the first line of defence and contribute to microbe killing by phagocytosis, release of granules and cytokine production (Tecchio et al. 2014). Granules contain hydrolytic enzymes such as neutrophil elastase and myeloperoxidases but also matrix metalloproteinases. Moreover, neutrophils can form neutrophil extracellular traps (NETs), a process also referred to as NETosis, in which a mixture of chromatin DNA, histones and granule contents is released (Kolaczkowska and Kubes 2013). Invading pathogens are trapped and immobilised in the NETs allowing for phagocytosis and potentially mediating direct killing (Brinkmann et al. 2004). It had previously

been assumed that NETosis essentially represents a form of cell death; however recent evidence suggests that neutrophils can remain functional following NETosis *in vivo* (Yipp et al. 2012).

Neutrophils are highly motile and are recruited to the site of inflammation via chemokines. Initially, chemokines are produced by tissue-resident cells such as macrophages, DCs and mast cells in response to PRR stimulation. Chemokines are essential for communication within the immune system and regulation of cell trafficking (Griffith et al. 2014). Chemokine gradients guide cells to the site of infection but they are also crucial in homing, for example to the LN via chemokine (C-C motif) ligand (CCL) 19/CCR7 interactions (Cyster 2005). Specificity of chemokines is achieved by distinct expression patterns of chemokine receptors. Neutrophils are attracted by a plethora of chemokines, specifically CCR1, chemokine (C-X-C motif) receptor (CXCR) 2 and BLT1 ligands (Griffith et al. 2014). Chemokines that specifically recruit neutrophils to the site of inflammation are CCL3 and CCL5 (CCR1 ligands) as well as LTB_4 (BLT1 ligand), while the CXCR2 ligands chemokine (C-X-C motif) ligand (CXCL) 1 (also KC) and CXCL2 (also MIP2) also attract monocytes. Neutrophils themselves also produce chemokines attracting cells from both adaptive and innate immunity and thus amplifying the immune response (Tecchio et al. 2014).

1.3. Transcriptional regulation of macrophages

Generally, gene expression is controlled by binding of TFs to the promoter region, thereby recruiting RNA Polymerase II (RNAP II) and enabling active

transcription. Cellular identity at a fundamental level is established by TFs that are upregulated during development and direct lineage fate. Similarly, the phenotype of differentially polarised macrophages is governed by distinct transcriptional regulators. Thus, cell fate and functions are governed by layers of transcriptional networks which are fine-tuned in response to a variety of stimuli. Macrophage activation via PRRs leads to downstream modulation of TF activity and expression that is specific to the stimulus encountered. Two of the major families of TFs involved in immune signalling are the nuclear factor κB (NF-κB) and the IFN regulatory factor (IRF) families.

1.3.1. Lineage defining transcription factors

Macrophage fate is induced during haematopoiesis by successively restricting the lineage potential of progenitors (refer to 1.2.1 Development of monocytes, macrophages and DCs, Haematopoiesis in the adult). The master regulator PU.1 is a RUNX1 (runt-related transcription factor 1) target gene, which is induced early at the HSC stage (see Figure 1.4) (Rosenbauer and Tenen 2007). While RUNX1 is essential for the development of all haematopoietic lineages (Okuda et al. 1996), PU.1 expression is indispensable for commitment to macrophage differentiation (Olson et al. 1995, Nerlov and Graf 1998). At a later stage, IRF8 is involved in promoting macrophage differentiation and supressing granulocyte fate (Holtschke et al. 1996, Tamura et al. 2000). Furthermore, PU.1 regulates Egr1- and Egr-2 which counteract neutrophil fate by activating macrophage specific genes (Nguyen et al. 1993, Laslo et al. 2006). The TFs c-Maf and MafB are required during the macrophage versus DC choice (Hegde et al. 1999, Bakri et al. 2005). KLF4 is another PU.1 target and important regulator

of monocyte/macrophage fate (Feinberg et al. 2007, Alder et al. 2008, Hettinger et al. 2013).

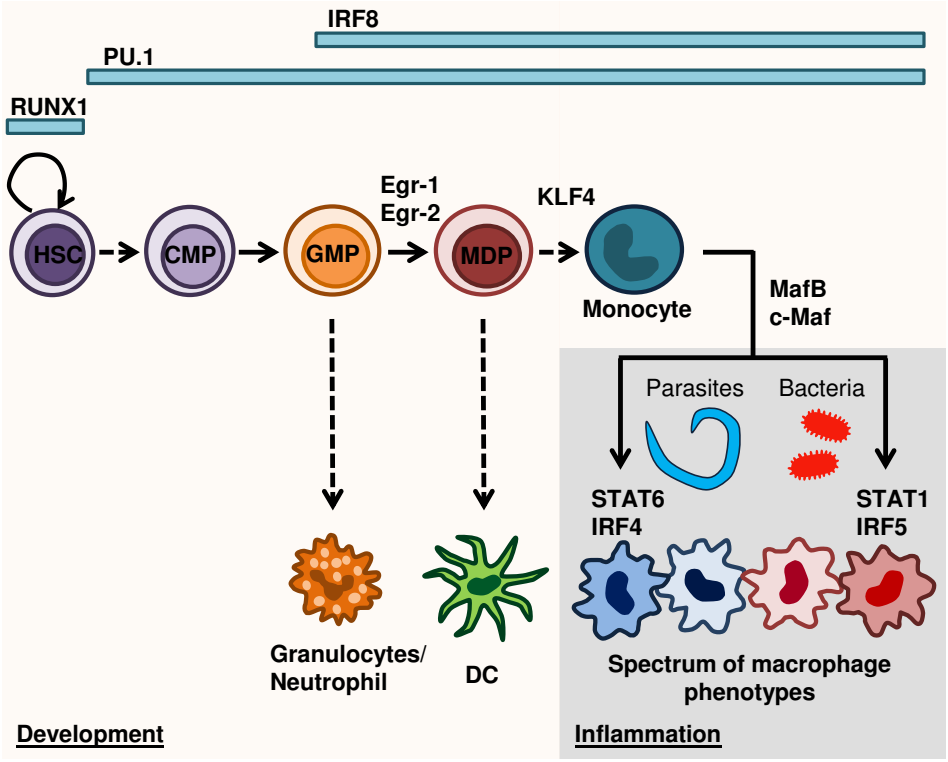

Figure 1.4. Transcriptional control of macrophage development and inflammatory phenotypes.

RUNX1 is required during early development in HSCs followed by the onset of PU.1 expression. PU.1 is the master regulator of the myeloid lineage and crucial throughout differentiation. IRF8, Egr-1 and Egr-2 are involved in supressing granulocyte and neutrophil genes while promoting macrophage fate. KLF4 is required for monocyte/macrophage differentiation and MafB and c-Maf counteract DC fate. During inflammation macrophages are shaped by the cytokine environment which depends on the nature of the infectious insult. Parasites lead to a Th2 driven disease activating STAT6 and IRF4 in macrophages. Bacterial pathogens on the other hand cause a Th1 or Th17 type response which leads to STAT1 and IRF5 activation. Importantly, macrophage phenotypes *in vivo* are manifold and thus represented as a spectrum.

PU.1 acts as the master regulator of the myeloid lineage, as it not only directs development but also orchestrates the genomic landscape of macrophages. This is illustrated by the finding that PU.1 binds to myeloid specific enhancer sites throughout the genome in macrophages (Ghisletti et al. 2010, Heinz et al. 2010). Enhancers are cis-regulatory elements that can be bound by multiple

regulatory factors and thereby influence the gene expression profile and thus cell identity. A characteristic mark of enhancer sites themselves is the abundance of monomethylated histone 3 lysine 4 (H3K4me1) (Heintzman et al. 2007). Interestingly, environmental cues have recently been shown to dictate the tissue-resident macrophage enhancer repertoire (Gosselin et al. 2014, Lavin et al. 2014). It has thus become increasingly clear that the control of transcriptional networks is complex and highly dynamic to adapt to the cell's functions (Natoli 2010).

1.3.2. Transcriptional mechanisms in activated macrophages

TLR signalling

Macrophages and other innate cells sense invading pathogens via intra- and extracellular PRRs that bind to evolutionary conserved PAMPs. One of the best characterised classes of PRRs are TLRs, which are transmembrane proteins localised on the cell surface or intracellularly in the vesicular compartment. 12 TLRs have been identified in mice that recognise different sets of PAMPs. Upon ligand binding, TLR signalling occurs via either the MyD88 dependent or the TRIF dependent pathway (Takeuchi and Akira 2010). The MyD88 pathway leads to activation of TRAF6, which in turn activates the inhibitor of kappa B (I-κB) kinase complex, resulting in degradation of the NF-κB inhibiting protein I-κB (Cao et al. 1996, Brubaker et al. 2015). NF-κB blockade is thereby removed allowing for NF-κB translocation to the nucleus and activation of cytokine gene expression such as TNF-α and IL-12 (Bonizzi and Karin 2004). TRIF signalling also activates NF-κB and additionally IRF3, which induces transcription of the type I IFNs, IFN-α and IFN-β (Doyle et al. 2002, Yamamoto et al. 2003). TLR4

is a prototypical TLR and was the first functionally characterised member of the TLR family (Medzhitov et al. 1997). Signalling of TLR4 is initiated upon LPS binding, which is derived from the outer membrane of Gram-negative bacteria (Poltorak et al. 1998). LPS is commonly used in experimental setups to mimic bacterial infection, both *in vitro* and *in vivo*.

Transcriptional control of macrophage phenotypes

Macrophage phenotypes are shaped during inflammation in response to the cytokine cues received from the environment (see Figure 1.4). Depending on the nature of the signal this induces different transcription programmes defining macrophage phenotypes (Lawrence and Natoli 2011). IFN-γ driven phenotypic changes are mediated by Janus kinase-signal transducer and activator of transcription (JAK-STAT) signalling, which ultimately leads to STAT1 phosphorylation and dimerisation (Darnell et al. 1994). STAT1 homodimers bind to gamma-activated sequences (GAS) in the promoters of genes, such as *Nos2* and *Il12b*, to induce mRNA expression (Varinou et al. 2003). The requirement for STAT1 signalling during inflammatory diseases is illustrated by susceptibly of *Stat1*$^{-/-}$ mice to viral and microbial infections (Durbin et al. 1996, Meraz et al. 1996). In macrophages that were exposed to IL-4 or IL-13, signalling occurs through the IL-4Rα via JAK-STAT6 (Takeda et al. 1996). Some of the IL-4 target genes include *Arg1* or *Mrc1*, which are generally associated with alternatively activated macrophages (Martinez et al. 2009). Furthermore, the TF PPARγ can be induced by STAT6 and has been shown to promote an anti-inflammatory macrophage phenotype in obesity (Bouhlel et al. 2007, Odegaard

et al. 2007). Importantly, STAT1 and STAT6 are known to antagonise each other and their effects are thus mutually exclusive (Ohmori and Hamilton 1997).

Members of the IRF family of transcription factors are also involved in controlling macrophage phenotypes. IRF5 has been shown to be important for establishment of a pro-inflammatory phenotype (Krausgruber et al. 2011) and will be discussed in more detail in the next section (1.4 The transcription factor IRF5). IRF4 on the other hand has been shown to contribute to the regulation of genes associated with anti-inflammatory macrophages such as *Arg1* (Satoh et al. 2010). In the context of helminth infection, the demethylase Jumonji domain containing-3 (Jmjd3) controls activity of the *Irf4* locus and thereby affects macrophage properties. This study highlights the influence of epigenetics on macrophage gene expression as an additional layer of transcriptional control. Epigenetic changes in specific histone marks have been shown to modulate gene expression levels in addition to TF mediated control (Alvarez-Errico et al. 2015). Histone lysine and arginine residues can be post-translationally modified leading to differential recruitment of co-factors (Kouzarides 2007). Different modifications of lysine residues can in fact mediate different effects; H3K27me3 for example has been associated with transcriptional repression whereas H3K4me3 has been linked to active transcription (Kouzarides 2007). Methylation status is controlled by the activity of respective histone methyltransferases and demethylases. Jmjd3 is a H3K27 demethylase and has not only been shown to regulate *Irf4*, as described earlier, but it has also been implicated in the control of LPS response genes (De Santa et al. 2007, De Santa et al. 2009).

1.4. The transcription factor IRF5

IRF5 is one the nine members of the IRF family of transcription factors. IRFs are involved in multiple processes within both the innate and adaptive immune system. As described earlier, different IRFs are involved in regulating the development and inflammatory phenotypes of myeloid cells. Upon activation, IRFs bind to IFN stimulated response elements (ISREs) in the promoters of their target genes and initiate transcription. To fulfil their functions in host defence against viral and bacterial pathogens, IRFs often cooperate with other TFs. IRF5 has been shown to play an important role in regulating genes involved in both anti-viral and microbial responses, such as type I IFNs and pro-inflammatory cytokines, respectively.

1.4.1. IRF5 gene and protein structure

The human *IRF5* gene (*hIRF5*) consists of nine exons and three different promoters lead to the expression of several variants of exon1 (Mancl et al. 2005). In combination with complex splicing of the *IRF5* transcript, this generates multiple mRNA variants (Graham et al. 2006). Expression of these is cell type specific and additionally some variants seem to associate with different diseases such as systemic lupus erythematosus (SLE) (Mancl et al. 2005, Stone et al. 2013). Some studies have been carried out to characterise the *hIRF5* locus further, detecting binding sites for multiple TFs including PU.1, IRF4, NF-κB and Sp1 (Kozyrev and Alarcon-Riquelme 2007, Clark et al. 2013). The human and mouse *Irf5* genes are highly homologous, yet there is a major difference regarding transcript variants (Paun et al. 2008). The mouse *Irf5* gene also contains nine exons but only one major transcript is expressed in most

tissues (Paun et al. 2008). A single splice variant exists in the BM, containing a deletion spanning from exon 4 to exon 6, which is expressed at a very low frequency and displays impaired transcriptional activity (Paun et al. 2008). Of note, it has been reported that *Irf5* transcript levels in the spleen vary between mouse strains and females show consistently higher IRF5 expression (Shen et al. 2010). Overall, this suggests a more complex regulation of the human *IRF5* locus while murine *Irf5* may be controlled in a simpler fashion. Nevertheless, it remains unknown how exactly and by which factors *Irf5* transcription is controlled, both in human and mouse.

The mouse IRF5 protein shows 87% homology to the full length human protein, translated from transcript variant 5, and was shown to behave similarly in response to TLR signalling (Paun et al. 2008). Murine IRF5 is a 498-amino acid protein containing two domains: a well-conserved N-terminal DNA-binding domain (DBD) and a C-terminal IRF association domain (IAD). The DBD is essential for its function as a TF by recognising ISREs in target genes while the IAD allows for the formation of homo- or hetereodimers (Tamura et al. 2008). The IAD is furthermore important for interactions with other proteins acting as transcriptional co-factors such as RelA, a member of the NF-κB TF family (Saliba et al. 2014).

IRF5 expression has been detected in many immune cells, including NK cells, B-cells, DCs and macrophages (Heng et al. 2008). For details regarding the expression pattern of IRF5 in different cell types and tissues, refer to section 4.1.

1.4.2. Functional properties of IRF5

Originally, IRF5 was reported to be activated during antiviral responses and induce type I IFN expression (Barnes et al. 2001). Additional roles for IRF5 in apoptosis (Barnes et al. 2003, Hu et al. 2005), parasite (Paun et al. 2011) and fungal (del Fresno et al. 2013) infections as well as inflammation (Takaoka et al. 2005, Krausgruber et al. 2011, Yang et al. 2012, Courties et al. 2014, Dalmas et al. 2015) have since been described.

IRF5 acts as a tumour suppressor by inducing cell cycle arrest and apoptosis, independent of p53 (Barnes et al. 2003, Hu et al. 2005, Yanai et al. 2007). Moreover, it has recently been demonstrated that IRF5 contributes to the innate immune system's anti-tumour response following activation downstream of Dectin-1 (Chiba et al. 2014). Dectin-1 is a CLR known to recognise fungal wall components and IRF5 is in fact required for Dectin-1 mediated immunity to *Candida albicans* infection (del Fresno et al. 2013).

We have previously identified IRF5 as the major regulator of the pro-inflammatory macrophage phenotype and potent inducer of Th1/Th17 responses (Krausgruber et al. 2011). IRF5 is responsible for directly inducing expression of key pro-inflammatory cytokines such as IL-6, IL-12, and IL-23 (Takaoka et al. 2005, Krausgruber et al. 2011). Furthermore, IRF5 has been shown to cooperate with RelA to regulate subsets of target genes, including for example TNF-α (Krausgruber et al. 2010, Saliba et al. 2014). Specifically, IRF5:RelA co-recruitment to PU.1-marked enhancers and promoters of inflammatory genes has been observed in response to LPS to establish an

inflammatory gene programme (Saliba et al. 2014). Moreover, it has also been reported that IRF5 can suppress expression of anti-inflammatory cytokines such as IL-10 (Krausgruber et al. 2011). These data show that IRF5 controls gene expression by inducing or suppressing target genes and that its functions can be mediated in collaboration with co-factors (Feng et al. 2010, Eames et al. 2012).

Upon activation following virus infection or downstream of TLR4, 7 and 9 signalling, IRF5 is post-translationally modified, which leads to its translocation to the nucleus and target gene expression (Barnes et al. 2001, Schoenemeyer et al. 2005, Honda and Taniguchi 2006, Ryzhakov et al. 2015). A recent study also reports IRF5 activation in response to *Staphylococcus aureus* induced TLR8 signalling (Bergstrom et al. 2015). Phosphorylation in response to viral infection has been described for several viruses, including Newcastle disease virus and Sendai virus, which ultimately induces expression of type I IFNs (Barnes et al. 2001, Barnes et al. 2002, Ikushima et al. 2013, Ren et al. 2014). Kinases involved in TLR signalling pathways have been reported to phosphorylate IRF5, namely TBK-1, IKKβ, IKKε and RIP2 (Schoenemeyer et al. 2005, Cheng et al. 2006, Chang Foreman et al. 2012, Ren et al. 2014, Ryzhakov et al. 2015). The E3 ubiquitin ligase TRAF6 has been shown to ubiquitinate IRF5, which in consequence facilitates nuclear translocation of IRF5 (Balkhi et al. 2008). In contrast, ubiquitination by the E3 ligase TRIM21 leads to degradation of IRF5 (Lazzari et al. 2014). Furthermore, IRF5 can directly interact with the TLR signalling adaptor molecules MyD88, TRAF6 and IRAK1 (Takaoka et al. 2005, Balkhi et al. 2008) (see 1.3.2 Transcriptional

mechanisms in activated macrophages). Interestingly, IRF5 and IRF4 compete for MyD88 binding and exert opposing effects on TLR signalling (Negishi et al. 2005). These data further underline the contrasting roles of IRF4 and IRF5 in shaping macrophage gene expression profiles (see 1.3.2 Transcriptional mechanisms in activated macrophages). To conclude, post-translational modifications clearly play an important role in IRF5 activation although the exact mechanisms and kinases involved *in vivo* remain to be elucidated (Ryzhakov et al. 2015).

1.4.3. Association of IRF5 with autoimmune diseases

IRF5 is involved in regulating Th17 responses that are prevalent in inflammatory autoimmune disease. It has indeed been shown that IRF5 associates with autoimmunity both on a genetic and a functional level (Eames et al. 2015). Genome-wide association studies (GWAS) have been performed to identify mutations, mainly single nucleotide polymorphisms (SNPs), which are more prevalent in cohorts with a specific disease compared to healthy controls. Several polymorphisms in the *IRF5* gene have been described, and for some of these functional consequences have been demonstrated in terms of increased expression levels or splicing (Eames et al. 2015).

SLE is a heterogeneous autoimmune disease that shows a strong association with IRF5 (Eames et al. 2015) and is characterised by a high abundance of antinuclear antibodies (ANAs) in predominantly female patients. Nuclear ‘self’ components such as chromatin, histones and double-stranded DNA are recognised by ANAs thereby breaking tolerance and resulting in a pathogenic

autoimmune response manifesting in multiple organs (Liu and Davidson 2012). ANAs have also been identified in other autoimmune diseases such as systemic sclerosis and RA (Lyons et al. 2005). Moreover, SLE patients commonly exhibit an IFN-signature correlating with disease severity (Kanayama et al. 1989, Bengtsson et al. 2000). IRF5 is known to regulate IFN expression during anti-viral responses (see above) but has also been linked to IFN levels in SLE (Niewold et al. 2008, Stone et al. 2012). Importantly, increased levels of IRF5 have been detected in SLE patients (Feng et al. 2010, Stone et al. 2013). The role of IRF5 has further been highlighted by studies using various mouse models of SLE where loss of IRF5 confers disease protection. In this context, $IRF5^{-/-}$ mice show reduced disease severity, increased Th2 but decreased Th1 differentiation and consistently lower IFN-α levels (Richez et al. 2010, Tada et al. 2011, Xu et al. 2012, Yang et al. 2012).

RA is a chronic autoimmune disease of the joints, which will be described in more detail in the next section. In contrast to SLE, IRF5 only shows a weak to moderate genetic association with RA (Eames et al. 2015). In addition, results from different studies are less consistent or even contrary as some actually did not detect association of *IRF5* with RA (Rueda et al. 2006, Garnier et al. 2007). However, two polymorphisms have repeatedly been identified in independent studies analysing multiple European nationalities (Dieguez-Gonzalez et al. 2008, Stahl et al. 2010, Dawidowicz et al. 2011). Recently, Zhu et al. showed that IRF5 is expressed in RA synovial fluid and can be induced in macrophages by Anti-citrullinated protein antibodies (ACPAs), which are specific for RA (Zhu et al. 2015). This study suggests a functional role for IRF5 in RA synovial

macrophages, as they demonstrated that an ACPA-induced switch in the ratio of pro-inflammatory versus anti-inflammatory phenotype correlated with IRF5. Mechanistic studies assessing different models of RA in IRF5$^{-/-}$ mice however have not been conducted conclusively. One study reported no difference in IRF5$^{-/-}$ mice using the model of collagen-induced arthritis (CIA) (Savitsky et al. 2010) although this may be due to the reduced susceptibility observed in mice on the C57BL/6 background (Inglis et al. 2007, Backlund et al. 2013). Further research will thus be required to clarify by which mechanisms exactly IRF5 may contribute to RA disease pathology.

Inflammatory bowel disease (IBD) is an inflammatory disorder of the gut comprising different forms, which affect distinct parts of the intestines (Maloy and Powrie 2011). Polymorphisms in the *IRF5* gene causing gain-of-function have been reported to show a weak to moderate association with IBD (Dideberg et al. 2007, Anderson et al. 2011). Interestingly, *IRF5* polymorphisms have also been associated with asthma, an allergic Th2 driven disease of the lung (Wang et al. 2012). However, in this context increased IRF5 appears to be related to protection while lower expression represents a risk factor. Taken together, current evidence suggests that an increase in IRF5 contributes to the disease susceptibility and pathology of multiple inflammatory autoimmune diseases. While strong genetic and functional links have been demonstrated for IRF5 in SLE, less conclusive data is available for other autoimmune diseases such as RA and IBD.

1.5. Rheumatoid arthritis

RA is a chronic inflammatory disease of the joints that affects approximately 1% of the population. The disease aetiology is not fully understood but both environmental and genetic risk factors contribute to disease onset and progression. As in many autoimmune diseases, women are affected to a greater extent than men (by a factor of three in RA). Patients suffer from debilitating joint destruction caused by the chronic inflammation, in some cases accompanied by additional extra-articular disease features. Current standard treatments are immunosuppressive drugs such as methotrexate, corticosteroids and biologicals, such as TNF inhibitors. Although anti-TNF-α therapy has brought major improvements for many RA patients, there also is a considerable proportion of partial or non-responders, accounting for 30-40% of treated patients which therefore warrants further research to identify new pathological targets and more effective medicines.

1.5.1. Disease aetiology, phenotype and treatment

Although the definitive steps in RA pathogenesis are still unknown, some important external and internal contributing factors have been identified. Smoking has been reported as a major environmental influence inferring risk even when discontinued (Stolt et al. 2003, Klareskog et al. 2006). Known genetic risk factors are polymorphisms in the *HLA-DRB* region, the human MHC, which strongly associates with RA (Gregersen et al. 1987) and weaker links with genes such as *PTPN22* have also been described (Begovich et al. 2004). The two main autoantibodies present in the majority of RA patients are rheumatoid factor (RF) and ACPAs. RF recognises the Fc portion of the IgG

molecule but can also be detected in the context of other diseases or even healthy individuals (Mewar and Wilson 2006). In contrast, ACPAs are exclusively present in RA recognising citrullinated proteins that as such are not RA specific (Willemze et al. 2012). Interestingly, ACPAs can be detected in the serum many years before onset of disease, which suggests a role for initial break of tolerance (Catrina et al. 2014). Moreover, ACPA levels correlate with development of a more erosive pathology as the disease progresses (van Venrooij et al. 2011). These and other data firmly link antibody producing B-cells to RA pathology (Edwards and Cambridge 2001, Cambridge et al. 2003). Although T-cells have also been demonstrated to contribute to disease progression, their specific functional role is so far insufficiently understood. Specifically Th1 and Th17 cells have been described to perpetuate inflammation by secreting cytokines such as IFN-γ and IL-17 leading to synovial fibroblast and macrophage activation (Lubberts 2015). T-cells thereby enhance the pro-inflammatory environment in the joint, which ultimately causes cartilage destruction and bone erosion. Targeting the Th17 related IL-17-IL-23 pathway has been explored as a potential new line of therapy in combination with anti-TNF-α (Lubberts 2015).

Arthritic joints are initially characterised by pain, redness and swelling due to the high influx of inflammatory cells (see Figure 1.5). Activated neutrophils are present in large numbers in RA synovial fluid and pannus where they promote inflammation and cause tissue damage (Wright et al. 2014). Moreover, infiltrating macrophages and proliferating resident synovial fibroblast cause considerable thickening of the synovial lining (Burmester et al. 1983). Synovial

fibroblasts secrete matrix degrading enzymes such as collagenase and matrix-metalloproteinases that diminish cartilage integrity (McInnes and Schett 2011). This aggressive synovial tissue resulting from the synovial hyperplasia and inflammatory infiltrate is referred to as pannus (McInnes and Schett 2011). Pannus invasion causes both destruction of the joint cartilage and bone erosions due to osteoclast formation and activation (Redlich and Smolen 2012). The cytokine environment in fully manifested RA is dictated by activated innate immune cells such as macrophages and fibroblasts that in consequence promote osteoclast differentiation (McInnes and Schett 2007, Neumann et al. 2010). Accordingly, therapies targeting pivotal inflammatory cytokines such as TNF-α and IL-6 have been particularly successful (Feldmann 2002). Current baseline treatment involves disease-modifying anti-rheumatic drugs (DMARDs), most commonly methotrexate, and steroids or non-steroidal anti-inflammatory drugs (Scott et al. 2010). Although TNF inhibitors are the most widely prescribed biologicals, additional therapies targeting IL-6R (tocilizumab), IL-1 (anakinra), B-cells (e.g. rituximab) or T-cell co-stimulation (abatacept) are also available (Smolen and Aletaha 2015). Since RA is a systemic disease, consequences of the chronic inflammation can also involve tissues other than the joints. Hence, RA patients present with a higher risk of conditions affecting the cardiovascular system, the lung or the liver and cancers, for example lymphomas (Scott et al. 2010).

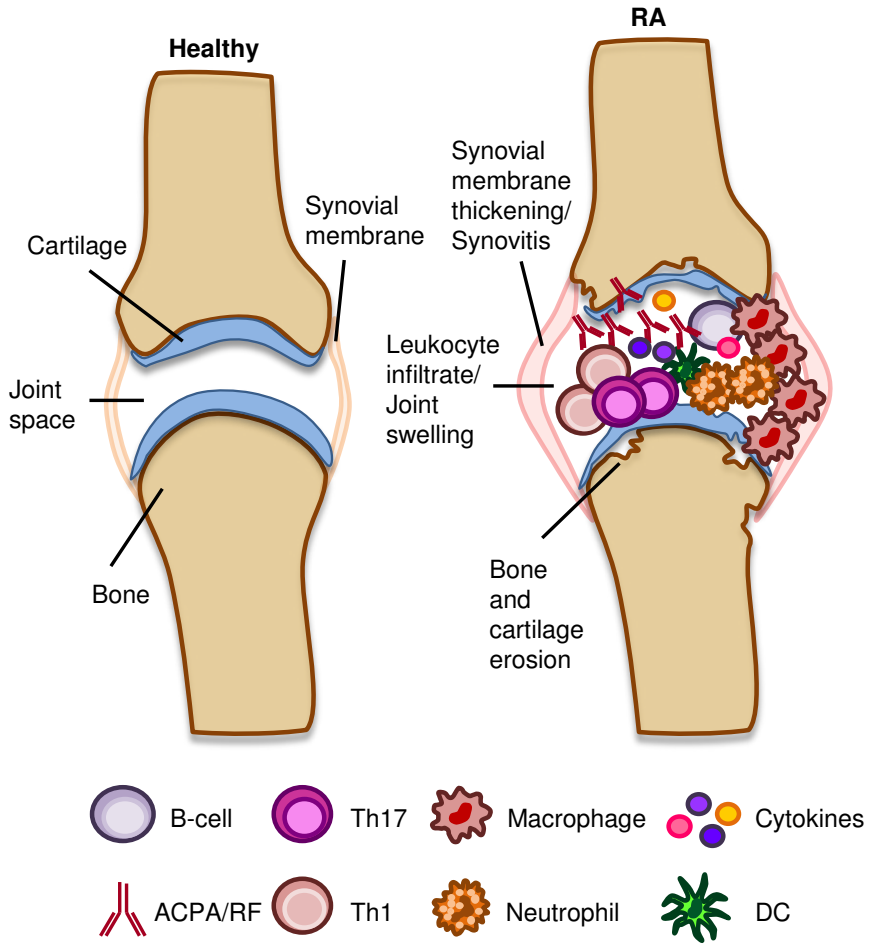

Figure 1.5. Schematic representation of a healthy and RA joint.

The RA joint is characterised by joint swelling caused by infiltration of different immune cells into the joint space. Ultimately this process results in hyperplasia and inflammation of the synovial membrane as well as bone and cartilage erosion.

1.5.2. Macrophages in RA

Macrophages are the main TNF-α producing cell in the inflamed RA joint and their key role is illustrated by the efficacy of TNF inhibitors in disease therapy. Upon activation by cytokines or immune complexes (consisting of antigen bound by autoantibodies), macrophages drive inflammation in the joint by shaping the cytokine environment (see Figure 1.6) (Feldmann et al. 1996, McInnes and Schett 2007, Kennedy et al. 2011). Secretion of cytokines and chemokines perpetuates the inflammatory response by recruiting additional

innate immune cells such as monocytes and neutrophils but also by inducing T-cell differentiation. IL-23 is an important cytokine in RA (Murphy et al. 2003) that stabilises the phenotype of Th17 cells, which are argued to be the one of the key effectors in autoimmunity generally and RA specifically (Miossec and Kolls 2012). Synovial fibroblasts also become activated in response to macrophage-derived cytokines and in turn provide feedback loops to activate macrophages (McInnes and Schett 2007). In response to TNF-α and IL-1β fibroblasts produce RANKL (receptor activator of NF-κB ligand) (Shigeyama et al. 2000) and M-CSF (Hamilton et al. 1993, Seitz et al. 1994), which are essential for formation of osteoclasts, the bone's resident macrophage equivalent (Yoshida et al. 1990, Dougall et al. 1999). Macrophage-derived TNF-α, IL-6 and IL-1 can further amplify osteoclast functions, directly or indirectly (Bertolini et al. 1986, Lam et al. 2000, Redlich and Smolen 2012). In healthy individuals, bone resorption by osteoclasts is balanced by bone-forming osteoblasts (Sims and Gooi 2008), while in RA at sites of inflammation, osteoclast activity is chronically induced causing severe bone erosion (Redlich and Smolen 2012).

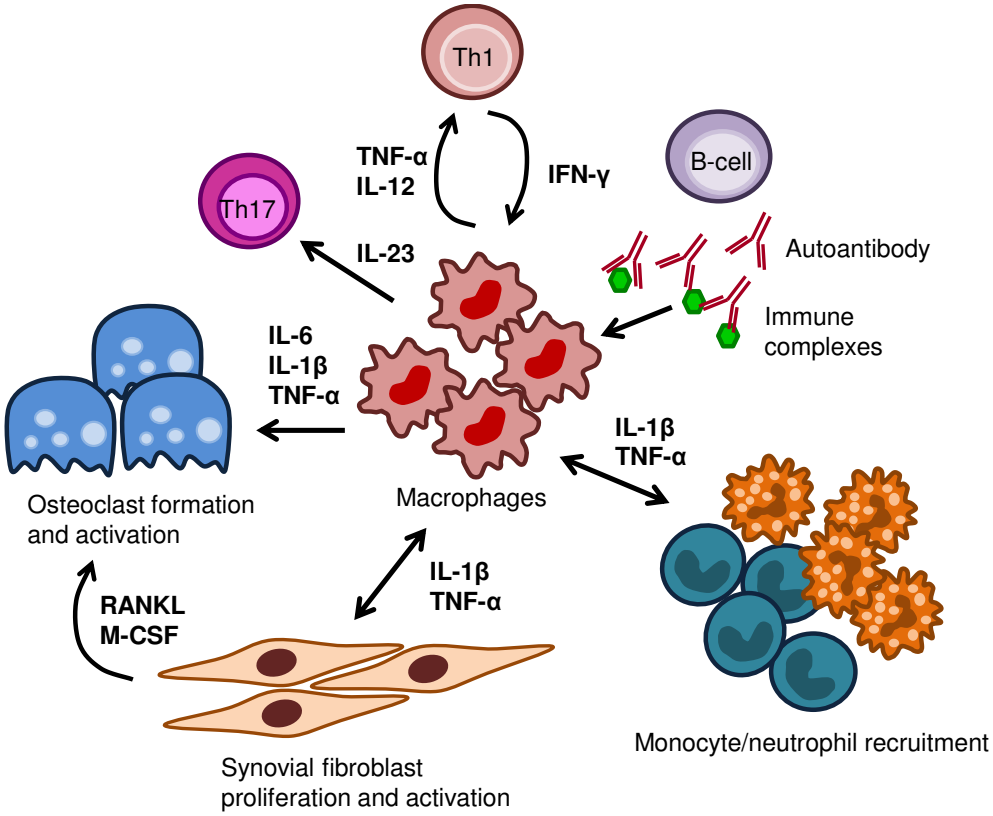

Figure 1.6. Overview of the role of macrophages in RA.

Macrophages produce cytokines which in turn promote inflammation by recruitment of additional immune cells, T-cell polarisation and fibroblast activation. Activated fibroblast secrete RANKL and M-CSF inducing osteoclast differentiation which is enhanced by macrophage derived TNF-α and others. Immune complexes formed by autoantibodies and antigens activate macrophages. Additionally, macrophages are influenced by cell-cell contact or cytokines produced by T-cells, fibroblasts and innate immune cells.

Macrophages further contribute to disease progression by production of ROS, NO intermediates, matrix-degrading enzymes and antigen presentation (McInnes and Schett 2011). GM-CSF has been shown to promote arthritis probably by enhancing macrophage survival and functions (Hamilton 2008). Macrophages are indeed one of the most abundant cell types at the site of inflammation in RA (Tak and Bresnihan 2000, Smeets et al. 2001) and clinically effective therapies have been shown to reduce macrophage numbers in the joint (Haringman et al. 2005). In addition, depletion of macrophages using

clodronate-containing liposomes has been demonstrated to be beneficial for disease pathogenesis (Barrera et al. 2000).

Other therapies targeting monocytes/macrophages by using specific targeting vectors such as lipoplexes or dendrimers have been shown to be effective in experimental mouse models (Davignon et al. 2013). The contribution of monocytes to the macrophage population in the joints and the origin of resident synovial macrophages are largely uncharacterised. A recent study, however, analysed murine myeloid populations in the ankle synovium, identifying embryonically- and monocyte-derived macrophages (Misharin et al. 2014) (also refer to chapter 4 sections 4.1 and 4.3). Thus, macrophages play a key role in RA by orchestrating the cytokine environment, which enhances inflammation and contributes to cartilage and bone destruction.

1.5.3. Mouse models of RA

To elucidate the mechanisms underlying RA pathology and to explore potential drug targets, multiple mouse models of arthritis have been established (McNamee et al. 2015). Different models mimic different phases of the human disease and can thus differ in the requirement for innate and adaptive immunity. CIA and antigen-induced arthritis (AIA) involve an immunisation step and hence rely on the adaptive immune system. In CIA, genetically susceptible mice are immunised with type II collagen in complete or incomplete Freund's adjuvant (CFA and IFA, respectively), which leads to a chronic and progressive disease (Holmdahl et al. 1989). AIA usually involves immunisation with methylated bovine serum albumin (mBSA) in CFA followed by intra-articular injection of antigen in one knee and saline in the contralateral knee as a negative control

(van den Berg et al. 2007). Antigen challenge in AIA causes an acute and localised inflammatory response, in contrast to CIA and RA that affect multiple joints. AIA therefore minimises the number of mice used (100% penetrance) and furthermore is not limited by strain susceptibilities. Since many genetic knockout mice are on the C57BL/6 background that is less susceptible to CIA (Inglis et al. 2007, Backlund et al. 2013), AIA is an especially useful model in this context. The model of serum transfer induced arthritis uses immune complexes from K/BxN mice and requires innate immunity. K/BxN mice spontaneously develop arthritis and transfer of their serum is sufficient to cause arthritis in the ankle joints of recipients on many different genetic backgrounds (Monach et al. 2008). This model has been shown to be independent of the adaptive immune response and pathology is largely neutrophil dependent (Wipke and Allen 2001). All models display elements of arthritis including joint swelling, leukocyte infiltrate and bone erosion but vary in kinetics and underlying mechanisms of disease induction and pathology. Whilst it is agreed they do not fully mimic RA and therefore interpretation should be restricted to understanding of discrete pathways, they are useful tools in which to manipulate immunological processes in a complex disease setting that is difficult to recapitulate by current *in vitro* methodologies.

1.6. Aims

Previous work in the Udalova laboratory has implicated IRF5 in the regulation of a pro-inflammatory phenotype in human *in vitro* differentiated macrophages (Krausgruber et al. 2011). Therefore, I wanted to explore the role of IRF5 in inflammatory macrophages in an *in vivo* disease setting using mouse models.

The first aim of my thesis was thus to transfer the previous findings to the murine system and extend existing knowledge by characterising the expression pattern in several differently generated *in vitro* differentiated macrophages (Chapter 3). I hypothesised that the IRF5 expression pattern is the same in the murine equivalents of human *in vitro* differentiated cells. I characterised differentially generated *in vitro* BM-derived macrophages with regards to surface marker expression, LPS response and IRF5 expression levels. During this part of my project, I could show that IRF5 expression in the murine in vitro system is similar to the previously described pattern in human *in vitro* differentiated macrophages.

Following on from the *in vitro* results, I then wanted to compare the results of my *in vitro* studies to the expression of IRF5 *in vivo* within different cell populations in murine tissues in the steady state (Chapter 4). Data from my own *in vitro* studies in chapter 3 and previously published data lead me to specifically investigate the IRF5 expression pattern in multiple myeloid cell populations. Based on the combined results of the *in vitro* and *in vivo* expression studies, I hypothesised that IRF5 is expressed by pro-inflammatory macrophages in a disease setting generally and specifically in the knee joints during AIA. The high IRF5 levels in both macrophages and monocytes that I observed in arthritic joints prompted me to elucidate the functional role of IRF5 in acute inflammatory diseases, including AIA and acute lung injury, by analysing the disease progression in animals lacking IRF5 (Chapter 5). Due to the previously described role of IRF5 in controlling pro-inflammatory gene expression, I hypothesised that IRF5 is in involved in regulating the

inflammatory response of macrophages at the site of inflammation and thereby driving recruitment of additional immune cells.

2. Material and Methods

2.1. *In vitro* experiments

2.1.1. Generation of bone marrow-derived cells

All murine cells were maintained at 37°C, with 5% CO_2 and 95% humidity.

Isolation of whole bone marrow

Mice were sacrificed by Schedule 1 method using CO_2 inhalation followed by cervical dislocation. Femurs and tibia were dissected and removed by dislocating the ankle and hip joints. Skin and muscle tissues surrounding the bones were removed with scissors. Remaining muscle tissue was detached by first soaking bones in 70% ethanol for up to 5 minutes and then using a tissue (Kimtech) to manually remove the excess muscle. Cleaned bones were cut open at both ends and the BM was then flushed out into a 50 ml tube (Falcon) with up to 10 ml of PBS (phosphate buffered saline, Gibco) using a 27G needle (BD) and 10ml syringe (BD). Bones were flushed with PBS until no visible BM was left and bones appeared clear and white. All the BM progenitors from a single mouse were collected in the same tube and then centrifuged (Scanspeed 1580MGR, GRS-750-4 rotor) at 515 x g for 5 min at room temperature. The resulting pellet was resuspended in 1 ml of BM culture medium (BM medium) consisting of RPMI-1640 medium with L-glutamine (Lonza) supplemented with 10% FBS (Foetal Bovine Serum, Labtech), 1% penicillin/streptomycin (P/S, Lonza), 0.01% 2-mercaptoethanol (Gibco). A 10 µl aliquot of the cell suspension was counted with a haemocytometer before diluting the cell suspension to a concentration of $5x10^6$ cells/ml in BM medium.

Bone marrow-derived macrophages

To generate *in vitro* differentiated macrophages, BM progenitors from IRF5 wild type and knockout mice were cultured in BM medium supplemented with either recombinant murine GM-CSF (20 ng/ml; Peprotech) or recombinant human M-CSF (100 ng/ml; Peprotech). Specifically, $5x10^6$ BM cells, obtained as described above, were seeded in a bacterial petri dish (Sterilin) in 10 ml of BM medium with added cytokine. Cells differentiated with GM-CSF were supplied with fresh GM-CSF on day three and six of culture to maintain a sufficiently high level for differentiation. On day three 10 ml of BM medium with 20 ng/ml GM-CSF were added to culture dishes. On day six 10 ml of the cell culture suspension were transferred to a 50 ml tube, centrifuged at 515 x g for 5 min and the pellet resuspended in fresh BM medium with 20 ng/ml GM-CSF. The cell suspension was then added back to the respective cell culture dishes. As M-CSF is produced by macrophages themselves, it does not need to be supplied after the start of culture.

After eight days of differentiation, cells were washed with 10 ml PBS once and then harvested with 3-4 ml Versene (EDTA; Lonza) for up to 15 min at 37°C. Cells were resuspended in BM medium, counted and re-plated in tissue culture plates (BD) as required and then stimulated with LPS (100 ng/ml; Alexis Biochemicals).

For GM-CSF differentiated macrophages (GM-BMDMs) medium contained 10 ng/ml GM-CSF during LPS stimulation. M-CSF differentiated macrophages (M-BMDMs) did not require additional M-CSF. In some cases, however, murine recombinant IFN-γ (5 ng/ml; Peprotech) or IL-4 (10 ng/ml; Peprotech) were added to M-BMDMs 18 h prior to LPS stimulation to obtain differently skewed

macrophage populations. Equally, GM-CSF (20 ng/ml) was sometimes added to M-BMDMs 18 h before LPS stimulation. Alternatively, GM-CSF treated BMDMs were sometimes left unstimulated and instead treated with Actinomycin D (ActD, Sigma), 6 h after GM-CSF addition. ActD prevents active transcription and thereby allows for assessment of mRNA stability.

2.1.2. Protein detection

Enzyme linked immunosorbent assay (ELISA)

Secreted cytokines in cell culture supernatants of *in vitro* differentiated cells were quantified using ELISA. Supernatants of stimulated cells were transferred into tubes, centrifuged for 5 min at 1,071 x g at room temperature and stored at -20°C until needed. For cytokine detection, 96 well plates (Nunc) were coated with 50 µl capture antibody in PBS per well and incubated at 4°C on a shaker overnight. All antibodies used and their respective dilutions can be found in Table 2.1. The following day, plates were washed once with PBS-T 0.05%, PBS containing 0.05% Tween-20 (Sigma). Residual liquid was removed by inverting the plate and blotting it against clean paper towels. Plates were then blocked with 100 µl per well of 1% BSA (high quality bovine serum albumin, Sigma) in PBS for 1 h at room temperature (RT). A seven point standard curve was created using serial 1:3 dilutions of the purified protein of interest in 1% BSA in PBS (see Table 2.1). The top standard was prepared at a concentration of 1,000 - 5,000 pg/ml. Samples were diluted 1:2 or 1:4 in 1% BSA in PBS. Following blocking, plates were washed three times using PBS-T 0.05% before addition of 50 µl sample/standard per well. Samples/standards were performed in triplicate and incubated overnight at 4°C on a shaker to allow for protein

capture. After three wash steps as described above, 50 µl of corresponding biotinylated detecting antibody (see Table 2.1) in 1% BSA in PBS were added to each well and left for 1 h on a shaker at RT. Three washes were performed as before and 50 µl of biotin binding streptavidin-HRP in 1% BSA in PBS per well were added. Plates were left on a shaker for 1h at RT before three final wash steps. The HRP substrate TMB (Cell Signaling) was added at a volume of 50 µl per well to induce a quantifiable colour change, relative to the amount of protein captured. Plates were observed during the resulting blue colour change to ensure that samples did not develop darker than the standard curve colour. To terminate the enzymatic reaction 50 µl 1M H_2S0_4 (Sigma) were added leading to a colour change to yellow. Absorbance was read at 450 nm by a spectrophotometric ELISA plate reader (Labsystems Multiscan Biochromic) and analysed using Ascent Labsystems software.

Table 2.1. ELISA reagents used to detect murine cytokines.

Name	Dilution	Clone or catalogue #	Company
Recombinant murine IL-10	N/A	Cat.# 39-8181	eBioscience
IL-10 capture	1:500	Cat.# 88-7105	eBioscience
IL-10 detect, biotinylated	1:1000	Cat.# 88-7105	eBioscience
Recombinant murine IL-12p70	N/A	Cat.# 14-8121	eBioscience
IL-12 p35 capture	1:125	Clone C18.2	eBioscience
Recombinant murine IL-23	N/A	Cat.# 14-8231	eBioscience
IL-23 p19 capture	1:125	Clone G23.8	eBioscience
IL-12/IL-23 p40 detect, biotinylated	1:1000	Clone C17.8	eBioscience
Streptavidin-HRP	1:400	Cat.#DY998	R&D

Protein isolation

Cells were harvested with Versene and cell pellets were stored at -80°C until cell lysis. Pellets were then resuspended with macrophage lysis buffer (20 mM Tris pH 8, 300 mM NaCl, 1% v/v NP40, 10% v/v Glycerol; all by Sigma)

containing freshly added protease inhibitors (Complete protease inhibitor cocktail, Roche). Samples were incubated on ice for 30 min before cellular debris was removed by centrifugation for 15 min, at 16,000 x g at 4°C (Heraeus Biofuge Fresco). Lysates were transferred into new tubes and stored at -80ºC. To determine the protein concentration of whole cell lysates a BCA test (Fisher Scientific) was performed according to the manufacturer's instructions. Samples were measured in duplicate and absorbance was read at 540 nm by a spectrophotometric ELISA plate reader. Data were analysed using Ascent Labsystems software.

Western Blot

Proteins were resolved by size using SDS polyacrylamide gel electrophoresis (SDS-PAGE). 5-7 µg of total protein were mixed with an appropriate volume of 4X loading buffer (200 mM Tris pH6.8, 400 mM DTT, 8% w/v SDS (0.2 µ), 0.4% w/v Bromophenol Blue, 40% v/v Glycerol; all by Sigma) and heated to 95°C for 5 min. The resulting denatured and reduced proteins were separated at 160 V on a pre-cast NuPAGE® Novex 4-12% Bis-Tris gel (Life technologies) immersed in NuPAGE® MOPS SDS running buffer (Life technologies) for approximately 120 min until fully resolved. To estimate the weight of resolved proteins, a full-range rainbow molecular weight marker (GE Healthcare) was run in parallel.

Following SDS-PAGE, proteins were transferred onto a membrane to allow for protein detection using antibodies. PVDF membranes (GE Healthcare) were dehydrated in methanol for a few minutes before transfer. The gel containing the resolved proteins was placed on two pieces of filter paper soaked in transfer

buffer (25 mM Tris-base, 192 mM Glycine, 15% v/v Methanol; all by Sigma) followed by the membrane and two pieces of soaked filter paper. The assembly was placed in a transfer cassette in between two transfer buffer-soaked sponges and inserted into a precooled transfer tank filled with transfer buffer. A constant voltage of 72 V was applied for 2 h at 4°C.

After protein transfer membranes were blocked with 5% milk in PBS-T (PBS with 0.1% tween) on a shaker for 1 h at room temperature. Rabbit α-IRF5 antibody (1:1,000; ab21689, Abcam) or mouse α- beta-actin (1:10,000; A5441, Sigma) were diluted in PBS-T containing 2% BSA and incubated with the membranes overnight at 4°C with gentle agitation. The following day, the membranes were washed three times with PBS-T, rotating on a shaker for at least 10 minutes between each wash step. HRP-conjugated secondary antibodies (donkey α-rabbit, NA934, GE Healthcare or rabbit α-mouse, P0260, Dako) were diluted 1:5,000 in PBS-T with 5% milk and incubated with the membranes for at least 1h at room temperature on a shaker. Immuno-complexes were detected using the chemiluminescent substrate solution ECL (Fisher Scientific), visualised using X-ray film RX NIF sheets (FujiFilm) and developed using an AGFA Cruis-60 automatic film processor (AGFA-Gaevert).

2.1.3. Chromatin immunoprecipitation sequencing (ChIP-Seq)

ChIP-Seq experiments mentioned in this thesis were performed by Dr. David Saliba (Udalova group) and are described in detail in (Saliba et al. 2014) .

Briefly, $300x10^6$ GM-CSF-derived macrophages (IRF5 KO and WT) stimulated with LPS for 0 or 2 h were fixed for 10 min with 1% formaldehyde (Sigma), quenched with 125 mM Tris pH 7.5 (Sigma) and washed with ice-cold PBS.

Nuclear lysates were isolated as described previously (De Santa et al. 2007) and sonicated with a Bioruptor (Diagenode) to obtain chromatin fragment sizes that average 500bp. Lysates were immunoprecipitated with 10 µg of IRF5 antibody (rabbit, ab21689, Abcam) and ChIP was performed as described previously (Ghisletti et al. 2010). ChIPped DNA was quantified with the Quant-iT dsDNA High Sensitivity Assay Kit (Life technologies) and DNA yields ranged from 10 – 20 ng. The ChIP-Seq datasets were generated using 50bp paired end sequencing (Accession number: E-MTAB-2661). Peaks were detected using MACS2 algorithm at 20% FDR and full analysis of this data set has been published in (Saliba et al. 2014). IRF5 binding peaks after 2 h LPS (filtered over $IRF5^{-/-}$ dataset) were assigned to genomic regions using GREAT (McLean et al. 2010) with standard settings (basal plus extension). The identified gene regions were then subjected to GO (gene ontogeny) categories and PANTHER pathway analysis to identify functional categories or pathways that were enriched in the IRF5 dataset.

2.2. Murine *in vivo* experiments

The experimental animal procedures used in this work were approved by the Kennedy Institute of Rheumatology Ethics Committee and the UK Home Office. All mice were housed in individually ventilated cages at constant temperatures and were provided with food and water ad libitum.

The use of animals in the experiments described in this thesis was performed after careful thought and consideration of the three ‘R’s which aim to refine, reduce and replace the use of animals in scientific research. Alternatives to *in vivo* models were considered when planning experiments: *in vitro* studies were

performed extensively prior to the use of murine *in vivo* disease models (Chapter 3) but also following on from *in vivo* experiments (Chapter 5.2.10 IRF5 controls chemokine gene expression *in vitro*). Animals were thus only used when it was deemed necessary and justified, namely to elucidate complex mechanisms underlying inflammatory diseases (Chapter 4 and 5). We chose the AIA model (described in detail in 2.2.2 Models used in this study) which displays 100% penetrance and in which the contralateral joint of the same animal is used as a negative control for the arthritic joint. Therefore, a lower number of mice are used in AIA as compared to other arthritis models such as CIA or K/BxN serum transfer (see also 1.5.3 Mouse models of RA). During all *in vivo* experiments, mice were monitored and assessed regularly to ensure minimal distress and suffering occurred. Wherever possible and as much as cell numbers obtained allowed, multiple analyses were performed on samples derived from any one experiment. In addition, samples used in this thesis such as RNA extracted from knee joints were used by other members of the group maximising the amount of information obtained from each animal and thereby reducing the overall number of mice used in the department.

2.2.1. Mice used in this study

IRF5 deficient mice

IRF5$^{-/-}$ mice were bred on a C57Bl/6 background and their generation has been described previously (Takaoka et al. 2005). The mice develop normally and no overt difference was observed in haematopoietic cell populations. IRF5$^{-/-}$ mice do not express IRF5 protein due to a disruption of exon 2 which is the first coding exon in the *Irf5* gene. Mice deficient in IRF5 have been shown to be

resistant to septic shock and to produce a reduced amount of pro-inflammatory cytokines (Takaoka et al. 2005).

As a recent study identified a spontaneous mutation in some colonies of IRF5$^{-/-}$ mice, experimental animals were genotyped for a mutation in the *Dock2* gene (Purtha et al. 2012); all mice used in this study were determined to be free of this homozygous mutation. The IRF5-/- line was genotyped for the DOCK2 mutation as described previously (Yasuda et al. 2013). Briefly, DNA was obtained from ear clips using REDExtract-N-Amp (Sigma) and PCR was performed using the following primers which detect the DOCK2 mutation as a 305bp product (Figure 2.1): DOCK2In29.4F GAC CTT ATG AGG TGG AAC CAC AAC C; DOCK2InR22.3.1R GAT CCA AAG ATT CCC TAC AGC TCC AC. Genotyping for the IRF5 allele was performed using the following primers: IRF5 Common CAC GGT CTG CTC CTG TCT AA, IRF5 KO CCT CCC CTA CCC GGT AGA AT, IRF5 WT CTT GAA GAT GGT GTT GTC CC. A 650bp product identified the WT allele while the IRF5 knock-out allele was identified by a 550bp product. Heterozygous mice were identified by the presence of both products. The following PCR programme was used for IRF5 genotyping PCRs:

1. 95°C 3 min
2. 95°C 30 sec ┐
3. 56°C 30 sec ├ 35 cycles
4. 72°C 1 min ┘
5. 72°C 10 min
6. 4°C ∞

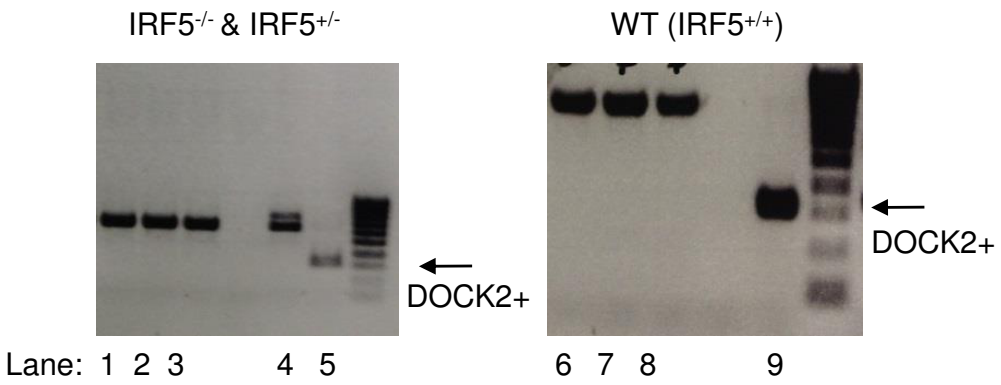

Figure 2.1. Genotyping of IRF5 deficient mice.

PCR reactions were performed to detect the IRF5 genotype and DOCK2 mutation status. Genomic DNA from IRF5$^{-/-}$ (Left panel, Lanes 1-3) and WT (Right panel, Lanes 6-8) did not result in a PCR product for the DOCK2 mutation (305bp; +ve controls Lanes 5 and 9). PCR products for IRF5 alleles were IRF5$^{-/-}$ 550 bp lanes 1-3; WT 650bp lanes 6-8; IRF5$^{+/-}$ both 650 and 550 bp lane 4).

IRF5 myeloid specific knockout

To generate a myeloid specific deletion of *Irf5*, we used the Cre-lox system. This technique uses Cre recombinase induced recombination of genes that contain its target *loxP* sites. Tissue or cell specific deletions can be achieved by creating genetically modified animals where Cre recombinase expression is driven by a promoter that is expressed only by certain subsets of cells or tissues. If these mice are crossed to a mouse strain containing *loxP* sites flanking the gene of interest, a cell or tissue specific knockout can be generated. In this study, we used *LysM*^{cre} mice (B6.129P2-*Lyz2*$^{tm1(cre)Ifo}$/J, Jackson laboratory stock number 004781) where the Cre recombinase is inserted into the *Lyz2* gene which shows restricted expression within the myeloid lineage including monocytes, macrophages and granulocytes (Clausen et al. 1999, Hume 2011). Cre insertion disrupts *Lyz2* expression but homozygous mice are normal in size and do not show any overt phenotypes. *LysM*^{cre} mice were crossed to *Irf5*$^{fl/fl}$ mice (C57BL/6-*Irf5*^{tm1Ppr}/J, Jackson

laboratory stock number 017311) containing *loxP* sites inserted into exon 2 of the *Irf5* gene. *Irf5*$^{fl/fl}$ mice are also phenotypically normal in steady state. *LysM*^{cre} *Irf5*$^{fl/fl}$ mice have been used recently to study the role of IRF5-expressing macrophages in obesity (Dalmas et al. 2015).

WT controls for those experiments were either *Irf5*$^{fl/fl}$ mice or obtained from crosses of mice that were heterozygous for the *LysM*^{cre} and *Irf5*^{flox} alleles, resulting from the breeding process of *LysM*^{cre} *Irf5*$^{fl/fl}$ mice. Progeny of those crosses that were negative for both alleles were kept to establish a matched WT control strain.

Genotyping was performed as described above for IRF5$^{-/-}$ using primer sets to detect both the *LysM*^{cre} and the *Irf5 loxP* alleles. For the *LysM*^{cre} allele the following primers were used: oIMR3066 mutant CCC AGA AAT GCC AGA TTA CG, oIMR3067 common CTT GGG CTG CCA GAA TTT CTC and oIMR3068 WT TTA CAG TCG GCC AGG CTG AC giving rise to two different products (Figure 2.2).

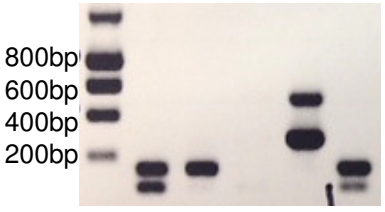

Figure 2.2. Genotyping of *LysM*^{cre} *Irf5*$^{fl/fl}$ mice.

PCR to detect the *LysM*^{cre} *Irf5*$^{fl/fl}$ alleles using genomic DNA derived from ear clips. PCR products for the WT alleles were 350bp for *LysM*^{cre} and 269bp for *Irf5 loxP* in lanes 1,2,4; mutant alleles were 700bp for *LysM*^{cre} and 449bp for *Irf5 loxP* in lane 3.

The WT allele is identified by a 350bp product while the Cre allele gives rise to a 700bp product; heterozygous mice display both PRC products. The *Irf5 loxP* allele was identified using the primers Lox5861F CGT GTA GCA CTC CAT GCT CT and Lox6309R AGG GCC TGT CCA GAA TTA GG. A 269bp product identified the WT allele and a 449bp product is found in *Irf5*$^{fl/fl}$ mice. The following PCR programme was used for genotyping PCRs:

1. 95°C 5 min
2. 95°C 45 sec
3. 56°C 45 sec
4. 72°C 45 min

(2–4: 35 cycles)

5. 72°C 5 min
6. 4°C ∞

CCR2 deficient mice

The full strain name of CCR2 deficient mice is B6.129S4-*Ccr2*^{tm1Ifc}/J (Jackson laboratory stock number 004999). Animals were kindly provided by Prof. Tonia Vincent. Under homeostatic conditions, the loss of CCR2 does not seem to have any effect as these mice are viable, fertile and of normal size. However, under inflammatory conditions Ly6C^{+} monocytes that lack CCR2 cannot exit the BM, which abolishes monocyte trafficking to the sites of inflammation (Boring et al. 1997). This can subsequently have a plethora of effects on the overall immune response. These mice have also been widely used to assess the contribution of circulating monocytes to tissue-resident macrophage populations (Guilliams et al. 2013, Hashimoto et al. 2013, Bain et al. 2014).

CX_3CR1 GFP mice

The CX_3CR1 GFP mouse strain (B6.129P-*Cx3cr1*^{tm1Litt}/J, Jackson laboratory stock number 008451) was crossed to the B6 IRF5 WT strain to generate GFP heterozygous mice. $CX_3CR1^{GFP/GFP}$ mice were kindly provided by Prof. Fiona Powrie. In the steady state, homozygous mice do not display any abnormalities. As the *Cx3cr1* locus is disrupted in GFP/GFP homozygous mice, they are CX_3CR1 deficient. To monitor CX_3CR1-expressing cells without complete loss of the receptor, heterozygous mice retaining an intact allele were used (Jung et al. 2000). These mice were used to analyse CX_3CR1 expression, which could be detected in peripheral monocytes, microglia, a subset of DCs and NK cells. Importantly, due to the extended half-life of more than 24h of GFP, GFP^+ cells do not necessarily still express CX_3CR1 at the moment of analysis (Jung et al. 2000).

2.2.2. Models used in this study

Antigen-induced arthritis

We induced arthritis as described previously (Egan et al. 2008, Asquith et al. 2009). To immunise mice with 100 µg mBSA (Sigma) the following mixture was prepared on ice: 400 µl CFA (BD Difco), 380 µl PBS (Gibco), 20 µl mBSA at a concentration of 40 mg/ml in dH_20. A 1 ml syringe (BD) was used to create an emulsion by mixing the components at least 100 times until the colour of the liquid changed to white and its consistency became more viscous. Initially, mice were sedated using inhaled isofluorane anaesthesia and subsequently immunised with 100 µg of mBSA (Sigma) (Figure 2.3). The antigen in adjuvant

was administered subcutaneously at the base of the tail in two sites with a volume of 50 µl per injection using a 27G needle (BD) and 1 ml syringe.

Seven days post immunisation, animals were sedated using Hypnorm (Vetapharma, diluted 1:10 in dH_20) using 150 µl per mouse injected intra-peritoneal with a 27G needle. The knee joint regions of mice were shaved to allow for precise intra-articular injection. To induce arthritis we performed an intra-articular injection of mBSA (200 µg in 10 µl of sterile PBS) or the same volume of PBS alone using a sterile 33-gauge micro-cannula.

Knee thickness was assessed daily using callipers measuring both mBSA and PBS knees. At day two or seven following intra-articular injection, mice were sacrificed and the knee joints were excised. Spleen, blood and inguinal LNs were harvested occasionally in addition to knee joints. For precise tissue harvest protocols refer to 2.2.3 Tissue preparation.

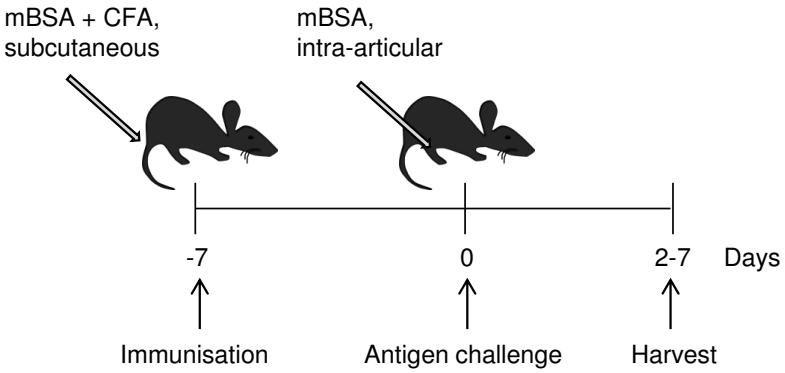

Figure 2.3. Schematic representation of the experimental set up for AIA.

IRF5$^{-/-}$ and WT mice were immunised subcutaneously at the base of the tail with mBSA in complete Freud's adjuvant. Seven days later, mBSA antigen or PBS as a control was injected directly into the knee joints. Disease severity was assessed by measuring swelling of the knees with callipers daily until mice were sacrificed. Knees were collected at day two or seven after antigen challenge.

Acute lung injury

Following short anaesthesia with isofluorane, mice were administered LPS (1 mg/ml; Alexis Biochemicals) at a dose of 1 mg/kg body weight intranasally (i.n.) (Figure 2.4). First, the weight of mice was assessed to determine the appropriate amount of LPS. LPS solution was pipetted onto the nostrils of mice shortly before they were coming out from anaesthesia and thus using their breathing reflex to deliver LPS i.n. Mice were sacrificed 24 h after the challenge, bronchoalveolar lavage was performed and lavage fluid was collected. Subsequently, the whole lung was harvested and both were processed for further analyses. Processing techniques are described in detail in 2.2.3 Tissue preparation.

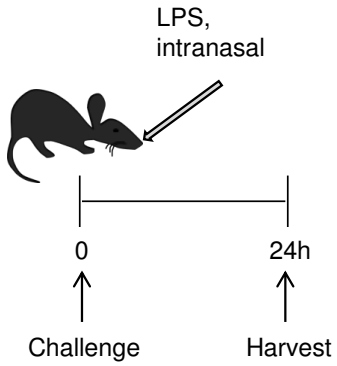

Figure 2.4. Schematic of the experimental set up for the acute lung injury model.

Mice are dosed with LPS at 1 mg/kg body weight and sacrificed 24 h post challenge. Bronchoalveolar lavage fluid (BAL) was collected and analysed for its cellular content and chemokine concentration.

Air pouch

Mice were anaesthetised with inhaled isofluorane and 3 ml of air were injected subcutaneously to create a dorsal air pouch using a 27G needle and a 5 ml syringe (Figure 2.5). Three days later a top-up of 3 ml of air was delivered to

isofluorane sedated animals. Six days after creation of the air pouch, mice were challenged with 100 µg zymosan (Sigma) in 500 µl PBS injected directly into the air pouch. Animals were sacrificed 4 h later and infiltrating cells were harvested from the air pouch.

Air pouch models performed to obtain neutrophils for migration assays (2.2.5 *Ex vivo* analyses, Neutrophil migration) were conducted by Dr. Adam Byrne (Udalova group).

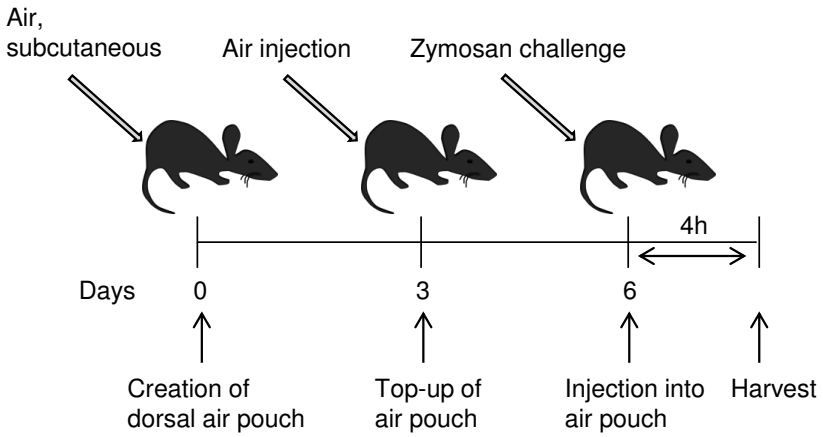

Figure 2.5. Schematic of the experimental procedures for the air pouch model.

Dorsal air pouches were created by subcutaneous injection of air in IRF5$^{-/-}$ and WT mice. Three days later, air pouches were topped up with air. Six days after air pouch creation, mice were challenged with zymosan which was injected directly into the air pouch. 4 h after challenge mice were sacrificed and air pouch infiltrate was collected for further experiments.

2.2.3. Tissue preparation

Blood

Mice were sacrificed by CO_2 inhalation and cardiac puncture was performed immediately before blood started to clot. For cardiac puncture, mice were placed on the back and the chest area was sprayed with 70% ethanol. A 27G needle with a 1 ml syringe was inserted just below the sternum and kept in

parallel to the rib cage. Once the needle entered the heart, a vacuum was created by pulling the plunger leading to blood retrieval. To improve blood recovery, the needle could be moved back and forth slightly or the syringe could be moved around its own axis carefully without letting go of the plunger. Prior to transferring 300 µl blood to a 1.5 ml tube containing 10 µl heparin (1 U/µl; Sigma), the needle was removed from the syringe to avoid clotting.

The remaining blood was collected in a separate 1.5 ml tube for serum collection. Tubes were kept at 4°C in the fridge overnight and centrifuged at maximum speed for 15 min the following day. Serum was transferred in a fresh tube and stored at -80°C until further analysis.

Blood treated with heparin was used for further analysis of blood cells. Weight of the blood tubes was recorded to determine the exact volume collected which was used to calculate the number of cells per ml blood after FACS (Fluorescence-activated cell sorting) analysis. Erythrocytes were removed from the blood cell suspension by red blood cell lysis. Therefore, 1 ml of red blood cell lysis buffer (Sigma) was added for 10 min at room temperature. After incubation cells were centrifuged for 5 min at 615 x g at room temperature. Supernatant was removed and the pellet was once again resuspended in red blood cell lysis buffer to remove all the erythrocytes. Following another centrifugation step the remaining cell pellet was resuspended in 400 µl of complete medium (RPMI-1640 medium with L-glutamine supplemented with 10% FBS, 1% P/S). Cells were diluted 1:10 in Trypan blue solution (Sigma) for live cell counting with a haemocytometer.

Knee and ankle joints

Control and mBSA injected knee joints were excised by first carefully removing the surrounding skin and muscles and then cutting the adjacent femur and tibia as close to the actual joint as possible to reduce BM contamination. The joint was transferred to 1 ml of RPMI medium with L-glutamine without supplements in a 24 well tissue culture plate. To obtain the ankle joint, the tibia was cut just above the ankle. The skin of the paw was then removed and the tips of the toes were cut off before transferring the joint to 1 ml of RPMI medium with L-glutamine without supplements.

Tissue digest and cell liberation was achieved by adding 25 µl of Liberase TL (12.5 mg/ml in sterile H_20; Roche) and 10 µl of DNase I (100 mg/ml in PBS, Roche) to the medium followed by a 90 min incubation at 37°C in a tissue culture incubator. Digested tissues were pushed through a 70 µm cell strainer (Falcon) using the plunger of a 2 ml syringe. The resulting cell suspension was centrifuged at 515 x g for 5 min at 4°C and then resuspended in 1 ml complete medium. Live cell counting was performed as described above using Trypan blue and a haemocytometer.

Bronchoalveolar lavage fluid

Bronchoalveolar lavage fluid (BAL) was collected by lavaging the lung after the animal has been sacrificed. For this, the trachea was exposed carefully without damaging surrounding vessels first by blunt dissection of the surrounding tissue. Scissors were only opened along the trachea rather than across to avoid any damage. Before cannulation, the tracheal membrane was removed by blunt dissection. To hold the cannula in place, a surgical thread was positioned

around the trachea and tied in a loose knot. Finally, the trachea was held with a pair of forceps as anterior as possible and a small incision was made, again as anterior as possible. Without letting go of the incised trachea, a cannula was now introduced into the trachea and fixed by tightening the surgical thread before letting go of the forceps. Lavage was then performed by injecting 0.4 ml of PBS with a 1 ml syringe connected to the cannula. Lavaged liquid was immediately recovered in the same syringe and collected in 1.5 ml tube. This procedure was performed three times in total and all the lavage fluid from one mouse was pooled. BAL was centrifuged at 222 x g for 5 min at 4°C and the resulting supernatants were stored at -80°C for further analysis. If necessary, red blood cell lysis was performed on the remaining pellet for 2 min using red blood cell lysis buffer as described in the section 'Blood' earlier. Cells were then resuspended in 100-200 µl of complete medium and counted with Trypan blue as previously described.

Lungs

Whole lungs were collected from the chest cavity of sacrificed mice. The chest cavity was exposed by first cutting along the midline of the rib cage and removing the surrounding skin. Second, the muscle below the rib cage was cut open to access the diaphragm. The lower end of the sternum was cut into to create a small opening of the cavity. Closed scissors were then carefully run along the diaphragm to ensure that lungs were not attached to it before cutting the diaphragm open completely. Next, the rib cage was opened up by cutting along the midline to expose the organs inside the cavity. Forceps were placed below the lungs and heart and then lifted and cut out with scissors. On a blue

towel, the individual lung lobes were dissected and the large left lobe was cut into small pieces on a petri dish and transferred to a 15 ml tube (Falcon) containing 1 ml of RPMI medium with L-glutamine. Tissue was digested in a total volume of 5 ml containing 40 µg/ml DNase I (Roche) and 20 µg/ml collagenase VIII (Sigma) in complete medium. For optimal cell liberation, tubes were shaken at 200 rpm for 45 min at 37°C throughout the digest period. Digested lung tissues were pushed through a 70 µm cell strainer with the plunger of a 1 ml syringe. The cell suspension was centrifuged at 515 x g for 5 min at 4°C and then resuspended in 1.5 ml complete medium. Cells were counted as described above using Trypan blue and a haemocytometer.

Lymph nodes

Inguinal LNs are located on the lower flank of the animal and were collected in 1 ml of RPMI medium with L-glutamine without supplements. LNs did not need to be digested and were immediately passed through a 70 µm cell strainer using the plunger of a 2 ml syringe. The resulting cell suspension was centrifuged at 515 x g for 5 min at 4°C and resuspended in 1 ml complete medium before cell counting. Cells were counted as described before using Trypan blue and a haemocytometer.

Spleen

Spleens were collected in 1 ml of RPMI medium with L-glutamine without further supplements. Tissue digestion was not needed and spleens were immediately passed through a 70 µm cell strainer with the plunger of a 2 ml syringe. The cell suspension was then centrifuged at 515 x g for 5 min at 4°C and resuspended

in 1 ml complete medium prior to cell counting using Trypan blue and a haemocytometer.

Air pouch infiltrate

To collect the cells infiltrating the air pouch in response to zymosan, 3 ml of PBS were injected directly into the pouch using a 27G needle and 5 ml syringe. To obtain the infiltrate, 3 ml of PBS were injected into the air pouch. The skin on top of the air pouch was carefully cut and the lining was exposed without piercing it. Skin around the incision was blunt dissected to further expose the air pouch. Whilst holding on to the edge of the skin, the air pouch was opened with a small cut. The infiltrate was then collected from the air pouch using a 5 ml syringe. The cell suspension was centrifuged at 515 x g for 5 min at 4°C and resuspended in 1 ml complete medium followed by cell counting.

2.2.4. Disease assessment and analysis

Histological methods

Histological slides were prepared by the Kennedy Institute's histology facility and all analyses were performed by Dr. Adam Byrne (Udalova group).

Arthritic knees were fixed in 10% buffered formalin. Knees were decalcified in 10% EDTA and dehydrated prior to embedding in paraffin wax. Coronal sections were stained with Haematoxylin and Eosin. Joints were scored in a blinded manner for degree of joint space infiltrate, bone erosion and synovial thickening. The inflammation score was based on joint space infiltrate.

For immunohistochemical analysis, paraffin-embedded sections were stained with APC conjugated Ly6G (clone 1A8, Biolegend) or isotype control and positive cells were viewed under fluorescence microscopy. Total cells/nuclei in the same section were stained with 4'-6-diamidino-2-phenylindole (DAPI, ProLong gold, Life Technologies).

Cytokine detection

BAL supernatants were collected after lavage fluid had been centrifuged to pellet the cellular contents, as described previously (2.2.3 Tissue preparation, Bronchoalveolar lavage fluid). Supernatants of knee cells were collected from cultures of liberated cells that were incubated for 3 h at 4°C. Secreted cytokines in those supernatants of knee cells and BAL were quantified using Luminex magnetic bead-based assay. All reagents and specific microplates were purchased as part of the mouse magnetic Luminex screening assay kit (R&D).
500 µl of microparticle cocktail were diluted with 5 ml assay diluent RD1W and vortexed prior to adding 50 µl per well to a 96 well microplate. Samples were diluted 1:2 with calibrator diluent RD6-52 and 50 µl per well were added to the microplate. Standard cocktails were reconstituted with calibrator diluent RD6-52 as per manufacturer's protocol to obtain a 1X solution. A six point standard was then prepared using three fold dilutions in calibrator diluent RD6-52. 50 µl of each standard were added per well. Samples and standards were measured in duplicates. The plate was sealed securely and incubated for 2 h, at RT on a shaker. The plate was then washed three times with 100 µl 1X wash buffer using a magnetic microplate holder (Life technologies) to retain magnetic beads within the plate. 500 µl biotin antibody cocktail were diluted in 5 ml assay diluent

RD1W. The diluted biotin antibody cocktail was added at 50 µl per well and incubated shaking for 1 h, at RT. Three wash steps were repeated as before and 50 µl of 1X streptavidin-PE were added per well. The plate was incubated for 30 min at RT on a shaker and then washed three more times. Finally, microparticles were resuspended in 100 µl wash buffer and incubated for 2 min. Measurements were performed using a Luminex 100 analyser (Luminex corporation) within 90 min of resuspension.

Levels of CXCL1 in supernatants of *LysM*^{cre} *Irf5*$^{fl/fl}$ knee cells were analysed using an ELISA kit (R&D, catalogue # DY453). ELISA was performed as described in 2.1.2. In this experiment, supernatants were collected after synovial cells were spun down following enzymatic digest (procedure described in 2.2.3, Knee and ankle joints). To account for variation in cells being liberated, the total amount of CXCL1 was normalised to total cell numbers.

Serum antibody levels

ELISAs to detect levels of antibodies in murine serum were performed by Dr. Adam Byrne (Udalova group). Serum was collected from mice at day two of AIA, as described in 2.2.3, Blood. Levels of IgG1 and IgG2a were determined by ELISA using the antibodies listed in Table 2.2.

Table 2.2. Antibodies used to detect IgG levels in serum.

Antigen	Dilution	Clone or catalogue #	Company
IgG1 capture	1:250	Clone A85-3	BD
IgG1 detect, biotinylated	1:250	Clone A85-1	BD
IgG2a capture	1:250	Clone R11-89	BD
IgG2a detect, biotinylated	1:250	Clone R19-15	BD

2.2.5. *Ex vivo* analyses

Neutrophil migration

TAXIScan was operated by Dr. James E. Pease (Imperial College London) and analysis was performed by Dr. Adam Byrne (Udalova group).

For real time analysis of migrating neutrophils, a 12-channel TAXIScan (Nitta et al. 2007) was employed and used with a 5µm chip according to the manufacturer's protocol (Effector Cell Institute). Sequential image data were generated from individual jpegs processed with ImageJ (National Institutes of Health), equipped with the manual tracking and chemotaxis tool plugins (Ibidi). Euclidean distances refer to the total Euclidean distance travelled by individual cells in a particular experiment.

Cell proliferation assay

Inguinal LNs were harvested from immunised mice (see 2.2.3 Tissue preparation, Lymph nodes). Cell suspensions were plated at 200,000 – 300,000 cells per well in a 96 well U bottom plate. Cells were stimulated with either α-CD3 (clone 145-2C11), mBSA antigen (50µg/ml) or media alone (naïve) for 48h at 37°C. To determine proliferation, replicating DNA was stained using the Click-iT® EdU kit according to the manufacturer's protocol (Life technologies). Briefly, 10 µM Edu was added 2 h prior to the end of stimulation. Extracellular staining and flow cytometry were performed as described below in 2.3.2 Flow cytometry**.**

2.3. Cellular analyses used *in vitro* and *in vivo*

2.3.1. Gene expression studies

RNA isolation

Total RNA was extracted from joints of mice or *in vitro* differentiated macrophages with the RNeasy Mini kit according to the manufacturer's instructions (Qiagen). Any contaminating genomic DNA was removed during this protocol using the RNase-Free DNase Set (Qiagen). RNA concentration was quantified using the NanoDrop™ 1000 (Thermo Scientific) and stored at -80°C.

cDNA synthesis

The High Capacity cDNA Reverse Transcription Kit (Life Technologies) was used to synthesise cDNA from total RNA. The total amounts of RNA used varied from 200 ng up to 1 µg, depending on the quantity isolated. The following reaction mix was prepared:

10 µl RNA

2 µl 10X RT buffer

0.8 µl 25X dNTP mix (100nM)

2 µl 10X RT random primers

4.2 µl RNase/DNase free H_2O (Ambion)

1 µl Reverse Transcriptase

20 µl total

RNA from at least one representative sample was added to a reaction mix lacking the reverse transcriptase enzyme as a 'no-RT' control for genomic DNA contamination. Reverse transcription was performed in a thermal cycler using the following conditions:

1. 25°C for 10 min
2. 37°C for 120 min
3. 85°C for 5 min
4. 4°C ∞

When cDNA synthesis was completed, samples were diluted 1:3 or 1:4 in RNase/DNase free H_2O prior to quantitative PCR (qPCR). Samples were stored at -20°C until needed.

Quantitative real-time PCR

To determine mRNA expression levels using qPCR, the following reaction was assembled and run in duplicate on a 384 well plate (Life technologies):

2.4 µl cDNA
3 µl Takyon Low ROX dTTP blue master mix (Eurogentec)
0.3 µl TaqMan probe (Life Technologies, see Table 2.3)
0.3 µl RNase/DNase free H_2O
7 µl total per well

Table 2.3. TaqMan probes used.

Gene	Catalogue #
Ccl3	Mm00441259_g1
Ccl4	Mm00443111_m1
Cxcl1	Mm04207460_m1
Cxcl2	Mm00436450_m1
Cxcl3	Mm01701838_m1
Cxcl5	Mm00436451_g1
Cxcl10	Mm00445235_m1
Fizz1	Mm00445109_m1
Hprt	Mm00446968_m1
Ifng	Mm00801778_m1
Il1b	Mm00434228_m1
Il6	Mm00446190_m1
Il10	Mm00439614_m1
Il12b	Mm00434174_m1
Il17a	Mm00439619_m1
Il23a	Mm00518984_m1
Irf5	Mm00496477_m1
Mrc1	Mm00485148_m1
Nos2	Mm00440502_m1
Socs1	Mm00782550_s1
Tnfa	Mm00443258_m1

The reactions were performed on a ViiA™7 system (Life technologies) according to the following cycling programme:

1. 95°C 3 min
2. 95°C 3 sec ┐ 45 cycles
3. 60°C 30 sec ┘

Levels of mRNA are quantified by measuring the accumulation of a fluorescent signal. The cycle threshold value (Ct) is the number of cycles required for the signal to cross the fluorescence threshold, as in exceeding the background level. The resulting data were analysed using the comparative Ct (or ΔΔCt)

method where the Ct values of the samples are compared to those of a control. Here, control samples used were either unstimulated *in vitro* differentiated cells or WT PBS knees. All Ct values are normalised to the endogenous housekeeping gene *Hprt*.

2.3.2. Flow cytometry

Pre-staining procedures

Single cells of murine tissues or *in vitro* generated cells obtained as described previously were resuspended in PBS in 96 well U-bottom plate. To distinguish between live and dead cells, a viability dye (LIVE/DEAD®, Life technologies) was used that can only penetrate dead cells lacking an intact cell membrane. Therefore cells were washed once with 150 µl PBS by centrifugation at 586 x g for 3 min at 4°C and then incubated for 15 min at 4°C with 10 µl of the diluted viability dye (1:1000). The dye was removed by washing twice with PBS, followed by one wash with FACS buffer consisting of 0.5% BSA (Sigma) and 0.01% NaN_3 sodium azide (10% stock, Sigma) in PBS, pH 7.4. To avoid nonspecific binding of antibodies to the Fcγ receptors FcγRIII/CD16 and FcγRII/CD32 on myeloid cells during staining, cells were incubated for 10 min at room temperature with 1:100 Fc-Block (clone 2.4G2, BD). Staining procedures varied depending on detection of extracellular or intracellular antigen and are described in detail below. Antibodies directly coupled to the following fluorophores were used: Allophycocyanin (APC), APC-Cy7, Alexa Fluor (AF) 700, Brilliant Violet (BV) 605, BV711, fluorescein isothiocyanate (FITC), Pacific Blue (PB), phycoerythrin (PE), PE-Cy7, PE-CF594, PerCP, PerCP-Cy5.5 and V500. Some antibodies were used conjugated to different fluorophores,

depending on the staining panel composition. Antibodies were purchased from BD, eBioscience or Biolegend.

Staining for surface markers

Surface marker expression was assessed to identify specific cell populations within heterogeneous cell suspensions. The following antibodies coupled to the indicated fluorophores were used: CD45 PerCP/ PerCP-Cy5.5 (clone 30-F11), CD11b APC-Cy7/FITC/V500 (clone M1/70), F4/80 BV711/FITC/PE-Cy7 (clone BM8), Ly6C PE/PE-Cy7 (clone AL-21), Ly6G APC (clone RB6-8C5), GR-1 PE-CF594 (clone 1A8-Ly6g), CD64 PE (clone X54-5/7.1), CD11c PB/BV605 (clone N418 or HL3), MHC II PE/AF700 (clone M5/114.15.2), CD206 APC (clone C068C2), CD19 APC (eBio1 D3), CD4 PE-Cy7 (clone RM4-5), γδ TCR PE (clone eBioGL3). All antibodies were diluted 1:200 in FACS buffer and samples were incubated for 1 h at 4°C in a staining volume of 10 µl. Following three washes using FACS buffer, cells were fixed with 50 µl Cytofix buffer (BD), overnight at 4°C. If no intracellular staining was performed, samples were processed the following day as described in the section ‘Sample acquisition and analysis’ below.

Cytokine and Foxp3 detection

To allow for staining of intracellular cytokines or Foxp3, cell suspensions were stimulated for 3 h prior to staining. The stimulation mixture contained PMA (Phorbol myristate acetage, 20 ng/ml, Merck), Ionomycin (1 µM, Merck) and Brefeldin A (12.5 µg/ml, Sigma) for T-cell stainings and LPS (100 ng/ml), Brefeldin A and Monensin (1:1000, BD GolgiStop) for myeloid cytokine panel.

Extracellular staining was performed as above but cells were fixed and permeabilised overnight using the fixation/permeabilisation buffer (Foxp3 staining set, eBioscience) instead. Cells were washed the next day with 1X permeabilisation buffer (Foxp3 staining set, eBioscience) followed by staining with pro-IL-1β PE (clone NJTEN3), IL-17a APC (clone eBio17B7), IFN-γ FITC (clone XMG1.2) or Foxp3 PB (clone FJK-16s) antibodies. Antibodies were diluted 1:200 in 1X permeabilisation buffer and samples were incubated for 1 h at 4°C in a staining volume of 10 µl. Samples were washed with 1X permeabilisation buffer two times and then prepared as in the section 'Sample acquisition and analysis' below.

Intracellular staining of IRF5 and CXCL1

To detect IRF5 or CXCL1, cell suspensions underwent a two-step staining protocol using primary and secondary antibodies as neither antibody is available directly conjugated to a fluorophore. Samples were thus stained with rabbit α-IRF5 antibody (1:200, ab21689, Abcam) or goat α-CXCL1 (1:20, AF-453-NA, R&D), diluted in 1X permeabilisation buffer and incubated for up to 1 h at 4°C. For CXCL1, a set of samples was stained as controls using goat IgG (1:20, AB-108-C, R&D). Primary antibody staining was followed by secondary staining with α-rabbit or α-goat Alexa Fluor 488 (Life Technologies), diluted 1:500 in 1X permeabilisation buffer and incubated for a maximum of 20 min at 4°C. IRF5 stained samples were washed five times using 1X permeabilisation buffer after primary and secondary antibody incubation to minimise background staining.

Sample acquisition and analysis

Finally, all samples were washed with FACS buffer once and resuspended in 150 µl FACS buffer. Cell suspensions were transferred to 5 ml FACS tubes (BD) for acquisition. Joint derived samples were transferred into specific FACS tubes with a cell strainer cap (BD) to allow filtering the cell suspensions through a 35 µm nylon mesh prior to measurement. Samples were acquired using a FACS Canto II or Fortessa X-20 (BD). The resulting data were analysed with Flow Jo software, version 7.6 (Treestar).

2.3.3. Mass cytometry

Mass cytometry is a recently established method similar to flow cytometry to analyse cells for the expression of intracellular and extracellular proteins (Figure 2.6). It also relies on antibodies to detect a specific antigen but these are conjugated to elemental isotopes instead of fluorophores. The advantages of metal labels compared to fluorophores are the greater number of available tags which can also be used in combination due to the lack of spectral overlap occurring in fluorescence (Bendall et al. 2012). The mass of these heavy metal ion tags is then determined using inductively coupled plasma mass spectrometry (ICP-MS). Briefly, cells are first nebulised to obtain single cell droplets, followed by ionisation in argon plasma allowing for detection of the ionised metal tags by time-of-flight mass spectrometry.

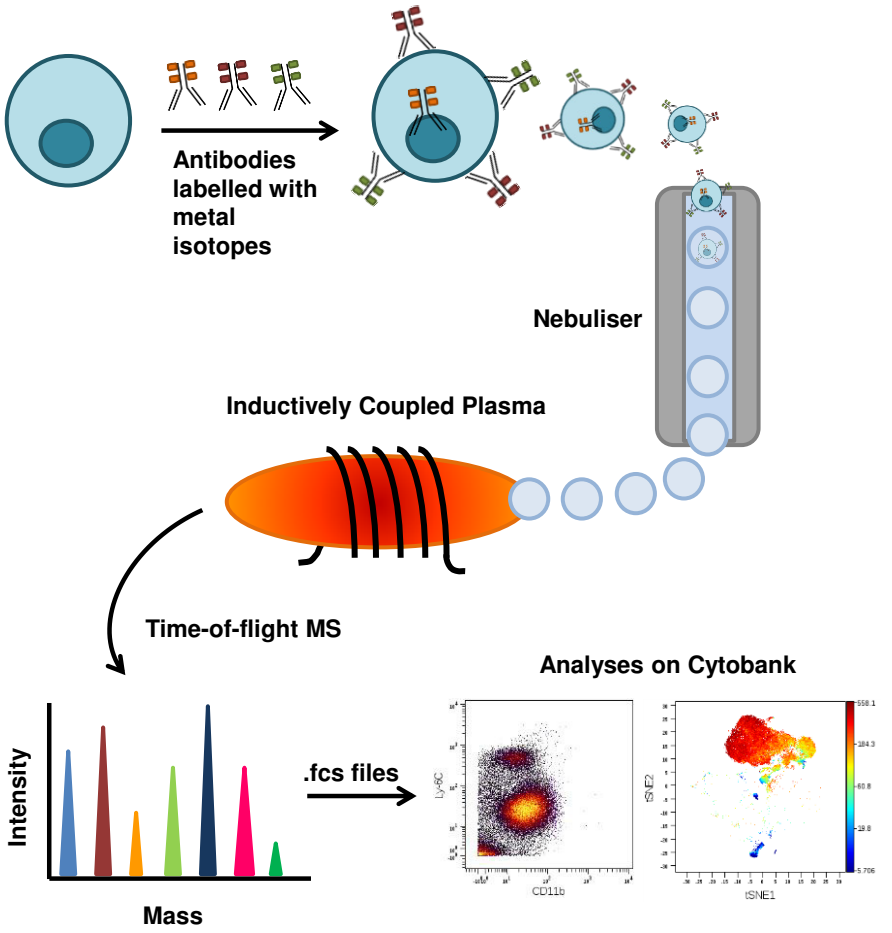

Figure 2.6. Schematic of mass cytometry work flow.

Mass cytometry is a technique based on inductively coupled plasma mass spectrometry coupled with phenotypical analysis of individual cells. Staining of cells is performed with antibodies labelled with heavy metal isotopes and both intracellular and extracellular antigens can be detected. Stained cell suspensions are passed through a nebuliser into argon plasma to ionise the metal tags. Mass of those tags is then analysed using time-of-flight MS where mass and intensity of the isotopes is determined for each cell. Data is converted into .fcs files which are uploaded into Cytobank. Data sets can then be analysed using conventional two dimensional dot plots (example picture on the left) or multidimensional analyses such as viSNE (right hand site).

Sample preparation

For analysis of BM and *in vitro* differentiated cells, cells were isolated and cultured as before (see 2.1.1 Generation of bone marrow-derived cells). Whole BM and unstimulated BMDMs were prepared for CyTOF as detailed in the next section.

Cells from mBSA knees were liberated as described previously (see 2.2.3 Tissue preparation) and prepared for storage at -80°C until later analysis. To adequately store cell suspensions, they were first centrifuged for 5 min at 1,320 x g and then resuspended in $10x10^6$ cells per 500 µl of complete medium. 500 µl of freezing medium (50% RPMI w/ L-glutamine, 30% FBS, 20% DMSO, 160ug/ml Ascorbic Acid) were added per 500 µl of cell suspension to obtain a 1:1 ratio. 1 ml of this mixture was used per cryovial (Greiner Bio-One) and frozen down slowly in a freezing container (Nalgene). The freezing container was kept at room temperature and immediately transferred to -80°C after addition of cells in cryovials. Samples were stored at -80°C until used for CyTOF analysis. At the day of staining, cells were thawed quickly at 37°C and added slowly drop by drop to pre-warmed complete medium. Cells were allowed to rest at 37°C for 20-30 min before counting. $2.5x10^6$ cells in 1 ml were added to a 24 well plate and stimulated for 3 h at 37°C to allow for T-cell cytokine staining as for FACS (refer to 2.3.2 Flow cytometry**,** Cytokine and Foxp3 detection).

Extracellular staining

All staining reagents purchased from Fluidigm were prepared specifically to minimise heavy metal contamination that could interfere with mass spectrometry analysis.

A total of $3\text{-}5x10^6$ cells resuspended in any volume in complete medium in 15 ml Falcon tubes were spun down for 3 min, 515 x g at RT or 4°C. Cells were washed once with cell staining buffer (CSB, Fluidigm) before resuspension in 1 ml CSB and transferred to 1.5 ml tubes. Samples were then centrifuged for 3

min at 615 x g and resuspended in 1 ml of 1X 103Rhodium nucleic acid intercalator (Fluidigm) in PBS (without BSA) and incubated for 15 min at RT. The intercalator cannot permeate live cell membranes and is thus used for discrimination of live and dead cells. Following incubation, cells were spun down and washed once with 1 ml of CSB. The pellet was then resuspended in 50 µl Fc block (1:10 in CSB) and incubated for 10 min at RT. Antibodies were diluted 1:100 and added in a volume of 50 µl for a total staining volume of 100 µl and incubated for 20 min at RT. Staining panels used can be found in Table 2.4. Following incubation with the antibody cocktail, cells were washed twice with 1 ml CSB. Whole BM and *in vitro* differentiated cell samples were not stained for intracellular antigens, so they then underwent the final intercalator and fixation step. Cells were resuspended in 1 ml Fix & Perm Buffer (Fluidigm) containing 1X 191/193Iridium intercalator (Fluidigm) and incubated at 4°C overnight. The second intercalator also binds to nucleic acids but since cells are permeabilised it will be able to enter all nuclei. This step ensures that live nucleated cells can be identified by the mass spectrometer while excluding antibodies bound to debris or each other. Dead cells will be identified by double positive staining for Rhodium and Iridium intercalators.

Table 2.4. Antibodies used for CyTOF staining.

BM and in vitro differentiated cells were stained for all extracellular markers. Inflamed knees were stained for the same markers, except TCRB. Additionally, knees were analysed for intracellular proteins which are in italic.

Antigen	Metal tag	Catalogue #	Clone	Expressed by
B220	176Yb	3176002B	RA3-6B2	B-cells
CD3	152Sm	3152004B	145-2C11	T-cells
CD4	172Yb	3172003B	RM4-5	T-cell subset
CD8	168Er	3168003B	53-6.7	T-cell subset
CD11b	148Nd	3148003B	M1/70	Myeloid cells
CD11c	142^{Nd}	3142003B	N418	DCs (Macrophages)
CD19	149Sm	3149002B	6D5	B-cells
CD25	151Eu	3151007B	3C7	Activated T-/B-cells & myeloid precursors
CD44	171Yb	3171003B	IM7	Myeloids & other cell types
CD45	147Sm	3147003B	30-F11	All haematopoietic cells
CD62L	160Gd	3160008B	MEL-14	Lymphocytes
CD69	145Nd	3145005B	H1.2F3	Activated T-/NK cells
F4/80	159Tb	3159009B	BM8	Macrophages/Eosinophils
GR1	141Pr	3141005B	RB6-8C5	Neutrophils
Ly6C	150Nd	3150010B	HK1.4	Monocytes
MHCII	174Yb	3174003B	M5/144	Antigen presenting cells
NKp46	153Eu	3153006B	29A1.4	NK cells
TCRB	169Tm	3169002B	H57-597	T-cells
Foxp3	158Gd	3158003A	FJK-16s	Regulatory T-cells
IL-17	169Tm	3169005B	TC11-18H10.1	Produced by T-cells
IFN-γ	165Ho	3165003B	XMG1.2	Produced by T-/NK cells

Intracellular staining

After extracellular staining and two washes as described above, cells derived from knee joints were resuspended in 1 ml Fix & Perm Buffer and incubated for 20 min at RT. This was followed by two washes using 1X permeabilisation buffer (Foxp3 staining set, eBioscience; diluted in Maxpar water, Fluidigm). Antibodies detecting intracellular proteins were used 1:100 in 1X permeabilisation buffer in 100 µl and incubated for 30 min at RT. Next, samples were washed once with 1X permeabilisation buffer followed by one wash with

CSB. Pellets were resuspended in 1 ml Fix & Perm Buffer containing 1X 191/193Iridium intercalator and incubated at 4°C overnight.

Mass spectrometry and analysis

Samples were centrifuged at 2,460 x g for 3 min and washed once with CSB before cells were counted using a light microscope and a cell counting chamber. Just before samples were acquired using a CyTOF mass cytometer (DVS Sciences), they were spun at 2,460 x g for 3 min and resuspended in ultrapure MiliQ water. The concentration was adjusted to 300,000 cells per 500 µl and the cell suspension was passed through a filter FACS tube. Cell suspensions were acquired by the mass cytometer by slowly pushing the plunger of a 1 ml syringe connected to the instrument. Firstly, cells were nebulised to generate single cell droplets which then enter the ICP where metal tags are ionised (Figure 2.6). Mass of the elements is determined by analysing the time-of-flight with a mass spectrometer. The resulting data were transferred onto the Cytobank platform (http://www.cytobank.org/) and analysed using Cytobank's viSNE tool (Amir el et al. 2013). This method analyses multi-dimensional data and plots cells on a two dimensional space. viSNE visualisation is based on the t-Distributed Stochastic Neighbour Embedding (t-SNE) algorithm resulting in a biaxial plot that uses t-SNE dimensions to provide a representation of the single-cell data. The closer cells are together on this two dimensional plot, the more similar they are in high-dimensional space. Colour is utilised as a third dimension to visualise additional features of cells, in this thesis colour indicates intensity of surface marker expression.

2.4. Statistical analyses

Statistical analysis was carried out using GraphPad v6.0 (GraphPad Software) using two-way ANOVA with Bonferroni's correction (multiple comparisons) or Mann-Whitney tests (comparisons between two groups).

3. Analysis of IRF5 expression *in vitro*

3.1. Introduction

Macrophages are immune cells involved in recognition of pathogenic stimuli and the initiation and resolution of inflammation. They can adapt to various different environmental signals giving rise to several subtypes with distinct functions (Mosser and Edwards 2008). Previously, these subtypes have been classified as M1 (classically activated) and M2 (alternatively activated) macrophages, mainly based on *in vitro* experiments. In addition, several phenotypes were described to be associated with M2 macrophages, for example M2-like or tumour associated macrophages (Biswas and Mantovani 2010). *In vitro*, pro-inflammatory M1 macrophages secrete high levels of IL-12 and IL-23 but low levels of IL-10, whereas anti-inflammatory M2 macrophages secrete low levels of IL-12 and IL-23 but high levels of IL-10 (Gordon 2003). However, the concept of M1/M2 macrophages has lately been challenged as oversimplified to fully represent the spectrum of macrophage phenotypes observed in response to a variety of stimuli (Xue et al. 2014). This concept has been further challenged by the discovery of true tissue-resident macrophages that do not rely on monocyte input, which also highlights macrophage diversity in tissues *in vivo* (Ginhoux et al. 2010, Hashimoto et al. 2013, Yona et al. 2013). Tissue-resident macrophages are derived embryonically from the yolk sac and can undergo local self-renewal. Various tissues are characterised by different ratios of tissue-resident to recruited macrophages (Sieweke and Allen 2013). Overall, there have been fundamental changes in recent years regarding our knowledge and understanding of macrophage identity and subtypes (Gautier and Yvan-Charvet 2014, Ginhoux and Jung 2014).

Nevertheless, *in vitro* differentiated macrophages can be a useful tool to analyse molecular processes and signalling pathways. Several reports have described protocols for generating *in vitro* differentiated macrophages which recently have been aimed to be standardised by the macrophage community (Murray et al. 2014). PBMCs (peripheral blood mononuclear cells) are most commonly used as macrophage progenitors in human studies, while murine experiments usually rely on the use of BM due to a higher yield of progenitors. In general, many methods utilise M-CSF to differentiate progenitors, followed by priming with various stimuli. Addition of IFN-γ followed by LPS stimulation has been used to acquire classically activated macrophages whereas addition of IL-4 or IL-13 without LPS yields alternatively activated macrophages (Gordon 2003). Another method used GM-CSF in order to generate pro-inflammatory (M1) macrophages or alternatively M-CSF treatment for anti-inflammatory (M2) differentiation, usually followed by LPS challenge for both subtypes (Verreck et al. 2004, Fleetwood et al. 2007). The current standardised nomenclature however avoids calling GM-CSF-derived cells M1 macrophages (Murray et al. 2014). GM-CSF differentiation is also used by some groups to generate DCs *in vitro* (Inaba et al. 1992, Sallusto and Lanzavecchia 1994, Caux et al. 1996). Helft et al. recently examined these GM-CSF-derived cultures in detail and revealed heterogeneity of those cells (Helft et al. 2015). In this study, two distinct populations were identified as macrophages and DCs although no real corresponding counterparts *in vivo* could be determined. Under physiological conditions, M-CSF is detected in low steady state levels whereas GM-CSF has been shown to be increased upon stimulation with inflammatory stimuli, such as IL-1, TNF-α or LPS (Verreck et al. 2006, Hamilton 2008).

Distinct macrophage subsets are not only characterised by differences in the inflammatory response but more importantly display differential expression of key TFs shaping the enhancer landscape, both *in vitro* and *in vivo* (Lawrence and Natoli 2011, Gosselin et al. 2014, Lavin et al. 2014). As described earlier, we identified the transcription factor IRF5 as the major regulator of the pro-inflammatory macrophage phenotype (Krausgruber et al. 2011). Both GM-CSF and IFN-γ treated macrophages displayed increased IRF5 expression (Krausgruber et al. 2011). IRF5 directly induces the expression of pro-inflammatory cytokines such as IL-6, IL-12 and IL-23 whilst repressing transcription of anti-inflammatory cytokines such as IL-10 (Takaoka et al. 2005, Krausgruber et al. 2011). Furthermore, IRF5 is involved in various inflammatory processes such as the Type I IFN response to virus infection and pathogen recognition receptor signalling downstream of TLR4, 7 and 9 (Honda and Taniguchi 2006). Upon viral infection, IRF5 is phosphorylated and thereby translocated to the nucleus where it binds to the regulatory regions of its target genes (Barnes et al. 2001). While post-translational activation of IRF5 has been studied to some extent (Ryzhakov et al. 2015), much less is known about the transcriptional regulation of *Irf5*.

We analysed various murine *in vitro* differentiated macrophage subtypes regarding their IRF5 expression, LPS response and surface receptor expression to extend the previously conducted studies in human *in vitro* differentiated macrophages. Moreover, we aimed to investigate which of the stimuli applied could induce IRF5 transcriptionally as the specific regulation of the *Irf5* gene remains to be elucidated.

3.2. Results

3.2.1. IRF5 expression is induced during *in vitro* differentiation by GM-CSF

In order to assess the levels of IRF5 during differentiation *in vitro*, BM progenitors were treated with either GM-CSF or M-CSF for a total of nine days (Figure 3.1A). Samples were taken at day zero from whole BM and from BMDM cultures at days three, six and nine of differentiation. Protein expression of IRF5 in those samples was analysed using western blot and flow cytometry.

Western blot of whole cell lysates revealed that GM-CSF strongly induced IRF5 protein levels in BM progenitors during differentiation, reaching the highest level of expression at day six (Figure 3.1B). Although IRF5 levels were decreased at the final day of differentiation compared to day six, they were still increased compared to day zero. M-CSF treated cultures on the other hand, only showed a slight increase at day three compared to whole BM levels but expression was reduced at the later time points. Similarly to GM-BMDMs however, IRF5 expression in M-BMDMs on day nine was still higher than at the start of differentiation. Comparing the effect of the two cytokines, it can be observed that GM-CSF was able to induce much higher levels of IRF5 than M-CSF throughout the process of differentiation.

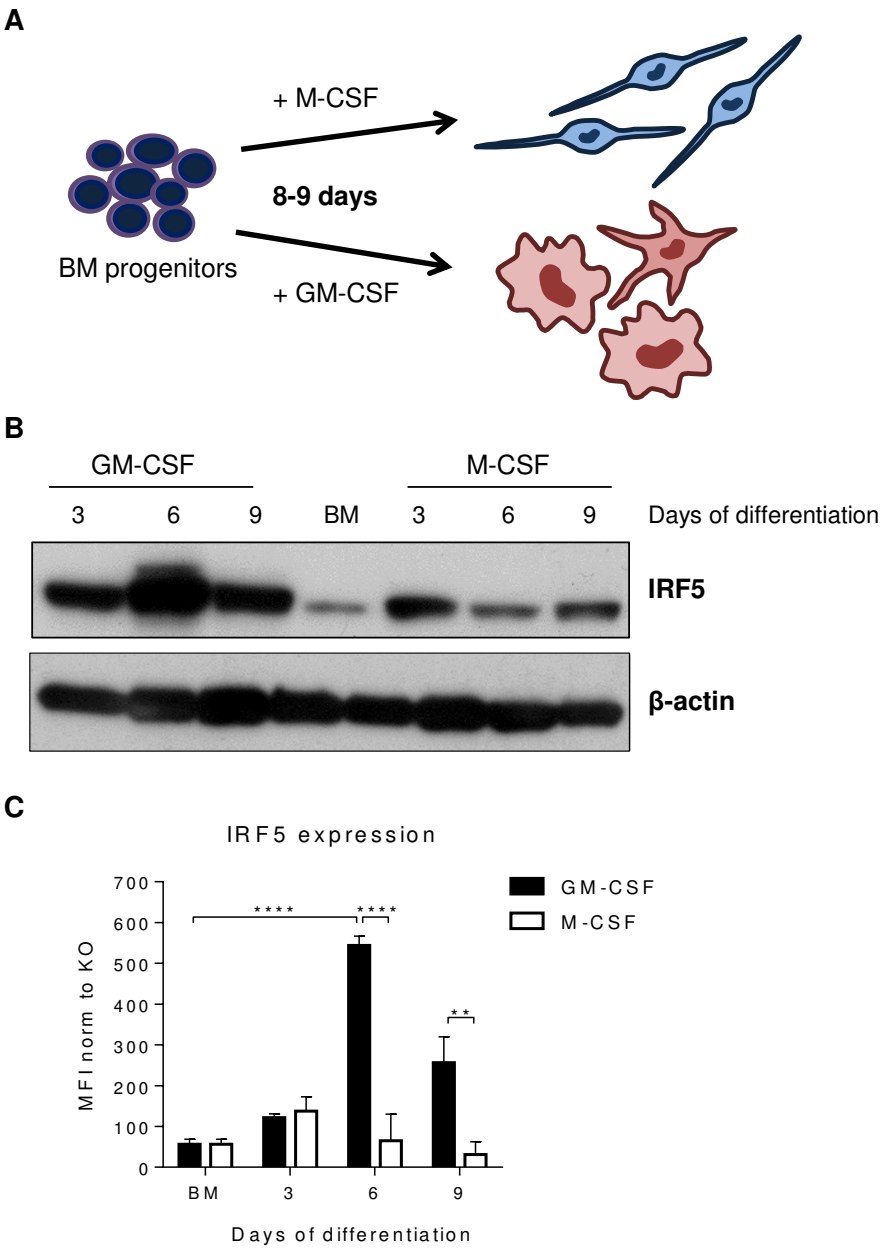

Figure 3.1. IRF5 is induced during differentiation in GM-CSF BM-derived macrophages.

BM derived progenitors were differentiated *in vitro* with GM-CSF or M-CSF for nine days. Protein and FACS samples were collected from BM at day three, six and nine of differentiation. **A.** Schematic representation of the *in vitro* differentiation protocol using GM-CSF (20ng/ml) or M-CSF (100ng/ml). **B.** Protein levels of IRF5 and β-actin were determined by western blot analysis. Experiment is representative of n=3. **C.** Cells were stained for intracellular IRF5 and staining was quantified by mean fluorescence intensity (MFI). MFI was normalised by subtracting MFI values of IRF5 knock-out cells from WT MFI values. Error bars represent the standard error of the mean (SEM) for n=3. Statistical analysis was performed by 2-way ANOVA and Bonferroni's multiple comparison. ** p≤0.01; **** p≤0.0001

The overall pattern of expression is mirrored when flow cytometric analysis was used to quantify intracellular IRF5 staining by MFI (Mean fluorescence intensity, Figure 3.1C). GM-CSF induced IRF5 expression peaked at day six (544±22.8) of differentiation. This increase was significant compared to levels in BM (56.3±12.4) on both day six and nine (256.3±63.4; $p \leq 0.05$ but not shown in Figure 3.1C). M-CSF treated cell cultures however did not show any significant increase of IRF5 levels over the period of differentiation though the highest MFI value was reached on day three (137.3±35.1). Moreover, GM-BMDMs express significantly more IRF5 than M-BMDMs from day six onwards. GM-CSF can thus induce IRF5 expression to a greater extent than M-CSF during differentiation of BMDMs *in vitro*.

3.2.2. GM-CSF and M-CSF induce progenitor differentiation into different myeloid cell types

Ly6G$^+$ and Ly6C$^+$ populations are lost in the process of differentiation

In order to characterise how the cellular composition changed over time, cell cultures were examined using FACS on day zero, three, six and nine of differentiation. Cells were stained for expression of several surface markers. CD11b was used to identify myeloid cells and the graphs shown display CD11b$^+$ gated populations (Figure 3.2). In whole BM less than half of the cells were CD11b$^+$ but this steadily increased throughout differentiation with both GM-CSF and M-CSF. On day three, 60-70% of all cells were CD11b$^+$ and from day six onwards the vast majority (80-95%) of cells expressed CD11b (Figure 3.2A).

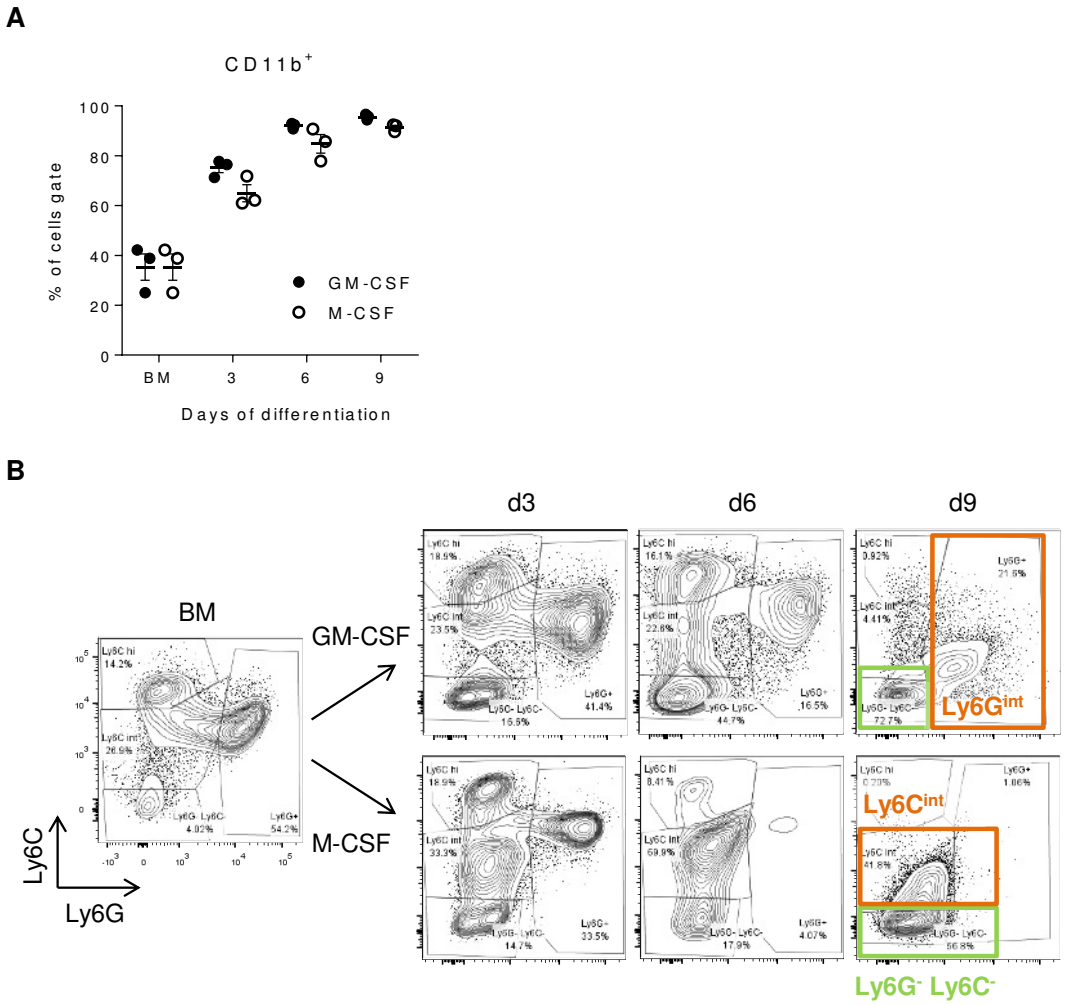

Figure 3.2. BM neutrophil and monocyte populations are not maintained during *in vitro* differentiation.

BM progenitor cells were isolated from WT mice and differentiated with GM-CSF or M-CSF for nine days. FACS samples were taken from whole BM and at day three, six and nine of differentiation. Cells were stained for the surface markers CD11b, Ly6G and Ly6C. CD11b is used as a marker for myeloid cells. Ly6G is expressed by neutrophils and progenitors in the BM while Ly6C is mostly expressed on monocytes and their progenitors. **A.** The amount of $CD11b^+$ myeloids shown as a percentage of size gated cells over time. **B.** The sub-populations highlighted in green ($Ly6G^-$ $Ly6C^-$) or orange (Ly6G intermediate or Ly6C intermediate) in day nine plots are further analysed in the following figure. The depicted populations were first gated by size and for CD11b expression. Plots are representative of n=3.

Ly6G and Ly6C were used to identify neutrophils and monocytes respectively, two major myeloid populations present in the BM (Figure 3.2B). Samples were analysed for Ly6G and Ly6C expression throughout the time course to assess persistence of those two populations. Flow cytometry confirmed that in

untreated BM, the largest myeloid populations consisted of $Ly6G^+$ neutrophils and $Ly6C^{int}$ / $Ly6C^+$ monocytes with only a minor $Ly6G^-$ $Ly6C^-$ population (Figure 3.2B). Although there was still a large population of $Ly6G^+$ neutrophils present in both cell cultures at day three, their numbers had decreased already compared to day zero. This reduction was even more apparent on day six, from which point onwards the neutrophil population was almost completely absent in M-CSF cultures. GM-CSF cultures showed a less drastic decrease on day three and a $Ly6G^{int}$ population appeared instead on day nine. $Ly6C^{int}$ / $Ly6C^+$ monocyte populations remained mostly unchanged in terms of numbers during the first six days when cells were differentiated with GM-CSF, while M-CSF cultures showed a considerable increase in $Ly6C^{int}$ cells. At the final day of differentiation, the majority of cells were $Ly6G^-$ $Ly6C^-$ in both conditions. However, while $Ly6G^-$ $Ly6C^-$ cells were the dominant population in GM-BMDMs next to the $Ly6G^{int}$ cells, in M-BMDMs almost half of the cells were $Ly6C^{int}$. Of note, it is likely that the $Ly6G^{int}$ population represents a technical artefact (as discussed below, section 3.3). Taken together, these data show that GM-CSF and M-CSF induced differentiation into $CD11b^+$ myeloid cell populations is concurrent with the loss of BM resident $Ly6G^+$ neutrophils and $Ly6C^+$ monocytes over time.

GM-CSF and M-CSF induce distinct cellular phenotypes

We then wanted to investigate the expression of cell surface markers on BM-derived cells in more detail, following differentiation at day nine. To determine whether cells could be characterised as macrophages or DCs, we used the expression markers F4/80, CD64, CD11c and MHC II. F4/80 and CD64 are

most commonly associated with macrophages, although they can also be expressed by eosinophils or DCs (as detailed in 1.2.1 Development of monocytes, macrophages and DCs, Nomenclature and identification). CD11c and MHC II have been widely used to identify DCs, yet these have also been found on some macrophage populations such as alveolar macrophages in the lung (see 1.2.1, Nomenclature and identification). We chose to analyse the major subsets present in each cell culture, the Ly6G^{-} Ly6C^{-} population (highlighted in green Figure 3.2B and left hand panel Figure 3.3) in both cultures and Ly6G^{int} cells in GM-BMDMs or Ly6C^{int} cells in M-BMDMs (highlighted in orange in Figure 3.2B and right hand panel Figure 3.3).

When generally comparing GM-CSF and M-CSF derived cells, the most striking differences were observed in terms of F4/80 and MHC II expression, independent of Ly6G/Ly6C subsets. Neither subset in GM-BMDMs expressed much F4/80 while M-CSF differentiation led to 79-92% double positive F4/80^{+} CD64^{+} cells (Ly6G^{-} Ly6C^{-} and Ly6C^{int} respectively) (Figure 3.3A). Even though F4/80 expression could not be detected on GM-BMDM subsets, a substantial proportion of both subsets were CD64^{+} (25-39%, Ly6G^{-} Ly6C^{-} and Ly6G^{int}). The fraction of CD11c-expressing cells within M-CSF-derived populations was comparable in the two subsets although not identical, ranging from around 55 to 65% (Figure 3.3B). In contrast, GM-CSF differentiated subsets were almost entirely CD11c^{+}. However, MHC II expression levels varied, with 65% and 32% of cells being MHC II^{hi} in Ly6G^{-} Ly6C^{-} and Ly6G^{int} subsets respectively. Of note, only a small proportion of GM-BMDMs were actually MHC II^{-}, as CD11c^{+} cells were either MHC II^{hi} or MHC II^{int}. On the other hand, only a minor fraction of M-BMDMs were MHC II^{+} in either subset. Overall, the Ly6G^{-} Ly6C^{-} and Ly6G/C^{int}

subsets showed a similar distribution pattern within GM-BMDMs or M-BMDMs respectively but displayed differences with respect to the exact proportions of each subset.

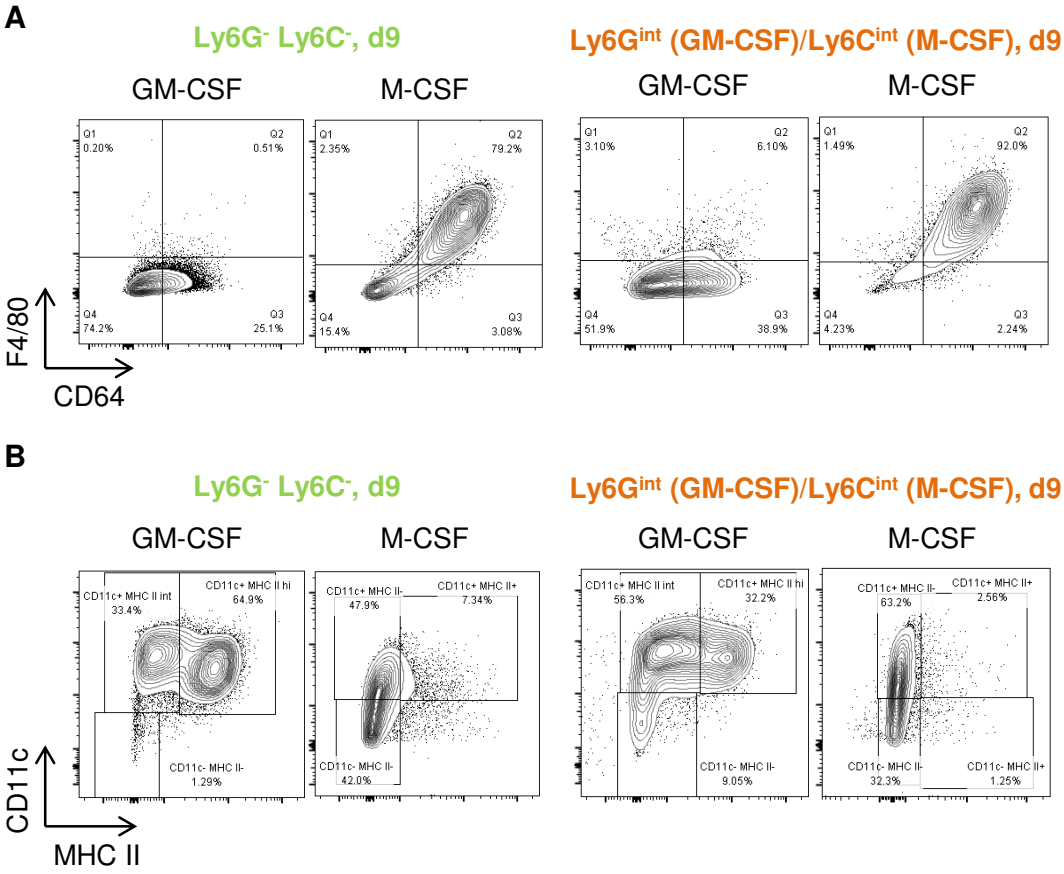

Figure 3.3. GM-CSF and M-CSF induce discrete subpopulations upon *in vitro* differentiation.

After differentiation with GM-CSF or M-CSF for nine days, FACS samples were taken and stained as described in the previous figure. Additionally, the expression of F4/80, CD64, CD11c and MHC II was analysed in the major sub-populations present at the final day of differentiation. F4/80 and CD64 are used as markers for a macrophage phenotype. CD11c and MHC II are commonly used to identify DCs although they can also be expressed on some macrophage populations. **A. and B.** As highlighted in the previous Figure 3.2, the most abundant populations are Ly6G^{-} Ly6C^{-} cells (in green, Figure 3.2A) and Ly6G^{int} in GM-BMDMs or Ly6C^{int} in M-BMDMs (in orange, Figure 3.2B). The phenotype of these populations was examined for macrophage and DC marker expression. Plots are representative of n=3.

As *in vitro* cell cultures were not FACS sorted prior to experiments in this study, we determined receptor expression on cells gated for size and thereby excluding debris. This population represents the cells that were ultimately used for *in vitro* experiments. In addition to the above mentioned markers CD64, F4/80, CD11c and MHC II, we also analysed expression levels of CD206 which is found on regulatory macrophages (see 1.2.1, Nomenclature and identification).

Cell surface receptors on the size gated population confirmed that macrophage associated markers F4/80, CD64 and also CD206 were found to a greater extent on M-BMDMs, while the DC related markers CD11c and MHC II were higher on GM-BMDMs (Figure 3.4A). Moreover, the two populations differentially expressing MHC II in GM-CSF cultures could be clearly distinguished. The graph displaying CD11b expression confirmed that most cells were $CD11b^+$ with no major differences between GM- and M-BMDMs. Intensity of surface receptor expression generally showed the same pattern as the contour plots and histograms: F4/80 and CD64 were detected in significantly higher amounts in M-BMDMs, whereas CD11c and MHC II levels were significantly greater in GM-BMDMs (Figure 3.4B). CD206 expression was markedly increased in M-CSF differentiated cells compared to GM-CSF treated cells. Overall, greater differences between GM-BMDMs and M-BMDMs were observed for the macrophage related markers F4/80 and CD64. Mean differences for those were 2360 and 3473 respectively compared to 1958 for CD11c and 1657 for MHC II.

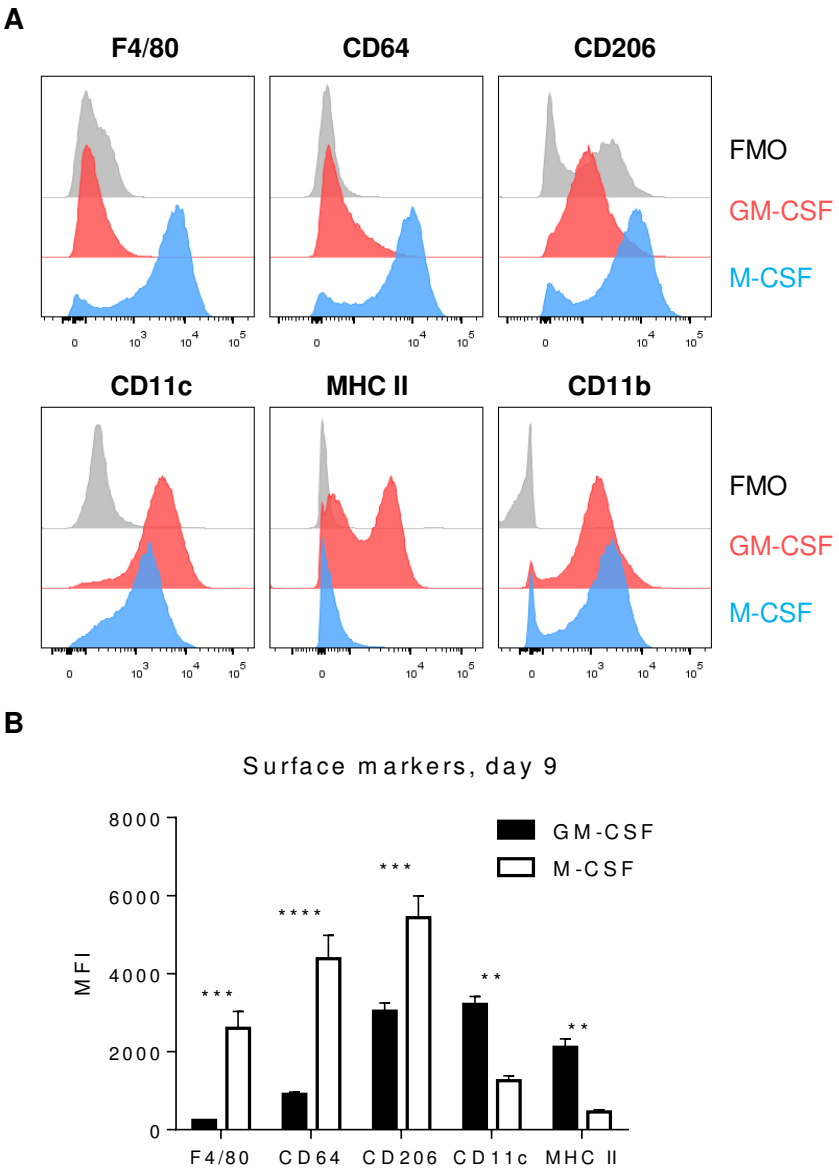

Figure 3.4. Surface markers are expressed differently in GM-CSF and M-CSF derived cells.

After differentiation with GM-CSF or M-CSF for nine days, FACS samples were collected and stained for the expression of CD11b, F4/80, CD64, CD206 and MHC II. F4/80 and CD64 are used as macrophage markers, while CD11c and MHC II are used to identify DCs. CD206 is associated with a regulatory macrophage phenotype. **A.** Histograms of surface markers are shown in the size gated cell population but without any further sub-gates. FMOs are depicted in grey, GM-CSF derived cells in red and M-CSF differentiated cells in blue. **B.** Surface marker expression was quantified by MFI. Error bars represent the SEM for n=3. Statistical analysis was performed by 2-way ANOVA and Bonferroni‘s multiple comparison. * p≤0.05; ** p≤0.01; *** p≤ 0.001; **** p≤0.0001

To conclude, GM-CSF and M-CSF induced different surface receptor expression patterns *in vitro.* M-CSF favoured a relatively homogenous F4/80^{+} CD64^{+} MHC II^{-} (CD11c$^{+/-}$) macrophage phenotype while GM-CSF led to a more heterogeneous F4/80^{-} CD11c^{+} MHC II$^{int/hi}$ (CD64$^{+/-}$) DC/macrophage phenotype.

MHC II^{hi} and MHC II^{int} cells in GM-CSF cultures express equal levels of IRF5

Helft et al. recently analysed two subsets of GM-CSF differentiated BM-derived cells in great detail (Helft et al. 2015). In this study, two major subsets were identified: CD11c^{+} CD11b^{hi} MHC II^{int} (CD115^{+} MerTK^{+}) and CD11c^{+} CD11b^{int} MHC II^{hi} (CD115^{-} CD135^{+}), and were extensively characterised in terms of gene expression and functional properties. The authors conclude that MHC II^{hi} cells show phenotypic similarities to DCs while MHC II^{int} cells possess macrophage properties.

We thus used our flow cytometry data to compare our results to the subsets analysed in this study and furthermore determine the IRF5 expression levels in the subsets. We could in principle identify two similar populations that were CD11c^{+} and either MHC II^{hi} or MHC II^{int} (Figure 3.5A), as described previously. We quantified surface marker expression in those subsets using MFI for F4/80, CD64, CD206 and CD11b (Figure 3.5B). CD64 was the only marker that showed a significant difference for MHC II^{hi} vs MHC II^{int} subpopulations. When IRF5 levels were determined in those cells, we found it to be equally expressed in both subsets (Figure 3.5C). Hence, both subpopulations of the GM-CSF-derived cells are suitable for the purpose of *in vitro* studies regarding the

regulation of *Irf5* gene expression (this chapter) and IRF5-dependent genes (Chapter 5), although both are likely to differ from primary cells (Chapter 4).

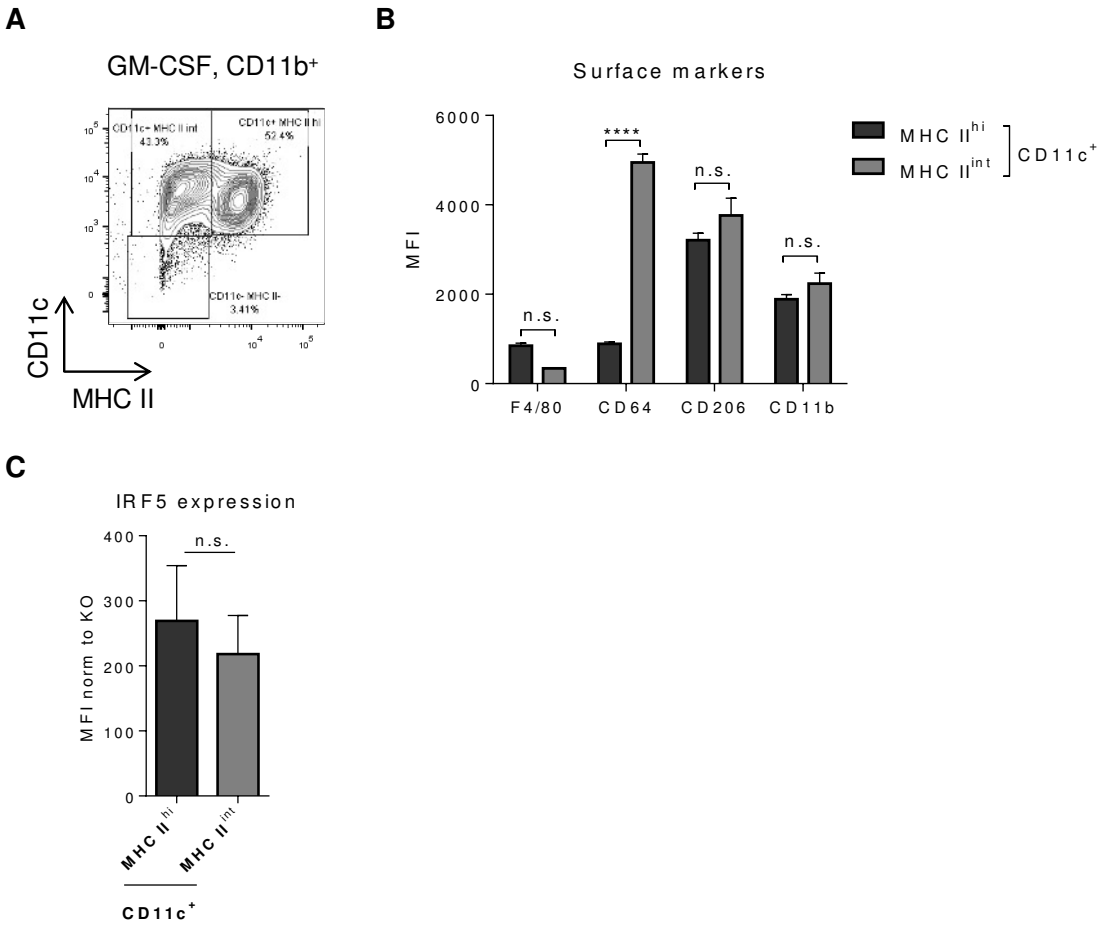

Figure 3.5. GM-CSF cultures contain CD11c+ MHC II^{hi} and MHC II^{int} populations.

Following differentiation with GM-CSF for nine days, FACS samples were taken and stained for the expression of CD11b, CD11c and MHC II as before. CD11c and MHC II are mainly expressed by DCs but can also be found on macrophage populations. **A.** Size and CD11b^{+} gated cells were analysed for phenotypic marker expression. Plot is representative of n=3. **B.** Surface marker expression was quantified by MFI in CD11b^{+} CD11c^{+} MHC II$^{hi/int}$ sub-populations. **C.** Levels of IRF5 were assessed using MFI in the same sub-populations as in (B.). MFI was normalised by subtracting MFI values of IRF5 knock-out cells from WT MFI values Error bars represent the SEM for n=3. Statistical analysis was performed by one-tailed Mann-Whitney U test in (C) or 2-way ANOVA and Bonferroni's multiple comparison in (B). **** p≤0.0001

3.2.3. Mass cytometry highlights heterogeneity of GM-CSF-derived cultures

We then aimed to use mass cytometry (CyTOF) to further analyse the composition and phenotype of GM-CSF and M-CSF cell cultures. CyTOF allows for the reliable detection of a greater number of markers in a single experiment than flow cytometry, as it does not rely on fluorescence and hence no spill over between channels occurs. We used a panel of 18 antibodies containing basic myeloid, B-, T- and NK cell markers, described in detail in 2.3.3 Mass cytometry. Whole BM as well as GM-BMDMs and M-BMDMs after nine days of differentiation were stained for mass cytometry and the obtained data were analysed using viSNE. The resulting cell clusters were manually assigned cellular identities based on expression of highly expressed markers (Schematic in Figure 3.6A, visual plots of myeloid related antigen expression in Figure 3.6B&C). Four main clusters were identified in whole BM (shown in purple in Figure 3.6A): two large $CD11b^+$ myeloid clusters of $GR1^+$ neutrophils and $Ly6C^+$ monocytes as well as two less abundant clusters consisting of $CD3^+$ $TCRB^+$ T-cells and $CD19^+$ $B220^+$ MHC II^+ B-cells. Clusters pre-dominantly found in GM-BMDMs (depicted in red, Figure 3.6A) differed mainly in the expression of F4/80, MHC II and CD11c and thus represented macrophage or DC populations. M-BMDMs largely consisted of one single cluster defined by its uniform expression of high levels of F4/80.

A

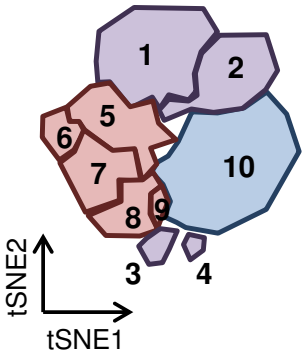

Cluster #	Characterised by	Cell type
1	GR1^{+}	Neutrophils
2	Ly6C^{+}	Monocytes
3	CD19^{+} B220^{+} MHC II^{+}	B-cells
4	CD3^{+} TCRB^{+}	T-cells
5	MHC II^{int} F4/80^{int}	Macrophages / DCs
6	MHC II^{hi} F4/80^{-}	Macrophages / DCs
7	MHC II^{int} F4/80^{-}	Macrophages / DCs
8	MHC II^{lo} F4/80^{-}	Macrophages / DCs
9	MHC II^{-} CD11c^{+}	Macrophages / DCs
10	F4/80^{hi} MHC II^{-}	Macrophages

B

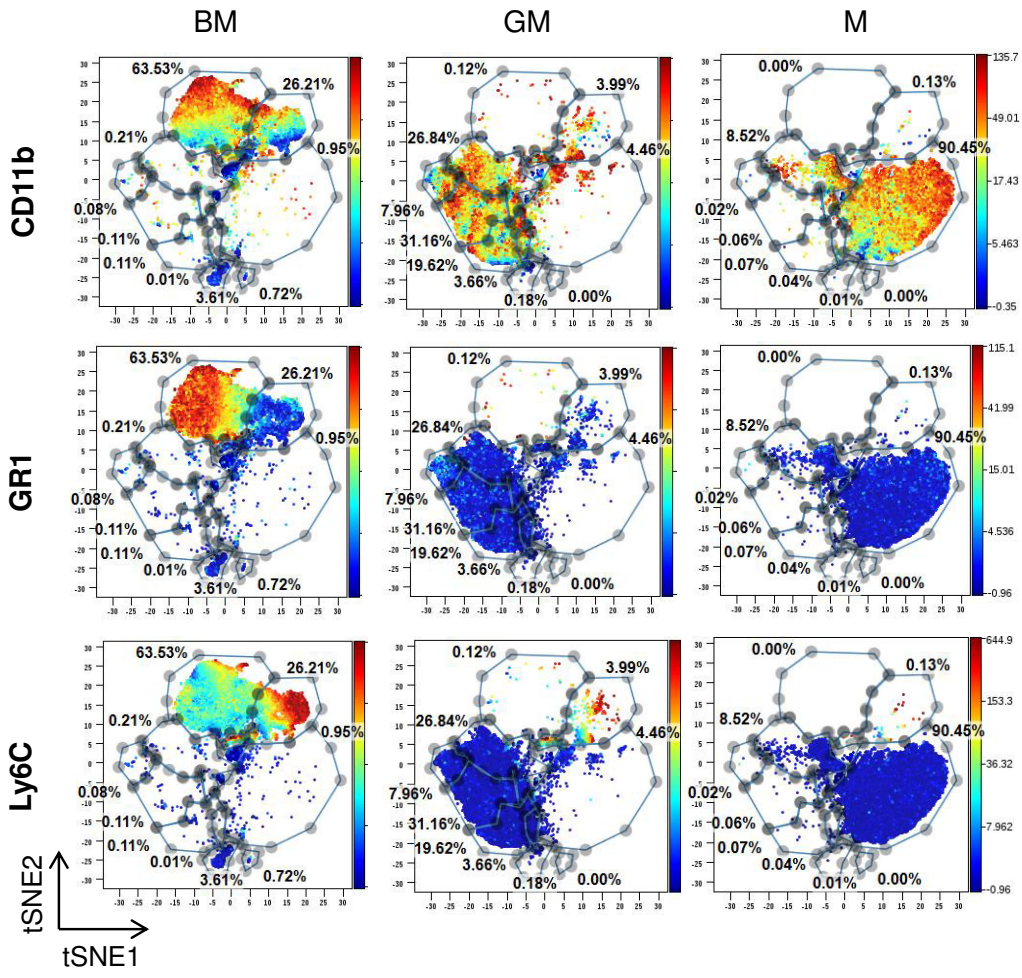

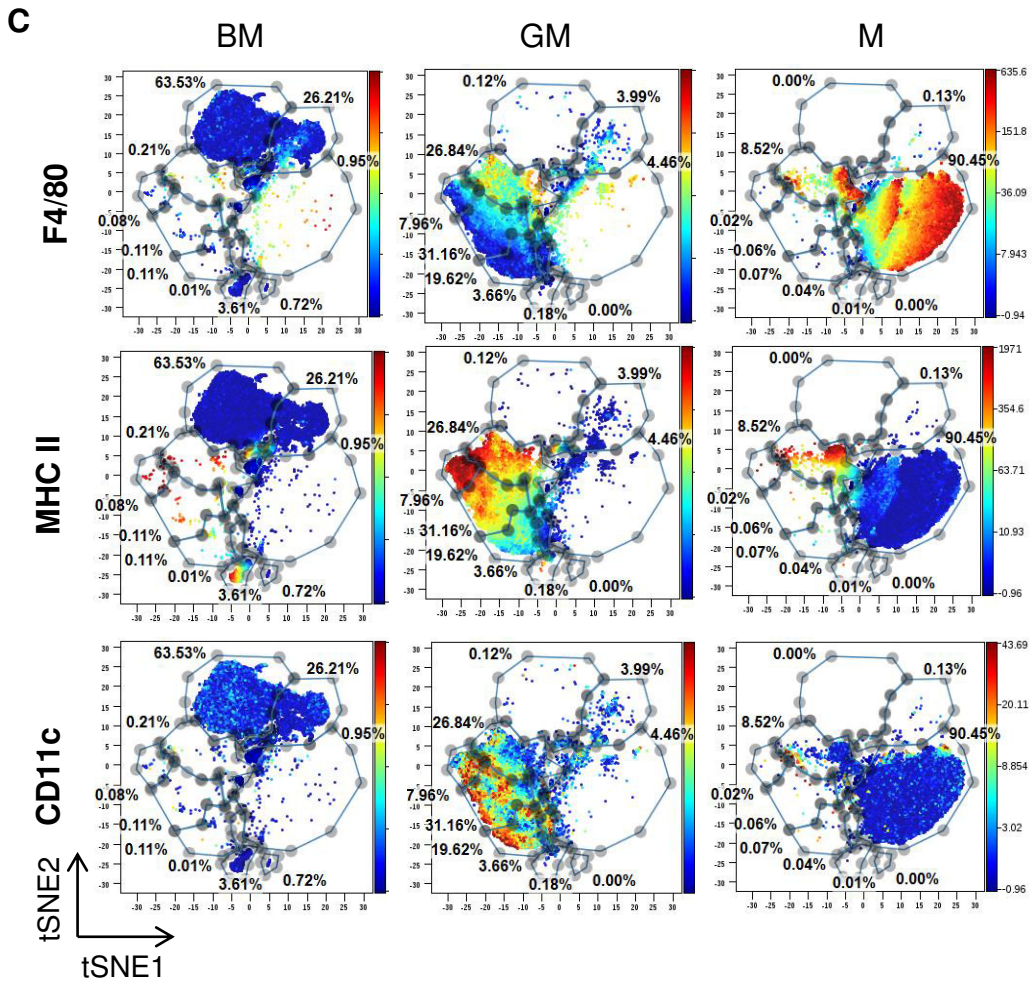

Figure 3.6. GM-CSF and M-CSF differentiation leads to distinct myeloid clusters.

BM progenitors were differentiated for eight days and samples were then stained for mass cytometry with an 18 marker panel. The panel contained markers for myeloid cell populations as well as T-cells, B-cells and NK cells (see 2.3.3 Mass cytometry). Data was analysed using viSNE on cytobank visualising the location of each individual cell in a multidimensional space on a dot plot using two tSNE dimensions. Cells with similar properties will be grouped together whereas cells that do not share expression patterns will be further apart. **A.** Schematic representation of the manually assigned clusters. Clusters predominantly found in BM are shown in purple; the clusters identified in GM-BMDMs are red while the most abundant cluster in M-BMDMs is blue. The table lists the main markers that were used to assign the clusters and the respective cell types associated with these markers. **B. and C.** Images show the expression levels of several extracellular myeloid markers in the different clusters found in BM, GM-BMDMs and M-BMDMs. Expression levels are indicated by the scale on the right hand site, red indicating high expression and blue showing low expression. Data show samples from one mouse.

General myeloid cell types were first determined by analysing expression patterns of CD11b, GR1 and Ly6C (Figure 3.6B). CD11b was highly expressed by most cells in all three samples, although as expected the B- and T-cell clusters in whole BM were CD11b$^-$. Furthermore, there was some variation in the expression levels within neutrophils and monocytes found in BM. GR1 expression was confined to the neutrophil cluster in whole BM and was largely absent in differentiated cells (Table 3.1). M-BMDMs did not contain any GR1$^+$ cells and in GM-BMDMs only very few cells fell within the neutrophil cluster. Ly6C expression showed a similar pattern as it was mostly absent in GM-CSF and M-CSF treated cultures, while highly expressed by the monocyte cluster in BM and to a lesser extent by neutrophils. Ly6C$^+$ monocytic cells were more abundant in GM-BMDMs than in M-BMDMs although they were only detected at low frequencies in both cultures.

Table 3.1 Proportions of identified cell clusters within BM and *in vitro* differentiated cell populations.

Samples were gated on CD45$^+$ live and percentages of each cluster are expressed proportionally. Cluster identity indicates the cell type associated with each cluster, unless marker expression could be interpreted ambiguously. Thus, for clusters identified in GM-BMDMs the characterising markers are given.

Cluster #	% of CD45$^+$ live			Cluster identity
	Whole BM	GM-BMDMs	M-BMDMs	
1	63.53	0.12	0.00	Neutrophils
2	26.21	3.99	0.13	Monocytes
3	3.61	0.18	0.01	B-cells
4	0.72	0.00	0.00	T-cells
5	0.21	26.84	8.52	MHC II^{int} F4/80^{int}
6	0.08	7.96	0.02	MHC II^{hi} F4/80$^-$
7	0.11	31.16	0.06	MHC II^{int} F4/80$^-$
8	0.11	19.62	0.07	MHC II^{lo} F4/80$^-$
9	0.01	3.66	0.04	MHC II$^-$ CD11c$^+$
10	0.95	4.46	90.45	F480^{hi} macrophages

Next, we looked at the markers F4/80, MHC II and CD11c to further identify macrophages and DCs, as previously in flow cytometry (Figure 3.6C). Only a small proportion of BM cells fell into the F4/80^{+} clusters found in GM-BMDMs and M-BMDMs. In GM-BMDMs one cluster was found that showed intermediate F4/80 expression while the remaining clusters were negative. M-CSF differentiated cells however did not only entirely express F4/80 but also mostly at high levels. The F4/80^{hi} cluster comprised 90% of all M-BMDMs and was the main cluster present. The largest MHC II-expressing clusters were found in GM-BMDMs, ranging from MHC II^{lo} to MHC II^{hi} clusters. Only a minority of cells differentiated with GM-CSF did not express MHC II. The only shared cluster showing actual overlap between M-BMDMs and GM-BMDMs could be determined based on its MHC II^{int} F4/80^{int} expression. This cluster was more abundant in GM-BMDMs where it represented 26.84% of CD45^{+} live cells, whereas it was only 8.52% in M-BMDMs. In whole BM, B-cells were the main MHC II^{+} population although minor fractions of MHC II-expressing cells were observed within macrophage/DC clusters identified in GM-BMDMs. CD11c expression was mainly confined to GM-BMDMs where it showed a scattered expression pattern across clusters. Only one small cluster in GM-BMDMs could be defined as entirely CD11c^{+}, and MHC II^{-}, which was essentially absent in both BM and M-BMDMs. Of note, NKp46 staining or markers related to specific T-cell subsets such as CD69 and CD25 could not be detected reliably.

In conclusion, differentiation with GM-CSF and M-CSF ablates BM-derived neutrophil and monocyte populations and induces distinct phenotypes. Specifically, GM-CSF treated cell cultures are highly heterogeneous and

contain several different MHC II and CD11c-expressing populations whereas M-BMDMs consist of a mostly homogeneous F4/80^{hi} population.

3.2.4. GM-BMDMs and M-BMDMs display distinct cytokine expression profiles upon LPS challenge

In order to functionally characterise *in vitro* differentiated macrophages/DCs with regards to their inflammatory properties, we assessed IRF5 expression and cytokine responses of LPS challenged BMDMs. IRF5 has been shown to be essential for establishing a pro-inflammatory phenotype, thus we chose to analyse two cytokines: anti-inflammatory IL-10 and pro-inflammatory IL-12. BM progenitors were treated with either GM-CSF or M-CSF as described before and stimulated with LPS at day nine for 0, 1, 4, 8 and 24 h. Transcript and protein levels of IRF5, IL-10 and IL-12 were determined for each time point.

As in previous experiments (Figure 3.1C, day 9), IRF5 levels in unstimulated cells were considerably higher in GM-CSF compared to M-CSF differentiated macrophages (Figure 3.7A). Upon LPS stimulation, IRF5 mRNA and protein expression was induced in M-BMDMs and further induced in GM-BMDMs. *Irf5* mRNA levels increased between 4-8 h but protein levels were already higher after 1 h post stimulation (Figure 3.7A).

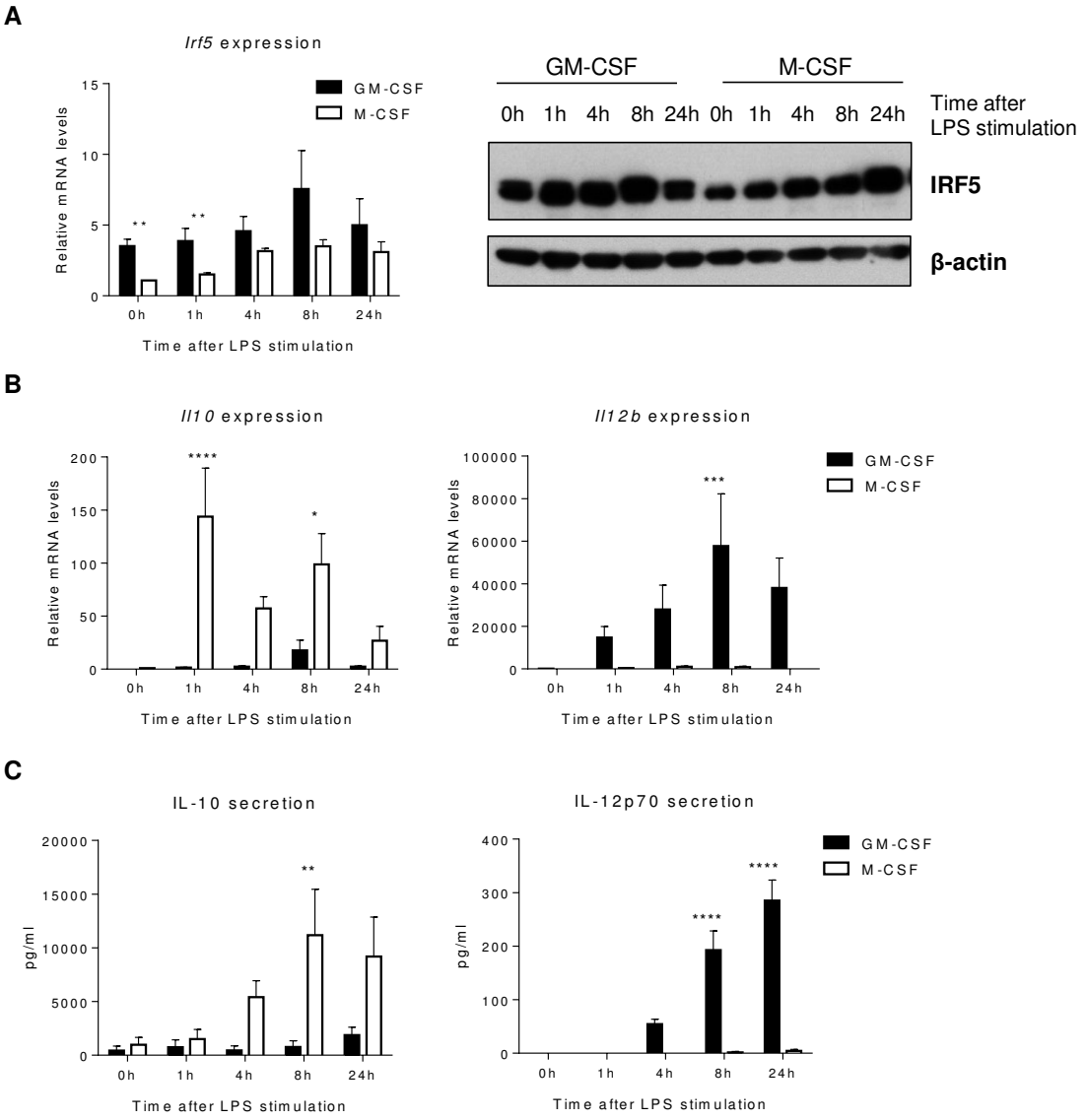

Figure 3.7. IRF5 levels and cytokine profiles of LPS stimulated macrophages.

BMDMs were differentiated with GM-CSF or M-CSF for eight days. All cells were challenged with LPS for the indicated time periods. **A.** *Irf5* transcript levels were measured by Realtime PCR. Error bars represent the SE for n=6. Statistical analysis performed by one-tailed Mann-Whitney U test, ** p≤0.01. Protein levels of IRF5 and β-actin were determined by western blot. Experiment is representative for three independent experiments. **B. and C.** At each time point RNA (top panel) and supernatants (bottom panel) were collected. mRNA expression was determined by Realtime PCR and cytokine concentrations were measured by ELISA. Error bars represent the SEM for n=5. Statistical analysis performed by 2-way ANOVA and Bonferroni's multiple comparison. * p≤0.05; ** p≤0.01; *** p≤ 0.001; **** p≤0.0001

As expected, GM-BMDMs and M-BMDMs were found to display differential behaviour to LPS challenge regarding their cytokine expression (Figure 3.7B and C). Transcription and secretion of the cytokine IL-10 was elevated in M-CSF differentiated macrophages compared to GM-CSF treated cells. LPS stimulation of M-BMDMs resulted in increased IL-10 expression on both transcript and protein level. At 24 h, *Il10* mRNA returned to an almost basal level, whereas protein secretion remained high. IL-10 protein secretion was significantly higher following 8 h stimulation with LPS in M-BMDMs whereas GM-BMDMs only showed basal IL-10 expression. The pro-inflammatory cytokine IL-12 was found to be expressed at much higher levels in GM-CSF-derived macrophages whereas M-BMDMs showed only minimal expression. The differences in cytokine expression were statistically significant on both the transcript and protein levels. *Il12b* mRNA was induced upon LPS stimulation in GM-BMDMs, with the highest levels observed 8 h post stimulation. Secretion of IL12p70 was increased from 4 h of stimulation onwards.

To conclude, GM-CSF differentiated BMDMs express high levels of IRF5 and produce IL-12 following stimulation with LPS, whereas M-CSF differentiated BMDMs express lower levels of IRF5 and produce IL-10.

3.2.5. IFN-γ increases levels of IRF5 and moderately affects cytokine production

IFN-γ but not IL-4 induces both IRF5 transcript and protein expression

We next aimed to assess levels of IRF5 in *in vitro* differentiated macrophages that are commonly referred to as classically and alternatively activated macrophages (Murray et al. 2014). Both are derived from BM progenitors that

are differentiated with M-CSF for 8-9 days and are then treated for 18 h with IFN-γ or IL-4 to generate classically or alternatively activated macrophages respectively (Figure 3.8A).

IRF5 transcript and protein levels were determined 18 h after addition of IFN-γ and IL-4. GM-BMDMs and M-BMDMs were analysed for comparison and as experimental controls. In accordance with previous data, GM-BMDMs expressed higher levels of IRF5 than M-BMDMs. Stimulation with IFN-γ led to a significant increase in *Irf5* mRNA expression comparable to levels observed in GM-BMDMs (Figure 3.8B). IRF5 expression was analysed by western blotting of whole cell lysates. Protein levels of IRF5 were also augmented following IFN-γ incubation compared to M-BMDMs although they did not reach the level observed in GM-BMDMs. IL-4 addition however did not have any effect on levels of IRF5, neither transcript nor protein levels changed. As a control for cytokine activity, transcript levels were determined for the known IFN-γ target gene *Socs1* (Sakamoto et al. 1998) and the IL-4 inducible *Mrc1* (Stein et al. 1992) (Figure 3.8C). *Socs1* expression was significantly increased upon IFN-γ but not IL-4 stimulation of M-BMDMs whereas *Mrc1* induction was exclusively observed with IL-4 treatment. Thus, both cytokines were functional and used in adequate concentrations to assert their known transcriptional effects. In conclusion, *Irf5* transcription and protein expression can be induced to some extent by IFN-γ in mouse M-CSF-derived BMDMs, similarly to the previously observed induction in human monocytes (Krausgruber et al. 2011). IL-4 however does not seem to affect levels of IRF5 in this system.

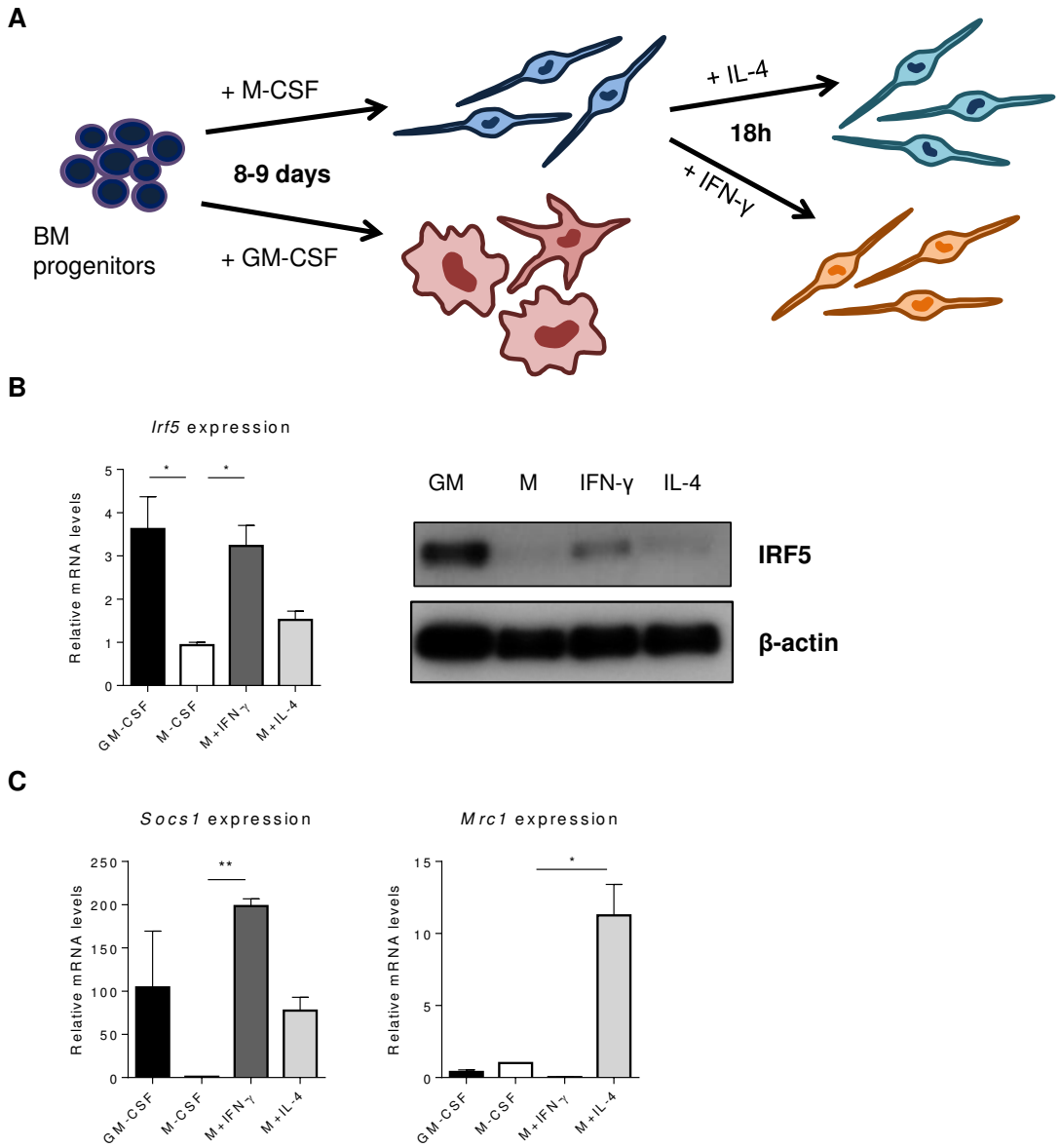

Figure 3.8. IRF5 levels are induced by IFN-γ in M-BMDMs but remain unaffected by IL-4.

BMDMs were differentiated with GM-CSF or M-CSF for eight days. M-BMDMs were treated with IFN-γ or IL-4 for 18 h prior to mRNA and protein collection. **A.** Schematic illustration of the *in vitro* differentiation protocol using GM-CSF or M-CSF. On day eight, IL-4 (10 ng/ml) or IFN-γ (5 ng/ml) was added to M-CSF differentiated cells for 18 h. **B.** Transcript levels were measured by Realtime PCR. Error bars represent the SEM for n=3. Protein levels of IRF5 and β-actin were determined by western blot. Experiment is representative for four independent experiments. **C.** *Socs1* mRNA induction was measured as a control for IFN-γ efficiency since it is a known IFN-γ target gene. Equally, *Mrc1* levels of induction were determined as a control for IL-4 activity. Error bars represent the SEM for n=2-3.
Statistical analysis performed by either one-tailed Mann-Whitney U test or two-tailed unpaired t- test. * p≤0.05; ** p≤0.01; *** p≤ 0.001

Il10 transcript levels are reduced after IFN-γ incubation

We next sought to determine the effect of IFN-γ and IL-4 on the cytokine expression profiles of anti-inflammatory IL-10 and pro-inflammatory IL-12. Cells were stimulated with LPS for up to 24 h following 18 h treatment with IFN-γ or IL-4. GM-BMDMs and M-BMDMs displayed similar patterns as before and showed significantly different expression of IL-10 and IL-12 upon LPS challenge. While addition of IL-4 did not alter cytokine expression compared to cells cultured with M-CSF only, IFN-γ treatment did affect the LPS response (Figure 3.9A and B).

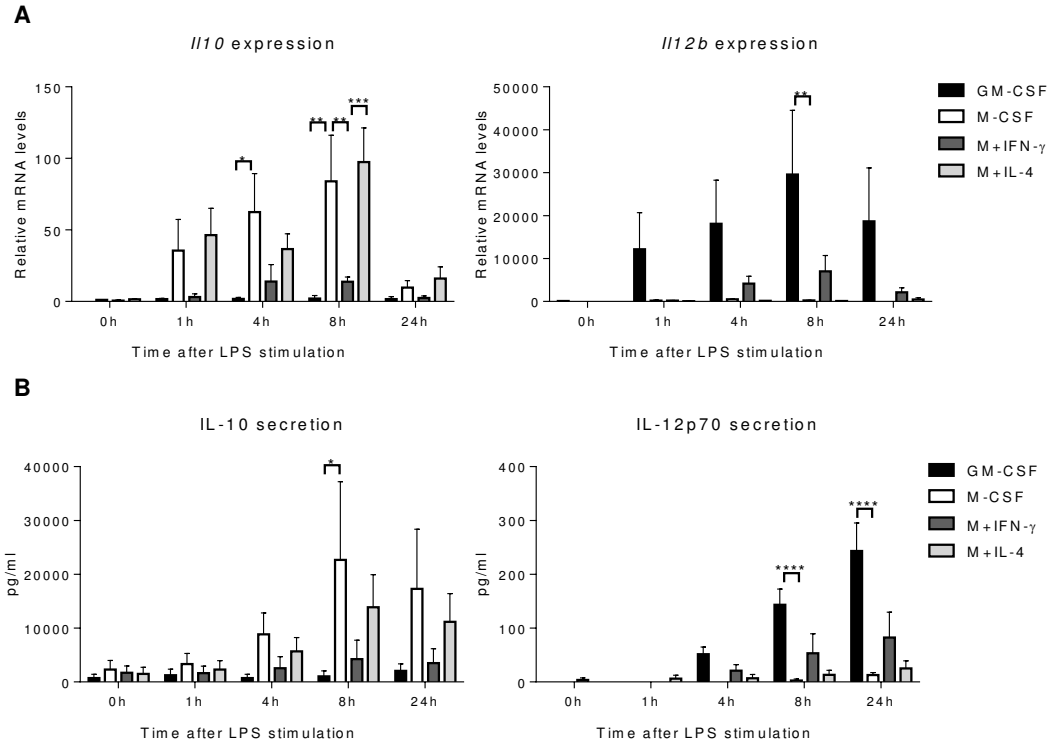

Figure 3.9. The cytokine expression profile upon LPS stimulation is altered by IFN-γ addition.

Macrophages were differentiated *in vitro* with GM-CSF or M-CSF. On day eight, IFN-γ or IL-4 was added to M-CSF derived cells for 18 h prior to stimulation with LPS for up to 24 h. **A. and B.** At each time point RNA (top panel) and supernatants (bottom panel) were collected. Transcript levels were measured by Realtime PCR and cytokine concentrations in supernatants were measured using ELISA. Error bars represent the SEM for n=3. Statistical analysis performed by 2-way ANOVA and Bonferroni's multiple comparison. * p≤0.05; ** p≤0.01; *** p≤ 0.001; **** p≤0.0001

Il10 transcript levels were significantly reduced after 8 h of LPS stimulation in classically activated macrophages compared to M-BMDMs with or without IL-4. Although protein levels did not reach statistical significance, a trend for less IL-10 secretion in the presence of IFN-γ could be observed. The same held true for IL-12 mRNA expression and secretion, IL-4 did not have any effect whereas IFN-γ slightly increased the amounts produced. The changes in IL-12 levels caused by IFN-γ addition were however not statistically significant. Thus, IL-4 treated M-BMDMs remain unaltered regarding their cytokine expression profiles for IL-10 and IL-12 while IFN-γ reduces IL-10 production.

3.2.6. GM-CSF increases levels of IRF5 and alters cytokine expression in M-CSF differentiated macrophages

GM-CSF induces transcription of Irf5 in M-BMDMs

In order to assess whether GM-CSF could initiate *Irf5* transcription even after differentiation, we added GM-CSF to M-CSF differentiated macrophages on day eight and assessed *Irf5* mRNA levels at different time points up to 48 h later (Figure 3.10A). Additionally, protein levels of IRF5 were determined 48 h after GM-CSF addition using flow cytometry. Transcript levels were significantly increased upon GM-CSF treatment in M-BMDMs from 4 h post treatment onwards, compared to untreated 0 h (Figure 3.10B). Expression levels peaked at 8 h when they were as high as levels detected in GM-BMDMs. *Irf5* mRNA levels started to decrease within 24 h and returned to basal levels of expression after 48 h. GM-BMDMs displayed similar kinetics of *Irf5* expression and levels were significantly higher than in M-BMDMs up to 24 h (p values at least ≤0.01, statistics not shown in the graph). However, amounts of *Irf5* transcript were

decreased after 48 h and reached the same basal level as M-BMDMs that had received GM-CSF. M-BMDMs without GM-CSF only showed a slight increase in transcript levels that was lower than in both GM-BMDMs and treated M-BMDMs. At 48 h post treatment, IRF5 protein expression was quantified using MFI normalised to IgG stained controls. Even though mRNA levels were no longer different at that time point, protein levels were still significantly increased in GM-CSF treated BMDMs compared to M-BMDMs. GM-CSF-derived cells showed the highest levels of expression as observed before. To conclude, IRF5 expression is increased on transcript and protein levels upon incubation with GM-CSF.

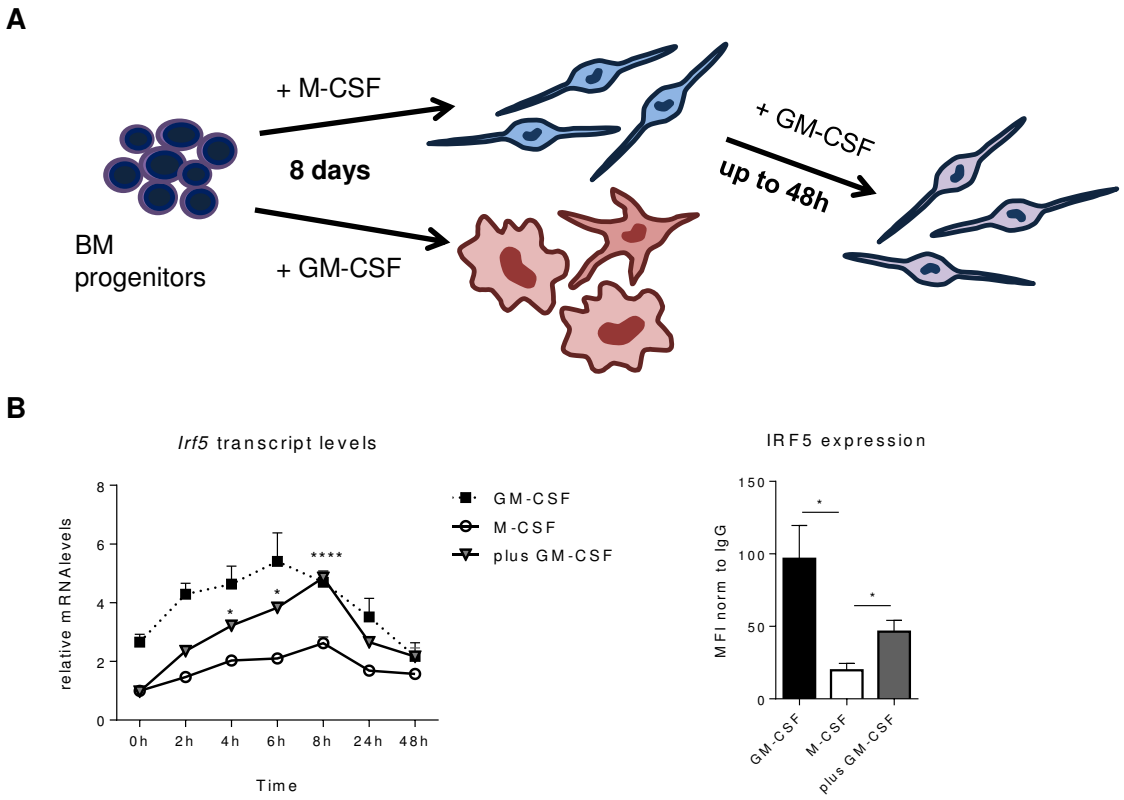

Figure 3.10. GM-CSF induces *Irf5* transcription in M-BMDMs.

BM-derived cells were differentiated as described previously. GM-CSF was added to M-CSF macrophages at the final day of differentiation as additional stimulus. **A.** Schematic of the macrophage differentiation protocol using GM-CSF (20 ng/ml) or M-CSF (100 ng/ml). On day eight, 20 ng/ml of GM-CSF were added to M-BMDMs. **B.** *Irf5* transcript levels were measured with Realtime PCR at several time points after GM-CSF addition. Protein levels of IRF5 were determined after 48h incubation with GM-CSF by FACS. MFI was calculated and normalised to IgG stained controls by subtracting the MFI value of IgG stained control samples from IRF5 stained samples. Error bars represent the SEM for n=3-4. Statistical analysis performed by 2-way ANOVA and Bonferroni's multiple comparison or one-tailed Mann-Whitney U test. * p≤0.05; ** p≤0.01; *** p≤ 0.001; **** p≤0.0001

Next, we aimed to verify whether the increase in *Irf5* transcript levels could be attributed to *de novo* transcription or was due to augmented mRNA stability (Supplementary Figure S8.1). To block active transcription just before the peak of *Irf5* expression was reached, cells were treated with ActD 6 h post stimulation with GM-CSF. ActD is known to prevent elongation mediated by the RNA polymerase complex and thus abolishes transcription. Samples were collected every hour for up to 6 h following ActD addition to analyse remaining mRNA

levels by qPCR. As expected transcript levels decreased upon ActD treatment as transcription was inhibited. Linear regression analysis was used to compare the kinetics of mRNA stability. The calculated functions were not significantly different in either untreated or treated M-BMDMs, as measured by differences in slope, elevation or intercept. The mRNA half-life was thus not significantly different either and the mean and standard deviation were calculated as 3.7 h±0.1. Hence, preliminary data based on n=1 experiment suggest that GM-CSF can induce *de novo* transcription of the *Irf5* gene in M-CSF differentiated macrophages.

Inflammatory cytokine expression is attenuated by GM-CSF treatment

We then wanted to investigate whether GM-CSF treatment also affected the cytokine expression profiles of those cells. Hence, we challenged cells with LPS as before for up to 24 h following incubation with GM-CSF for 18 h analogous to experiments using IFN-γ and IL-4. Transcript levels and secretion of the cytokines IL-10 and IL-12 were determined as in previous experiments. Prior treatment with GM-CSF led to a significant reduction in *Il10* mRNA production in M-CSF-derived macrophages, throughout the entire time course (Figure 3.11A). Transcript levels were decreased from 1 h post stimulation and GM-CSF treated M-BMDMs generally only showed a minor increase in mRNA levels overall. Although it could be observed that they still expressed significantly higher levels than GM-BMDMs, as did untreated M-BMDMs ($p \leq 0.05$ at least, statistics not shown). This was however not reflected in the secreted protein levels detected in supernatants (Figure 3.11B). IL-10 production was not altered in M-BMDMs

and levels were significantly higher than in GM-BMDMs, as seen before, independent of GM-CSF incubation.

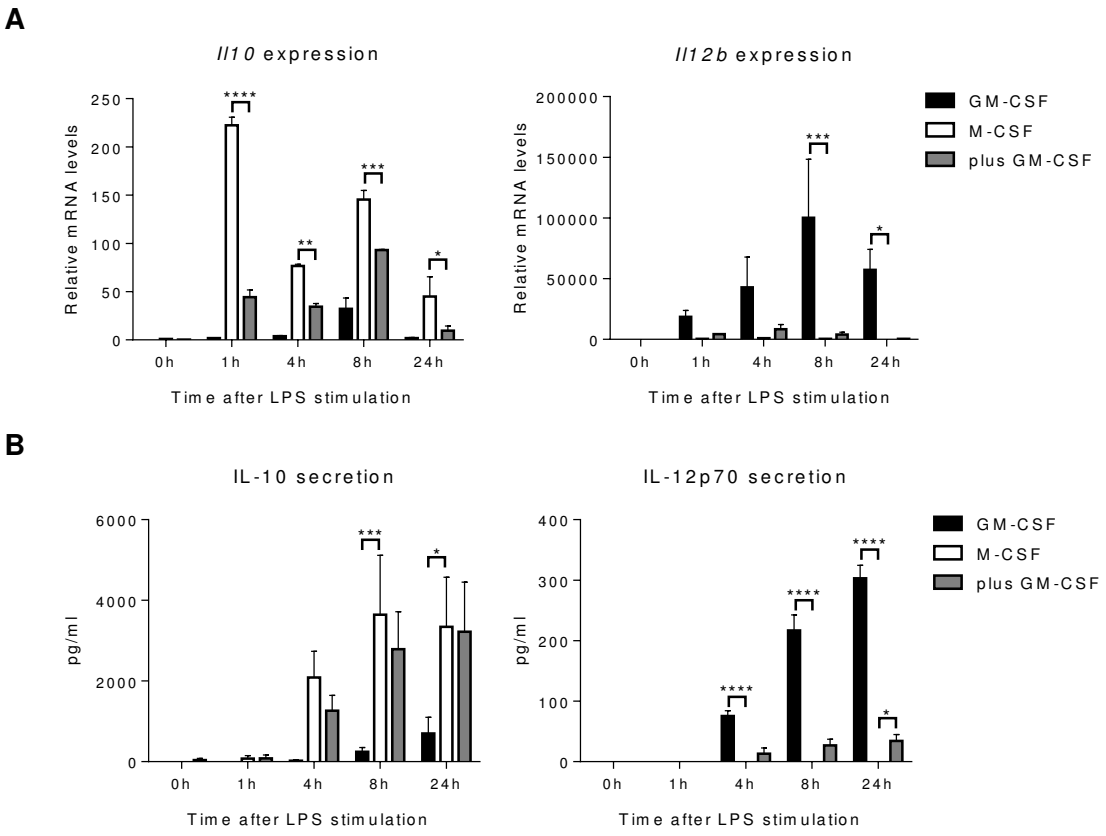

Figure 3.11. GM-CSF alters LPS induced cytokine expression in M-BMDMs.

BMDMs were differentiated as described previously. GM-CSF was added to M-CSF macrophages at 20 ng/ml for 18 h. Subsequently all cells were stimulated with LPS for the indicated periods of time. **A. and B.** At each time point of LPS stimulation RNA (top panel) and supernatants (bottom panel) were collected. Error bars represent the SEM for n=2-5. Statistical analysis performed by 2-way ANOVA and Bonferroni's multiple comparison or one-tailed Mann-Whitney U test. * p≤0.05; ** p≤0.01; *** p≤ 0.001; **** p≤0.0001

Il12b mRNA expression was not affected in the presence of GM-CSF but IL12-p70 secretion showed a minor but statistically significant increase 24 h after LPS stimulation when compared to M-BMDMs (Figure 3.11A and B). As discussed in section 3.2.4, GM-CSF differentiated cells produced significantly more IL-12 than M-BMDMs throughout and still 10-fold more than GM-CSF

treated M-BMDMs at 24 h. These data show that GM-CSF driven IRF5 expression modulates the LPS response of M-CSF *in vitro* differentiated macrophages to some extent.

3.2.7. Transcriptional regulation of the *Irf5* locus in GM-CSF-derived cells

To further gain insight into potential factors involved in transcription at the murine *Irf5* locus, we chose to analyse publicly available ChIP-Seq datasets from Gerber et al. (GEO accession number GSE36104) (Garber et al. 2012). In this study, murine *in vitro* differentiated macrophages/DCs were analysed that had been generated using a similar culture protocol to the one described here (for details refer to 2.1.1 Generation of bone marrow-derived cells). To assess whether the locus was transcribed at all, we examined the distribution of some basic markers of active transcription such as RNAP II binding and presence of the histone marks H3K4me3 and H3K27ac over the *Irf5* genomic locus (Heintzman et al. 2009). Furthermore, we scrutinised datasets for H3K4me1 and the myeloid master regulator PU.1, which were also found to mark enhancers. TFs generally important within the macrophage compartment were also analysed such as CEBPB and STAT1, the latter acting downstream of IFN-γ amongst others. Moreover, we chose to examine the potential influence of members of the IRF family such as IRF1 and IRF4. CTCF was used as a general marker for regulatory regions within genomic sites. Datasets of unstimulated cells (and 2h LPS challenged for STAT1) were obtained from the GEO database and visualised using the integrative genomics viewer (IGV) (Robinson et al. 2011). Binding of RNAP II and abundance of H3K4me3 as well

as H3K27ac upstream of the *Irf5* gene and within the first intron indicated that this region was transcribed in the cells used in this study (Figure 3.12).

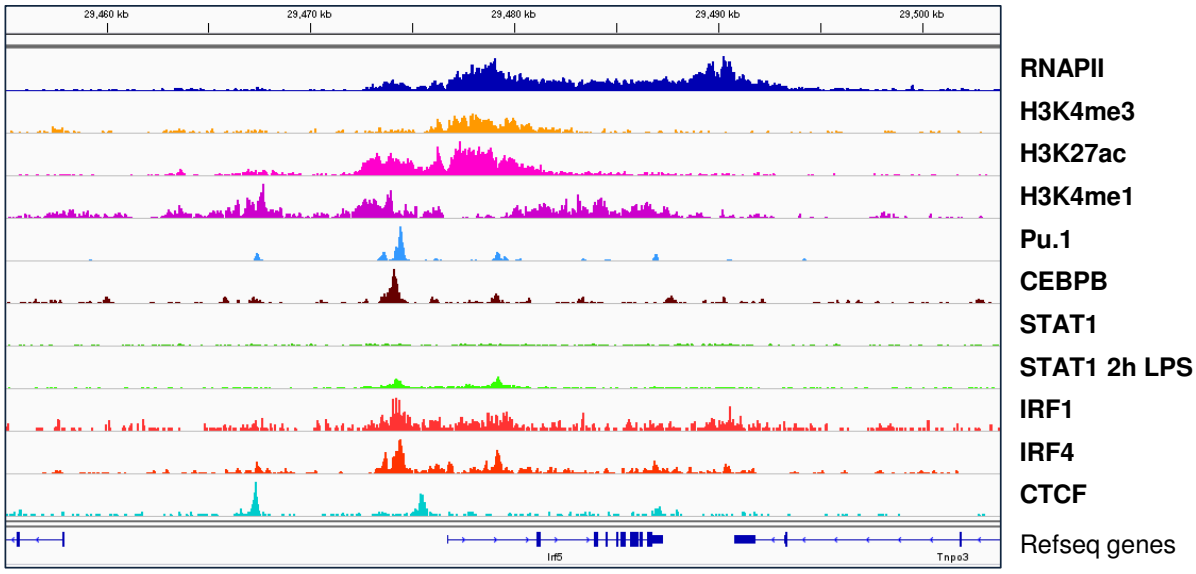

Figure 3.12. TF binding and histone modifications at the *Irf5* locus in GM-CSF differentiated cells.

Publicly available datasets generated (Garber et al. 2012) were used to examine the murine *Irf5* locus in unstimulated *in vitro* generated BM derived cells (except STAT1 binding which is also shown for 2 h post LPS stimulus). Garber et al. performed ChIP-Seq experiments for various transcription factors and histone modifications in unstimulated and LPS treated cells. Selected datasets were obtained and analysed using the IGV. The top four lanes display RNA polymerase II binding as well as histone modifications associated with open chromatin regions. The following lanes are several transcription factors that may be involved in *Irf5* transcription. CTCF in the second last lane is a factor described to mark regulatory regions or boundary sites in the genome. At the very bottom the Refseq genes track can be found showing the annotated genes of the chromosomal region displayed. Upstream of *Irf5* lies the *Kcp* gene and downstream the *Tnpo3* gene.

There was also a substantial amount of H3K4me1 detected further upstream of the promoter region, however there was no real overlap with PU.1 binding peaks. On the other hand, there was one distinct PU.1 peak in close proximity to the first exon. At the same position, we found binding of both members of the IRF family and LPS induced STAT1. One CEBPB binding site could be detected that was near by the upstream PU.1 peak. There were two major CTCF peaks,

one of which overlapped with H3K4me1 binding further upstream whereas the other one was located near the gene start site.

To conclude, several TFs can be found in close proximity to the *Irf5* promoter region after differentiation and may be involved in regulating expression of the locus. Nevertheless, more work is needed to functionally validate the role of these TFs in regulation of *Irf5* transcription.

3.3. Discussion

IRF5 has been previously shown to be involved in the pro-inflammatory response to microbial and viral stimuli. High levels of IRF5 expression are associated with a pro-inflammatory macrophage phenotype (Krausgruber et al. 2011) and lack of IRF5 protects mice from exacerbated inflammation in different disease models (Eames et al. 2015). Here, we have shown that murine *in vitro* differentiated macrophages characterised by high levels of IRF5 display a pro-inflammatory phenotype in terms of surface receptor expression and cytokine response to LPS (Figure 3.13), as observed in their human counterparts. Expression of IRF5 is induced during differentiation of BM progenitors with GM-CSF but not M-CSF and these cells display distinct phenotypes. M-BMDMs consist of a relatively homogenous population while GM-BMDMs are a much more heterogeneous mixture of cells. Mass cytometry further highlighted diversity of GM-CSF treated cells, in line with recent work by Helft et al. (Helft et al. 2015). Furthermore, we observed that transcription of *Irf5* in M-BMDMs was induced following 18 h treatment with the inflammatory stimuli GM-CSF and IFN-γ, which consequently displayed a modulated LPS response. Thus, we

establish a species-invariant role of IRF5 in controlling the inflammatory macrophage phenotype *in vitro*.

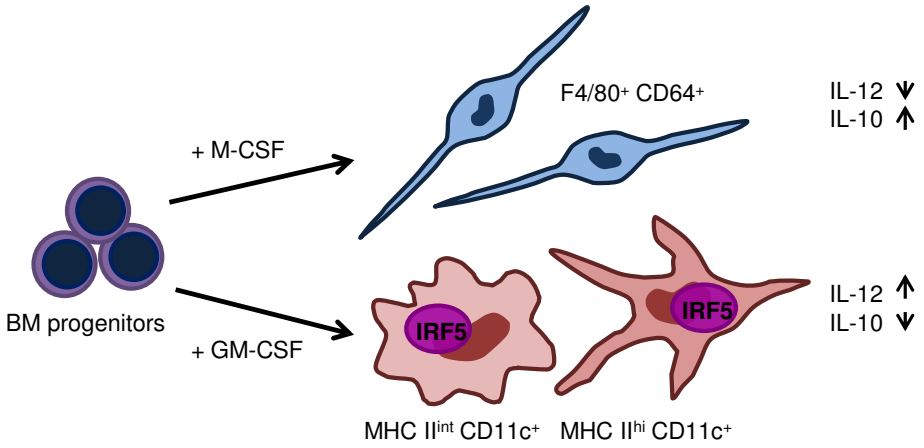

Figure 3.13. GM-CSF drives IRF5 expression and a distinct pro-inflammatory phenotype *in vitro*.

BMDMs generated *in vitro* using M-CSF and GM-CSF display different phenotypes, both with regards to surface receptor expression and LPS response. M-BMDMs are a homogenous population of F4/80$^+$ CD64$^+$ cells that produce IL-10 upon LPS stimulation. GM-BMDMs are a heterogeneous CD11c$^+$ population that differs in the degree of MHC II expression. These cells produce IL-12 in response to LPS rather than IL-10. Moreover, M-BMDMs and GM-BMDMs differ in their IRF5 expression which is induced during differentiation with GM-CSF but not M-CSF.

GM-CSF and M-CSF both play important roles in the development of myeloid cell populations, namely granulocytes, DCs and macrophages, respectively (Burgess and Metcalf 1980, Hamilton 2008). IRF5 is upregulated during the differentiation process in GM-CSF treated cultures. Functional implications of these data may be that IRF5 potentially has a role in the developmental process of myeloid cells. Interestingly, it has been previously observed that IRF5 expression is enriched as monocyte precursors progress from the MDP to cMoP and ultimately Ly6C^{hi} monocyte stage (Hettinger et al. 2013). Since IRF5 is a TF it is possible that it controls genes involved in reinforcing lineage commitment such as *MafB*, *c-Maf*, *Egr1*, *Irf8*, *Klf4* (Geissmann et al. 2010). Alternatively, IRF5 may be co-regulating these genes that are crucial for fate

decisions by collaborating with TFs such as PU.1, which is essential for monocyte development (Nerlov and Graf 1998, Dakic et al. 2005, Auffray et al. 2009). It has been suggested before in the context of macrophage polarisation and the inflammatory response that IRF5 may cooperate with PU.1 (Lawrence and Natoli 2011, Saliba et al. 2014).

Although monocytes are characterised as $CD115^{+}$ (MCSF-R) and completely depend on M-CSF in their development *in vivo* (Cecchini et al. 1994, Dai et al. 2002), cMoPs have been shown to respond to both M-CSF and GM-CSF *in vitro* (Hettinger et al. 2013). Thus far though, the role of IRF5 in myeloid cells has mainly been described in the context of autoimmunity and response to bacterial or viral challenge (Honda and Taniguchi 2006, Ryzhakov et al. 2015) rather than as a developmental TF. To elucidate the potential role of IRF5 in myeloid fate decisions, analysis of different myeloid progenitor populations in the BM of $IRF5^{-/-}$ mice may indicate whether there are any developmental defects. *In vitro* and *in vivo* experiments using sorted precursors of $IRF5^{-/-}$ mice could be used to assess their precursor potential. Subsequent transfer of purified IRF5 deficient precursors into a WT host would provide information about the resultant progeny and the effect of intrinsic loss of IRF5. Future research would need to address these questions as well as identify potential IRF5 target genes that could be involved in lineage commitment.

While both M-CSF and GM-CSF are crucial in the development of myeloid cell subsets, there are fundamental differences in their biological functions. In the physiological situation, M-CSF is detected in low steady state levels (Hamilton 2008), whereas GM-CSF has been shown to be increased upon stimulation with

inflammatory stimuli, such as IL-1, TNF or LPS (Verreck et al. 2006). M-CSF has long been known to be crucial in monocyte and macrophage development (Witmer-Pack et al. 1993, Dai et al. 2002, Sasmono et al. 2003) and has thus been used from early on to generate macrophages *in vitro* (Stanley 1997). GM-CSF on the other hand displays pleiotropic effects as it can induce the differentiation of multiple myeloid lineages (Burgess and Metcalf 1980) and has been shown to be involved in the maintenance and differentiation of macrophages, DCs and neutrophils.

This effect is apparent when analysing Ly6G and Ly6C expression on the differentiating cells (Figure 3.2), where a substantial $Ly6G^{hi}$ population is maintained in GM-CSF cultures up to day six but is absent in M-CSF treated cells. At day nine, one fifth of GM-CSF-derived cells show intermediate Ly6G expression, which may represent a neutrophil population. However, no equivalent of this population was found by mass cytometry where the $GR1^{+}$ cluster is basically absent in GM-CSF cultures (Figure 3.6). Of note, different antibody clones were used and GR1 is reported to detect Ly6C, although to a lesser extent than Ly6G (Fleming et al. 1993). Mass cytometry however seems more likely to identify *bona fide* neutrophils as viSNE clustering is based on the expression pattern of several markers. Moreover, when we analysed the surface marker expression of macrophage and DC markers (Figure 3.3), in both sub-populations present at day nine, the expression patterns were essentially the same and varied only slightly with regards to proportions. A neutrophilic population would have been expected to be entirely $CD11c^{-}$ and $CD64^{-}$. Thus, the $Ly6G^{int}$ staining is likely to be an artefact due to macrophage autofluorescence or spill over from other channels. $Ly6C^{int}$ cells within M-CSF

cultures may represent a transitional stage in macrophage development as monocytes can down-regulate Ly6C expression upon differentiation into macrophages (Tamoutounour et al. 2012, Bain et al. 2013, Plantinga et al. 2013, Tamoutounour et al. 2013).

In agreement with M-CSF enforcing a macrophage phenotype, M-CSF cultures show a largely homogenous expression pattern for the macrophage markers CD64 and F4/80. *In vitro* differentiation with GM-CSF has been used to generate both macrophages and DCs (Inaba et al. 1992, Caux et al. 1996), especially in combination with IL-4 (Sallusto and Lanzavecchia 1994). Using GM-CSF alone yields a heterogeneous mixture of cells that are almost entirely $CD11c^{+}$ and express high or intermediate levels of MHC II. When comparing GM-BMDMs and M-BMDMs (Figure 3.4), differences are more pronounced when analysing macrophage associated markers like F4/80, CD64 and CD206. This may be due to the high level of heterogeneity of the GM-CSF cultures masking some effects. Hence, we analysed subsets that were recently identified and examined in depth by Helft and colleagues (Helft et al. 2015). In this study, two main cell populations were characterised so called GM-Macs and GM-DCs that were $CD11c^{+}$ $CD11b^{hi}$ MHC II^{int} $CD115^{+}$ $MerTK^{+}$ and $CD11c^{+}$ $CD11b^{int}$ MHC II^{hi} $CD115^{-}$ $CD135^{+}$, respectively. Importantly, there were still cells within the MHC II^{hi} population that did not fall into this category. Even though our panel did not include CD115, MerTK or CD135, the two main populations could still be distinguished based on their differential MHC II expression. We analysed some of the key surface markers used in the study by Helft et al. and could confirm that CD64 expression is much higher in the MHC II^{int} macrophage population

(Figure 3.5). In our hands however, F4/80 and CD11b were not differentially expressed within the two populations. A potential reason for these differences could lie in the variations within differentiation protocols. The protocol we have used differs slightly from the one applied by Helft et al. in terms of culture length and use of tissue culture treated plastic. This may result in different cell yields and populations. In conclusion, these data to some extent clarify the identity of GM-CSF-derived cell cultures as both macrophages and DCs. Thus interpretation of data generated using these cultures may be complicated as subtle or less pronounced effects may be hidden due to heterogeneity. Nevertheless, since IRF5 expression within these populations seems to be equal, conclusions drawn with regards of IRF5 molecular functions should still be valid.

Mass cytometry is a new technique combining mass spectrometry with the principles of classical flow cytometry. Due to the lack of potential spill over as fluorophores are replaced with heavy metal tags on antibodies, it allows for a much higher number of antibodies in one panel. In flow cytometry, the highest number is currently 18 whereas for mass cytometry panels are currently reaching 45, but will probably be extended as the technique evolves (Bendall et al. 2012). We applied mass cytometry on whole BM, GM-CSF and M-CSF treated cell cultures (Figure 3.6). This allowed us to compare our conventional flow cytometry data to data generated using an 18 marker panel including additional cell types. When using data from all three samples, viSNE clustering clearly distinguished between them as most clusters were predominantly associated with origin and only little overlap occurred. This confirmed previous

observations that GM-CSF and M-CSF induced different phenotypes (Verreck et al. 2004, Fleetwood et al. 2007, Krausgruber et al. 2011) and our own flow cytometry data. Clusters identified in BM showed the expected cell types although due to the limited panel specific progenitor populations could not be identified. M-CSF-derived cells consisted of one homogenous cluster which again underlines the more restricted cellular fate imposed by M-CSF. GM-CSF however leads to a diverse mixture of cell subsets going beyond the two main subsets described in (Helft et al. 2015). These studies are however only preliminary as many macrophage and DC markers such as CD64, MerTK, CD103 and others are to be incorporated into future panels allowing for more detailed analysis of different subsets. Moreover, it would be important to establish IRF5 staining for mass cytometry to use in this context and for future *in vivo* studies. This would be especially interesting if coupled with additional intracellular stainings of cytokines or TFs such as STATs. Such experiments would enable us to analyse the differences in cells with high or low levels of IRF5. Taken together, mass cytometry in the future will be extremely useful to characterise the highly heterogeneous and diverse macrophage and DC populations, especially *in vivo*.

The IRF5 expression pattern *in vitro* is also exhibited by unstimulated human macrophage counterparts, with significantly higher IRF5 expression in GM-CSF *in vitro* differentiated human macrophages compared to those differentiated with M-CSF(Krausgruber et al. 2011). Upon LPS challenge, *Irf5* mRNA levels increased between 4-8 h but protein levels were already higher 1 h post stimulation (Figure 3.7A). We therefore hypothesised that LPS-induced

production of IRF5 was most likely due to a combination of two factors: (1) increased mRNA levels and (2) protein stabilisation, possibly related to activation by phosphorylation or ubiquitination (Balkhi et al. 2008, Chang Foreman et al. 2012). IRF5 has been shown to be essential for the pro-inflammatory phenotype of human monocyte-derived GM-CSF macrophages upon LPS stimulation. However, mRNA and protein levels in human M-CSF-derived macrophages are not further induced upon LPS stimulation, suggesting some species-specific or cell source-specific differences in LPS-regulated IRF5 production.

We also noted that IRF5 levels increased in M-BMDMs upon LPS stimulation but did not result in significant induction of pro-inflammatory cytokines (Figure 3.7B and C). Thus, we hypothesised that this could be due to a lower functional activity of IRF5 in M-BMDMs, as IRF5 protein is subject to post-translational modifications such as phosphorylation and ubiquitination (Balkhi et al. 2008, Balkhi et al. 2010, Chang Foreman et al. 2012, Lu et al. 2015). However, the status of post-translational modifications for IRF5 in LPS stimulated macrophages is yet to be determined. Furthermore, the availability of activating co-factors potentially required for IRF5 mediated induction of pro-inflammatory cytokines might be different in M-BMDMs compared to GM-BMDMs. Thus, consistent with its proposed role as a master regulator of the pro-inflammatory macrophage phenotype and in accordance with data for human *in vitro* differentiated macrophages (Krausgruber et al. 2011), GM-CSF differentiated BMDMs express high levels of IRF5 and produce IL-12 following stimulation with LPS, whereas M-CSF differentiated BMDMs express lower levels of IRF5 and produce IL-10. These data confirm the study of Fleetwood et al. (Fleetwood

et al. 2007) that suggested GM-CSF and M-CSF induce distinct BMDM phenotypes.

Little is known about transcriptional activation of *Irf5* but it has been shown to be a p53 target gene in the context of apoptosis in mice (Mori et al. 2002, Barnes et al. 2003). We confirmed that IRF5 is expressed in pro-inflammatory macrophages and transcription can be induced by GM-CSF and IFN-γ (Figure 3.8 and Figure 3.10). Induction of *Irf5* transcript by GM-CSF does not seem to be due to a change in mRNA stability (Supplementary Figure S8.1) although these results are preliminary and will need to be repeated. GM-CSF addition following differentiation with M-CSF also altered the cytokine expression profile, in line with previous data by Fleetwood et al. (Fleetwood et al. 2007), which is likely due to the increase in IRF5 expression. Publicly available datasets generated by Garber et al. further showed a transcriptionally active *Irf5* locus in GM-CSF-derived macrophages as measured by histone markers associated with open chromatin (Garber et al. 2012). Since *Irf5* transcription is induced by GM-CSF and IFN-γ, it is likely regulated by members of the JAK/STAT signalling pathway as these cytokines activate STAT5 (van de Laar et al. 2012) and STAT1/2, respectively (Hu and Ivashkiv 2009) (Figure 3.14Figure 3.14. Transcription of *Irf5* is induced by GM-CSF and IFN-γ.). However, other downstream factors may be involved in regulation of the *Irf5* locus such as MAPK, PI3K, NF-κB or other IRFs (van de Laar et al. 2012, Martinez and Gordon 2014). Further experiments such as luciferase assays using plasmids containing the *Irf5* promoter region and ChIP experiments will be needed to ultimately establish the transcription factor network controlling *Irf5* expression.

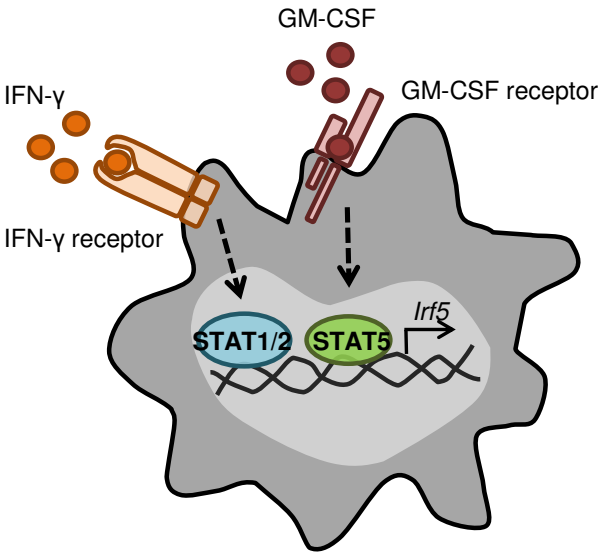

Figure 3.14. Transcription of *Irf5* is induced by GM-CSF and IFN-γ.

The pro-inflammatory stimuli GM-CSF and IFN-γ are able to induce *Irf5* transcription in *in vitro* differentiated macrophages. Activation of transcription at the gene locus is likely to be mediated by members of the STAT transcription factor family downstream of those cytokines. However, the exact mechnanisms remain to be elucidated.

4. IRF5 expression in macrophages *in vivo*

4.1. Introduction

As we observed that IRF5 is highly expressed in pro-inflammatory *in vitro* differentiated macrophages (Chapter 3), we sought to transfer these findings into an *in vivo* setting. IRF5 expression *in vivo* thus far has been detected in human lymphoid tissues and blood lymphocytes (Barnes et al. 2001), in mammary epithelial cells (Bi et al. 2011), as well as in populations of human DCs, macrophages, monocytes, NK cells and B-cells (Mancl et al. 2005, Krausgruber et al. 2011). Moreover, IRF5 expression and loss thereof has been detected in human tumours, both in primary tissues and cell lines such as breast cancer and leukaemia (Mori et al. 2002, Barnes et al. 2003, Li et al. 2008, Bi et al. 2011). In mice, splenic macrophages and DCs have been shown to express IRF5 (Takaoka et al. 2005), however it remains unknown to what extent this depends on the tissues or environmental context. Furthermore, $IRF5^+$ cells were detected in lungs following HDM stimulation in a murine asthma model (Draijer et al. 2013). Recently, Ericson et al. detected expression of *Irf5* mRNA in neutrophil data sets generated by the ImmGen consortium (Ericson et al. 2014). IRF5 was moreover highlighted as a TF expressed in microglia and perivascular macrophages of the normal brain (Zeisel et al. 2015). There is also some evidence regarding IRF5 expression in macrophages in the context of different disease models such as spinal microglia in neuropathic pain (Masuda et al. 2014), macrophages in adipose tissue during obesity (Dalmas et al. 2015) and myocardial macrophages following infarcts (Courties et al. 2014).

Macrophages play a key role in autoimmune diseases such as RA, a degenerative disease characterised by joint inflammation and bone destruction

(Kennedy et al. 2011). At the site of inflammation, macrophages are present in high numbers and their depletion ameliorates disease severity (Van Lent et al. 1998, Barrera et al. 2000, Smeets et al. 2001). More specifically, macrophages contribute to RA pathogenesis by secreting pro-inflammatory cytokines and thereby taking part in the Th1/Th17 response (Chabaud et al. 2001, Nistala et al. 2010). In recent years there has been a growing understanding of the heterogeneity of macrophages (Davies et al. 2013, Xue et al. 2014). The exact nature of myeloid cells in the arthritic joint as well as in other inflammatory diseases is thus a topic of major interest, as it will not only provide clues about pathogenesis but also contribute towards more effective therapeutics. The phenotype and origin of macrophages in the knee joint in the steady state or during inflammatory arthritis are not known. Recent work by Misharin et al. demonstrated that the ankle synovial lining of naïve mice consists of a heterogeneous population of macrophages, with the majority being true tissue-resident cells and about a fifth originating from the BM (Misharin et al. 2014).

Currently existing murine models of arthritis recapitulate different aspects of the human disease (Asquith et al. 2009). For example, K/BxN serum transfer induced arthritis is a mouse model of sterile inflammatory arthritis that represents only the effector part of the disease. In this model, non-classical ($Ly6C^-$) monocytes enter the joint and differentiate into classical inflammatory macrophages to drive joint pathology (Misharin et al. 2014). During resolution, macrophages are ‘alternatively activated’ and thus promote resolution and repair. The situation in models of RA that involve induction as well as effector phases, or more importantly in human RA, remains to be understood. Here, we use the model of acute inflammatory AIA, which is characterised by a Th17

dependent localised inflammation in the knee joint (Egan et al. 2008). AIA relies on subcutaneous immunisation with mBSA plus CFA, followed by intra-articular injection of mBSA into the knee joint seven days later. In response to the antigen challenge, infiltration of polymorphonuclear and mononuclear cells, pannus formation and erosion of bone and cartilage can be observed (Brackertz et al. 1977).

Our aim was to explore the expression pattern of IRF5 within different myeloid cell populations in the joints and other tissues as well as to profile the phenotype of IRF5-expressing macrophages in acute inflammatory arthritis.

4.2. Results

4.2.1. Ly6C^{hi} monocytes and macrophages express high levels of IRF5 in multiple tissues at steady state

To extend IRF5 expression studies beyond *in vitro* differentiated cells, we sought to investigate the expression pattern in different tissues under homeostatic conditions. A selection of tissues were obtained from naïve mice and IRF5 expression was determined focusing mainly on the myeloid populations. We chose to examine BM, blood and spleen, in addition to the lung where resident macrophage and monocyte populations as well as other myeloids such as neutrophils are present. BM and blood contain large numbers of haematopoietic cells, especially monocytes that can give rise to some tissue-resident macrophages and infiltrating inflammatory macrophages/DCs (Ginhoux and Jung 2014). The spleen is a lymphoid organ mainly consisting of B- and T-cells but is also important for blood filtering (Mebius and Kraal 2005). However,

the spleen additionally contains a substantial monocyte reservoir and various distinct macrophage populations (den Haan and Kraal 2012). The lung is not only a respiratory organ but also a large mucosal site that is continuously exposed to inhaled pathogens and particles. Thus, the lung possesses a network of myeloid cells involved in immune surveillance, such as two discrete resident macrophage subsets, termed interstitial macrophages and alveolar macrophages, respectively (Hussell and Bell 2014, Byrne et al. 2015).

Tissues were collected from WT animals and cell populations were analysed for IRF5 expression using flow cytometry. Levels of IRF5 expression were quantified using MFI and normalised to stained IRF5$^{-/-}$ samples. All samples were stained for CD45 and live cells as well as for panels assessing mainly myeloid but also partially other cell populations that are described in detail in the sections below.

Bone marrow

BM cells were isolated from tibiae and femurs and analysed using flow cytometry for expression of the markers CD11b, F4/80, CD64, Ly6C and Ly6G, respectively. We identified macrophages based on F4/80 and CD64 expression, as both monocytes and neutrophils lacked these markers (see 1.2.1 section Nomenclature and identification). Monocytes were Ly6C$^{hi/lo}$, whereas neutrophils were Ly6G^{+}, as in previous experiments (chapter 3.2). Expression of IRF5 was absent in CD45^{-} cells but expressed by all myeloid subsets analysed (Figure 4.1A). Within those, Ly6C^{hi} monocytes showed the highest level of IRF5 expression (MFI 557.3±41.7), which was increased by 2-3 fold compared to Ly6C^{lo} monocytes or macrophages (147.7±34.3 or 202.5±51.3, p≤ 0.0001 or p≤

0.001 respectively). Neutrophils on the other hand only expressed negligible amounts of IRF5 but were more abundant than macrophages and Ly6C^{lo} monocytes.

Blood

Whole blood was collected from mice and samples were stained for the markers CD11b, F4/80, CD64, Ly6C and Ly6G as above. In addition, we stained for CD19 to identify B-cells and MHC II and CD11c to identify DCs. The Ly6C^{hi} monocyte subset again expressed the highest levels of IRF5 (MFI 2532.9±310.7, $p \leq 0.05$ at least compared to other cell types), displaying levels twice as high as the Ly6C^{lo} subset (1032.2±130.8) (Figure 4.1B). In CD11b^{+} DCs observed levels were comparable to Ly6C^{lo} monocytes, whereas neutrophils in the blood expressed very little IRF5 (152.3±57.6). Macrophages are by definition absent from the blood stream as they are only found within tissues (Ginhoux and Jung 2014). Here, B-cells were also examined and showed IRF5 expression as expected, although considerably lower than monocytes and DCs reaching a value of 647.3±133.3. About half of the live haematopoietic cells in the blood were B-cells while DCs, monocytes and neutrophils together represented below 10% of CD45^{+} live cells.

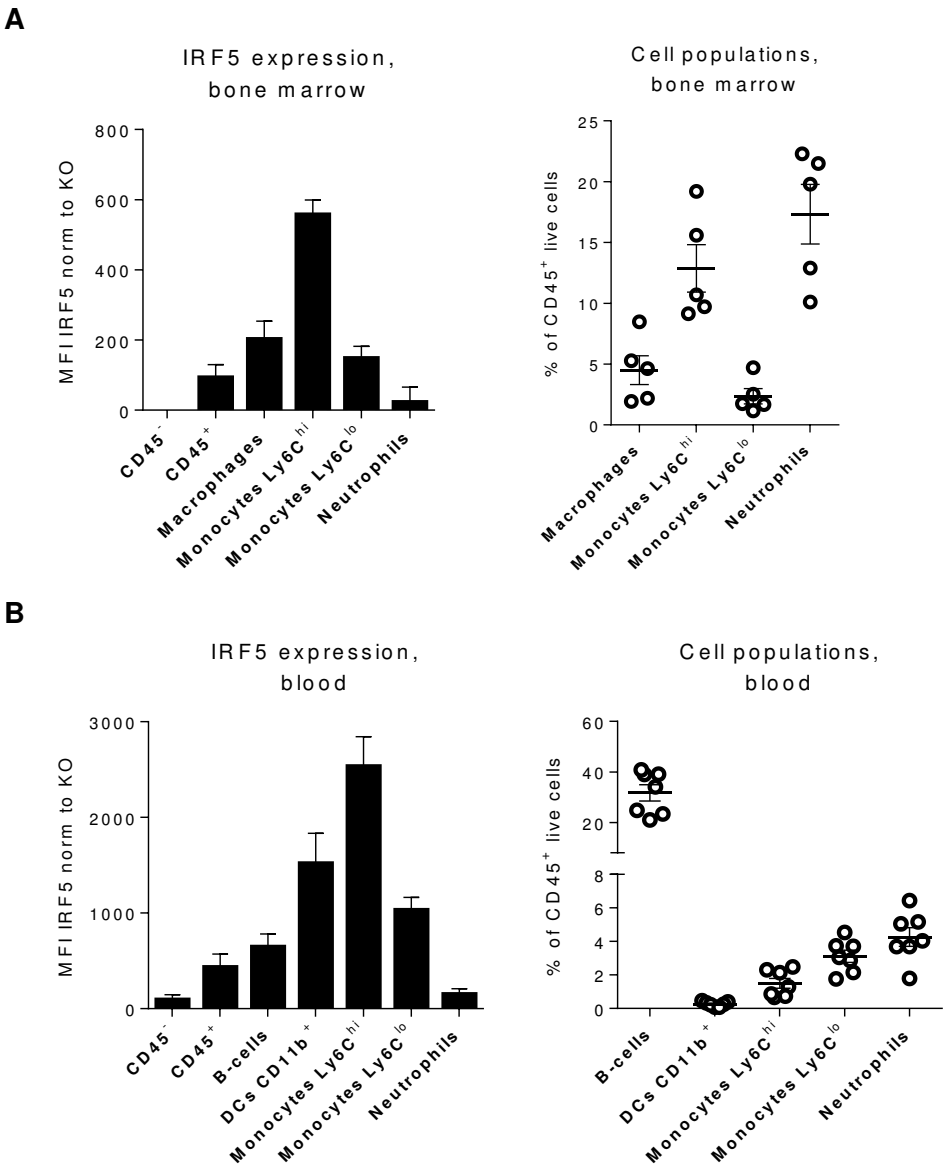

Figure 4.1. Monocytes are the major IRF5-expressing cells in the BM and blood of naïve mice.

Whole BM was isolated from femurs and tibias of naïve WT mice. Whole blood was collected from naïve WT mice and erythrocytes were lysed prior to staining. Cells were analysed by FACS for expression of the surface markers CD45, CD11b, F4/80, CD64, Ly6C and Ly6G as well as intracellular IRF5. All cell populations were gated on $CD45^+$ live. IRF5 expression was quantified by calculating the MFI of each cell type and normalised by subtracting the IRF5 KO MFI values. **A.** In the BM, macrophages were defined as $CD11b^+$ $CD64^+$ $F4/80^+$, monocytes as $CD11b^+$ $F480^-$ $Ly6C^{hi/lo}$ and neutrophils as $CD11b^+$ $F4/80^-$ $Ly6G^+$. Error bars represent the SEM of n=5. **B.** The FACS panel used for blood additionally contained the markers CD19, Siglec F, CD11c and MHC II. Siglec F was used to exclude eosinophils. B-cells were defined as $CD19^+$ MHC II^+. All myeloid cells were $CD11b^+$ but negative for CD19, Siglec F and Ly6G, except for $Ly6G^+$ neutrophils. DCs were identified as double positive MHC II^+ $CD11c^+$. Two populations of monocytes can be found in the blood and they are distinguished based on their differential Ly6C expression. Macrophages do not enter the circulation and are thus absent in blood. Error bars represent the SEM of n=7.

Spleen

Spleens were excised from healthy animals and were subjected to flow cytometric analysis. The same FACS panel was used as for blood, consisting of CD11b, F4/80, CD64, Ly6C, Ly6G, CD19, CD11c and MHC II. Next to large B- and T-cell populations, the spleen also consists of monocytes, DCs and different types of macrophages. Macrophages differ in their expression of CD11b and were defined as $CD11b^-$ red pulp macrophages or $CD11b^+$ macrophages (Mitchell et al. 2010). The highest levels of IRF5 were detected in the $Ly6C^{hi}$ monocyte subset followed by $CD11b^+$ DCs which still expressed more than 50% less (622.4±78.1 vs 245.4±28.1, $p \leq 0.0001$ compared to all populations). Similar levels were observed for $CD11b^-$ DCs, $CD11b^+$ macrophages, $Ly6C^{lo}$ monocytes and neutrophils, which all expressed moderate levels of around MFI 100 (Figure 4.2A). B-cells showed some IRF5 expression (53.6±17.8) although again lower than most myeloid populations, except red pulp macrophages that only displayed little expression (15.1±8.7). As expected B-cells represented the most abundant cell population in the spleen (50% of $CD45^+$ live) while the percentage of myeloid cells ranged from 0.2-4.5%. Within those, macrophages and monocytes were present at greater numbers than DCs and neutrophils.

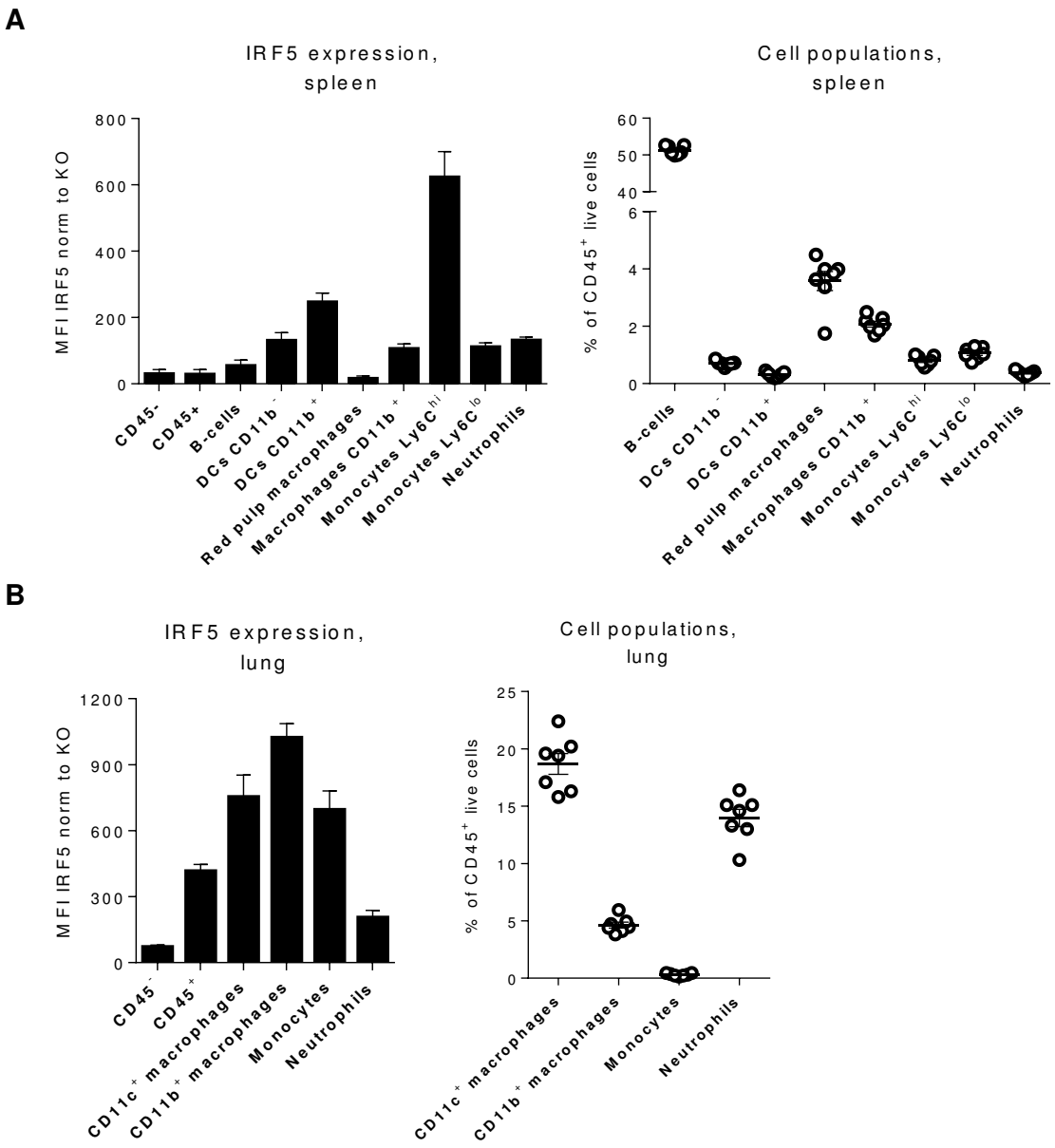

Figure 4.2. Monocytes and macrophages are the main IRF5-expressing cells in naïve spleens and lungs.

Spleens were excised from naïve WT mice and subjected to red blood cell lysis. Cells from whole lungs were isolated using tissue digestion. Cells were analysed by FACS for expression of the surface markers CD45, CD11b, CD11c, F4/80, CD64, Ly6C and Ly6G as well as intracellular IRF5. All samples were first gated on $CD45^+$ live. IRF5 expression of each cell type was quantified using MFI and normalised by subtraction of IRF5 KO MFI values. **A.** The staining panel used for spleens contained the additional markers CD19, Siglec F and MHC II. Siglec F was used to exclude eosinophils. B-cells were $CD19^+$ MHC II^+. All myeloid cells were negative for CD19, Siglec F and Ly6G, except neutrophils which are $Ly6G^+$. DCs were identified as $F4/80^-$ $CD64^-$ $CD11c^+$ MHC II^+ and either $CD11b^+$ or $CD11b^-$. Red pulp macrophages were defined as $CD11b^-$ $F4/80^+$ $CD64^+$ while other macrophages were $CD11b^+$ $Ly6C^-$ $CD64^+$ $F4/80^+$. The two monocyte populations present are distinguished based on their differential Ly6C expression. **B.** Two populations of macrophages can be found in the lung, both express CD64 and F4/80 but not Ly6C. They are distinguished based on their differential

CD11b and CD11c expression. Alveolar macrophages express high levels of CD11c while interstitial macrophages highly express CD11b. Monocytes are defined as $CD11b^{+}$ $F480^{dim}$ $Ly6C^{hi}$. Macrophages and monocytes were all $Ly6G^{-}$. Neutrophils were defined as $CD11b^{+}$ $Ly6G^{hi}$.
Error bars represent the SEM of n=7.

Lung

Whole lungs were collected from animals under steady state conditions and analysed using flow cytometry. The markers chosen were CD11b, F4/80, CD64, Ly6C, Ly6G, CD11c and MHC II. The two macrophage subsets in the lung are $F4/80^{+}$ $CD64^{+}$ but differ in their expression of CD11b and CD11c and are identified as $CD11b^{+}$ interstitial and $CD11c^{+}$ alveolar macrophages, respectively (Misharin et al. 2013). These cells were the major IRF5-expressing cell types present in the lung and $CD11b^{+}$ macrophages displayed similar levels as $CD11c^{+}$ macrophages (MFI 1022.3±64.1 and 752.8±99.7 respectively, Figure 4.2B). Both macrophage subsets express significantly more IRF5 than neutrophils (204.0±33.2, $p \leq 0.0001$). $Ly6C^{hi}$ monocytes, on the other hand show IRF5 levels comparable to $CD11c^{+}$ macrophages (694.5±85.9) but significantly lower than $CD11b^{+}$ macrophages ($p \leq 0.05$). Monocytes were the least abundant (0.3% of $CD45^{+}$ live cells), followed by interstitial macrophages reaching 4.6% while alveolar macrophages and neutrophils were present in greater numbers (18.7% and 13.9%).

Taken together, these data show that *in vivo* $Ly6C^{hi}$ monocytes and macrophages express the highest levels of IRF5, in several different tissues. Nevertheless, other myeloid cells such as DCs and, to a lower extent, neutrophils also express IRF5. We also confirmed IRF5 expression in B-cells.

4.2.2. Mice develop characteristics of arthritis in mBSA challenged knees

In order to explore expression of IRF5 and inflammatory macrophages in a disease setting, we utilised the murine model of antigen-induced arthritis. WT mice were immunised with mBSA in CFA and after seven days arthritis was induced by intra-articular injection of mBSA (affected knee) or PBS (control knee) (see 2.2.2, Antigen-induced arthritis). Seven days after antigen challenge, affected and control knees were collected and subjected to histological analysis to verify the previously described disease pathology (Lawlor et al. 2001). Knee joints challenged with PBS show no signs of disease as indicated by intact bone structures, a clear joint space and a thin synovial membrane consisting of 1-2 cell layers (Figure 4.3). Joints that were injected with mBSA however displayed clear indications of arthritis. We could observe areas of bone erosion, visible thickening of the synovial membrane, massive cellular infiltrate and exudate in the joint space. We could therefore confirm that during AIA WT mice develop arthritic disease in the antigen-challenged but not in the control knee.

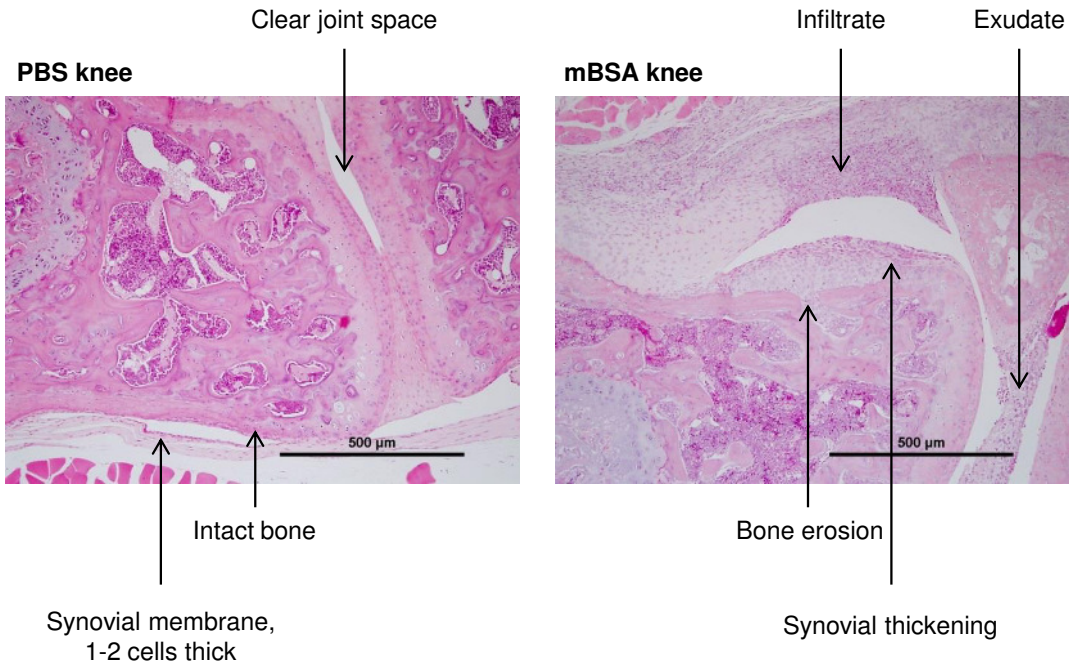

Figure 4.3. Intra-articular mBSA injection causes arthritic pathology in the knee.

WT mice were immunised s.c. with mBSA and subjected to intra-articular challenge with mBSA or PBS as control seven days later. Mice were sacrificed on day seven of disease and knees were collected for histological analysis. Representative image of an mBSA knee show key characteristics of AIA pathology in comparison to a PBS control knee. Features of a healthy control knee are indicated on the left hand side. Signs of disease in an arthritic mBSA knee such as synovial thickening, leukocyte infiltration into the joint space and bone erosion are indicated on the right hand side. Images courtesy of Katrina Blazek (Udalova laboratory).

4.2.3. Gating strategy of myeloid cell types in the knee

To analyse myeloid cell populations in AIA, mice were first immunised and challenged with mBSA seven days later. Arthritic mBSA and PBS control knees were harvested two days after injection and subjected to FACS analysis. Gating of myeloid cell populations was performed as follows: First, samples were gated for $CD45^+$ haematopoietic live cells and were then plotted with regards to their CD11b and F4/80 expression. $CD11b^+$ $F4/80^{hi}$ cells were identified as macrophages that were further analysed for expression of CD64, Ly6C, MHC II and CD206 (Figure 4.4).

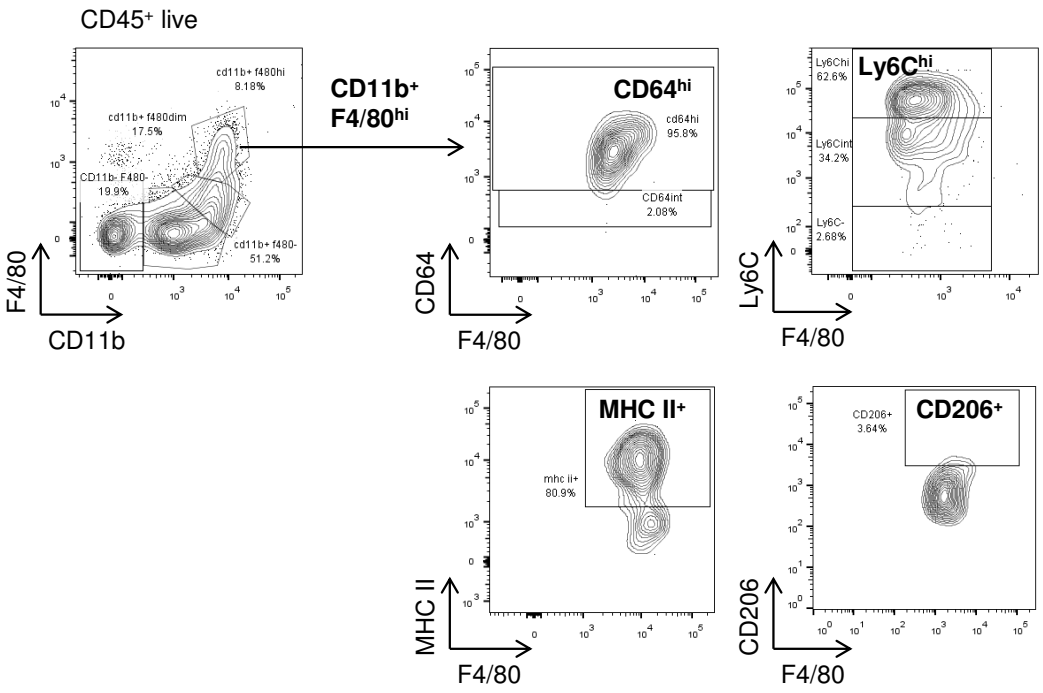

Figure 4.4. Gating strategy used to identify macrophage populations in the inflamed knee.

Images show representative plots of mBSA challenged joints collected at day two of AIA. A viability dye was used to exclude dead cells from the analysis. All samples were first gated on haematopoietic CD45$^+$ live cells. Gates were set based on FMO (fluorescence minus one) controls excluding any background staining or autofluorescence. Macrophages were defined as CD11b$^+$ F4/80^{hi} and then analysed for expression of CD64, Ly6C, MHC II and CD206.

The population of CD11b$^+$ F4/80^{dim} cells was defined as monocytes, almost entirely expressing Ly6C at different levels (Figure 4.5A). Neutrophils were part of the CD11b$^+$ F4/80$^-$ population within which they were specifically identified by high levels of Ly6G (Figure 4.5B). In some experiments, activated neutrophils were distinguished by pro-IL1β staining.

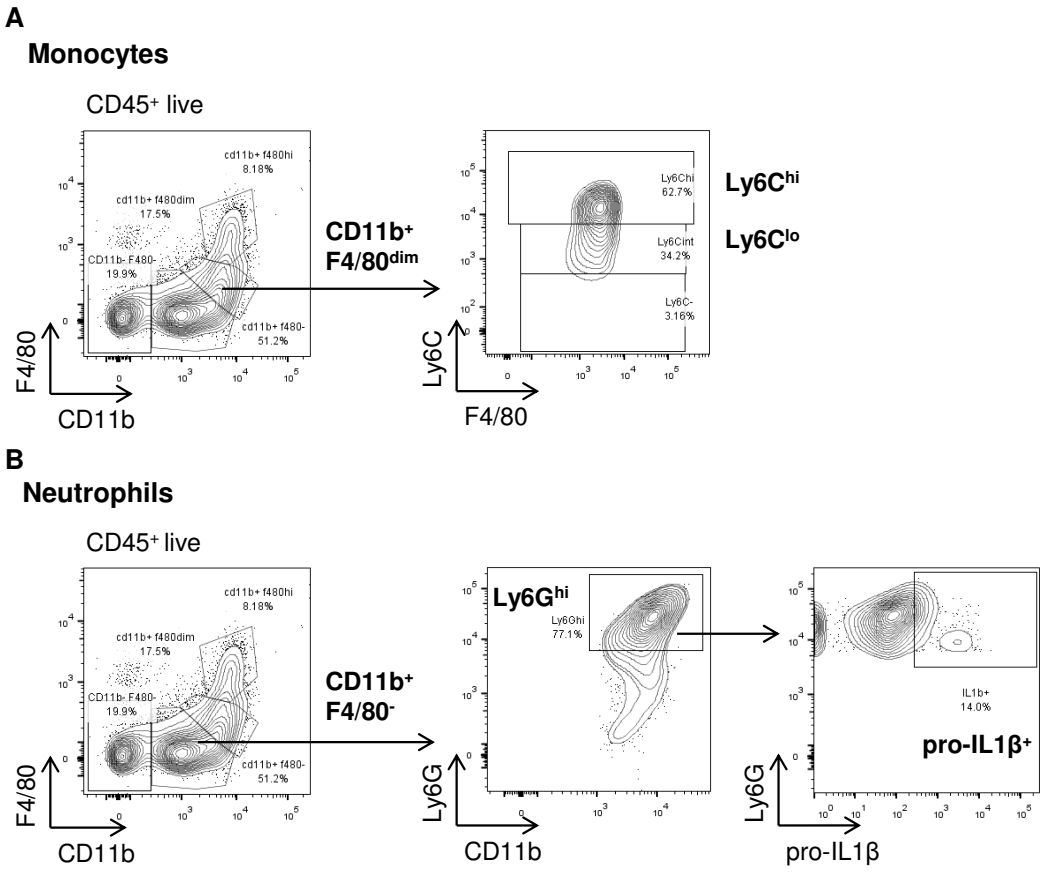

Figure 4.5. Gating strategy applied to detect monocytes and neutrophils in the challenged knee joint.

Plots are representative for mBSA knees collected at day two of AIA. Using a viability dye, dead cells were excluded from the analysis. All samples were gated on haematopoietic CD45$^+$ live cells before sub-gating. FMO controls were used to set all gates. Monocytes were defined as CD11b$^+$ F4/80^{dim} and Ly6C expression was analysed. Neutrophils were generally defined as CD11b$^+$ F4/80$^-$ Ly6G^{hi} and pro-IL1β allowed for identification of activated neutrophils.

Lastly, DCs were identified based on the expression of CD11c within the CD11b$^+$ F4/80$^-$ or CD11b$^-$ F4/80$^-$ gates (Figure 4.6).

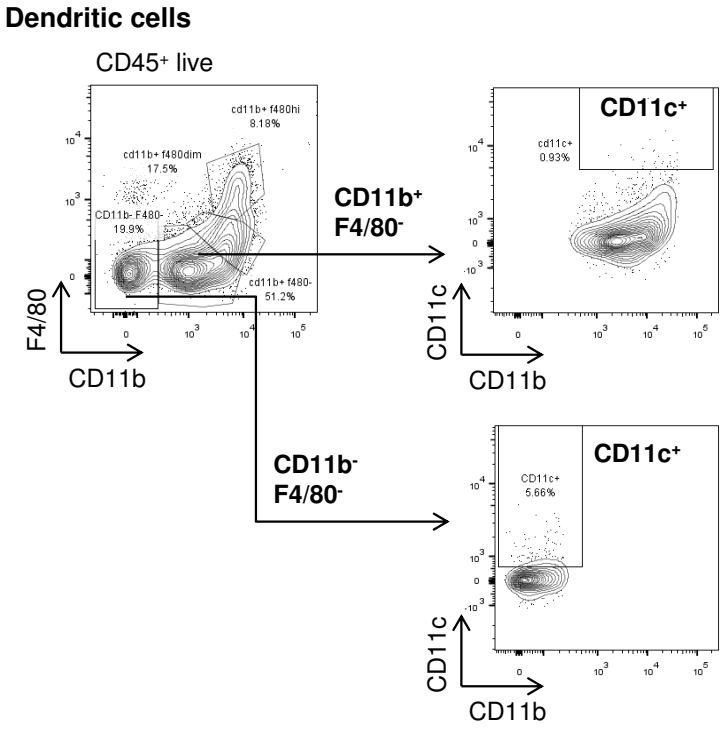

Figure 4.6. Representative FACS plots for the DC gating strategy.

Images shown are from mBSA knees collected after two days of AIA. Samples were gated on haematopoietic CD45$^+$ live cells prior to further gating. Gates were set based on background staining in FMO controls. Two DC populations were identified based on their CD11c expression in either the CD11b$^+$ F4/80$^-$ or CD11b$^-$ F4/80$^-$ gates.

4.2.4. Infiltration of monocytes and pro-inflammatory macrophages into the inflamed knee during AIA

Ly6C$^+$ monocytes and macrophages are recruited upon mBSA challenge

First, we investigated the monocyte and macrophage populations that are recruited into the knee upon mBSA challenge. Mice underwent AIA and both challenged and control knees were harvested two days after intra-articular injection and subsequently subjected to FACS analysis. As both Ly6C and CD64 can be used to establish macrophage identity (Gautier et al. 2012,

Epelman et al. 2014), we characterised monocytes and macrophages in the joint with regards to Ly6C and CD64 expression.

When comparing PBS and mBSA knees, a significant increase in monocyte numbers can be observed. Ly6C was expressed on 88% of all monocytes in the knee joints of challenged mice and about 55-60% of those were $Ly6C^{hi}$ (Figure 4.7A). The proportions of Ly6C expression within monocytes remained unaltered by inflammation.

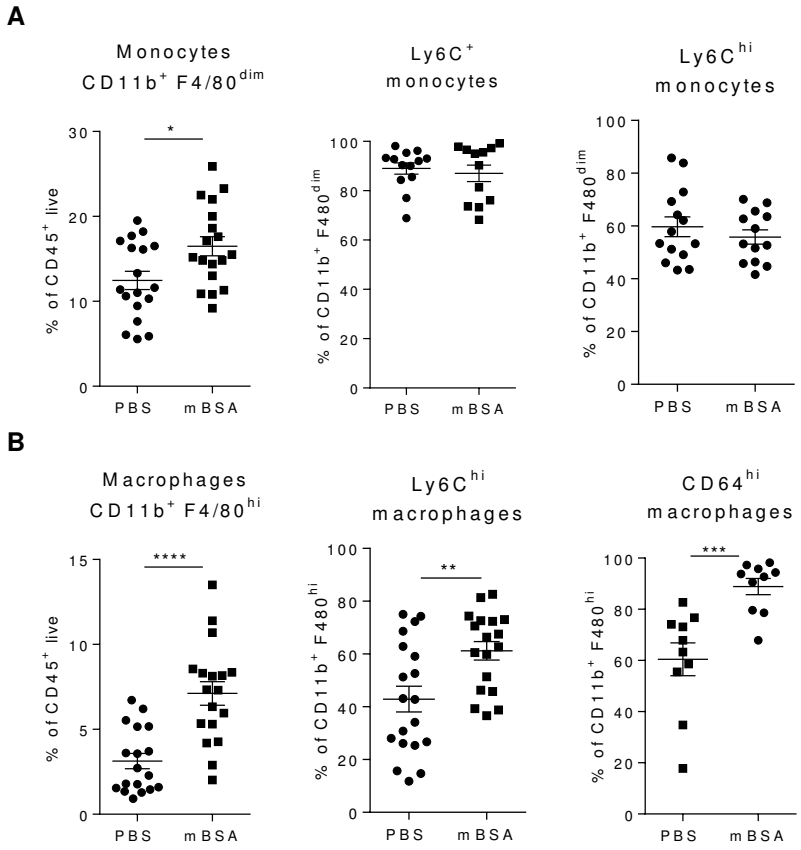

Figure 4.7. Ly6C^{hi} monocytes accumulate in the knee upon challenge and infiltrating macrophages display high expression of Ly6C and CD64.

WT mice were immunised with mBSA and subjected to intra-articular challenge with mBSA or PBS control seven days later. Knees were collected at day two of disease and stained for flow cytometry using antibodies against CD45, CD11b, F4/80, Ly6C and CD64. Ly6C and CD64 were used to examine the phenotype of CD11b^{+} F4/80^{hi} macrophages. All cells were first gated on CD45^{+} live. **A.** Monocytes were defined as CD11b^{+} F4/80^{dim} and then analysed for their Ly6C expression, shown as percentage of all monocytes. **B.** Macrophages were defined as CD11b^{+} F4/80^{hi} and examined regarding their Ly6C and CD64 expression. Ly6C and CD64 are expressed as a proportion of all macrophages.
Error bars represent the SEM of n=10-18. Statistical analysis performed throughout by one-tailed Mann-Whitney U test. * p≤0.05; ** p≤0.01; *** p≤ 0.001

Two days after antigen challenge, we also observed a significant increase in the number of CD11b^{+} F4/80^{hi} macrophages compared to PBS joints (Figure 4.7B). Similarly to monocytes, 61% of macrophages in the challenged knee are Ly6C^{hi} although this was increased significantly from 43% in control joints. In addition, 60% of macrophages in PBS treated knees and 90% of macrophages in the mBSA injected knees were CD64^{hi}.

These data demonstrate that the majority of monocytes that enter the knee during AIA are Ly6C^{hi}. Moreover, we could show that macrophages in inflamed joints retain high Ly6C expression and additionally are almost entirely CD64^{hi}.

Expression of pro-inflammatory markers increases in the inflamed knee

Next, we aimed to characterise the inflammatory phenotype of macrophages present during inflammation in the joint. Knee joints were harvested from mice on day two of AIA and subjected to flow cytometry as described in 2.3.2. Macrophage subsets were characterised by staining for MHC II (pro-inflammatory) and CD206 (anti-inflammatory). In addition, RNA was isolated from knees to study mRNA levels of *Irf5* and macrophage markers at the site of inflammation. The chosen markers were *Nos2* (iNOS) and *Fizz1* (Retln1a) associated with pro- and anti-inflammatory macrophages respectively (MacMicking et al. 1997, Gordon and Martinez 2010).

The percentage of pro-inflammatory MHC II^{+} macrophages was significantly increased in affected knees compared to control knees (Figure 4.8A). In contrast, the percentage of CD206^{+} macrophages was found to be significantly reduced after antigen challenge. In concurrence with surface marker expression, analysis of whole knee RNA extracts revealed that the expression of *Nos2* was significantly higher in mBSA injected knees whereas *Fizz1* expression was diminished (Figure 4.8B). Simultaneously, transcript levels of *Irf5* were significantly augmented in affected knees.

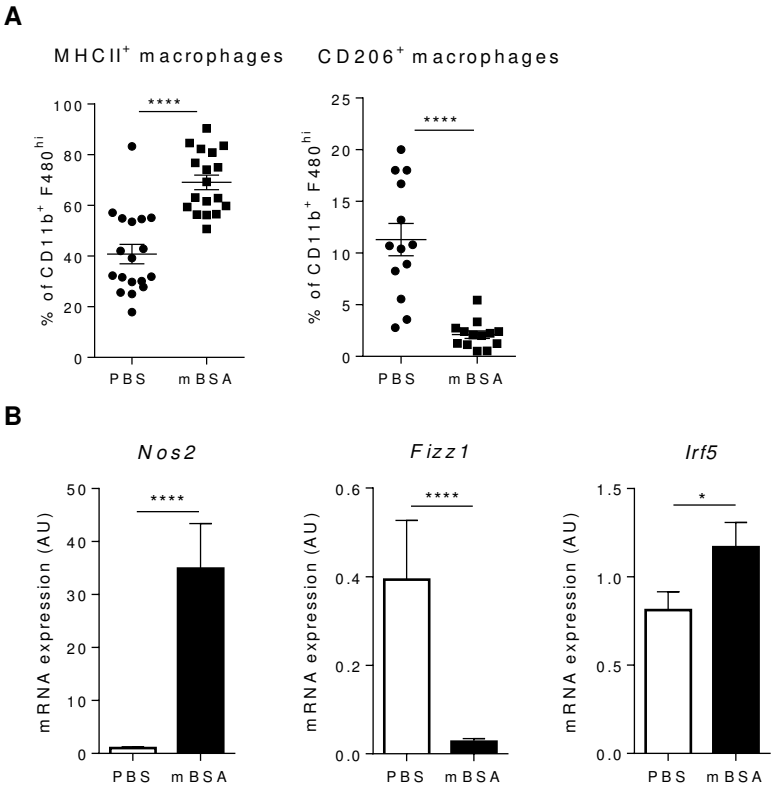

Figure 4.8. Pro-inflammatory macrophages accumulate at the site of inflammation in a mouse model of arthritis.

Mice were immunised with mBSA in CFA prior to intra-articular injection of mBSA or PBS control. Knees were collected at day two of disease. **A.** Cell suspensions obtained from whole knees were stained for flow cytometry analysis with antibodies against CD45, CD11b, F4/80, CD206 and MHC II. CD206 and MHC II are expressed as a percentage of macrophages, $CD11b^{+}$ $F4/80^{hi}$. **B.** Total RNA was isolated from whole knees and analysed by Real-time PCR for transcript expression of *Irf5*, *Nos2* and *Fizz1*. RNA was derived from experiments conducted by Katrina Blazek (Udalova laboratory).
Error bars represent the SEM of n=13-18. Statistical analysis performed throughout by one-tailed Mann-Whitney U test. * p≤0.05; ** p≤0.01; *** p≤ 0.001; **** p≤0.0001

Taken together, these results indicate that there is an increased amount of pro-inflammatory macrophages at the site of inflammation, which correlates with an increase in *Irf5* mRNA. These results also demonstrate that a number of macrophages did not fit into either category.

4.2.5. The main IRF5-expressing cells in the challenged joint are macrophages and Ly6C^{hi} monocytes

To specifically establish the cell populations in the knee that express IRF5, mBSA and PBS knees were collected at day two of disease and analysed using FACS as detailed above (Section 2.3.2). IRF5 staining was assessed within each cell type by two means: 1) MFI was used to quantify expression levels (Figure 4.9A) and 2) the percentage of positive cells was determined to identify the cells that display the largest IRF5^{+} proportion (Figure 4.9B).

In control knees, the highest levels of expression were found in Ly6C^{hi} monocytes and macrophages (MFI 939.2±83.2 and 605.7±111.6) (Figure 4.9A). They expressed similar levels of IRF5 that were significantly higher than those in neutrophils (40.5±17.5) and CD11b^{+} DCs (90.5±92.8). Ly6C^{lo} monocytes (170.4±32.9) and CD11b^{-} DCs (198.2±59.1) expressed intermediate levels that were significantly lower than Ly6C^{hi} monocytes but not macrophages. Upon antigen challenge, an overall increase of expression within haematopoietic cells could be observed, which was mainly due to the significantly augmented IRF5 levels in macrophages. Levels were increased by two fold to as high as in Ly6C^{hi} monocytes, while other cells only showed slight changes in expression if any. Thus in the inflamed knee, macrophages and Ly6C^{hi} monocytes expressed significantly more IRF5 than any other cell type ($p \leq 0.0001$). Of note, levels measured in the CD45^{-} population (likely to contain epithelial and stromal cells), were negligible and not affected by mBSA challenge.

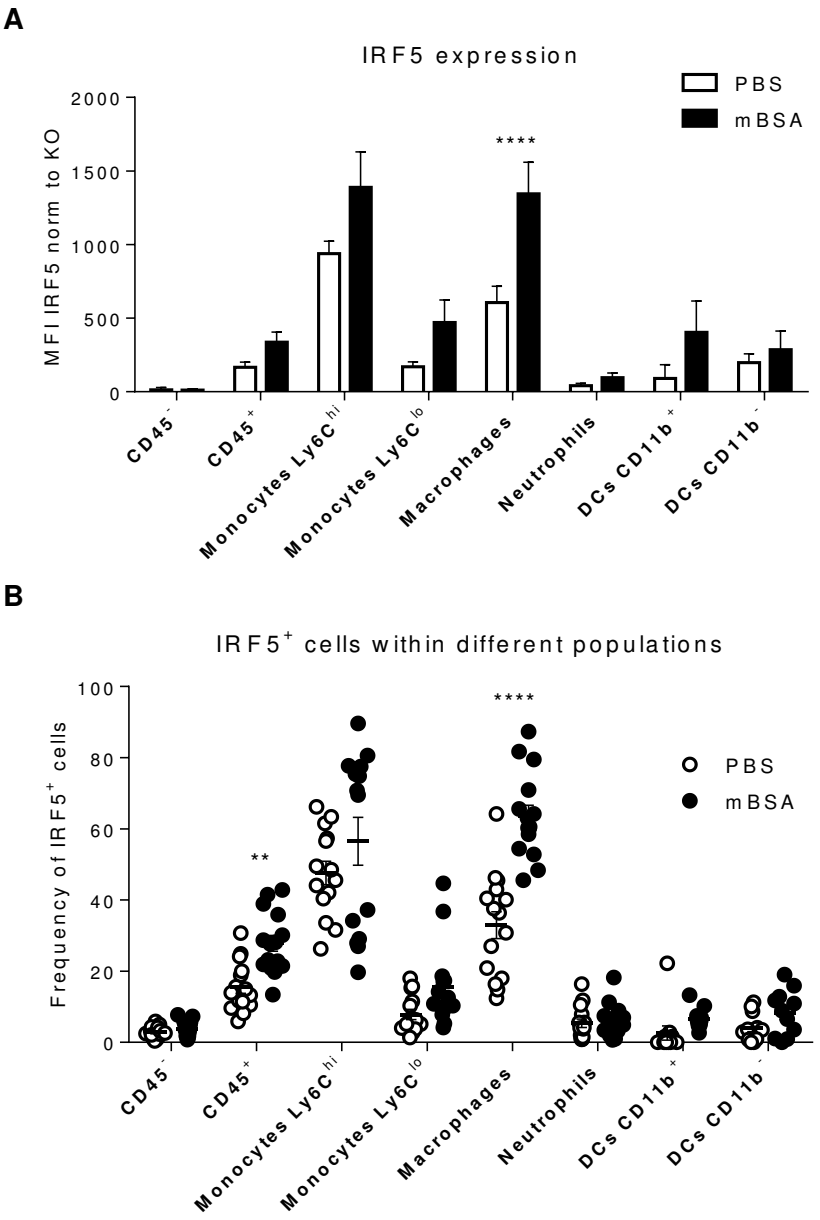

Figure 4.9. IRF5 expression is highest in Ly6C^{hi} monocytes macrophages and induced upon mBSA challenge in the knee.

Arthritic and control knees were harvested from WT mice two days after intra-articular challenge. Cell suspensions were created by digesting the knee tissues prior to FACS staining. Liberated cells were analysed for the surface markers CD45, CD11b, F4/80, Ly6C, Ly6G and CD11c as well as for intracellular IRF5. All cell populations were gated on CD45$^+$ live. Macrophages were defined as CD11b$^+$ F4/80^{hi} and monocytes as CD11b$^+$ F4/80^{dim} Ly6C$^{hi/lo}$. Neutrophils are CD11b$^+$ F480$^-$ Ly6G$^+$. DCs were CD11c$^+$ F4/80$^-$ and either CD11b$^+$ or CD11b$^-$. **A.** Levels of IRF5 were quantified by MFI of each cell type and normalised to stained IRF5 KO cells by subtracting IRF5 KO MFI values from IRF5 WT samples. **B.** The percentage of IRF5 expressing cells was determined within each of the populations indicated.
Error bars represent the SEM of n=11-15. Statistical analysis performed by 2-way ANOVA and Bonferroni's multiple comparison. ** p≤0.01; **** p≤0.0001

The largest proportion of IRF5$^+$ cells in PBS knees was found within Ly6C^{hi} monocytes, where 47.6%±3.3 cells expressed IRF5. The next highest proportion of IRF5-expressing cells was observed in macrophages (32.9%±3.8) and this proportion was significantly less than in Ly6C^{hi} monocytes ($p \leq 0.01$) (Figure 4.9B). In contrast, only a small fraction of Ly6C^{lo} monocytes, neutrophils and DCs, respectively, expressed IRF5 (in the range of 2-7%). Following mBSA injection, the number of IRF5-expressing cells doubled in macrophages so that circa 66% of macrophages were IRF5$^+$. However, the proportion of Ly6C^{hi} IRF5$^+$ monocytes was only slightly increased, amounting to just over half of the population. While there was no increase in the proportion of neutrophils that expressed IRF5, there was a minor rise in IRF5$^+$ DCs and Ly6C^{lo} monocytes although not statistically significant. About 3% of CD45$^-$ cells were positive for IRF5 but this remained unaltered by inflammatory conditions.

In conclusion, during inflammation, Ly6C^{hi} monocytes and macrophages are the predominant IRF5-expressing cells in the joint. Upon antigen challenge, macrophages show the biggest increase in both per-cell expression as well as proportions of IRF5$^+$ cells, whereas monocytes only show minor alterations in IRF5 expression.

4.2.6. Synovial macrophages express high levels of CX_3CR1

We next sought to further characterise the myeloid populations such as monocytes and macrophages recruited to the inflamed joint. We used $CX_3CR1^{+/GFP}$ mice in which monocytes, especially the circulating Ly6C^{lo} subset, and some DCs are marked by GFP expression (Jung et al. 2000, Geissmann et al. 2003). Moreover, CX_3CR1 expression is characteristic for microglia, the

resident macrophages of the brain that are derived exclusively from embryonic precursors (Ginhoux et al. 2010). However, not all tissue-resident macrophages express CX_3CR1 (Yona et al. 2013) and expression levels in synovial resident cells are not known. Hence, $CX_3CR1^{+/GFP}$ animals underwent AIA and were sacrificed on day two to investigate expression levels.

First, the number of GFP^+ cells within monocytes and macrophages (defined as $F4/80^{dim}$ $Ly6C^{hi/lo}$ and $F4/80^{hi}$ as before, Figure 4.10A) was determined. 30-35% of monocytes and 60% of macrophages expressed CX_3CR1 in control joints. The relative number of GFP^+ macrophages was comparable in PBS and mBSA knees. In both monocyte subsets however, there was a shift towards higher numbers of GFP-expressing cells following antigen challenge, so that almost half of the cells were GFP^+. Analysis of the CX_3CR1-GFP expression levels revealed that macrophages (in red) displayed a more uniform expression of GFP in comparison to monocytes (in blue) (Figure 4.10B). Both $Ly6C^{hi}$ and $Ly6C^{lo}$ monocytes displayed a wider distribution of fluorescence intensity.

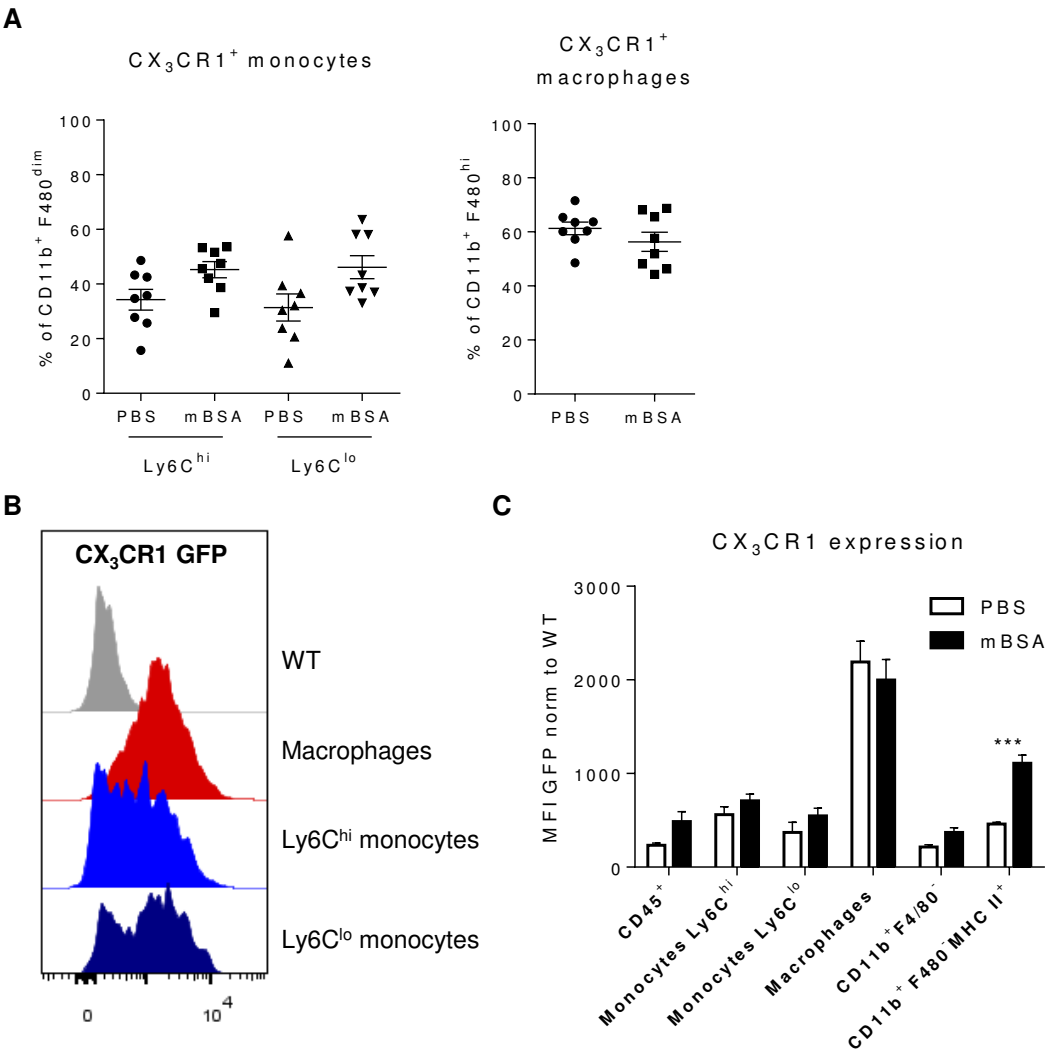

Figure 4.10. Macrophages in the knee express high levels of CX_3CR1.

$CX_3CR1^{+/GFP}$ mice were immunised with mBSA followed by intra-articular challenge with mBSA or PBS control seven days later. Knees were collected at day two of disease and analysed using flow cytometry with antibodies against CD45, CD11b, F4/80, Ly6C and MHC II. CX_3CR1 expressing cells were identified by GFP staining which was absent in WT mice. All cells were first gated on $CD45^+$ live. Monocytes were defined as $CD11b^+$ $F4/80^{dim}$ $Ly6C^{hi/lo}$ and macrophages were defined as $CD11b^+$ $F4/80^{hi}$. **A.** The percentage of CX_3CR1^+ cells was determined in all monocytes and macrophages. **B.** GFP expression was analysed in those cells in mBSA knees and is shown as a histogram. WT background levels are in grey, macrophages in red and monocytes are shown in shades of blue. **C.** Levels of CX_3CR1 were quantified using MFI and normalising it to WT background values by subtracting the WT MFI. The $CD11b^+$ $F4/80^-$ population contains both neutrophils and DCs, however the $CD11b^+$ $F4/80^-$ MHC II^+ gate was used as a proxy for DCs in the absence of CD11c in this panel. Error bars represent the SEM of n=8. Statistical analysis performed by 2-way ANOVA and Bonferroni's multiple comparison. *** $p \leq 0.001$

We next quantified the expression levels within monocytes, macrophages and CD11b^{+} F4/80^{-} (MHC II^{+}) populations (Figure 4.10C). Macrophages showed the greatest level of expression, which was significantly higher than any other cell type ($p \leq 0.0001$) in both control and inflamed joints (MFI 2190.4±221.9 and 1999.9±217.8). Of note, monocyte subsets in the knee displayed similar levels of GFP expression (Ly6C^{hi} 560.7±83.7 vs Ly6C^{lo} 371.0±108.6) that did show some increase, yet no significant changes, upon inflammation. In general, levels of GFP remained unaffected upon challenge in the majority of cell populations, with the exception of CD11b^{+} F4/80^{-} MHC II^{+} cells. In those, levels increased by two fold and reached the second highest expression levels (1110.7±85.9). DCs are the most likely contributors to this increase in GFP expression because they have been shown to express high levels of CX_3CR1, whereas neutrophils are CX_3CR1^{-} and do not usually express MHC II (Jung et al. 2000).

In conclusion, we have determined that in the inflamed joint, macrophages, rather than monocytes, are the predominant CX_3CR1-expressing cell.

4.2.7. CCR2^{+} monocytes give rise to inflammatory synovial macrophages

To elucidate the source of macrophages infiltrating the knee in response to mBSA challenge, AIA was performed on CCR2 deficient mice. In these mice, Ly6C^{+} monocytes fail to migrate from the BM. The influx of CD11b^{+} F4/80^{dim} monocytes and CD11b^{+} F4/80^{hi} macrophages was almost completely abolished in the mBSA challenged joints of CCR2$^{-/-}$ mice (Figure 4.11A). Furthermore, IRF5^{+} monocytes and macrophages were drastically reduced in CCR2$^{-/-}$ mice (Figure 4.11B). This was apparent in both PBS and mBSA injected knees.

Thus, the increase in macrophages, generally and also specifically in IRF5$^+$ cells, relies on infiltrating Ly6C^{hi} monocytes in antigen challenged knees.

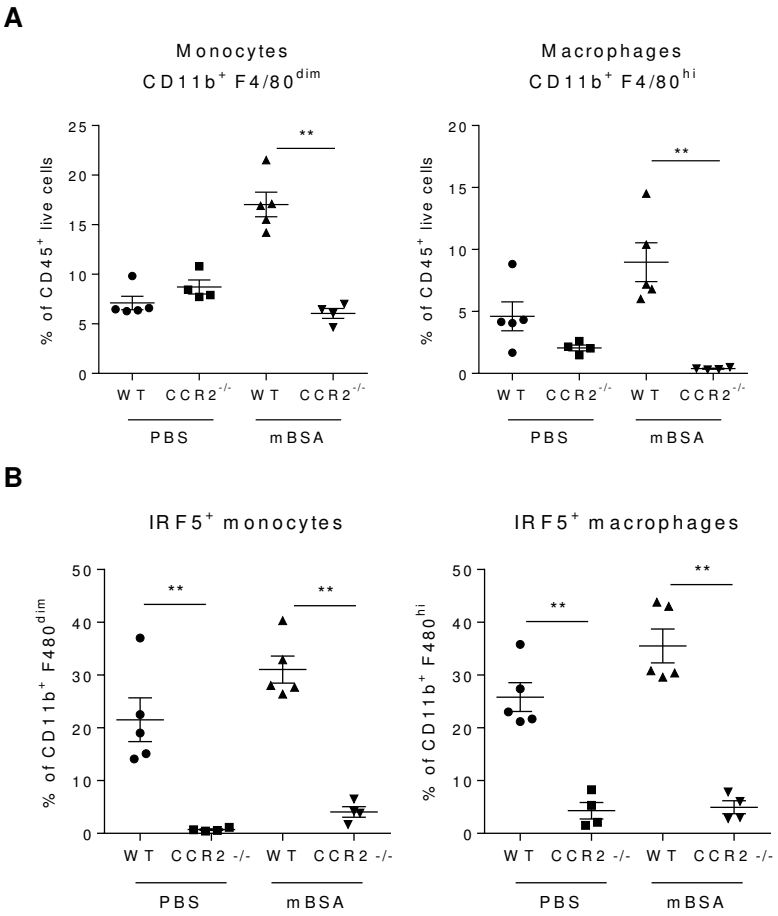

Figure 4.11. Infiltrating monocytes and macrophages are absent in CCR2$^{-/-}$ mice.

WT and CCR2$^{-/-}$ mice underwent AIA as described previously. CCR2$^{-/-}$ mice lack circulating monocytes in the blood and can be used to identify monocyte-derived cells. Inflamed and control knees were collected at day two of disease and subjected to FACS using antibodies against CD45, CD11b and F4/80. Cells were first gated on CD45$^+$ live to exclude debris and dead cells. **A.** The proportions of monocytes and macrophages in PBS and mBSA knees were determined in WT and CCR2$^{-/-}$ mice. Macrophages and monocytes are CD11b$^+$ and F4/80$^{hi/dim}$, respectively. **B.** IRF5 intracellular staining was performed to assess its expression levels within monocytes and macrophages. IRF5-expressing cells are displayed as a percentage of monocytes and macrophages.
Error bars represent the SEM of n=4-5. Statistical analysis performed throughout by one-tailed Mann-Whitney U test. ** p≤0.01

4.2.8. Macrophage populations in the mBSA injected knee are highly heterogeneous

In order to gain insight into the overall composition of cells in the inflamed knee, mass cytometry was performed using a panel of 20 markers (described in detail in 2.3.3 Mass cytometry). This panel contained basic myeloid, B-, T- and NK cell markers as well as antibodies detecting intracellular Foxp3, IFN-γ and IL-17. Pooled synovial cells derived from mBSA knees of five WT mice after two days of AIA were stained for mass cytometry and the resulting data were analysed using viSNE. The obtained cell clusters were manually assigned cellular identities based on expression of highly expressed markers (Schematic in Figure 4.12A, visual plots of myeloid related antigen expression Figure 4.12B).

The largest cluster was identified based on overall F4/80 expression although not entirely uniform, representing over a third of all cells. The second biggest cluster was $GR1^+$ and also made up about 30% of $CD45^+$ live events. 12% of the cells present in the inflamed joint consisted of $Ly6C^+$ monocytes. We also identified two MHC II^+ DC populations that were $CD11b^+$ or $CD11b^-$, representing about 3-4% each. Only minor fractions of CD19+ B-cells (<1%) and $CD3^+$ T-cells (~1%) could be detected. Although T-cells were identified using CD3, we were unable to reliably detect markers related to specific T-cell subsets such as CD69, CD25 or intracellular Foxp3, IFN-γ and IL-17. Additionally, NK cells could not be assessed as NKp46 staining was not detectable at all.

A

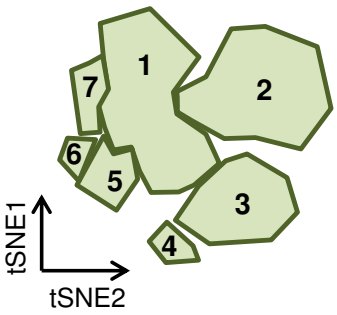

Cluster #	Characterised by	Cell type	% of CD45⁺ live
1	F4/80⁺	Macrophages	36.11
2	GR1⁺	Neutrophils	34.27
3	Ly6C⁺	Monocytes	11.59
4	CD3⁺	T-cells	0.99
5	CD11b⁻ MHC II^{int}	DCs	3.56
6	CD19⁺	B-cells	0.36
7	CD11b⁺ MHC II^{hi}	DCs	2.85

B

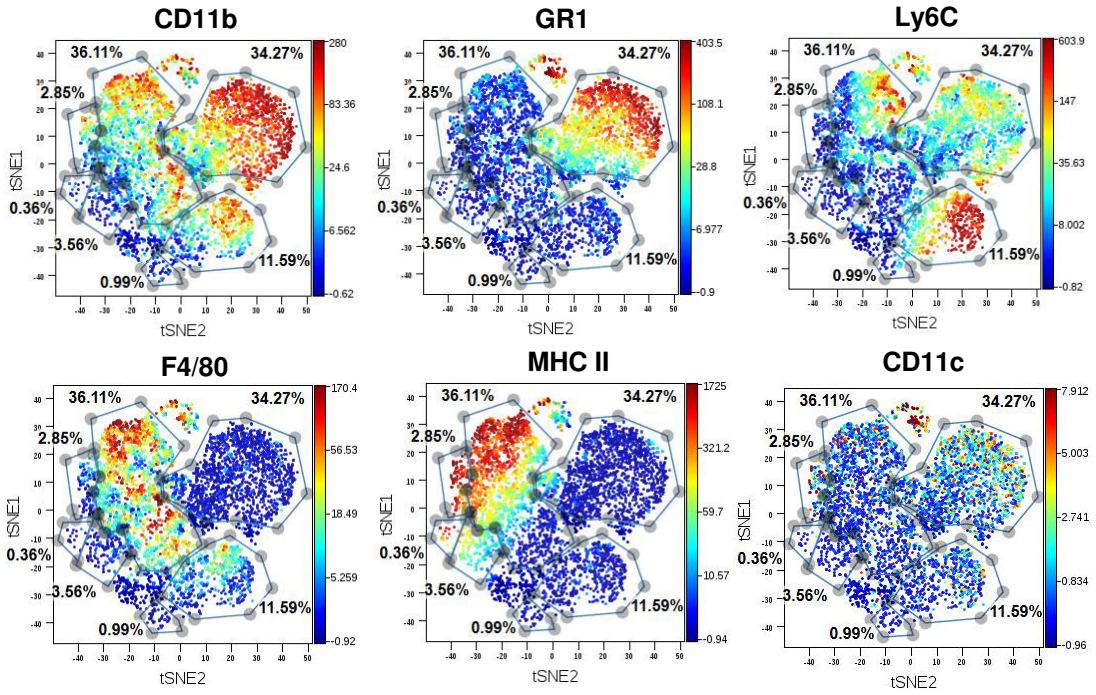

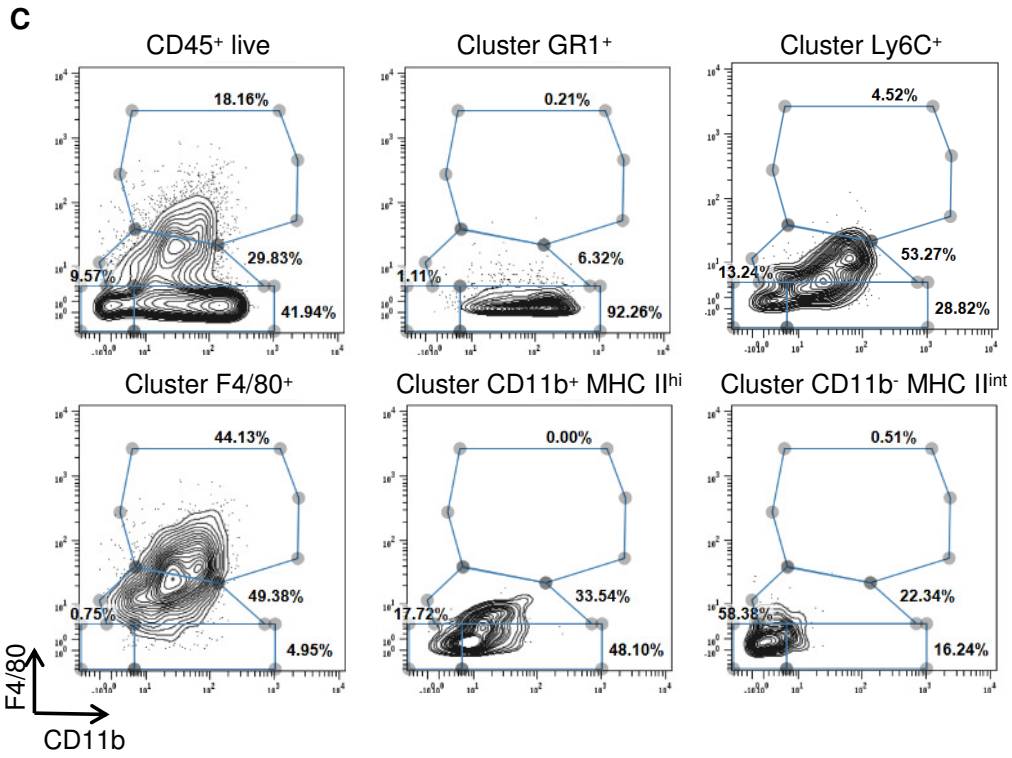

Figure 4.12. CyTOF reveals macrophage heterogeneity in inflamed knees.

mBSA challenged knees were harvested at day two of disease and samples were stained for CyTOF with a panel containing 20 markers. The panel contained markers for the main myeloid cell populations and basic T-cell, B-cell and NK cell markers. viSNE analysis on cytobank was used to plot the location of individual cells in a multidimensional space using two tSNE dimensions. The closer a cell is to another, the more similar their properties. **A.** Schematic representation of the manually identified clusters in the knee. The table shows by expression of which marker each cluster is characterised and what cell types this marker is most commonly expressed by. In addition, the percentage of each cluster of all CD45+ live events is shown. **B.** Images show the expression levels of selected myeloid markers in the different clusters. **C.** The individual myeloid clusters are shown as conventional contour plots to allow comparison with flow cytometry data. The axes display CD11b and F4/80 expression, as used for flow cytometry. Gates were drawn accordingly for $CD11b^+$ $F4/80^{hi}$, $CD11b^+$ $F4/80^{dim}$, $CD11b^+$ $F4/80^-$ and $CD11b^-$ $F4/80^-$.
Data show mass cytometry from a pooled sample containing cells derived from arthritic knees of five individual WT mice.

When the expression patterns were analysed in more detail, it could be observed that the majority of cells were $CD11b^+$ and of this population, neutrophils expressed the highest levels (Figure 4.12B). GR1 expression was restricted to cluster #2, which also partly expressed intermediate levels of Ly6C. The highest levels of Ly6C expression were found in the cluster that most likely represents monocytes. This cluster also partially showed intermediate F4/80

expression. Most F4/80 expression however was found in one large but rather heterogeneous cluster. Levels of F4/80 were highest in some cells within this cluster although expression was somewhat scattered and some cells also displayed intermediate levels. In addition, 39.5% of cells located in the F4/80^{+} macrophage cluster were also Ly6C^{+} (percentage not shown in graph). Furthermore, a large fraction of the macrophage cluster was found to be MHC II^{+} (83.4%, not shown in graph), ranging from high to intermediate expression levels. Other MHC II^{hi} cell types were CD11b^{+} DCs and B-cells while CD11b^{-} DCs were only MHC II^{int}. Moreover, expression of the DC associated marker CD11c was determined, and CD11c^{hi} cells were found to be scattered among all clusters rather than defining any cluster specifically. Of note, the cells found at the top of each graph showing high expression of all markers, are most likely to represent nonspecific staining of debris or dead cells that could not be gated out properly. Thus these were not assigned to a specific cluster.

Lastly, we aimed to compare mass cytometry data to previously obtained flow cytometry data. Therefore, the myeloid clusters were plotted on graphs showing CD11b vs F4/80 expression as used in flow cytometry gating (see 4.2.3 Gating strategy of myeloid cell types in the knee). Thereby, clusters could be compared in terms of location on these plots to the manually gated populations identified using FACS. As expected, the neutrophil cluster was almost entirely confined to the CD11b^{+} F4/80^{-} gate (Figure 4.12C). Of the Ly6C^{+} monocytes however, about half of the cells were not localised to the CD11b^{+} F4/80^{dim} gate that had been used to identify monocytes in flow cytometry. It could be observed though that only a minor fraction, below 5%, was found within the CD11b^{+} F4/80^{hi} macrophage gate. The F4/80^{hi} population indeed corresponded to 44.13% of

the F4/80^{+} macrophage cluster although its distribution was more widespread with about half of the cells localising to the F4/80^{dim} gate. The majority of cells belonging to either of the two DC clusters were found within one of the F4/80^{-} gates. These clusters however were not restricted in their distribution and were also found in adjacent gates.

Taken together, mass cytometry confirms the previously identified myeloid cell types in the inflamed knee but at the same time emphasises heterogeneity within the macrophage cluster.

4.2.9. Resident macrophage populations in the knee and ankle synovium are comparable but not identical

The phenotype and origin of macrophages in the knee joint in the steady state or during inflammatory arthritis are not known. Misharin et al. recently demonstrated that macrophages in the ankle synovial lining of naïve mice consist of a heterogeneous population: CD11b^{+} CD11c^{int} F4/80^{+} CD64^{+} MHCII^{-} are true tissue-resident cells, and CD11b^{+} CD11c^{int} F4/80^{+} CD64^{+} MHCII^{+} originate from the BM (Misharin et al. 2014). Applying a similar gating strategy, we find a higher representation of MHCII^{+} macrophages in the knee than in the ankle, while MHCII^{-} macrophages in the ankle show the opposite (Figure 4.13A). IRF5 levels in CD11b^{+} F4/80^{+} CD64^{+} macrophages are lower in the knee, which appears to be mainly due to the significant decrease in expression within MHCII^{-} macrophages (Figure 4.13B). In contrast, the MHC II^{+} subsets in the ankle and knee displayed equal levels of IRF5. These data highlight differences between the two joints in naïve animals.

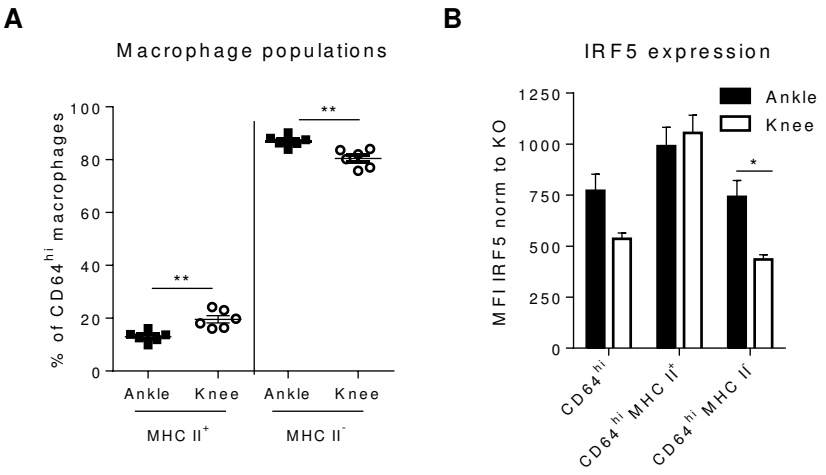

Figure 4.13. Synovial macrophages in the naïve knee and ankle are comparable but not identical.

Knee and ankle joints were collected from naïve WT mice. Cell suspensions were analysed by flow cytometry and stained with antibodies against CD45, CD11b, SiglecF, Ly6G, Ly6C, CD64 and MHC II. Gating was performed as described by (Misharin et al. 2014) to compare synovial macrophages in the knee and ankle. **A.** Macrophages are defined as $CD45^+$ live $CD11b^+$ Siglec F^- $Ly6G^-$ $CD64^{hi}$. Sub-populations of those $CD64^{hi}$ macrophages were either MHC II positive or negative. **B.** Intracellular IRF5 staining was quantified using MFI in $CD64^{hi}$ macrophages and MHC II^+ and MHC II^- sub-populations. MFI was normalised by subtracting MFI values of IRF5 KO from WT MFI values
Error bars represent the SEM of n=6. Statistical analysis performed was either one-tailed Mann-Whitney U test or by 2-way ANOVA and Bonferroni's multiple comparison. * p≤0.05; ** p≤0.01

4.3. Discussion

Translation of *in vitro* findings regarding myeloid populations can be challenging as macrophages or DCs *in vitro* rarely correspond to a specific *in vivo* counterpart, as demonstrated for GM-CSF-derived macrophages (Helft et al. 2015). This can most likely be attributed to a strong influence on the macrophage genomic landscape by the environment that dictates distinct transcriptional programmes (Gosselin et al. 2014, Lavin et al. 2014). Since we established in chapter 3 that IRF5 is highly expressed in pro-inflammatory macrophages *in vitro*, we aimed to identify and characterise IRF5-expressing cell populations *in vivo*. We observed that in four different steady state tissues,

blood, BM, spleen and lung, Ly6C^{hi} monocytes and macrophages respectively expressed the highest levels of IRF5. In the context of inflammation, using the model of antigen-induced arthritis, IRF5 expression is most strongly induced in macrophages following antigen challenge. Moreover, we could show that upon inflammation there is an influx of monocyte-derived macrophages that are CD64^{hi} Ly6C^{hi} and largely MHC II^{+} in the arthritic knee (Figure 4.14).

IRF5 expression in B-cells has previously been reported (Barnes et al. 2002, Mancl et al. 2005, Lien et al. 2010), which we could confirm for circulating B-cells in the blood and splenic B-cells that represent 50% of haematopoietic cells in the spleen. Moreover, we could confirm that IRF5 was expressed by different cells of the myeloid lineage including monocytes, macrophages, neutrophils and DCs (Mancl et al. 2005, Ericson et al. 2014). However, there were considerable differences within their expression levels at steady state. Ly6C^{hi} monocytes displayed the highest expression of IRF5 across tissues whereas levels varied for macrophages (Figure 4.1 and Figure 4.2). While both subsets of lung macrophages highly expressed IRF5, in line with (Draijer et al. 2013), different macrophages in the spleen showed relatively low expression (Figure 4.2). This is most likely due to the differential influence of the environment and its effect on macrophage gene expression (Gosselin et al. 2014, Lavin et al. 2014).

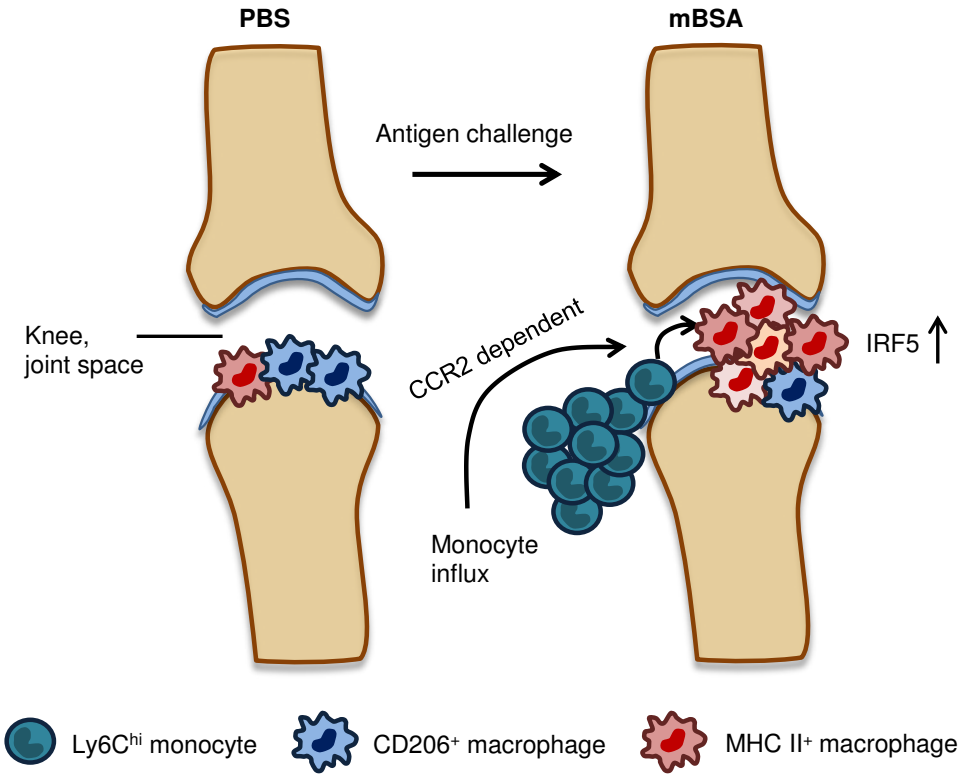

Figure 4.14. Pro-inflammatory IRF5-expressing macrophages in the arthritic knee are Ly6C^{hi} monocyte derived.

In WT mice undergoing AIA, mBSA challenge causes a CCR2 dependent influx of monocytes which in turn leads to an increase in macrophage numbers. Proportions of anti-inflammatory CD206^{+} macrophages are decreased in inflamed knees compared to PBS control knees whereas MHC II^{+} pro-inflammatory macrophages increase upon challenge. The MHC II^{+} population in fact represents the majority of synovial macrophages in the arthritic knee. However, mass cytometry revealed macrophage heterogeneity in the inflamed knee (represented by different shades of red in the macrophage population). Expression of IRF5 is increased following antigen challenge, specifically we observed a strong induction in macrophages. Overall, Ly6C^{hi} monocytes and macrophages express the highest levels of IRF5 in the joint while neutrophils and DCs only express low levels.

Myeloid cells in the lung are constantly exposed to inhaled antigens, so require a tight control of their activation status and thus displaying a rather immunoregulatory phenotype, characterised by the expression of receptors such as CD200R (Hussell and Bell 2014). Therefore, high IRF5 expression in alveolar macrophages seems somewhat counterintuitive as it has been mainly associated with a pro-inflammatory macrophage phenotype *in vitro* (Krausgruber et al. 2011), as described in chapter 3. However, it could be that

IRF5 expression in alveolar macrophages is related to the important role of GM-CSF in their development and maintenance (Guilliams et al. 2013, Schneider et al. 2014). As we could show in chapter 3, GM-CSF is able to induce expression of IRF5 at different stages of macrophage development. Thus, it may be that GM-CSF dependent induction of IRF5 occurs at some point during alveolar macrophage development. Alternatively, IRF5 expression could be induced or maintained in response to GM-CSF produced by the respiratory epithelium (Chen et al. 1988, Trapnell and Whitsett 2002, Higgins et al. 2008).

The main environmental stimulus driving the transcriptional landscape in spleen macrophages identified thus far is heme, which induces the TF SPI-C that drives differentiation (Kohyama et al. 2009, Haldar et al. 2014). Interestingly, SPI-C has also been shown to be important in the development of F4/80^{hi} BM macrophages (Haldar et al. 2014). We did detect intermediate IRF5 expression in BM macrophages (Figure 4.1), whereas IRF5 levels in red pulp macrophages in the spleen were negligible (Figure 4.2). This further highlights differences between tissue macrophages influenced by a network of environmentally driven TFs. It has to be noted however that even macrophages in the spleen vary depending on their localisation (den Haan and Kraal 2012). We identified two subsets of spleen macrophages that indeed differed in their IRF5 expression (Figure 4.2). Of note, we did not analyse the full spectrum of spleen macrophages due to a restricted panel of markers. For example, we were unable to identify marginal zone macrophages, which are F4/80^{-} CD209b^{+}. Further and more detailed analysis will be needed to determine the role of IRF5 in the different splenic macrophage populations.

Although neutrophils were recently reported to express IRF5 (Ericson et al. 2014), we only detected low expression levels that varied slightly depending on the tissue origin. Of note, little IRF5 was detected in the $CD45^-$ population, which contains stromal or epithelial cells, within all organs analysed. Overall, myeloid cells are the dominant IRF5-expressing populations in the tissues assessed, in line with previous reports (Mancl et al. 2005, Takaoka et al. 2005).

In the mouse model of sterile inflammatory arthritis (K/BxN model), which represents only the effector phase of human RA, circulating non-classical ($Ly6C^-$) blood monocytes are recruited to the joint and differentiate into classically activated inflammatory macrophages to drive joint pathology (Misharin et al. 2014). In contrast to the data derived from the K/BxN model we find that in AIA, which mimics both induction and effector phases of arthritis, over 90% of infiltrating monocytes were $Ly6C^+$, the majority being $Ly6C^{hi}$ (Figure 4.7). Moreover, their recruitment was almost completely abolished in the mBSA challenged joints of $CCR2^{-/-}$ mice, which are deficient in circulating $Ly6C^+$ monocytes (Figure 4.11). Thus, despite somewhat similar joint pathologies, the two models clearly differ in the types of circulating monocytes recruited to the joint. This difference is likely due to immunisation with CFA, which is composed of inactivated and dried mycobacteria and may predispose mice to preferentially recruit classical monocytes to the site of inflammation. Of significance, in RA patients it is the intermediate $CD14^{++}CD16^+$ (corresponding to $Ly6C^{int}$ in mouse) blood monocytes that appear to be significantly increased in RA patients, while non-classical $CD14^+CD16^{++}$ ($Ly6C^-$ in mouse) remained the same (Rossol et al. 2012).

These infiltrating monocytes likely differentiated into macrophages, which are also increased in terms of numbers after mBSA challenge in the knee joint. Their monocyte origin is based on the observation that F4/80^{hi} macrophages are absent in the joints of CCR2$^{-/-}$ mice (Figure 4.11) but also by their high expression of Ly6C and CD64 (Figure 4.7) (Gautier et al. 2012, Epelman et al. 2014, Schiwon et al. 2014). In agreement with our *in vitro* experiments, pro-inflammatory MHC II^{+} macrophages in arthritic joints displayed high levels of IRF5 and their increase correlated with elevated iNOS expression. In fact, macrophages were not only the cells expressing the highest levels of IRF5, but they were also the population with the largest increase in IRF5^{+} cells (Figure 4.9). Interestingly, the influx of IRF5^{+} monocytes and macrophages to the joint is abolished in CCR2$^{-/-}$ (Figure 4.11). As Ly6C^{hi} monocytes already express high levels of IRF5, it may be that IRF5 is upregulated in the process of monocyte differentiation and further induced upon tissue entry in response to inflammatory cues. This increase in IRF5 may be necessary to establish a mature macrophage phenotype and lead to activation of the pro-inflammatory gene programme regulated by IRF5 (Takaoka et al. 2005, Krausgruber et al. 2011, Saliba et al. 2014). These *in vivo* data confirm the findings in pro-inflammatory *in vitro* differentiated macrophages and suggest that upregulation of IRF5 expression is important in monocytes and their progeny in acute inflammation in the joint.

Reliable identification of macrophages and other myeloid cells is often difficult, especially *in vivo*, due to large numbers of macrophage subsets across tissues (Guilliams and van de Laar 2015). Macrophages *in vivo* are often defined as

generally F4/80$^{+/hi}$ (Austyn and Gordon 1981, Schulz et al. 2012) although this marker can also be expressed by eosinophils (McGarry and Stewart 1991) or certain DC subsets (Merad et al. 2013). Even though *in vitro* differentiated cells that expressed high levels of IRF5 were F4/80^{-}, we chose to identify macrophages *in vivo* as F4/80^{hi} (Figure 4.4). This discrepancy in F4/80 levels may be due to the challenging identification of corresponding cell populations *in vivo*, if possible at all, as mentioned earlier. This has been shown specifically for the macrophage subset in GM-CSF-derived cultures (Helft et al. 2015). However, we used CD64 as an additional marker to verify macrophage identity and indeed most *in vivo* macrophages are CD64^{+} (Figure 4.7). CD64 is also expressed by a subset of GM-BMDMs and we observed no difference in IRF5 expression within subsets present in GM-CSF cultures (Figure 3.5).

CD11c was only detected minimally in the knee (Figure 4.6, Figure 4.12) although it was highly abundant on GM-BMDMs and also on a proportion of M-BMDMs (Figure 3.3). This could either be because there simply are not many DCs or CD11c^{+} macrophages present in the synovium but it may also be a technical artefact. It is possible that CD11c is more susceptible to cleavage by the liberase enzyme during digest of the excised knees, as has been shown for CD4 and other markers when using dispase or alternatives (Egan et al. 2003). CD11c could be more sensitive to liberase digest than other surface markers as it has indeed been shown that different enzymes may affect various antigens to variable degrees (Goodyear et al. 2014). Of note, CD11c was readily detected in experiments using naïve lungs, which are digested using a different enzyme (see 2.2.3, Lungs) (Figure 4.2). Misharin et al. reported a population of CD11c^{hi}

$CD11b^+$ DCs in the naïve ankle synovium although they were not crucial for development of K/BxN arthritis (Misharin et al. 2014).

In conclusion, as expected macrophages *in vitro* and *in vivo* did not show a complete overlap in their surface marker expression, however they did share pro-inflammatory characteristics and importantly high levels of IRF5.

Mass cytometry in this chapter further underlined macrophage heterogeneity *in vivo*. The cluster containing macrophages showed that cells display varying degrees of F4/80 expression (Figure 4.12). Within this cluster we could also confirm the Ly6C- and MHC II-expressing fractions previously characterised using flow cytometry. When comparing contour plots derived from mass cytometry data to FACS plots, the overall pattern appeared similar when analysing CD11b versus F4/80 expression. Specifically, the clusters identified by viSNE analysis mostly corresponded to the manual gates although the populations showed a more widespread distribution. Since clustering relies on the overall expression pattern of various markers, it is likely that they will be less confined to a particular gate based only on the expression of two markers. These results also demonstrate that there are a substantial number of macrophages that do not fall in either of the classical categories of macrophage polarisation. This probably reflects the extent of macrophage plasticity and the wide spectrum of *in vivo* macrophage subtypes (Gautier et al. 2012). This especially holds true in a disease setting where macrophages might be at different stages of polarisation and where the inflammatory environment can be constantly changing. Moreover, transcriptional profiling of macrophages from different origins demonstrated heterogeneity of macrophage populations and

revealed tissue-specific transcriptional signatures (Gautier et al. 2012). This suggests that identification of subset specific TFs is needed to tease out the contribution of different macrophage subtypes in inflammatory processes, especially in disease-related chronic inflammation or autoimmunity that so far received less attention. We hypothesise that IRF5 could play a critical role in tracking inflammatory macrophages in various inflammatory diseases.

Based on our data thus far, we conclude that IRF5 is indeed an appropriate marker for detection of inflammatory macrophages in the arthritis disease model used. However, it has to be kept in mind that although IRF5 levels within macrophage populations increase, this may not necessarily translate into elevated protein activity since IRF5 phosphorylation status and cellular localisation are not taken into account. It has been shown that IRF5 undergoes post-translational modifications and is regulated by phosphorylation and ubiquitination (Balkhi et al. 2008, Balkhi et al. 2010, Chang Foreman et al. 2012). Furthermore, it has been reported recently that iNOS mediates nitration of tyrosine residues in IRF5, which impaired its DNA binding activity to the *Il12b* promoter (Lu et al. 2015). However, the role of IRF5 post-translational activation in the context of disease has not been studied extensively and further research will be required to elucidate this (Stone et al. 2012, Ryzhakov et al. 2015).

Recently, IRF5 was used as an indicator for pro-inflammatory macrophage infiltrate in house dust mite induced asthma animal models (Draijer et al. 2013). Although this study did not describe the phenotype of the IRF5-expressing macrophages in detail, it demonstrated that IRF5 can potentially be used as a marker in a different disease setting and tissue. This is particularly important

since IRF5 polymorphisms associate not only with RA but also with several other auto-immune diseases such as inflammatory bowel disease, asthma and SLE (Dideberg et al. 2007, Gathungu et al. 2012, Wang et al. 2012, Xu et al. 2013, Eames et al. 2015). It is worth noting however that FACS staining for IRF5 in macrophages is challenging due to relatively high background from secondary antibodies and macrophage autofluorescence. A reporter IRF5 mouse strain, similar to the described RelA-GFP knockin (De Lorenzi et al. 2009), would further facilitate analysis of IRF5 expression in macrophage populations and possibly other cell types in *in vivo* models. In addition, it would be helpful in the analysis of the intracellular localisation of IRF5 in response to stimulation.

Heterogeneity of tissue macrophages has been extensively analysed in the last few years, with possible co-existing mechanisms of macrophage development from recruited blood monocytes and local self-renewal of tissue-resident macrophages being described (Sieweke and Allen 2013). Fate mapping studies revealed that Kupffer cells, as well as lung, peritoneal and splenic macrophages are established before birth and self-replicate in adulthood uncoupled from the steady-state monocyte pool (Yona et al. 2013). However, the origin of synovial macrophages remained elusive until recently. Recent work by Misharin et al. using a series of elegant chimera experiments demonstrated that the synovial lining in the naïve mouse ankle joint contains a heterogeneous population of macrophages, with the majority being true tissue-resident cells ($MHCII^-$) while about a fifth originates from the BM ($MHCII^+$) (Misharin et al. 2014).

Of interest, expression of CX_3CR1 was mainly confined to the resident $MHCII^-$ synovial macrophages in the ankle. In the knee however, macrophages expressed high levels of CX_3CR1 independent of the inflammatory state and were largely MHC II^+ (Figure 4.10). Infiltrating macrophages in the knee are most likely derived from $Ly6C^{hi}$ monocytes based on their absence in $CCR2^{-/-}$ mice. Expression of CX_3CR1 could therefore not be explained by macrophages retaining GFP expression as $Ly6C^{hi}$ monocytes in the blood are $CX3CR1^{lo}$ (Geissmann et al. 2003). However, it may be possible that a high abundance of the ligand fractalkine in the joint environment favours accumulation of CX_3CR1-expressing macrophages. A high percentage of CX_3CR1^+ macrophages in the joints of mice undergoing CIA has indeed been described (Nanki et al. 2004). Moreover, CX_3CR1 and its ligand have been shown to be expressed in the synovium of rats and human synovial fluid samples (Ruth et al. 2001). The low levels of CX_3CR1 observed in monocytes in PBS and mBSA knees are in agreement with previously published data that monocytes in tissues display low to intermediate expression of CX_3CR1 in the steady state (Jakubzick et al. 2013).

We also noted some additional differences between macrophage populations in the two analysed joints (Figure 4.13). Firstly, there appears to be a shift towards a higher representation of MHC II^+ macrophages in the knee than in the ankle. Secondly, MHC II^- macrophages in the ankle express higher levels of IRF5 than those in the knee. Further more detailed analysis, such as fate mapping and BM chimera, will be necessary to ultimately determine the origin of synovial macrophage populations in the knee.

Overall, we were able to translate the findings of *in vitro* differentiated cells, described in chapter 3, to an *in vivo* setting. We could show that both at steady state and during inflammation monocytes, especially the Ly6C^{hi} subset, and macrophages express high levels of IRF5. Specifically, there is a large influx of IRF5^{+} monocytes and macrophages in arthritic knees. The phenotype of these macrophages could mostly be classified as pro-inflammatory, based on MHC II expression although there were a large number of unclassified cells. Mass cytometry further highlighted the heterogeneity of macrophages in the joint *in vivo*. Having established the presence of IRF5 in infiltrating pro-inflammatory macrophages, the importance of IRF5 in those remained to be addressed. Experiments clarifying the functional role of IRF5 in acute inflammatory diseases will be described in chapter 5.

5. Role of IRF5 in inflammatory diseases

5.1. Introduction

Myeloid cells play a critical role in the immune system's defence to external challenges and injury. They sense both microbial components and tissue damage, eliminate bacteria by phagocytosis and activate adaptive immune cells via the release of cytokines and chemokines. Under certain circumstances however the same cells can contribute to disease pathology. It remains one of the key challenges to understand how myeloid cell function is regulated to promote health but not disease.

Macrophages and neutrophils are the two major types of myeloid cells involved in inflammatory diseases, such as RA, which is a chronic degenerative disease of the joints affecting up to 1% of the population (Helmick et al. 2008). While the molecular pathogenesis of RA has been extensively studied, only some aspects have been understood. For example, excess TNF-α is known to be pathogenic as witnessed by the extensive use of TNF inhibitors, monoclonal antibodies and a receptor Ig fusion protein. In fact, most of the TNF-α in RA is produced by synovial macrophages. The increase in the number of sublining macrophages is an early hallmark of active rheumatic disease and a prominent feature of inflammatory lesions (Tak and Bresnihan 2000, Smeets et al. 2001). The degree of synovial macrophage infiltration correlates with the degree of joint erosion (Mulherin et al. 1996) and their depletion from inflamed tissue has a profound therapeutic benefit (Barrera et al. 2000). Neutrophils also play an important role in RA pathogenesis as suggested by their abundance in synovial fluid and within the pannus in patients with active RA (Mohr et al. 1981, Wittkowski et al. 2007, Wright et al. 2014). Moreover, the formation of NETs can

provide a source of destructive enzymes as well as autoantigens (Khandpur et al. 2013). As described earlier, there has been a growing understanding of the heterogeneity of macrophages (Davies et al. 2013), followed more recently by the awareness that neutrophils may also form distinct subsets. Neutrophil polarisation has so far been considered mainly in the context of cancer and infections (Kolaczkowska and Kubes 2013). However, high-dimensional analyses of neutrophil phenotypes and gene expression extended the notion of polarisation to the possibility of distinct neutrophil populations in relation to various tissues and biological processes (Becher et al. 2014, Ericson et al. 2014).

We have previously documented the importance of the TF IRF5 in defining the classical inflammatory phenotype of macrophages and thus promoting Th1 and Th17 responses (previous chapters 3 and 4 and (Krausgruber et al. 2011)). Furthermore, IRF5 has recently been reported to be expressed in neutrophils, specifically in neutrophils from synovial fluid of arthritic mice (Ericson et al. 2014). In chapter 4, we demonstrated an influx of IRF5-expressing macrophages in the mBSA challenged joint. Using IRF5 deficient animals, we now seek to investigate the role of IRF5 in antigen induced arthritis, with particular focus on its role in establishing the inflammatory macrophage phenotype. Moreover, we wished to assess the importance of IRF5 in regulating neutrophil influx and neutrophil function

5.2. Results

5.2.1. Knee swelling and cellular infiltrate are reduced in IRF5 deficient mice

Here, we aimed to determine the role that IRF5 plays in synovial physiology and function in the knee joints during inflammatory arthritis. $IRF5^{-/-}$ mice and WT controls were immunised with a subcutaneous injection of mBSA in CFA and seven days later knees were either challenged with an intra-articular injection of mBSA or PBS as a control in the contralateral knee (see 2.2.2, Antigen-induced arthritis). Post intra-articular challenge, disease severity was evaluated for seven days by measuring knee swelling daily. Knee joints were collected on day two or seven for histological analysis.

Arthritis severity was assessed through measurement of joint swelling which was then expressed as a percentage of the inflamed knee relative to the control knee. In WT mice, knee swelling was induced rapidly and peaked at day two after which it started to decrease (Figure 5.1A). Even though $IRF5^{-/-}$ mice showed a minor increase 24 h post challenge, swelling decreased by day two to a level that was significantly lower in comparison to WT animals. Moreover, reduced swelling corresponded to fewer cells being recovered from excised knee joints at day two of AIA (Figure 5.1B).

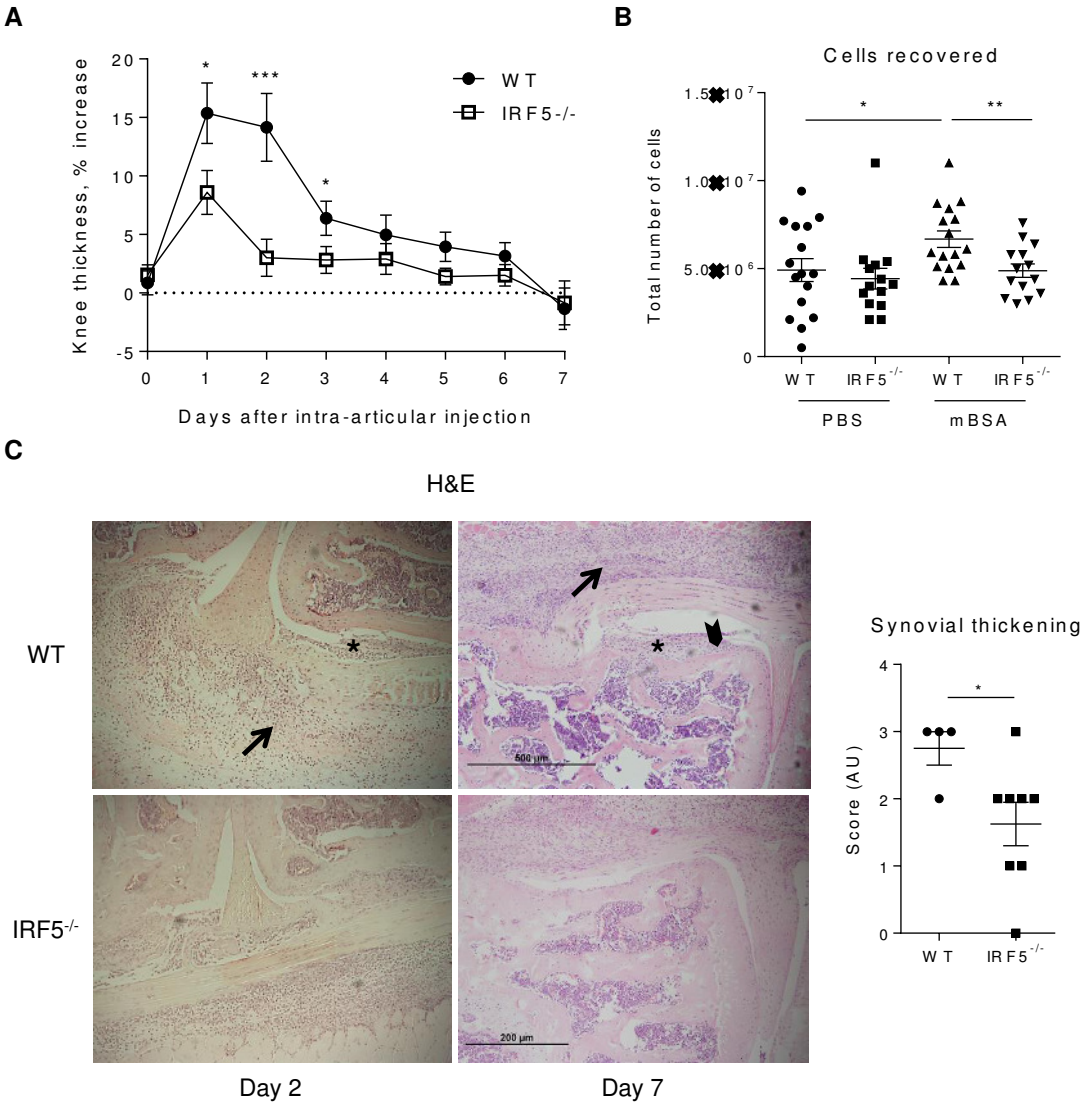

Figure 5.1. IRF5$^{-/-}$ mice display reduced disease severity and decreased cellular infiltrate in the joints.

WT and IRF5$^{-/-}$ mice underwent AIA as described previously, disease severity was assessed each day post intra-articular injection using callipers. Mice were sacrificed either on day two or seven of disease. **A.** Knee swelling in IRF5$^{-/-}$ and WT animals, expressed as a percentage of swelling of the mBSA challenged knee compared to the PBS knee. **B.** Total number of cells recovered from excised knee joints of IRF5$^{-/-}$ and WT animals at day two of AIA. Data show the mean and SEM derived from 10-16 mice from three independent AIA experiments (A. and B.). **C.** Representative images of the knee showing areas of synovial thickening (asterisk), leukocyte infiltration into the joint space (arrows) and bone erosion (arrowhead). Synovial thickening of inflamed knees at day two based was quantified based on examination of the histology slides. Images and analysis courtesy of Dr. Adam J. Byrne (Udalova laboratory). Data show the mean and SEM for n=4-8.
Each dot represents an individual mouse. Statistical analysis was performed by one-tailed Mann-Whitney U test. * p≤0.05; ** p≤0.01; *** p≤ 0.001

Knee pathology was further assessed histologically for the degree of inflammatory infiltrate into the synovium and joint cavity (indicated by arrows), synovial membrane thickness (denoted with asterisks) and bone erosion (indicated by an arrowhead) (Figure 5.1C). In WT animals, we observed both infiltrating leukocytes and membrane thickness two days after mBSA challenge. When synovial thickening was quantified, IRF5$^{-/-}$ mice displayed significantly lower scores in mBSA challenged knees than WT mice. On day seven, signs of bone erosion were detected in WT animals in addition to infiltrating cells and membrane thickness, which were all notably absent in IRF5$^{-/-}$ mice.

Thus, disease severity is attenuated in IRF5 deficient animals undergoing AIA.

5.2.2. Numbers of infiltrating monocytes, macrophages and DCs are not altered in IRF5$^{-/-}$ mice

Next, we sought to determine if the decreased swelling in IRF5$^{-/-}$ mice was due to a lack of infiltrating myeloid cells previously shown to express high levels of IRF5. Therefore, we used flow cytometry to determine the numbers of macrophages, monocytes and DCs in the synovial infiltrate of mBSA and PBS knees.

The observed difference in the number of cells recovered from mBSA challenged knees at day two compared to PBS controls was mirrored by the increase in myeloid cell numbers. As described earlier (Chapter 4), an influx of CD11b^{+} F4/80^{hi} macrophages and CD11b^{+} F4/80^{dim} monocytes could be detected in mBSA knees (Figure 5.2). Additionally, the percentage of CD11b^{+} F4/80^{-} CD11c^{+} DCs was increased in affected knees while there was no change in the number of CD11b^{-} F4/80^{-} CD11c^{+} DCs. However, the numbers of

monocytes, macrophages and DCs infiltrating the inflamed knee were unaffected by the loss of IRF5.

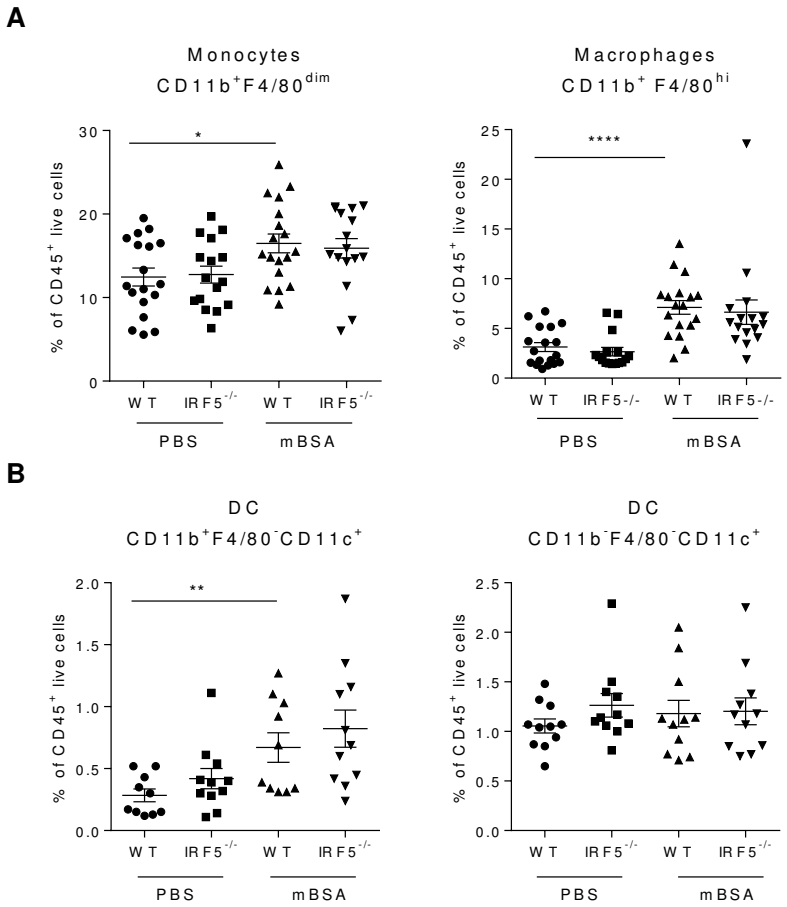

Figure 5.2. Influx of monocytes, macrophages and DCs into the inflamed knee remains unaffected by loss of IRF5.

Numbers of monocytes, macrophages (**A.**) and DCs (**B.**) recovered from excised knee joints of IRF5$^{-/-}$ and WT mice at day 2 of disease, expressed as a percentage of live CD45^{+} cells. Cells obtained from the joints were stained for flow cytometry using antibodies against the surface markers CD45, CD11b, F4/80 and CD11c. Data shown the mean and SEM derived from 10-18 mice from 3-4 independent AIA experiments. Each dot represents an individual mouse. Statistical analysis was performed by one-tailed Mann-Whitney U test. * p≤0.05; ** p≤0.01; *** p≤ 0.001

5.2.3. Macrophages display a different phenotype in the absence of IRF5

As our group has previously shown that IRF5 is involved in regulating pro-inflammatory macrophages, we aimed to investigate the macrophage phenotype in IRF5 deficient mice with AIA. Arthritic and control joints were

excised on day two of disease for either flow cytometric analysis of cellular subsets or RNA extraction and subsequent qPCR for analysis of gene expression. As before, the cell surface receptors CD64, Ly6C, MHC II and CD206 were used to analyse macrophage identity. Transcript levels of *Nos2* and *Fizz1* were analysed as markers for pro- or anti-inflammatory macrophages, respectively.

Although macrophage infiltration in the mBSA challenged knee was not affected, the proportion of $CD64^{hi}$ macrophages was reduced (Figure 5.3A). In contrast, the proportion of $Ly6C^{hi}$ macrophages remained unaltered by depletion of IRF5. Consistent with our previously reported observations, we observed a shift towards an alternatively activated macrophage phenotype in the $IRF5^{-/-}$ animals, with a lower number of macrophages expressing MHC II and a higher number expressing CD206 (Figure 5.3B). Concurrent with these data, *Nos2* expression levels in whole knee extracts were significantly lower in arthritic knees of $IRF5^{-/-}$ than in WT mice (Figure 5.3C). However, we did not observe a difference in *Fizz1* transcript levels, which were equally downregulated in WT and $IRF5^{-/-}$ mice upon antigen challenge.

To conclude, macrophages that lack IRF5 display an altered phenotype with decreased expression of CD64 and pro-inflammatory markers but increasing numbers of regulatory CD206+ cells.

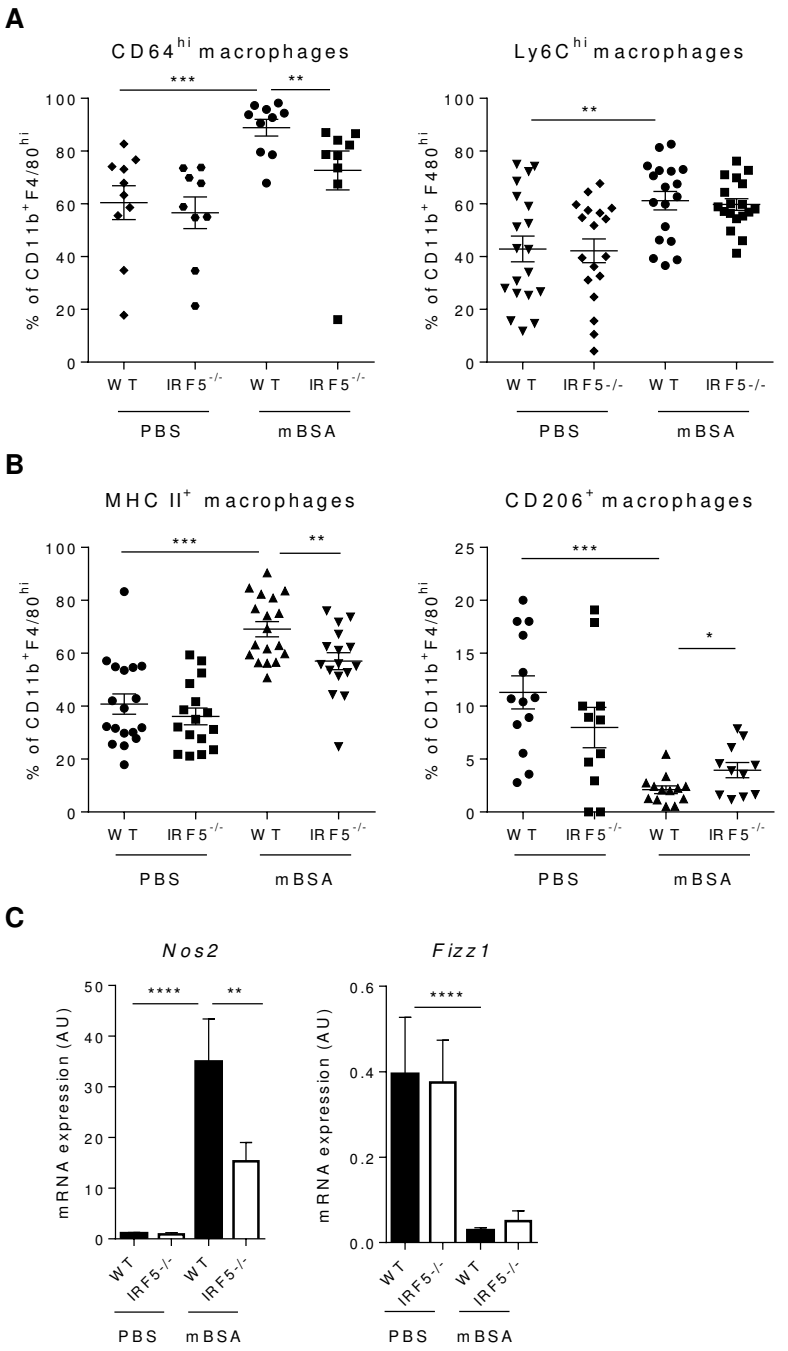

Figure 5.3. The phenotype of macrophages infiltrating the inflamed knee is changed in IRF5 deficient animals.

Joints of IRF5$^{-/-}$ and WT mice were harvested two days after mBSA challenge and subjected to further analysis. **A. and B.** Flow cytometric analysis of macrophage phenotype in PBS and mBSA knees. Numbers of CD64^{hi}, Ly6C^{hi}, MHC II^{+} and CD206^{+} macrophages expressed as a percentage of CD11b^{+} F4/80^{hi} cells. **C.** RNA was isolated from whole knee extracts and mRNA expression of *Nos2* and *Fizz1* was determined by qPCR. RNA was derived from experiments conducted by Katrina Blazek (Udalova laboratory).
Data shown the mean and SEM derived from 10-18 mice from 3-4 independent AIA experiments. Each dot represents an individual mouse. Statistical analysis was performed by one-tailed Mann-Whitney U test. * p≤0.05; ** p≤0.01; *** p≤ 0.001

5.2.4. Deletion of IRF5 leads to a dampened cytokine response in AIA

To assess the overall cytokine response in inflamed knees of IRF5 WT and KO mice, joints were collected at day two of disease and transcript levels were determined using qPCR. We chose pro-inflammatory cytokines known to be crucial in arthritis and expressed by macrophages and also synovial fibroblasts, such as IL-1, IL-6, IL-12, IL-23 and TNF-α. Moreover, the expression levels of several T-cell associated cytokines were measured as AIA is known to be a Th1/Th17 driven model (Egan et al. 2008). As IRF5 has been shown to be involved in regulating IL-10, we also analysed mRNA levels of this immunoregulatory cytokine as well as IL-4 and IL-13 which are all involved in Th2 immunity.

As expected, expression of all pro-inflammatory cytokines was induced in mBSA challenged knees in WT mice and not PBS (non-antigen challenged) controls (Figure 5.4A). In IRF5 deficient animals however, relative to WTs, transcript levels of *Il1b*, *Il6*, *Il12b* and *Tnfa* were significantly decreased in arthritic joints. While levels in mBSA knees were less than in WT mice, most cytokines were still elevated compared to PBS knees. *Il23a* expression was also reduced in IRF5$^{-/-}$ mBSA knees although this was not statistically significant compared to WT mBSA knees. In affected joints, the induction of cytokines promoting the differentiation and expansion of Th1/Th17-cells such as IL-12 and IL-23 corresponds to increasing mRNA levels of the key T-cell cytokines *Ifng* and *Il17a* in WT mice (Figure 5.4B). Accordingly, transcript levels of both are reduced in mice lacking IRF5. We also observed an increase in the mRNA levels of the Th2 related cytokines *Il10* and *Il13* in IRF5$^{-/-}$ mice whereas *Il4*

remained unaffected. However, differences were only significant in PBS and not mBSA knees.

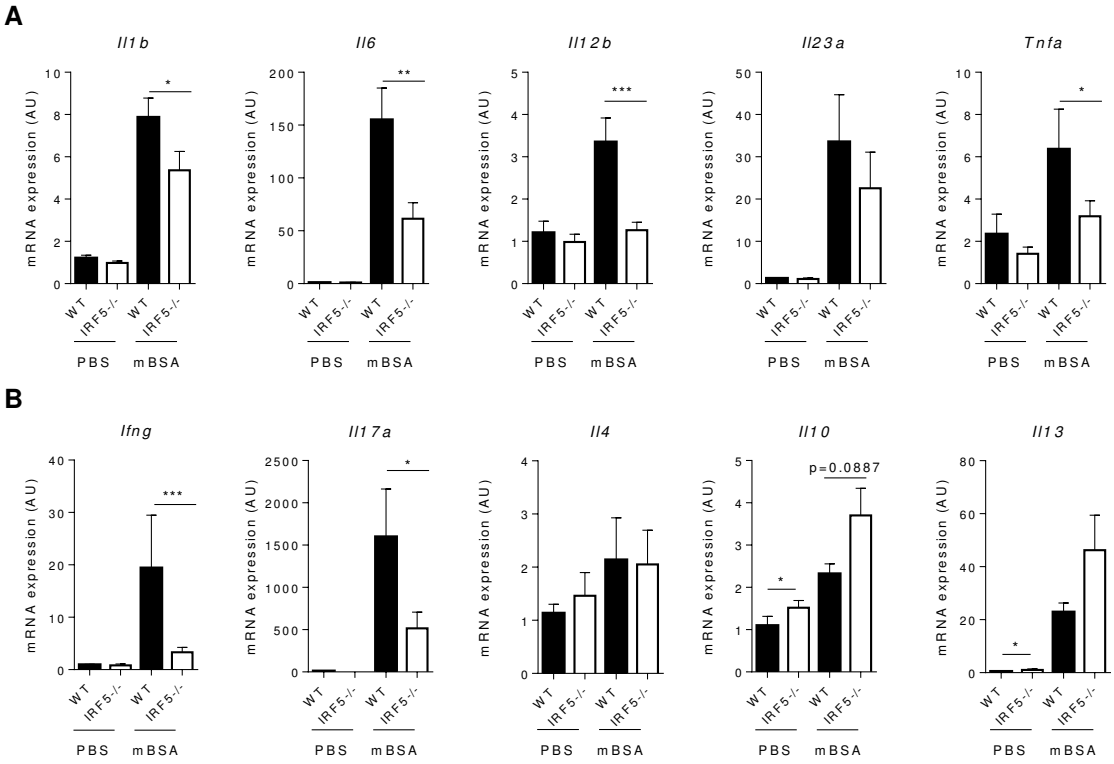

Figure 5.4. Expression of pro-inflammatory cytokines is reduced in IRF5$^{-/-}$ mice.

Knees of IRF5$^{-/-}$ and WT animals were excised two days after intra-articular challenge and analysed regarding their cytokine expression levels. RNA was isolated from whole knee extracts and transcript levels were determined by qPCR. **A.** Transcript levels of *Il1b, Il6, Il12b, Il23a* and *Tnfa* were analysed. These pro-inflammatory cytokines can be expressed in myeloid and endothelial cells in the arthritic joint. **B.** mRNA levels of T-cell related cytokines were determined using qPCR. IL-4, IL-10 and IL-13 are associated with an anti-inflammatory Th2 response whereas IFN-γ and IL-17 are involved in the pro-inflammatory Th1/Th17 response.
RNA was derived from experiments conducted by Katrina Blazek (Udalova laboratory). Data show the mean and SEM derived from 13-18 mice from 3 independent AIA experiments. Statistical analysis was performed by one-tailed Mann-Whitney U test. * p≤0.05; ** p≤0.01; *** p≤ 0.001

To conclude, mRNA expression of cytokines that are either produced by Th1/Th17 T-cells or facilitate their generation are reduced in the absence of IRF5.

5.2.5. T-cell responses in inflamed joints are reduced seven days after antigen challenge in IRF5$^{-/-}$ mice

Since cytokine levels involved in T-cell expansion and development were diminished in IRF5$^{-/-}$ mice, we sought to investigate the numbers of T-cells during the early and late stages of AIA. Different T-cell subsets were determined in tissues important for adaptive immune responses on day two and seven, respectively. In addition to the knee joints, inguinal LNs were harvested as they drain the site of immunisation at the base of the tail as well as the hind leg (Harrell et al. 2008). Notably, only inguinal LNs draining the arthritic knee were taken. Although popliteal LNs equally drain the hind leg they were not collected in these experiments. To assess circulating T-cell populations, blood was also collected.

T-cell subsets were identified using a flow cytometry panel containing antibodies against CD45, CD4, CD8a, γδTCR, IL-17a and IFN-γ (Figure 5.5). Dead cells were excluded using a viability dye. Cells were first gated as CD45^{+} live and then analysed for CD4 vs CD8a expression. CD4^{+} CD8a^{-} T-cells were further gated on Th1 cells producing IFN-γ and IL-17a producing Th17 cells. γδ T-cells producing IL-17a were also identified based on their expression of γδTCR.

Thus, knees, inguinal LNs and blood were collected from mice at day two and seven of AIA and subjected to flow cytometry analysis.

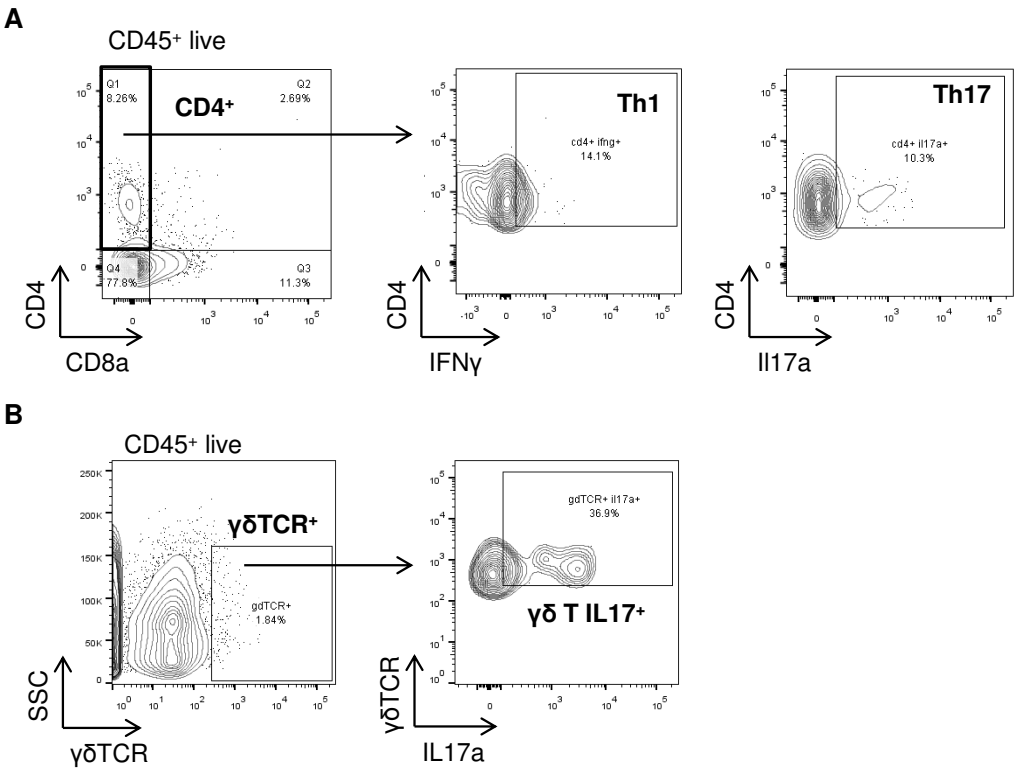

Figure 5.5. Gating strategy used to identify T-cell subsets in the inflamed knee.

Images shown are representative plots of mBSA challenged joints collected at day seven of AIA. A viability dye was used to exclude dead cells from the analysis and all samples were first gated on haematopoietic CD45$^+$ live cells. Gates were set based on FMO controls. **A.** T-cells were gated as CD4$^+$ CD8a$^-$ and then further gated on IL17a and IFNγ expression to identify T-cell subsets. **B.** IL17a producing γδ T-cells were first gated on γδTCR expression and then IL17a staining.

T-cells at the site of inflammation

Firstly, the overall influx of CD4$^+$ T-cells was assessed during the early and late stages of AIA (Figure 5.6A). Minimal CD4$^+$ T-cell populations were detected at day two which showed no significant increase upon antigen challenge. In contrast, by day seven the T-cell response in mBSA knees in WT animals was significantly increased compared to day two and to PBS joints. This increase in overall CD4$^+$ T-cells was however absent in mice that lack IRF5.

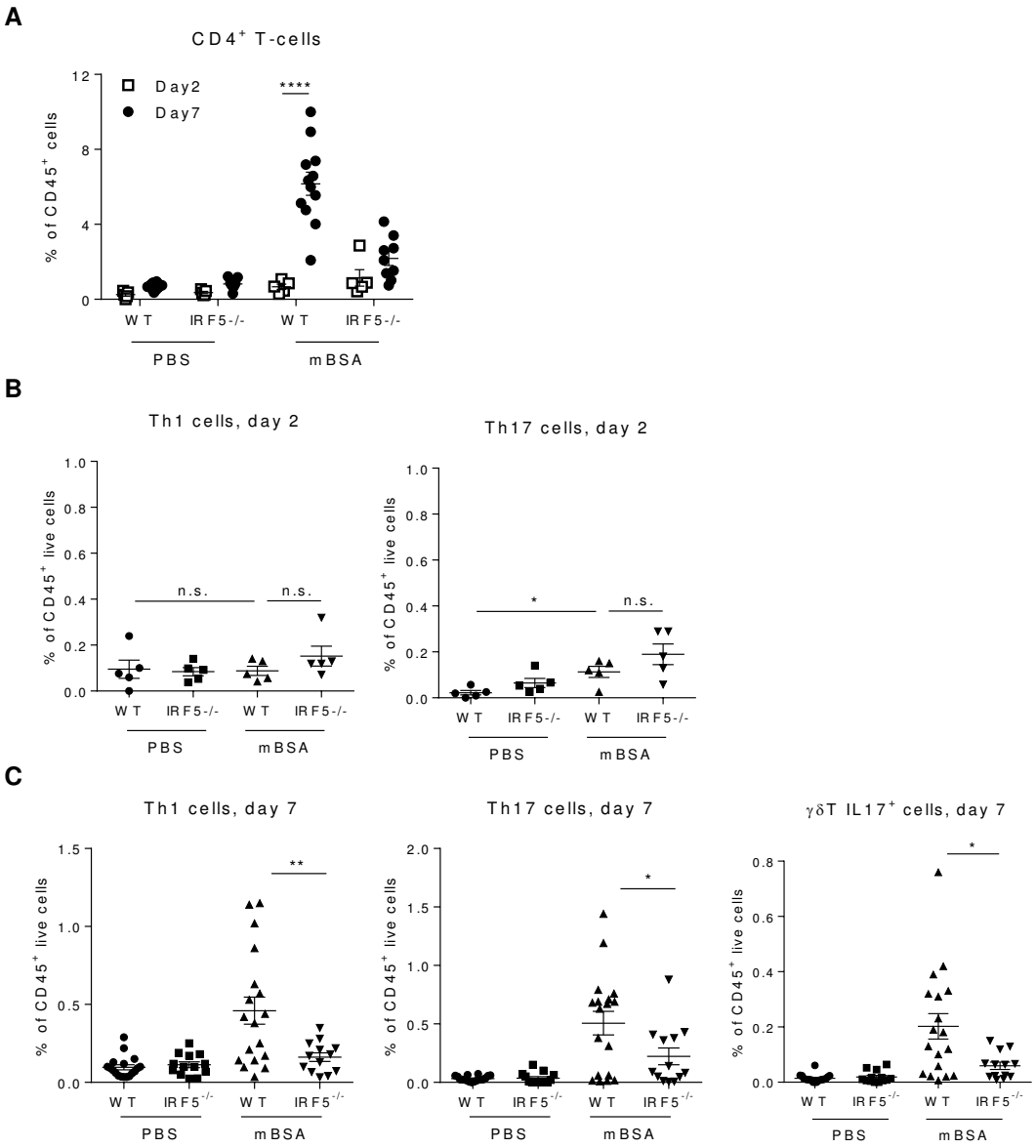

Figure 5.6. The T-cell response in the arthritic knee is diminished in the absence of IRF5.

IRF5 WT and KO were first immunised with mBSA and challenged with mBSA or PBS control seven days later. Knees were excised on day two or seven of disease to investigate the early and late T-cell responses. Flow cytometric analysis was used to identify Th1, Th17 and γδ IL17$^+$ T-cells in PBS and mBSA knees of mice. **A.** Cell suspensions obtained from knees were gated for CD45$^+$ live and CD4 expression to identify CD4$^+$ T-cells. For day two n=5, for day 7 n=9-12. Statistical analysis performed by 2-way ANOVA and Bonferroni's multiple comparison. **B and C.** The numbers of CD4$^+$ IFNγ (Th1) and Il17 (CD4$^+$ Th17 or γδ TCR$^+$) producing T-cells were expressed as a percentage of live CD45$^+$ cells. No γδ T-cells were detected on day two of disease. Data show the mean and SEM derived from n=5 at day two or n=13-18 for day seven from 3 independent AIA experiments. Statistical analysis was performed by one-tailed Mann-Whitney U test. * p≤0.05; ** p≤0.01; **** p≤0.0001

Secondly, T-cell subsets were analysed specifically at day two (Figure 5.6B) and seven (Figure 5.6C) of disease. Of note, γδ T-cells could not be detected in joints at day two. In early AIA, the numbers of IFN-γ producing Th1 cells were not increased following mBSA injection whereas IL-17 producing Th17 cells showed a small though statistically significant increase in WT but not IRF5$^{-/-}$ mice. Th1, Th17 and IL-17a^{+} γδ T-cells were all augmented in arthritic knees of WT mice but significantly reduced in IRF5 deficient mice at day seven. Hence, T-cell responses at the site of inflammation are more pronounced at the later stages of AIA in WTs but are diminished throughout when IRF5 is ablated.

T-cells in the draining lymph node

Inguinal LNs (draining both the affected knee and the site of immunisation) were collected two or seven days after intra-articular injection. Th1 and IL-17 producing γδ T-cells but not CD4^{+} IL-17a^{+} cells were present at significantly lower numbers in IRF5$^{-/-}$ mice at day two of AIA (Figure 5.7A). During late AIA, there were generally fewer T-cells compared to day two but percentages were equally low in IRF5 WT and KO animals (Figure 5.7B). To sum up, early but not late T-cell responses in the draining LN are affected by IRF5 deficiency.

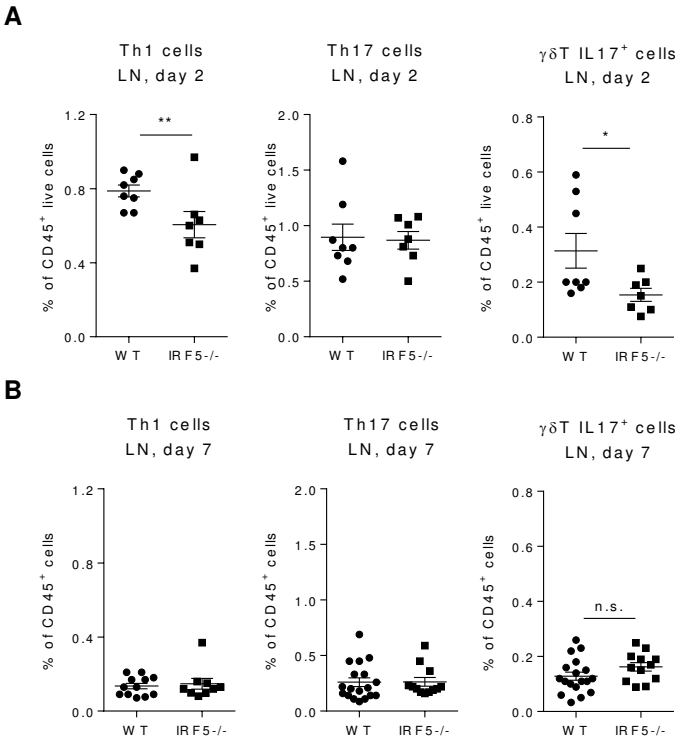

Figure 5.7. T-cell numbers in the lymph nodes are affected by loss of IRF5 during early but not late AIA.

IRF5 WT and KO were immunised with mBSA and challenged with mBSA or PBS control seven days later. LNs were collected on day two (**A.**) or seven (**B.**) of disease to determine the T-cell responses. Th1, Th17 and γδ IL17$^+$ T-cells were identified using flow cytometry. Cell suspensions were first gated for CD45$^+$ live. Th1 (CD4$^+$ IFNγ$^+$), Th17 (CD4$^+$ Il17a$^+$) and γδ IL17$^+$ T-cells (γδ TCR$^+$ Il17a$^+$) are expressed as a percentage of live CD45$^+$ cells. Data show the mean and SEM derived from n=7-8 from one experiment at day two or n=12-18 for day seven from 3 independent AIA experiments. Statistical analysis was performed by one-tailed Mann-Whitney U test. * p≤0.05; ** p≤0.01

T-cells in circulation

Few T-cells were detected in whole blood at early or late time points showing little or no change when comparing WT and IRF5$^{-/-}$ animals (Figure 5.8). The only significant difference could be observed for IL-17a$^+$ CD4$^+$ T-cells on day seven (Figure 5.8B). Thus, depletion of IRF5 does not seem to affect most circulating T-cells during AIA.

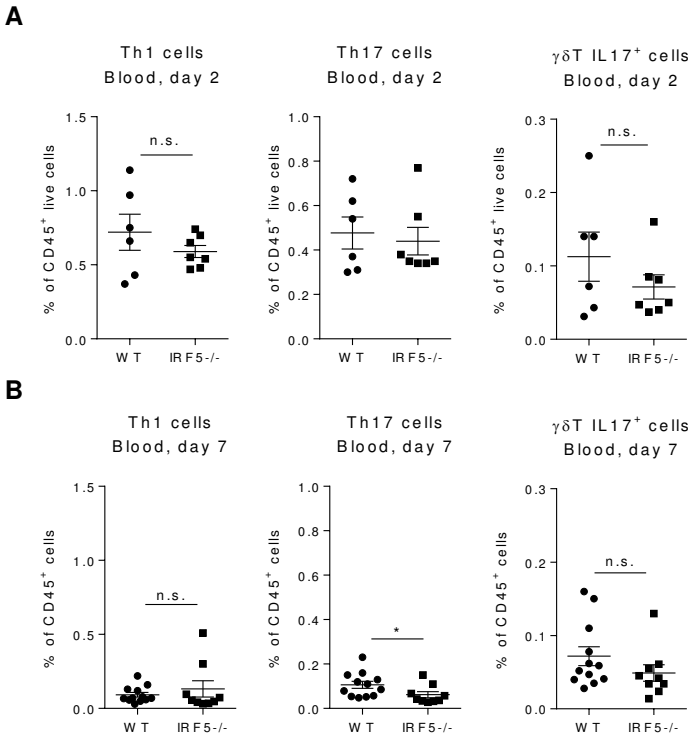

Figure 5.8. IRF5$^{-/-}$ mice have less Th17 cells in the blood at day seven of AIA.

Mice were immunised with mBSA and seven days later intra-articular challenge with mBSA or PBS as a control was performed. At day two (**A.**) or seven (**B.**) of AIA, blood was collected to analyse the T-cell populations in circulation. Th1, Th17 and γδ IL17^{+} T-cells were identified using flow cytometry by staining for CD45, CD4, γδ TCR, IFNγ and IL17a. Th1, Th17 and γδ IL17+ T-cells are expressed as a percentage of CD45^{+} cells. Data show the mean and SEM derived from n=6-7 from one experiment for day two or n=9-12 for day seven from 2 independent AIA experiments. Statistical analysis was performed by one-tailed Mann-Whitney U test. * p≤0.05

To conclude, the T-cell response in IRF5 deficient animals is diminished both at the site of inflammation in the joints and in the draining LNs in AIA.

5.2.6. Lymphocyte proliferation and B-cell numbers are unaffected by a lack of IRF5

To assess a potential effect of IRF5 deficiency on the immunisation process preceding the intra-articular challenge, inguinal LNs were harvested seven days after immunisation. LN cell suspensions were stimulated with α-CD3 or mBSA for 3 h and cell proliferation was measured. Since B-cells are also known to

express IRF5, we examined B-cell numbers in tissues of arthritic animals including the joints, inguinal LNs, blood and spleen. In addition, IgG1 and IgG2a antibody levels in serum as a measure of B-cell function were evaluated at day two of AIA.

Stimulation with either α-CD3 or mBSA resulted in a significant increase in lymphocyte proliferation, but proliferative responses were unaffected by IRF5 deficiency (Figure 5.9).

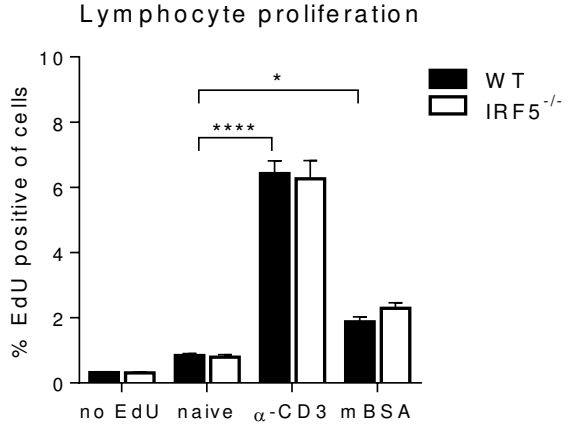

Figure 5.9. Lymphocyte proliferation is unaltered in IRF5 deficient mice.

WT and IRF5$^{-/-}$ mice were immunised with mBSA and CFA and LNs were collected seven days later. No further intra-articular challenge was performed on those mice as solely the immunisation process was investigated. LN cell cultures were stimulated with α-CD3 and mBSA for 48 h. Edu was added to the lymphocytes 2 h prior to the end of stimulation. Proliferation was assessed by determination of EdU^{+} cells using flow cytometry. The data are mean and SEM derived from 6 independent lymphocyte cultures. Statistical analysis was performed by 2-way ANOVA and Bonferroni's multiple comparison. * p≤0.05; ** p≤0.01, *** p≤ 0.001

We were unable to detect CD19^{+} B-cells in the joint in WT and IRF5$^{-/-}$ mice. The numbers of CD19^{+} B-cells in the blood, spleen and LN were unaffected (Figure 5.10A). Furthermore, the analysis of B-cell responses revealed no significant change in IgG1 but levels of IgG2a were reduced (Figure 5.10B), consistent with previously published observations (Savitsky et al. 2010).

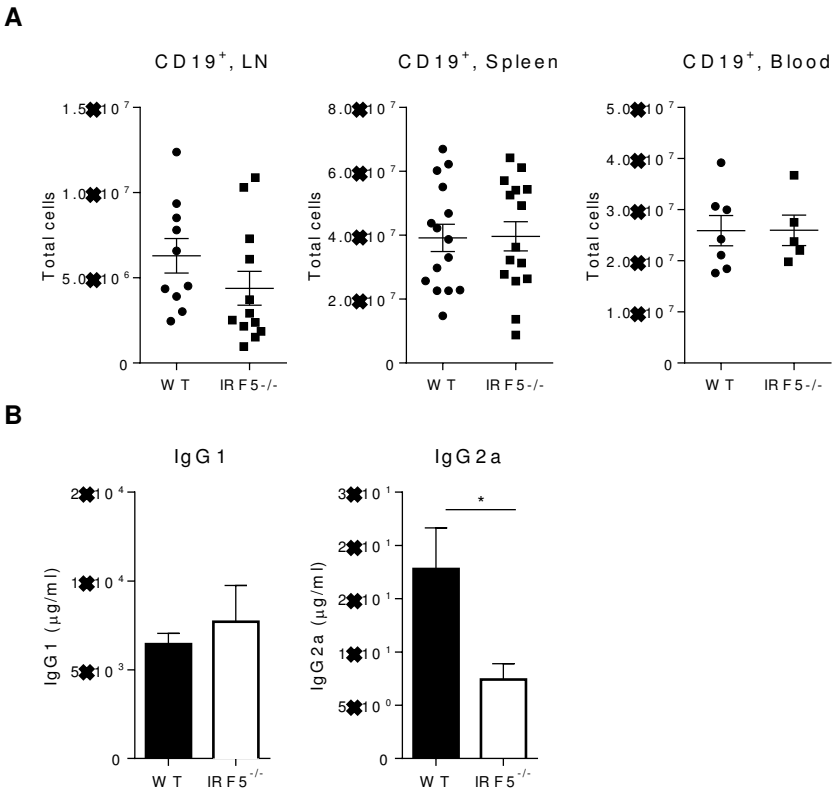

Figure 5.10. B-cell numbers and antibody responses in IRF5 deficient mice.

WT and IRF5$^{-/-}$ mice were immunised with mBSA and CFA and challenged with mBSA seven days later. Tissues and serum were obtained to analyse the response of the adaptive immune system in those animals. **A.** Total cell counts of CD19^{+} B-cells in the lymph nodes, spleens and blood of IRF5$^{-/-}$ and WT mice at day two of disease. Experiments were partly conducted by Katrina Blazek (Udalova laboratory). The data are mean and SEM derived from 5-15 independent cell preparations. Each dot represents an individual mouse. **B.** Levels of total IgG1 and IgG2a in the serum on day two of AIA. Serum data and analysis courtesy of Dr. Adam J. Byrne (Udalova laboratory). The data are mean and SEM using 3-5 mice from a representative AIA experiment. Statistical analysis was performed by two-tailed unpaired t- test. * p≤0.05

These data show that lack of IRF5 only moderately affects the systemic adaptive immune response but instead influences local inflammation at the site of antigen challenge.

5.2.7. Reduced swelling in inflamed knees of IRF5$^{-/-}$ mice correlates with fewer infiltrating neutrophils and decreased levels of CXCL1

IRF5$^{-/-}$ mice display limited neutrophil influx in response to mBSA injection

Since none of the cell populations analysed thus far (macrophages, monocytes, DCs, B- and T-cells) exhibited reduced numbers in IRF5$^{-/-}$ animals during early AIA, the difference in knee swelling and cellular infiltrate at day two remained unexplained. As neutrophils are known to be part of the early innate immune response, we examined whether neutrophil influx could be responsible for the observed reduction in disease severity at day two of AIA.

Due to the likelihood of a substantial contribution from the pool of BM neutrophils when harvesting knees for flow cytometry, we investigated infiltrating neutrophils by two independent methods based on their Ly6G expression. First, we determined overall neutrophil numbers by immunohistochemistry and confocal microscopy using knee sections stained for Ly6G^{+} cells where BM neutrophils could be excluded due to their localisation. Second, when flow cytometry was used to identify neutrophils, pro-IL1β was included as marker for activated neutrophils (Parsey et al. 1998), which were thereby characterised as Ly6G^{+} CD11b^{+} F4/80^{-} pro-IL1β^{+}. Immunohistochemical staining demonstrated a clear reduction in synovial neutrophil infiltrate in IRF5$^{-/-}$ animals (Figure 5.11A and B, representative pictures and quantification, respectively). This was confirmed by the significant decrease in synovial activated neutrophils in inflamed knees of IRF5$^{-/-}$ mice (Figure 5.11C). However, in IRF5 deficient arthritic mice at day two, the numbers of circulating neutrophils in the blood and in the spleen remain

unaltered (Figure 5.11D). Thus, ablation of IRF5 does not seem to affect the capability of neutrophils to exit the BM.

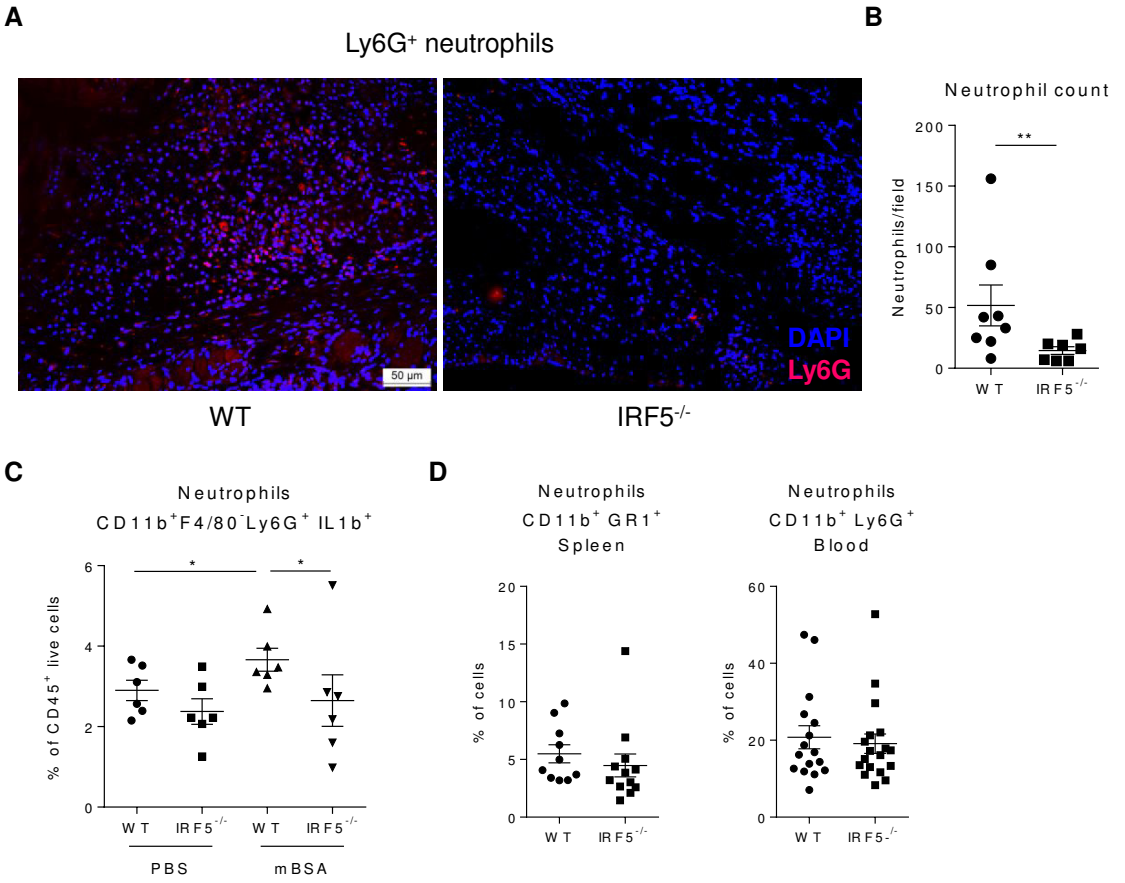

Figure 5.11. IRF5 ablation limits neutrophil influx in the inflamed knee.

Mice underwent AIA and were sacrificed at day two of disease. Knee joints were excised and subjected to either immuno-histochemistry or FACS. Spleens and blood were taken for flow cytometric analysis. **A. and B.** Ly6G$^+$ cells were detected within the synovial capsule of arthritic knees in IRF5$^{-/-}$ and WT mice, analysed by immuno-histochemical staining and confocal microscopy. Nuclei are stained with DAPI in blue, surface Ly6G is shown in pink. To quantify the reduction of neutrophils, the number of neutrophils per field was counted in mBSA knees of both IRF5 WT and KO mice, n=7-8. Images and analysis courtesy of Dr. Adam J. Byrne (Udalova laboratory). **C.** Control and challenged knees were analysed for the amount of pro-IL1β expressing neutrophils. Neutrophils were defined as previously, CD11b$^+$ F4/80$^-$ Ly6G$^+$. Prior to staining, cell suspensions were stimulated with LPS, Brefeldin A and monensin. Data show the mean and SEM for n=6. **D.** Numbers of CD11b$^+$ GR1$^+$/Ly6G$^+$ neutrophils shown as percentage of total cells in spleen and blood. Experiments were partly conducted by Katrina Blazek (Udalova laboratory). The data are mean and SEM for n=10-18 from 2-3 independent experiments.
Statistical analysis was performed by one-tailed Mann-Whitney U test. * p≤0.05; ** p≤0.01

To conclude, neutrophils are the only cell population analysed whose influx into mBSA challenged joints is diminished in the absence of IRF5.

IRF5 depleted neutrophils migrate normally

As it was observed previously that neutrophils themselves express some IRF5, we sought to examine whether their migratory capacity was affected by IRF5 deletion. To assess chemotaxis towards the neutrophil chemo-attractant CXCL2, we used the EZ-Taxiscan system, which allows visualisation of neutrophil movement (Nitta et al. 2007). Neutrophils were isolated from air-pouches by Dr. Adam Byrne, created on the dorsal surface of mice and injected with zymosan (Colville-Nash and Lawrence 2003) (see chapter 2.2.2, Air pouch). ~80% of the recovered cells after injection of 100 µg of zymosan were $CD11b^+$ $Ly6G^+$ neutrophils (Blazek et al. 2015). Migration of IRF5 deficient neutrophils towards the chemoattractant CXCL2 was not impaired when compared to WT neutrophils (Figure 5.12A). The Euclidean distance covered by neutrophils migrating towards the chemokine was equally increased in WT and $IRF5^{-/-}$ cells (Figure 5.12B). Notably, basal neutrophil movement, in the absence of any chemoattractant, was not affected either. Overall, we conclude that neutrophil intrinsic capacity to migrate is not affected in $IRF5^{-/-}$ animals.

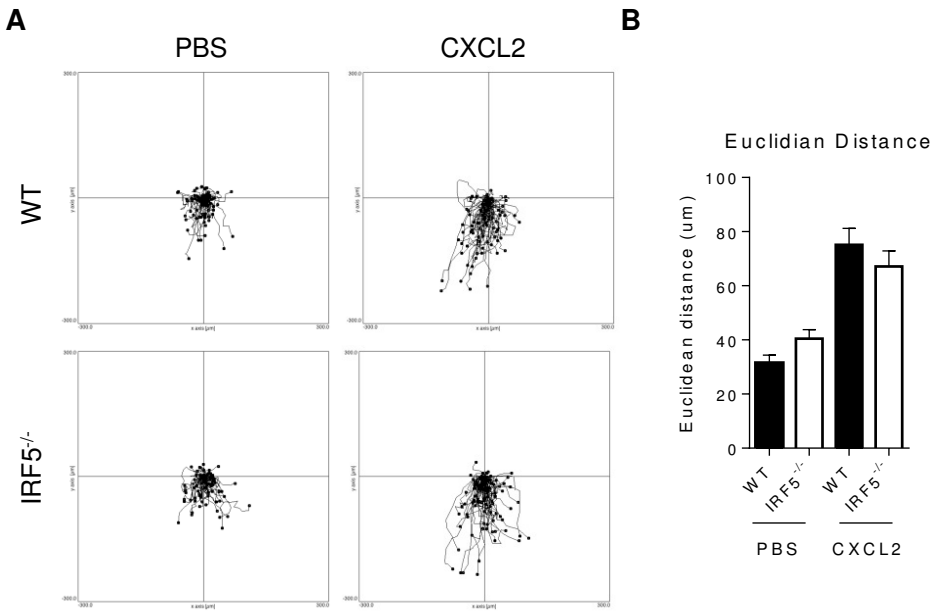

Figure 5.12.Neutrophils lacking IRF5 do not show any defects in their migratory capabilities.

A. The air pouch model was used to obtain a highly neutrophilic cell suspension from an inflammatory environment. Images show centre-zeroed tracks of neutrophilic infiltrate in an EZ-Taxiscan migrating towards PBS as a control or CXCL2; scale in µm. **B.** Tracks were analysed to calculate the Euclidean distance each cell travelled in a 45 minute time-period. Data shown are the average and SEM of 3 independent experiments each including 9-20 movies per treatment. Experiments were conducted and analysed by Dr. Adam J. Byrne (Udalova laboratory). Taxiscan was operated by Dr. James E. Pease (Imperial College London).

Levels of CXCL1 are reduced in inflamed joints of IRF5$^{-/-}$ mice

To assess whether neutrophil attracting chemokines produced by macrophages and other cells were altered in IRF5$^{-/-}$ mice, we analysed the levels of known neutrophil chemoattractants. The concentration of secreted CXCL1, CXCL2, CXCL10, CCL3, CCL4 and CCL5 was determined in the supernatants of synovial leukocytes isolated from mBSA treated knees using Luminex analysis. The levels of CXCL1 were significantly reduced while most other chemokines only showed a trend that was not significantly affected by loss of IRF5 (Figure 5.13). Hence, decreased levels of neutrophil attracting CXCL1 correspond to reduced numbers of neutrophils in the inflamed joint in IRF5$^{-/-}$ mice.

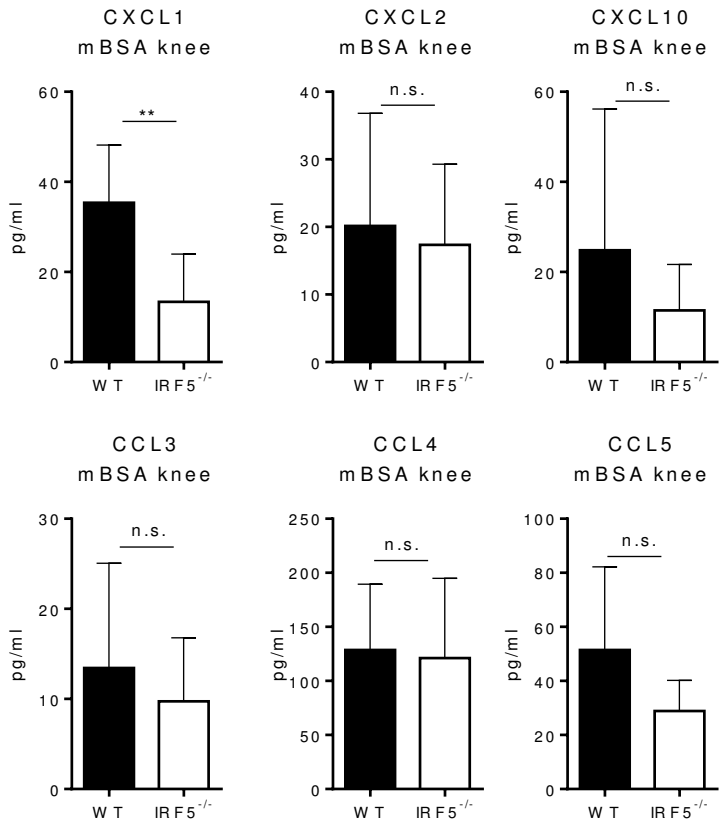

Figure 5.13. The neutrophil chemoattractant CXCL1 is reduced in the supernatants of synovial cells.

IRF5$^{-/-}$ and WT mice were subjected to AIA and knee joints were excised on day two of disease. Cells were liberated from the joints and left at 4°C for 3 h before supernatants were collected and chemokine levels were determined using Luminex. The neutrophil attracting chemokines CXCL1 and CXCL2 were analysed as well as CXCL10 which is involved in the Th1 response. Additionally, the chemokines CCL3, CCL4 and CCL5 which mediate macrophage and NK cell migration were investigated. Data are shown as mean and SEM for n=6. Statistical analysis was performed by one-tailed Mann-Whitney U test. ** p≤0.01

To conclude, neutrophil influx in the mBSA challenged knee is attenuated in IRF5$^{-/-}$ animals although IRF5 deficient neutrophils are able to migrate normally. This reduction in neutrophil numbers may be due to the decreased levels of the neutrophil chemoattractant CXCL1.

5.2.8. Myeloid specific IRF5 ablation leads to reduced neutrophil influx and CXCL1 secretion

To verify whether the observed effects were solely due to a deletion of IRF5 in myeloid cells, we generated a myeloid specific IRF5 knockout using *LysM*^{cre} *Irf5*$^{fl/fl}$ mice (referred to as IRF5 conditional KO, cKO). Myeloid specific IRF5 deficient mice underwent AIA as before and phenotypic key read-outs of the global IRF5$^{-/-}$ experiment described above were analysed. This included knee swelling, numbers of infiltrating neutrophils and expression of CXCL1 in the affected joint.

First, we wanted to estimate the efficiency of IRF5 deletion by examining levels of IRF5 in the inflamed knees of IRF5 cKO mice at day two of AIA, using flow cytometry (Figure 5.14). IRF5 expression was reduced by approximately 50% in Ly6C^{hi} monocytes and macrophages that expressed the highest levels of IRF5 overall, as observed previously. The effect on Ly6C^{lo} monocytes and CD11b^{+} DCs was less pronounced and not statistically significant, whereas IRF5 levels in CD45^{-} and CD11b^{-} DCs cell populations remained completely unaffected.

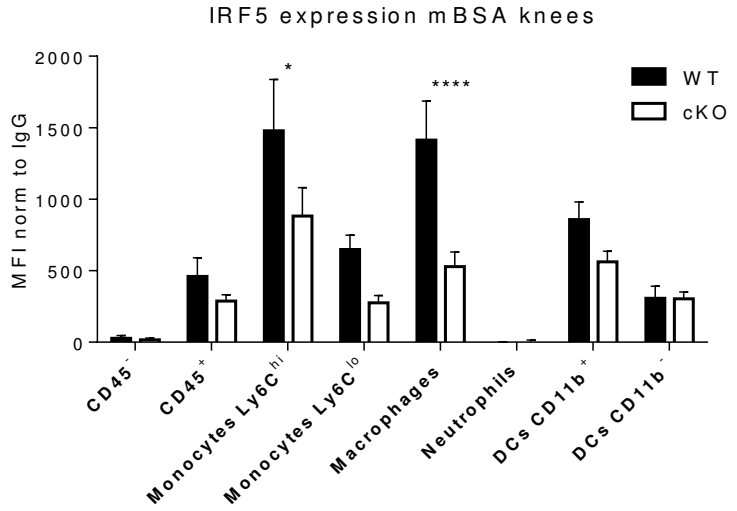

Figure 5.14. Only Ly6C^{hi} monocytes and macrophages show reduced IRF5 expression in arthritic knees of *LysM-cre Irf5*$^{fl/fl}$ mice.

WT and *LysM-cre Irf5*$^{fl/fl}$ mice underwent AIA as described before and were sacrificed on day two. Liberated knee cells were analysed for surface marker expression and intracellular IRF5. All cell populations were gated on CD45$^+$ live. Macrophages were defined as CD11b$^+$ F4/80^{hi}, monocytes as CD11b$^+$ F4/80^{dim} and neutrophils as CD11b$^+$ F480$^-$ Ly6G$^+$. DCs were CD11c$^+$ F4/80$^-$ and either CD11b$^+$ or CD11b$^-$. IRF5 levels were quantified by MFI and normalised by subtracting the MFI values of IgG controls from WT mice. Data show the mean and SEM derived from 3-14 mice from 2 independent experiments. Statistical analysis was performed by 2-way ANOVA and Bonferroni's multiple comparison. ** p≤0.01; *** p≤ 0.001

Second, we assessed knee swelling and neutrophil influx in IRF5 cKO mice. Knee swelling was reduced in IRF5 cKO mice at day one and two of disease (Figure 5.15A). Furthermore, quantification of knee sections stained for Ly6G$^+$ cells demonstrated a significant reduction in synovial neutrophil infiltrate in IRF5 cKO animals on day two (Figure 5.15B). Lastly, we analysed expression of CXCL1 in IRF5 cKO mice by two independent means; 1) in whole joint supernatants of excised knees and 2) cell type specific using flow cytometry. Total CXCL1 secretion was measured by ELISA in supernatants of synovial cells and levels of CXCL1 were indeed significantly reduced in samples derived from mBSA challenged knees of IRF5 cKO mice (Figure 5.15C). To specifically address which cells express less CXCL1 in IRF5 cKO mice, intracellular CXCL1

was detected by flow cytometry in synovial cell suspensions. Cells were obtained from PBS knees and stimulated *ex vivo* with LPS for 3 h. Macrophages were observed to be the main producers of CXCL1 with some contribution from Ly6C$^{hi/lo}$ monocytes and CD11b^{+} DCs. They were, however, the only cells to demonstrate a significant reduction in CXCL1 in IRF5 cKO mice (Figure 5.15D).

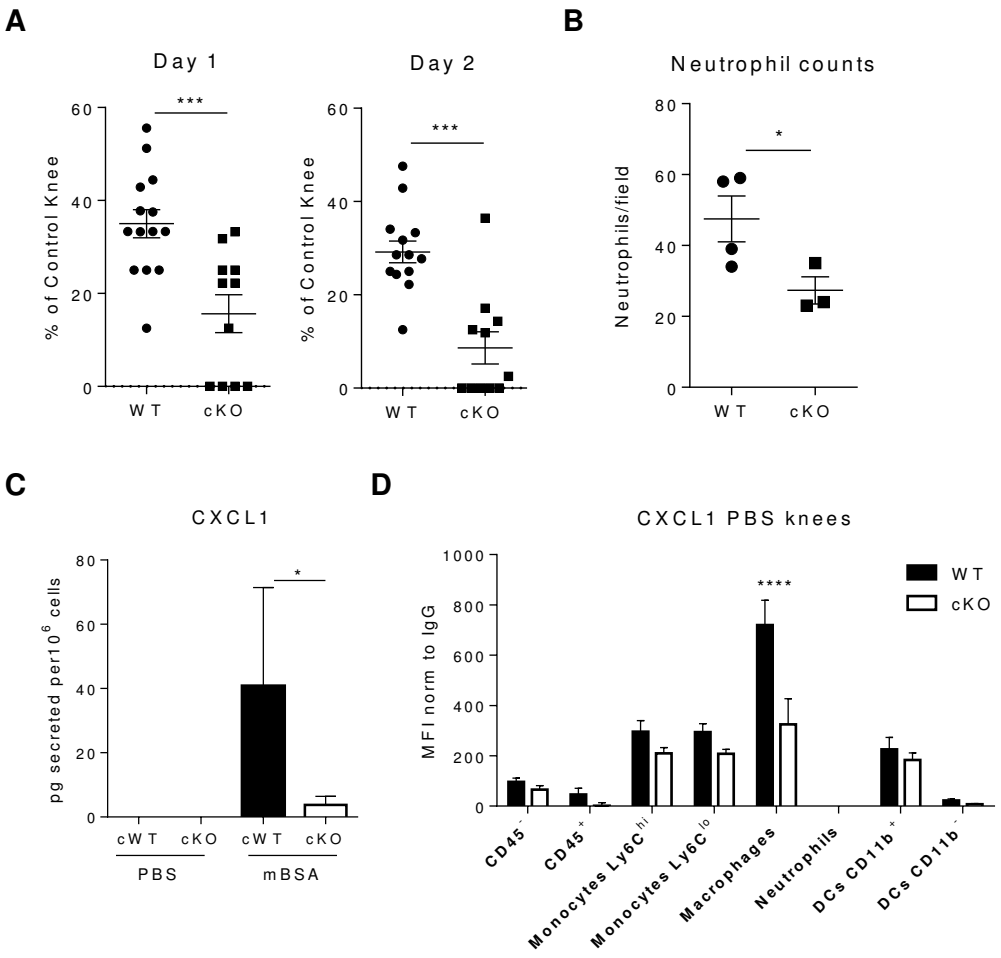

Figure 5.15. Myeloid specific IRF5 deficient mice show decreased knee swelling and neutrophil influx.

To induce AIA, WT and *LysM-cre Irf5*$^{fl/fl}$ mice were first immunised and then challenged intra-articularly with mBSA or PBS control. Disease severity was assessed every day using callipers. Mice were sacrificed on day two of disease and joints were collected. **A.** Knee swelling in *LysM-cre Irf5*$^{fl/fl}$ and WT mice, expressed as a percentage of swelling of the mBSA challenged knee compared to the PBS knee. Data show the mean and SEM derived from 11-14 mice from 2 independent experiments. **B.** Neutrophils were detected within the synovial capsule of inflamed knees by immuno-histochemical staining and confocal microscopy as in Figure 5.11. Neutrophils were quantified by counting the number of Ly6G$^+$ cells per field in mBSA knees. Analysis provided by Dr. Adam J. Byrne (Udalova laboratory). Data are mean and SEM for n=3-4. **C.** Levels of CXCL1 in the supernatants of synovial cells isolated from mBSA injected knees and PBS controls. Amount secreted was normalised to the total number of cells present. Data are shown as mean and SEM for n=5. **D.** Cells liberated from PBS knees were stimulated with LPS, Brefeldin A and monensin for 3 h. Samples were then stained for expression of the extracellular markers CD45, CD11b, Ly6G, F4/80 and MHC II to identify the different myeloid cell subsets. CXCL1 was detected by intracellular staining and samples were analysed by FACS. Expression levels of CXCL1 were quantified by MFI by subtracting MFI values of IgG stained controls. Data are mean and SEM for n=5.
Statistical analysis was performed by one-tailed Mann-Whitney U test or 2-way ANOVA and Bonferroni's multiple comparison (D.). * p≤0.05; ** p≤0.01; *** p≤ 0.001; *** p≤ 0.001

We therefore conclude that IRF5 cKO mice display reduced IRF5 levels in some populations of myeloid cells, especially Ly6C^{hi} monocytes and macrophages. Despite incomplete ablation achieved, these data indicate that IRF5 expression in macrophages is crucial for CXCL1 secretion, neutrophil influx and disease severity.

5.2.9. Lack of IRF5 reduces infiltrating neutrophils and CXCL1 in the lung upon LPS challenge

Next, we examined whether the reduction in neutrophil influx in IRF5$^{-/-}$ mice was confined to inflammation in the joint in arthritis models. As an alternative, we chose the well-established model of acute lung injury, which is characterised by a high influx of neutrophils into the challenged lung (Matute-Bello et al. 2008). IRF5$^{-/-}$ and WT mice were administered LPS intra-nasally at 1 mg/kg body weight and sacrificed 24 h later (see 2.2.2, Acute lung injury). IRF5$^{-/-}$ mice showed significantly less cellular infiltrate in bronchoalveolar lavage fluid (BAL) and more specifically, displayed a significant reduction in the number of neutrophils recruited into the lung 24 h post challenge (Figure 5.16A). Numbers of other infiltrating myeloid cells such as monocytes and macrophages were not affected in the lung, but the levels of secreted CXCL1 were significantly reduced once again (Figure 5.16B). To conclude, lack of IRF5 can also affect neutrophil influx and CXCL1 production in the LPS challenged lung.

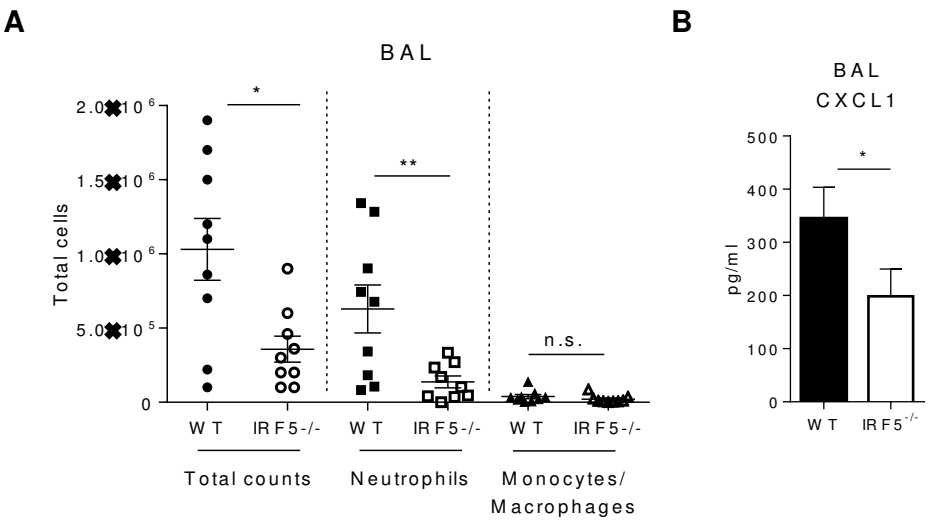

Figure 5.16. Neutrophil influx and CXCL1 levels in the LPS challenged lung of IRF5$^{-/-}$ mice are decreased.

WT and IRF5$^{-/-}$ mice were given LPS intranasally for 24 h. BAL was collected and analysed for its cellular content and chemokine concentration. **A.** Overall cell counts and total numbers of neutrophils and monocytes/macrophages were analysed in BAL. Cell numbers were determined using either flow cytometry or Wright-Giemsa stained cytospins. Each dot represents an individual mouse. **B.** Levels of CXCL1 in BAL of LPS challenged animals as quantified by ELISA or Luminex. Experiments and analysis conducted by both Dr. Adam J. Byrne and myself. Data shown are mean and SEM for n=9-10 from 2 independent experiments. Statistical analysis was performed by one-tailed Mann-Whitney U test. * p≤0.05, ** p≤0.01

5.2.10. IRF5 controls chemokine gene expression *in vitro*

To investigate whether IRF5 is recruited to genetic chemokine loci and whether the expression of chemokine genes are generally affected by the lack of IRF5, we utilised GM-CSF mouse BM cultures that represent a mixture of macrophages and DCs (Helft et al. 2015), both expressing similar levels of IRF5 (see Figure 3.5).

IRF5 binds to chemokine loci in GM-CSF differentiated cells

IRF5 ChIP-Seq data sets were generated by Dr. David Saliba in WT and IRF5$^{-/-}$ GM-BMDMs with 50 bp paired end sequencing following stimulation with LPS

for 0 h and 2 h in duplicate, as previously described (Saliba et al. 2014). After filtering out false positive IRF5 binding peaks detected in IRF5 deficient cells, 2538 bona fide binding peaks were mapped to gene promoter regions (up to 10 kb upstream and 0.5 kb of the TSS). The defined genes with IRF5 binding sites in their promoters were then subjected to gene ontology and PANTHER pathway analysis (Figure 5.17). The pathways and molecular functions that were enriched for IRF5 binding were related to inflammation and chemokines, cytokines as well as their receptor activities.

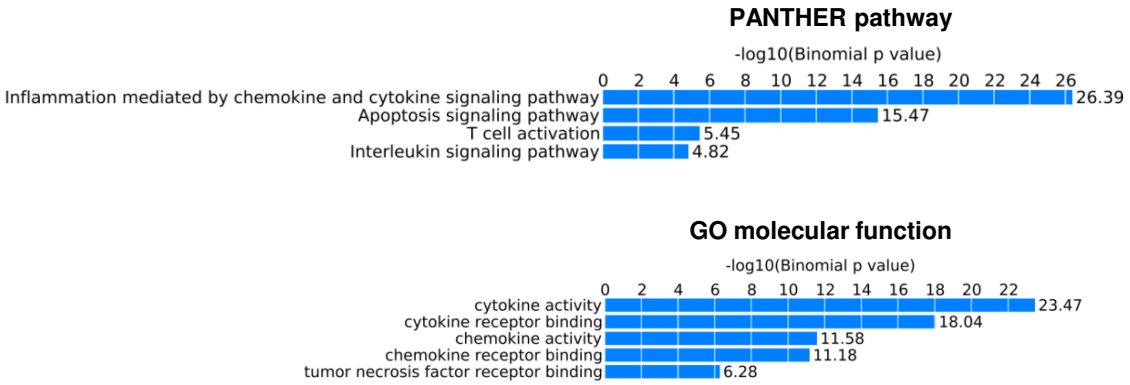

Figure 5.17. Binding sites of IRF5 in GM-BMDMs are associated with inflammatory cytokines and chemokines.

IRF5 WT and KO BMDMs were differentiated with GM-CSF for eight days and then stimulated with LPS for 2 h. ChIP-Seq for IRF5 was performed on those cells to determine genome wide IRF5 binding patterns. IRF5 peaks were assigned to genomic regions using GREAT and molecular functions and pathways were analysed using GO and PANTHER. Analysis and images courtesy of Dr. David G. Saliba (Udalova laboratory).

Moreover, chemokines where promoters were directly targeted by IRF5 in GM-BMDMs following 2 h stimulation with LPS included, amongst others, *Cxcl1, Cxcl2, Cxcl10, Ccl3, Ccl4* and *Ccl5* (Figure 5.18A and B). These data show that genomic regions bound by IRF5 are not only generally associated with chemokine activity but also specifically contain chemokine genes.

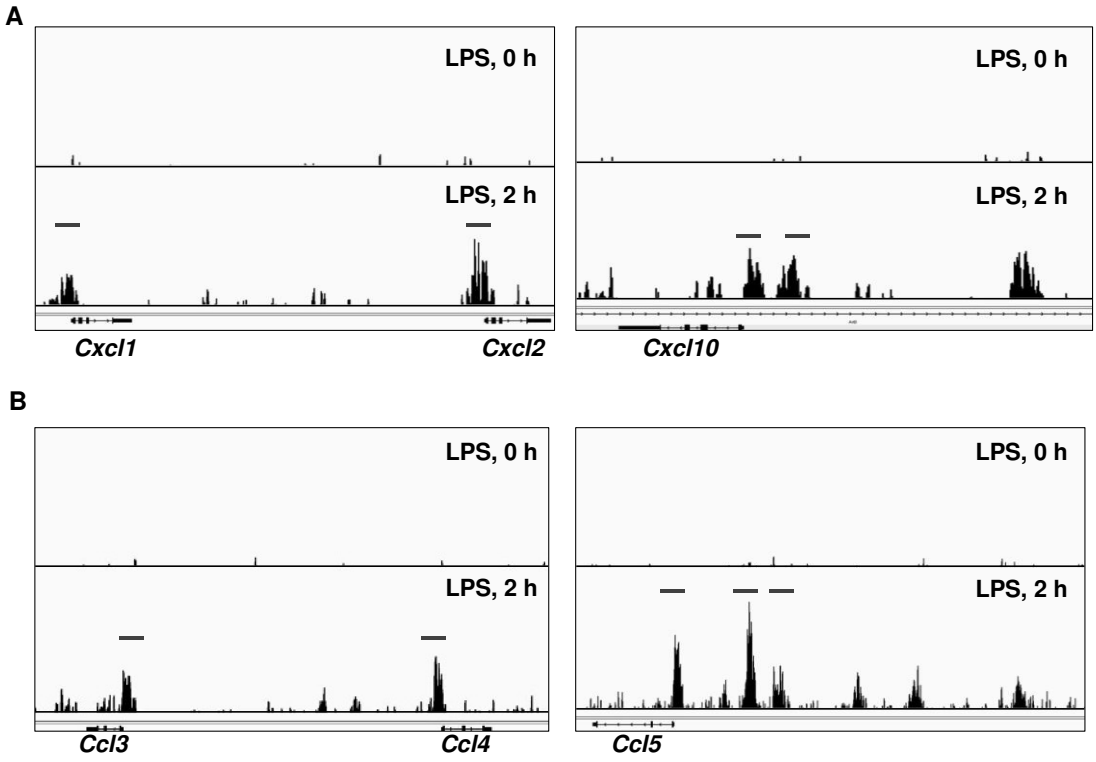

Figure 5.18. IRF5 binds to the promoters of chemokine genes in GM-BMDMs.

BMDMs were differentiated with GM-CSF for eight days and then either left unstimulated (0 h, upper panels) or stimulated with LPS for 2 h (lower panels). ChIP-Seq for IRF5 was performed to identify direct IRF5 target genes. Representative USCS tracks with IRF5 binding peaks are shown for the loci of *Cxcl1*, *Cxcl2* and *Cxcl10* (**A**) and members of the CCL family, *Ccl3*, *Ccl4*, *Ccl5* (**B**). Images courtesy of Dr. David G. Saliba (Udalova laboratory).

Chemokine expression is reduced in response to LPS in GM-BMDMs

To verify the functional consequences of IRF5 depletion in GM-BMDMs, we next examined mRNA expression of eight selected chemokines. These included the aforementioned chemokines in the previous section but included *Cxcl3* and *Cxcl5* as additional neutrophil attracting chemokines. IRF5$^{-/-}$ and WT GM-BMDMs were stimulated with LPS for 1 and 4 h and transcript levels were determined using qPCR. Expression of *Cxcl1*, *Cxcl2*, *Cxcl3*, *Cxcl5*, *Cxcl10*, *Ccl3* and *Ccl4* was significantly reduced in IRF5$^{-/-}$ macrophages (Figure 5.19A and B).

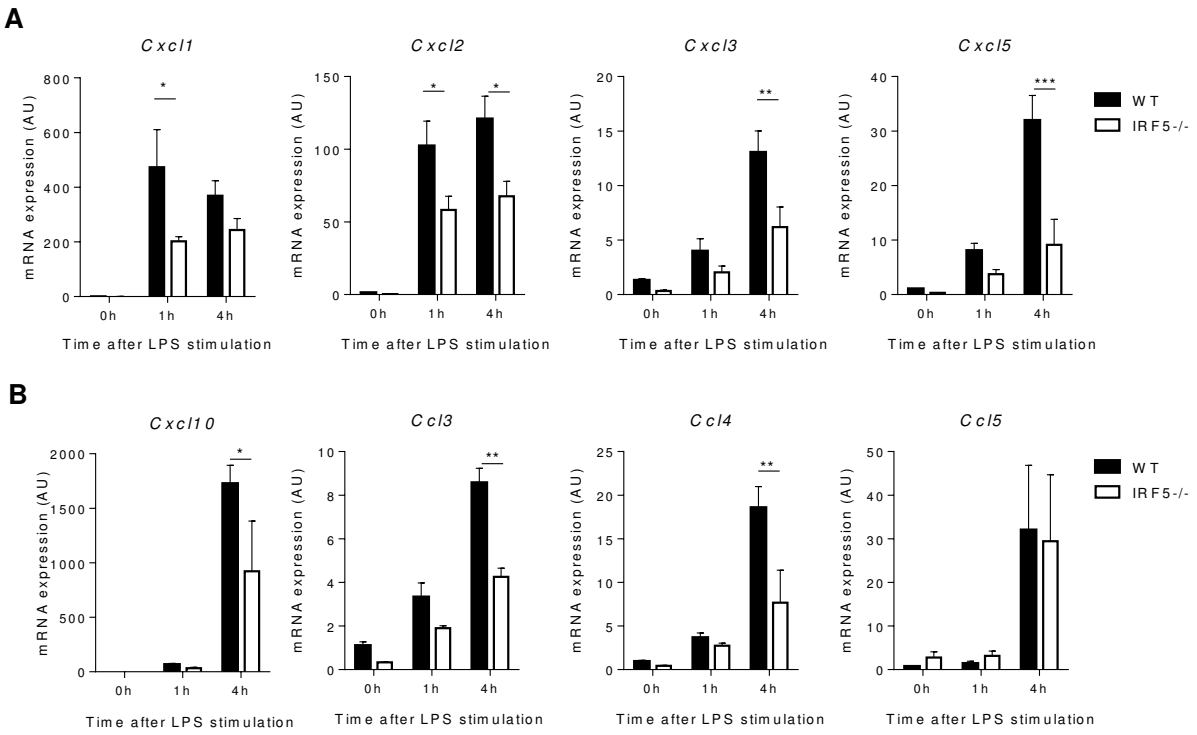

Figure 5.19. IRF5 controls chemokine network in GM-CSF derived macrophages.

BM progenitors were isolated from IRF5 WT and KO mice and differentiated with GM-CSF for eight days. Cells were then stimulated with LPS for 0 h, 1 h and 4 h. RNA was collected at each time point and mRNA levels were analysed using qPCR. Transcript expression is shown for the neutrophil chemoattractants *Cxcl1*, *Cxcl2, Cxcl3* and *Cxcl5* (**A**) as well as *Cxcl10*, *Ccl3*, *Ccl4, Ccl5* (**B**). RNA courtesy of Dr. David G. Saliba (Udalova laboratory). Data shown are the mean and SEM derived from n=3. Statistical analysis was performed by two-way ANOVA with Bonferroni's correction for multiple comparisons. * p≤0.05; ** p≤0.01; *** p≤ 0.001

In conclusion, we could show that IRF5 can directly bind to the regulatory regions of chemokine genes *in vitro* and ablation of IRF5 leads to reduced chemokine gene expression upon LPS challenge in GM-BMDMs.

5.3. Discussion

Neutrophil recruitment to the sites of infection has long been considered to be a key event in microbial clearance through their release of toxic molecules, including ROS and of cytokines and chemokines, which subsequently

orchestrate the propagation of inflammation. Consequently, their removal from the site of inflammation is vital for maintaining host health. Here, we demonstrate that deficiency of the TF IRF5, which has been previously shown to modulate the macrophage phenotype, also significantly reduces neutrophil trafficking to the sites of inflammation in various tissues (Figure 5.20). We unravel a systemic role for IRF5 in regulating chemokine gene expression in macrophages, including the secretion of major neutrophil chemoattractants, such as CXCL1, CXCL2, CXCL3 and CXCL5. Moreover, we show that IRF5 is critical for establishment of the $MHCII^{+}$ phenotype in monocyte-derived macrophages and the subsequent formation of a local Th1/Th17 response during antigen-induced arthritis.

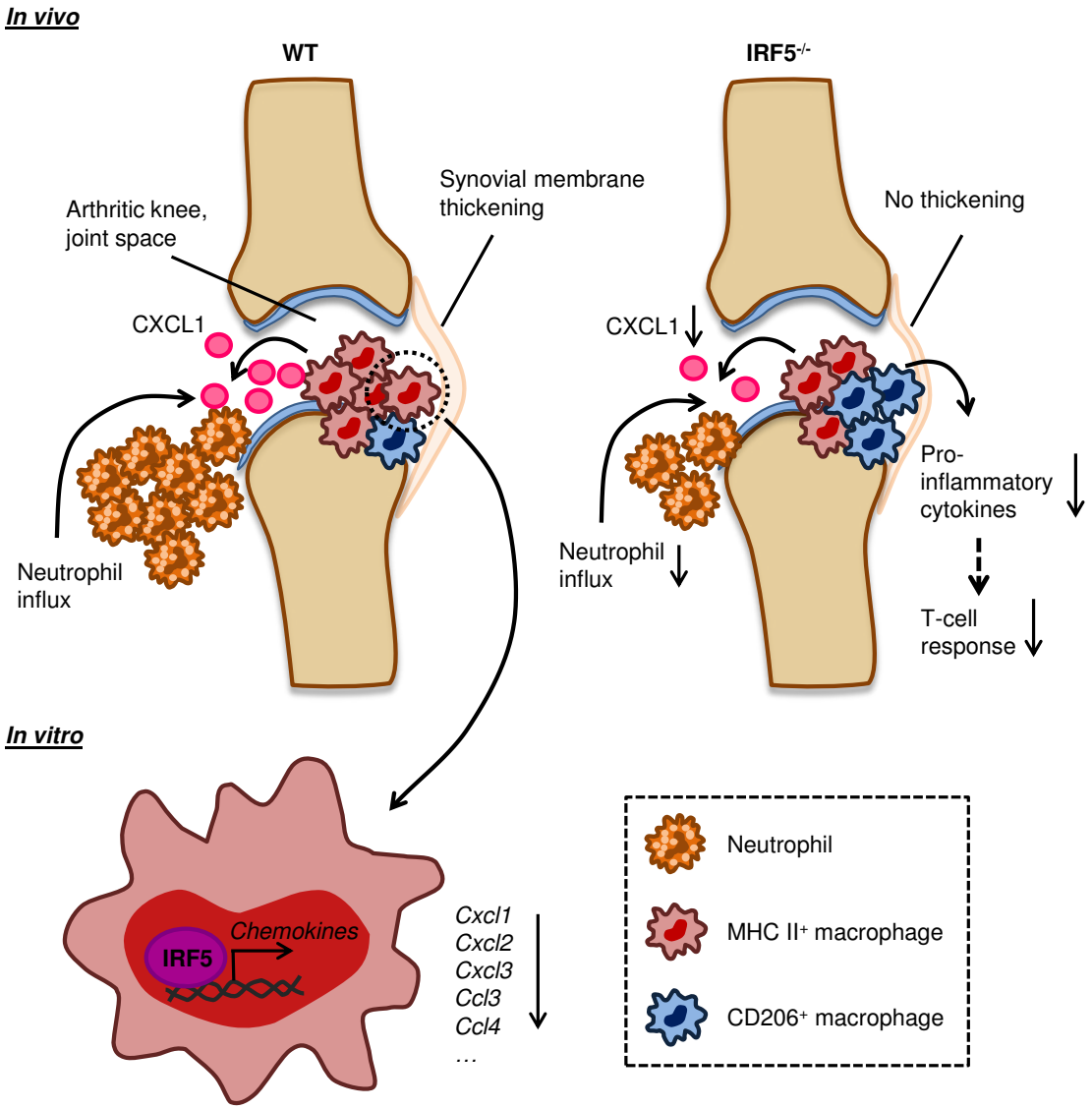

Figure 5.20. Lack of IRF5 causes a reduction in neutrophil influx and macrophage-derived CXCL1 in the arthritic knee.

IRF5 deficient mice display reduced knee swelling which is due to decreased infiltrating neutrophils in the joint at early stages of disease. Macrophage numbers remain unaffected by loss of IRF5, however the proportions of MHC II^{+} pro-inflammatory macrophages decrease while the CD206^{+} population increases. Moreover, levels of the neutrophil chemoattractant CXCL1 are reduced in the absence of IRF5, overall and specifically in synovial macrophages. IRF5 can generally regulate the expression of a network of chemokines in *in vitro* differentiated macrophages. Furthermore, ablation of IRF5 in AIA leads to a reduction in macrophage secreted pro-inflammatory cytokines and an overall altered inflammatory environment in the joint. Consequently, disease severity is also attenuated at later stages of the disease. Both the T-cell response in the knee as well as histological signs of membrane thickening and bone erosion are diminished in IRF5$^{-/-}$ mice.

Mice lacking IRF5 are resistant to lethal endotoxic shock (Takaoka et al. 2005) but cannot control *L. donovani* infection (Paun et al. 2008). They demonstrate a shift towards Th2 differentiation in a pristane-induced lupus model (Xu et al. 2012) and reduced disease severity in the MRL/lpr lupus model (Yasuda et al. 2014). Recent work unravelled the unorthodox role of IRF5 in diet-induced obesity, where its ablation induces massive tissue remodelling in the intra-abdominal adipose tissue and concomitant type-2 immune response. Consequently, IRF5-deficient mice are protected from obesity-induced metabolic dysfunction (Dalmas et al. 2015). Previously, $IRF5^{-/-}$ monocytes have been reported to show reduced migration and lower expression of CCR2 and CXCR4 in the pristane-induced lupus model into the peritoneal cavity (Yang et al. 2012). However, this difference was not observed in the BM and monocytes egress normally into circulation. Moreover, the influx of $Ly6C^{hi}$ monocytes into the peritoneal cavity upon thioglycollate stimulation remained unaffected. Our own data show that the influx of monocytes remains unaffected, both in the knee and in the lung (Figure 5.2 and Figure 5.16). Furthermore, numbers of both $CD11b^{+}$ and $CD11b^{-}$ DCs as well as overall $F4/80^{hi}$ macrophages were not changed in $IRF5^{-/-}$ mice. Thus, the observed effect on monocyte migration and receptor expression seems to be specific to pristane injection rather than a general property of monocytes lacking IRF5. This could be due to the fact that pristane is known to depend on TLR7 signalling (Lee et al. 2008) whereas CFA, which is used during immunisation in AIA, can activate different TLRs redundantly (Billiau and Matthys 2001).

Nevertheless, the presence of IRF5 appears to be important for differentiation of monocytes into $CD64^{hi}$ $MHCII^{+}$ macrophages in the arthritic joint (Figure 5.3). In

line with these observations and previously published studies (Takaoka et al. 2005, Krausgruber et al. 2011), expression of a number of pro-inflammatory cytokines produced by macrophages was reduced in whole joint RNA extracts of IRF5 deficient mice (Figure 5.4). Interestingly, transcript levels of the two Th2 related cytokines IL-10 and IL-13 were significantly higher in control knees of $IRF5^{-/-}$ mice. This finding suggests that IRF5 negatively regulates Th2 cytokine expression, in agreement with previously published data (Krausgruber et al. 2011, Paun et al. 2011, Dalmas et al. 2015). However, this difference could not be observed in antigen challenged knees where the acute pro-inflammatory response dominates and thereby is likely to overrule anti-inflammatory effects. These results combined with data from the previous chapters suggest that IRF5 is detrimental in regulating the establishment of an inflammatory phenotype in macrophages derived from infiltrating $Ly6C^{hi}$ monocytes in the joint.

Cytokine production by macrophages is important for shaping of the inflammatory environment and orchestrating adaptive immune responses at the site of inflammation (Mosser and Edwards 2008). Cytokines such as IL-6, IL-12 and IL-23 are crucial for differentiation of the Th1 and Th17 T-cell subsets, respectively (Zhu et al. 2010). Notably, mRNA expression levels of the key T-cell cytokines IL-17 and IFN-γ were reduced in IRF5 deficient mice at day two of disease in addition to macrophage secreted cytokines (Figure 5.4). However, numbers of IFN-γ and IL-17 producing T-cells were not affected at that stage of AIA (Figure 5.6). This could be because decreased transcript levels may not necessarily be due to decreased cell numbers in the arthritic joint but rather a cell intrinsic effect within T-cells present at that time point. When the T-cell

response was analysed at the later stages of AIA on day seven, numbers of Th1, Th17 and IL-17 producing γδ T-cells in WT mice were significantly increased compared to day two (Figure 5.6). Moreover, this T-cell response was impaired in mice lacking IRF5, most likely as a consequence of a less inflammatory environment due to the reduction in pro-inflammatory macrophages at the site of inflammation. Intrinsic effects of IRF5 ablation can be excluded as T-cells do not express IRF5 themselves, (Mancl et al. 2005, Heng et al. 2008). T-cells in the periphery (Figure 5.7 Figure 5.8) were only mildly affected during AIA, which is likely due to the nature of the model causing localised inflammation by intra-articular antigen injection (Egan et al. 2008).

To further exclude an effect of IRF5 deficiency on the immunisation process, for example due to impaired antigen presentation by IRF5$^{-/-}$ APCs, we analysed the proliferative response in LNs post immunisation (Figure 5.9). Proliferation of lymphocytes, consisting of T- and B-cells, derived from the draining LNs was not affected by IRF5 deficiency. Furthermore, B-cell numbers in the blood and lymphoid organs, spleen and LN, also remained unchanged (Figure 5.10). Serum levels of IgG1 antibodies were not different in WT and IRF5$^{-/-}$ mice whereas IgG2a antibody levels were reduced, which is in agreement with the previously documented role for IRF5 in the control of the *IgG2a* locus (Savitsky et al. 2010). Thus, the observed effects in IRF5$^{-/-}$ mice during AIA do not seem to be caused by the IRF5 deficiency in B-cells. There is however an effect on T-cell adaptive immunity in the joint at later stages of AIA, probably as a functional consequence of limited pro-inflammatory cytokine production at early stages, as has been previously shown *in vitro* (Krausgruber et al. 2011).

In vivo models of acute inflammation used in this study, which are characterised by a high influx of neutrophils into the site of inflammation (Grespan et al. 2008, Matute-Bello et al. 2008), demonstrated the impaired neutrophil recruitment in IRF5$^{-/-}$ mice (Figure 5.16). In both models, the levels of CXCL1, a chemokine previously implicated in neutrophil migration in both AIA joints (Coelho et al. 2008, Grespan et al. 2008, Lemos et al. 2009) and acute lung injury (Matute-Bello et al. 2008) were significantly reduced. Blocking neutrophil influx in to the joints, either with Ly6G antibodies or by interfering with neutrophil migration, e.g. by using the CXCR1/CXCR2 allosteric inhibitor, has been demonstrated to significantly reduce arthritis development in different mouse models of the disease, including AIA (Coelho et al. 2008). Moreover, antibody mediated blockade of CXCL1, a ligand for the CXCR2 receptor, led to a reduced number of neutrophils in the joint cavity of AIA mice (Grespan et al. 2008), mimicking the effect of the IRF5 deletion observed in this study.

Macrophages, neutrophils and epithelial cells can all secrete CXCL1 and promote neutrophil entry (Griffith et al. 2014). However, in the inflamed arthritic knee macrophages express the highest levels of IRF5, exceeding the IRF5 level detected in neutrophils by more than 10 times (Figure 4.9). Moreover, no difference in the secretion of CXCL1 was observed between WT and IRF5$^{-/-}$ BM-derived neutrophils in response to a range of TLR agonists (Ericson et al. 2014). To specifically address the effect of IRF5 deletion in myeloid cells we generated *LysM*^{cre} *Irf5*$^{fl/fl}$ mice. Both neutrophil influx and CXCL1 levels were reduced during AIA in those mice (Figure 5.15). Of interest, macrophages were the main CXCL1 producing cells in WT joints and the only cell type that showed a reduction in expression levels in cKO mice. Although the *LysM-cre* gene is

indeed expressed by macrophages, it is also expressed by other myeloid cells such as granulocytes (Clausen et al. 1999, Hume 2011). However, we observe that *LysM* cre driven depletion of IRF5 was most effective, although incomplete, in macrophages and Ly6C^{hi} monocytes in the inflamed knee (Figure 5.14). Other myeloid cells such as DCs and neutrophils were only affected to a much lower degree, if at all. Of note, incomplete deletion in Ly6C^{hi} monocytes has been previously observed by others when using *LysM-cre* mice (Jakubzick et al. 2008, Croxford et al. 2015). We thus conclude that the observed changes in CXCL1 in cKOs were due to loss of IRF5 in macrophages specifically. Future studies to verify these findings may be conducted by generating macrophage- and neutrophil-specific ablations of IRF5, using *Cx3cr1-cre* (Yona et al. 2013) and *hMRP8-cre* (Passegue et al. 2004) deletor mice, respectively. *Cx3cr1-cre* mice may be of especially useful as we observed high levels of CX_3CR1 expression specifically in synovial macrophages (Figure 4.10). Additionally, it would be interesting to use the *Ccr2*-creER^{T2}-mKate2 mice described recently that specifically and inducibly targets CCR2-expressing cells (Croxford et al. 2015). This would allow for a specific deletion of the IRF5^{+} infiltrating monocytes and macrophages which are absent in CCR2 deficient mice (Figure 4.11).

Furthermore, we observe a significantly lower mRNA expression of CXCL1 and other neutrophil attracting chemokines by BM-derived macrophages/DCs stimulated with LPS (Figure 5.19). It is possible though that other chemokines not detected by our assay or not tested may also have an effect on neutrophil influx. The global profiling of IRF5-bound sites in macrophages/DCs deficient in IRF5 has further highlighted the direct role for IRF5 in transcriptional regulation of key chemokine genes, and specifically the ones involved in neutrophil

trafficking (Figure 5.18). Moreover, we have previously shown that the expression of both IL-1α and IL-1β, which are potent chemoattractants for myeloid cells (Rider et al. 2011) are also under IRF5 control in GM-BM-DC/MPHs (Saliba et al. 2014). Taken together these data suggest that it is macrophage-specific chemokine production that is likely to be affected most by the lack of IRF5.

We observed that IRF5 deficiency alters the levels of CXCL1 chemokine secretion that leads to neutrophil recruitment in two independent models of acute inflammation. Others have reported that IRF5 regulates CXCL13 expression in breast cancer cells, and that it leads to enhanced B- and T-cell trafficking to tumour-conditioned media (Pimenta et al. 2015). IRF5 has also been implicated in the induction of chemokine expression in response to a virus infection in a B- cell line, affecting RANTES (CCL5), MIP-1α (CCL3) and CXCL10 (Barnes et al. 2002). Interestingly, CXCL10 has been shown to be negatively regulated by IRF5 in human *in vitro* differentiated macrophages (Krausgruber et al. 2011). Other chemokines such as CCL4 and CCL5, however, were shown to be positively regulated in the same study, in agreement with our data. The difference in the regulation of CXCL10 may be due to either technical differences in the cell systems used or a general species specific effect. Overall, these data show that IRF5 is important in regulating a network of chemokine genes that may differ depending on the cell type but potentially also on the type of disease.

Importantly, a very recent publication by Duffau et al. validates our findings regarding the role of IRF5 in regulating chemokine expression in the context of arthritis (Duffau et al. 2015). This study reports that IRF5$^{-/-}$ mice undergoing the K/BxN serum transfer model of arthritis also display reduced disease severity and lower levels of chemokines in the serum. In accordance with our *in vivo* and *in vitro* data, Duffau et al. observed a reduction in IL-1β, CXCL10, CXCL1, CCL3 and CCL5 in the serum of arthritic mice. Although we only observed significant differences for CXCL1 at the site of inflammation in arthritic knees during AIA and in the lung, this may be due to model-specific differences. This is further highlighted by the data regarding TLR involvement that implicates TLR3 and TLR7 but not TLR2/4 signalling in K/BxN arthritis (Duffau et al. 2015). As discussed above, AIA relies on immunisation using CFA, which can amongst others activate TLR4 and thus could induce different signalling cascades. One consequence of this differential TLR involvement may be the preferential recruitment of Ly6C^{hi} monocytes (Figure 4.7) as opposed to Ly6C^{lo} monocytes in the K/BxN model (Misharin et al. 2014). Moreover, TLR4 has been previously reported to be important in CIA, another mouse model of arthritis relying on immunisation with CFA (Pierer et al. 2011). Duffau et al. further showed that IRF5 deficient synovial fibroblasts express less CXCL1 and IL-6 upon TLR7 activation. However, these fibroblasts were cultured *in vitro* following isolation from non-inflamed joints, which may not necessarily reflect the processes *in vivo*. Furthermore, IRF5 expression levels were not determined in this cell population. We did not detect substantial IRF5 expression within the CD45^{-} population containing fibroblasts in arthritic knees (Figure 4.9). Moreover, our data derived from *LysM*^{cre} *Irf5*$^{fl/fl}$ mice suggest that it is macrophage-derived

CXCL1 which is affected by ablation of IRF5 (Figure 5.15). In conclusion, the recent study by Duffau et al. generally supports the finding that IRF5 is important in regulating chemokine expression in arthritis.

As mentioned earlier, one study observed no differences in the CIA model in the absence of IRF5 (Savitsky et al. 2010). Since it has recently been shown that C57BL/6 mice backcrossed to a *H-2*^{q} haplotype can develop more severe CIA than mice with a *H-2*^{b} haplotype (Backlund et al. 2013), this model should be repeated using backcrossed IRF5$^{-/-}$ mice. These experiments may allow for identification of previously hidden and more subtle differences. However, opposing results may also be due to the more systemic nature of CIA where swelling only occurs within approximately 21 days post-immunisation, compared to the acute inflammation occurring within hours or days during AIA or K/BxN serum transfer arthritis (McNamee et al. 2015). We demonstrated that lack of IRF5 is beneficial during AIA (Figure 5.1) and others obtained similar results using the model of K/BxN serum transfer (Duffau et al. 2015), highlighting a potential role for IRF5 in the early acute events of autoimmunity rather than prolonged systemic processes.

Neutrophils display marked abnormalities in phenotype and function in autoimmune diseases, including RA, systemic vasculitis, SLE (Kaplan 2013), complementing macrophage alterations. In these conditions, neutrophils may play a central role in the initiation and perpetuation of aberrant immune responses and organ damage. Here we show that inhibition of IRF5 activity leads to reduction in neutrophil influx at the sites of acute inflammation. Thus, in

addition to the previously suggested and recently confirmed role of IRF5 in balancing the arms of Th1/Th17 and Th2 adoptive immune responses (Krausgruber et al. 2011, Feng et al. 2012, Dalmas et al. 2015), IRF5 also plays a direct role in controlling the innate immune responses leading to host tissue damage. These results augment evidence suggesting that IRF5 blockade might be an effective therapeutic target.

6. General discussion

Macrophages are pivotal in shaping the inflammatory environment, which is crucial for host defence during infections but can become pathogenic in chronic autoimmunity (Motwani and Gilroy 2015). Accumulating data in recent years have uncovered the diversity and heterogeneity of macrophages *in vivo* (Epelman et al. 2014). However, the interplay between mostly embryonically-derived tissue-resident macrophages and inflammatory monocyte-derived macrophages depends on the nature of the stimulus and remains to be fully understood. Tissue-resident macrophages in the steady state display a regulatory phenotype and are involved in homeostasis and tissue maintenance (Davies et al. 2013). We could show that IRF5 is crucial in establishing a pro-inflammatory macrophage phenotype both *in vitro* and *in vivo* in acute inflammatory diseases. Data from different murine steady state tissues suggest that in accordance with its well-described role in inflammation, IRF5 expression in most tissue-resident populations is rather low, although not absent (Figure 4.1 and Figure 4.2). In contrast, expression levels are high in Ly6C^{hi} monocytes, which have been shown to be the predominant infiltrating monocyte subset in inflammation giving rise to pro-inflammatory macrophages (Serbina and Pamer 2006, Shi and Pamer 2011). Accordingly, IRF5 expression was especially induced in macrophages in response to inflammatory stimuli *in vitro* and acute inflammation *in vivo* (Chapters 3 and 4). Thus IRF5 is likely to be a critical factor in response to environmental challenges, such as inflammatory insults, by ensuring that monocytes and macrophages adopt the adequate gene expression profile.

Nevertheless, further experiments will be necessary to elucidate the role of IRF5 in specific tissue-resident macrophage subsets. To clarify the contributions of IRF5 depleted tissue-resident versus infiltrating monocyte-derived macrophages during AIA, it would be useful to perform BM chimera experiments in which knees are protected from radiation. Resident synovial macrophages would thereby persist in the joint and consequently be of host origin. Irradiated WT mice receiving IRF5 deficient BM would provide information specifically about the contribution of IRF5 in infiltrating monocyte-derived macrophages. The opposite experiment of transferring WT BM to $IRF5^{-/-}$ mice would allow for assessment of a potential role of IRF5 in the resident macrophage population. Although we could show that macrophages in the arthritic knee predominantly depend on the influx of $CCR2^{+}$ monocytes (Figure 4.11), this does not rule out a contribution of resident macrophages in initiation of the disease. It would be particularly interesting to determine if the kinetics of neutrophil influx are affected in this context and if so how. It could be that neutrophil recruitment is affected either initially when resident macrophages lack IRF5 or when the promotion of inflammation, and consequently further neutrophil influx, is reduced due to IRF5 deficiency in monocyte-derived macrophages. Overall, these experiments may be helpful in clarifying the distinct contributions of different IRF5-expressing macrophage populations in the joint.

Within the tissues analysed in this study, macrophages in the lung were the only tissue-resident population expressing high levels of IRF5 (Figure 4.2). As discussed before, this may be due to the high levels of GM-CSF in the lung

inducing IRF5 expression (Chapter 4.3.). As the lung is constantly exposed to external antigens, co-factors may be crucial in this context to prevent IRF5 from activating its pro-inflammatory target genes prematurely. IRF5 has indeed been shown to cooperate with other TFs, although this has been in a synergistic rather than an antagonistic context (Saliba et al. 2014). Alternatively, IRF5 activity may be controlled by post-translational modifications (Ryzhakov et al. 2015) or cellular localisation (Lin et al. 2005). Interestingly, higher levels of IRF5 have been found to be protective in the context of asthma, an allergic Th2 driven disease (Wang et al. 2012). Accordingly, $IRF5^{-/-}$ mice display aggravated disease in the house dust mite model of asthma (Byrne et al. manuscript in preparation). Importantly, these effects could be counteracted by adenoviral overexpression of IRF5, potentially opening up new therapeutic avenues in pulmonary conditions.

IRF5 is implicated in the pathogenesis of a murine model of arthritis and it is also associated with RA on a genetic level. Genetic association alone however only provides a limited amount of information and not a causal link to a certain disease. Equally, useful drug targets may not necessarily be identified in GWAS, such as TNF-α, which despite its success in RA therapy has not been highlighted by GWAS as RA associated marker. IRF5 has in fact also been detected as an expression quantitative trait locus (eQTL) for LPS-stimulated monocytes and monocyte-derived DCs (Kim et al. 2014, Lee et al. 2014). Moreover, a recent study found a potential functional connection between ACPAs and both IRF5 expression and pro-inflammatory macrophage phenotype (Zhu et al. 2015), in line with data presented in this thesis and

previously published (Krausgruber et al. 2011). Since ACPAs can be detected in patients prior to the onset of disease, they have been linked to early events in RA pathogenesis (van Venrooij et al. 2011, Catrina et al. 2014). Hence, IRF5 may be implicated in more acute inflammatory processes during or before onset of RA and contribute to increased disease susceptibility.

Since mouse models are limited in terms of their ability to mimic human pathogenesis accurately, further research will be necessary to fully translate these findings to RA. Recently, Soler Palacios et al. characterised macrophages in the synovial fluid and synovial membranes of RA patients (Soler Palacios et al. 2015). Interestingly, they reported that synovial fluid macrophages share phenotypic and transcriptomic properties with GM-CSF differentiated *in vitro* macrophages, which we have shown to highly express IRF5 (Krausgruber et al. 2011). Synovial membrane macrophages were shown to also express markers related to a pro-inflammatory phenotype. Although levels of IRF5 were not analysed in this study, these data provide evidence that synovial macrophages display a pro-inflammatory phenotype in active RA. Further experiments determining IRF5 expression levels in different macrophage populations of RA patients will be needed to clarify whether IRF5 controls pro-inflammatory macrophage phenotypes in RA. Moreover, it would be interesting to obtain samples from different stages of disease to analyse potential differences in expression. However, thus far results regarding association of IRF5 with a specific type of RA are inconsistent (Eames et al. 2015).

IRF5 expression is clearly induced by GM-CSF in mouse and human *in vitro* differentiated macrophages while M-CSF does not induce expression. This further suggests a role for IRF5 in the context of GM-CSF-induced inflammation rather than M-CSF mediated macrophage maintenance. GM-CSF is an important inflammatory cytokine with pleiotropic effects and has been shown to be involved in many autoimmune diseases (Hamilton 2008). Interestingly, it has recently been shown that GM-CSF signalling via STAT5 in $CCR2^{+}$ myeloid cells is necessary for the pathogenesis of experimental autoimmune encephalomyelitis (EAE), a mouse model for multiple sclerosis (Croxford et al. 2015). Since we observed that IRF5 is downstream of GM-CSF and infiltrating $IRF5^{+}$ cells are absent in the joints of $CCR2^{-/-}$ mice, it may be that a similar mechanism occurs in AIA involving highly IRF5-expressing $Ly6C^{hi}$ monocytes. Moreover, IRF5 may generally be one of the GM-CSF target TFs necessary to establish its downstream inflammatory signature. Since GM-CSF plays an important role in many diseases (Hamilton 2008, Hamilton and Achuthan 2013), it is possible that IRF5 contributes to the pathogenesis of additional yet unknown conditions such as multiple sclerosis and psoriasis.

GM-CSF has in fact been shown to play a role in RA experimentally (Campbell et al. 1998) and has also been detected in synovial biopsies of patients (Berenbaum et al. 1994). Therapies targeting GM-CSF, including both GM-CSF depletion and GM-CSFR blockade, have been developed and are in clinical trials (Burmester et al. 2014). The receptor antagonist mavrilimumab in fact showed promising results in RA patients in phase II trials (Burmester et al. 2013). This is in contrast with M-CSF blockade, which has so far not been

successful in clinical trials for RA (Hamilton and Achuthan 2013), despite showing beneficial therapeutic effects in mouse models of arthritis (Campbell et al. 2000, Hamilton 2008).

Due to the widespread effects of both GM-CSF and M-CSF, the risk of severe side effects also has to be considered. Especially since both of these factors are also involved in the development and maintenance of macrophage populations. IRF5 may be a useful alternative with a limited set of side effects. Nevertheless, since IRF5 is crucial in pathogen defence (Honda and Taniguchi 2006), patients may be more susceptible to infections when IRF5 is blocked. If distinct post-translational modifications of IRF5 could be linked to chronic inflammation, it may be possible to specifically target those to modulate IRF5 activity in a more restricted manner. Equally, a similar approach could be performed targeting specific IRF5 transcript variants, as it has been shown that SLE patients display a distinct IRF5 transcript signature (Stone et al. 2013).

Targeting IRF5 may also have therapeutic benefits in conditions characterised by large neutrophil influx, since we demonstrated that IRF5 controls expression of a chemokine network (Figure 5.18 and Figure 5.19). However, it remains unclear how IRF5 affects the interplay between macrophages and neutrophils in terms of functional capacities. As described earlier, macrophage-derived chemokines are crucial for neutrophil recruitment to the site of inflammation (Griffith et al. 2014).

Moreover, crosstalk between different macrophage populations has been reported to be necessary in initiating neutrophil recruitment to the epithelium of the urinary tract (Schiwon et al. 2014). In the context of bacterial infection,

inflammatory Ly6C$^+$ macrophages are required to instruct tissue-resident Ly6C$^-$ macrophages in the uroepithelium to produce CXCL2, which in turn recruits neutrophils. Our own data, however, suggest that AIA is more likely to depend on Ly6C$^+$ monocytes and macrophages, as discussed previously with regards to the K/BxN serum transfer arthritis model (see chapter 4.3), which is driven by Ly6C$^-$ monocytes (Misharin et al. 2014). In fact, up to 80% of the macrophages present in the arthritic knee during AIA are Ly6C^{hi} (Figure 4.7) and we demonstrated that they are the main CXCL1 producers in the joint (Figure 5.15). Differences may be due to tissue-specific requirements of the bladder as a barrier organ.

Intriguingly, it has recently been shown that NET release by neutrophils affects macrophage functions in atherosclerosis by priming them for cytokine production (Warnatsch et al. 2015). Thus, macrophage-neutrophil interactions are not unidirectional but consist of a crosstalk that can have functional consequences for both. Therefore, it would be interesting to analyse neutrophil intrinsic functions in the absence of IRF5, specifically by measuring the activity of key neutrophil enzymes such as myeloperoxidase and neutrophil elastase (Amulic et al. 2012). Moreover, NET formation at the site of inflammation should be assessed, especially since NETs have also been shown to be involved in RA (Khandpur et al. 2013). These experiments would be especially interesting in neutrophil- and macrophage-specific IRF5 knockouts (potential cre strains are discussed in chapter 5.3 Discussion). Using these conditional cell type specific ablations of IRF5 would allow teasing out the effects IRF5-expressing cell types have on one another. The resulting knowledge may also provide information

about the general biology of neutrophil-macrophage interactions during inflammation.

In conclusion, IRF5 is pivotal in inflammatory processes coordinated by macrophages by controlling their gene expression profiles. Ablation of IRF5 dampens acute inflammation, consequently affecting cells of both innate and adaptive immunity and thereby ultimately restricting the inflammatory response. Further research will be necessary to fully elucidate the mechanisms by which IRF5 contributes to human diseases. Nevertheless, targeting IRF5 may be beneficial in chronic diseases to prevent the long-term consequences of prolonged inflammation that cause severe tissue damage. However, IRF5 blockade in patients may not be easy to achieve as TFs are often considered “non-druggable”. Although other steps that target the regulation of IRF5 activation by modifying enzymes might be more tractable. Hence, IRF5 may be an interesting drug target to tackle a wide spectrum of autoimmune and acute inflammatory diseases.

7. References

Abbas, A. K., et al. (1996). "*Functional diversity of helper T lymphocytes*." Nature **383**(6603): 787-793.
Abraham, S. N. and A. L. St John (2010). "*Mast cell-orchestrated immunity to pathogens*." Nature Reviews Immunology **10**(6): 440-452.
Ajami, B., et al. (2007). "*Local self-renewal can sustain CNS microglia maintenance and function throughout adult life*." Nat Neurosci **10**(12): 1538-1543.
Ajuebor, M. N., et al. (1999). "*Role of resident peritoneal macrophages and mast cells in chemokine production and neutrophil migration in acute inflammation: Evidence for an inhibitory loop involving endogenous IL-10*." Journal of Immunology **162**(3): 1685-1691.
Alder, J. K., et al. (2008). "*Kruppel-like factor 4 is essential for inflammatory monocyte differentiation in vivo*." J Immunol **180**(8): 5645-5652.
Alvarez-Errico, D., et al. (2015). "*Epigenetic control of myeloid cell differentiation, identity and function*." Nat Rev Immunol **15**(1): 7-17.
Amir el, A. D., et al. (2013). "*viSNE enables visualization of high dimensional single-cell data and reveals phenotypic heterogeneity of leukemia*." Nat Biotechnol **31**(6): 545-552.
Amulic, B., et al. (2012). "*Neutrophil function: from mechanisms to disease*." Annu Rev Immunol **30**: 459-489.
Anderson, C. A., et al. (2011). "*Meta-analysis identifies 29 additional ulcerative colitis risk loci, increasing the number of confirmed associations to 47*." Nat Genet **43**(3): 246-252.
Arango Duque, G. and A. Descoteaux (2014). "*Macrophage cytokines: involvement in immunity and infectious diseases*." Front Immunol **5**: 491.
Arnold, L., et al. (2007). "*Inflammatory monocytes recruited after skeletal muscle injury switch into antiinflammatory macrophages to support myogenesis*." J Exp Med **204**(5): 1057-1069.
Artis, D. and H. Spits (2015). "*The biology of innate lymphoid cells*." Nature **517**(7534): 293-301.
Asquith, D. L., et al. (2009). "*Animal models of rheumatoid arthritis*." Eur J Immunol **39**(8): 2040-2044.
Auffray, C., et al. (2007). "*Monitoring of blood vessels and tissues by a population of monocytes with patrolling behavior*." Science **317**(5838): 666-670.
Auffray, C., et al. (2009). "*Blood monocytes: development, heterogeneity, and relationship with dendritic cells*." Annu Rev Immunol **27**: 669-692.
Austyn, J. M. and S. Gordon (1981). "*F4/80, a monoclonal antibody directed specifically against the mouse macrophage*." Eur J Immunol **11**(10): 805-815.
Backlund, J., et al. (2013). "*C57BL/6 mice need MHC class II Aq to develop collagen-induced arthritis dependent on autoreactive T cells*." Ann Rheum Dis **72**(7): 1225-1232.
Bain, C. C., et al. (2014). "*Constant replenishment from circulating monocytes maintains the macrophage pool in the intestine of adult mice*." Nat Immunol **15**(10): 929-937.
Bain, C. C., et al. (2013). "*Resident and pro-inflammatory macrophages in the colon represent alternative context-dependent fates of the same Ly6Chi monocyte precursors*." Mucosal Immunol **6**(3): 498-510.

Bakri, Y., et al. (2005). "*Balance of MafB and PU.1 specifies alternative macrophage or dendritic cell fate*." Blood **105**(7): 2707-2716.
Balkhi, M. Y., et al. (2008). "*Functional regulation of MyD88-activated interferon regulatory factor 5 by K63-linked polyubiquitination*." Mol Cell Biol **28**(24): 7296-7308.
Balkhi, M. Y., et al. (2010). "*IKKalpha negatively regulates IRF-5 function in a MyD88-TRAF6 pathway*." Cell Signal **22**(1): 117-127.
Barnes, B. J., et al. (2002). "*Multiple regulatory domains of IRF-5 control activation, cellular localization, and induction of chemokines that mediate recruitment of T lymphocytes*." Mol Cell Biol **22**(16): 5721-5740.
Barnes, B. J., et al. (2003). "*Interferon regulatory factor 5, a novel mediator of cell cycle arrest and cell death*." Cancer Res **63**(19): 6424-6431.
Barnes, B. J., et al. (2001). "*Virus-specific activation of a novel interferon regulatory factor, IRF-5, results in the induction of distinct interferon alpha genes*." J Biol Chem **276**(26): 23382-23390.
Barrera, P., et al. (2000). "*Synovial macrophage depletion with clodronate-containing liposomes in rheumatoid arthritis*." Arthritis Rheum **43**(9): 1951-1959.
Becher, B., et al. (2014). "*High-dimensional analysis of the murine myeloid cell system*." Nat Immunol **15**(12): 1181-1189.
Begovich, A. B., et al. (2004). "*A missense single-nucleotide polymorphism in a gene encoding a protein tyrosine phosphatase (PTPN22) is associated with rheumatoid arthritis*." Am J Hum Genet **75**(2): 330-337.
Bendall, S. C., et al. (2012). "*A deep profiler's guide to cytometry*." Trends Immunol **33**(7): 323-332.
Bengtsson, A. A., et al. (2000). "*Activation of type I interferon system in systemic lupus erythematosus correlates with disease activity but not with antiretroviral antibodies*." Lupus **9**(9): 664-671.
Berenbaum, F., et al. (1994). "*Evidence for GM-CSF receptor expression in synovial tissue. An analysis by semi-quantitative polymerase chain reaction on rheumatoid arthritis and osteoarthritis synovial biopsies*." Eur Cytokine Netw **5**(1): 43-46.
Bergstrom, B., et al. (2015). "*TLR8 Senses Staphylococcus aureus RNA in Human Primary Monocytes and Macrophages and Induces IFN-beta Production via a TAK1-IKKbeta-IRF5 Signaling Pathway*." J Immunol **195**(3): 1100-1111.
Bertolini, D. R., et al. (1986). "*Stimulation of bone resorption and inhibition of bone formation in vitro by human tumour necrosis factors*." Nature **319**(6053): 516-518.
Bettelli, E., et al. (2008). "*Induction and effector functions of T(H)17 cells*." Nature **453**(7198): 1051-1057.
Bi, X., et al. (2011). "*Loss of interferon regulatory factor 5 (IRF5) expression in human ductal carcinoma correlates with disease stage and contributes to metastasis*." Breast Cancer Res **13**(6): R111.
Billiau, A. and P. Matthys (2001). "*Modes of action of Freund's adjuvants in experimental models of autoimmune diseases*." J Leukoc Biol **70**(6): 849-860.
Biswas, S. K., et al. (2012). "*Macrophage polarization and plasticity in health and disease*." Immunol Res **53**(1-3): 11-24.
Biswas, S. K. and A. Mantovani (2010). "*Macrophage plasticity and interaction with lymphocyte subsets: cancer as a paradigm*." Nat Immunol **11**(10): 889-896.
Biswas, S. K. and A. Mantovani (2012). "*Orchestration of metabolism by macrophages*." Cell Metab **15**(4): 432-437.

Blazek, K., et al. (2015). "*IFN-lambda resolves inflammation via suppression of neutrophil infiltration and IL-1beta production*." J Exp Med **212**(6): 845-853.
Bonizzi, G. and M. Karin (2004). "*The two NF-kappa B activation pathways and their role in innate and adaptive immunity*." Trends in Immunology **25**(6): 280-288.
Boring, L., et al. (1997). "*Impaired monocyte migration and reduced type 1 (Th1) cytokine responses in C-C chemokine receptor 2 knockout mice*." J Clin Invest **100**(10): 2552-2561.
Bouhlel, M. A., et al. (2007). "*PPARgamma activation primes human monocytes into alternative M2 macrophages with anti-inflammatory properties*." Cell Metab **6**(2): 137-143.
Boyer, S. W., et al. (2011). "*All hematopoietic cells develop from hematopoietic stem cells through Flk2/Flt3-positive progenitor cells*." Cell Stem Cell **9**(1): 64-73.
Brackertz, D., et al. (1977). "*Antigen-induced arthritis in mice. I. Induction of arthritis in various strains of mice*." Arthritis Rheum **20**(3): 841-850.
Breton, G., et al. (2015). "*Circulating precursors of human CD1c+ and CD141+ dendritic cells*." J Exp Med **212**(3): 401-413.
Brinkmann, V., et al. (2004). "*Neutrophil extracellular traps kill bacteria*." Science **303**(5663): 1532-1535.
Brubaker, S. W., et al. (2015). "*Innate Immune Pattern Recognition: A Cell Biological Perspective*." Annual Review of Immunology Vol 33 **33**: 257-290.
Brunkow, M. E., et al. (2001). "*Disruption of a new forkhead/winged-helix protein, scurfin, results in the fatal lymphoproliferative disorder of the scurfy mouse*." Nat Genet **27**(1): 68-73.
Burgess, A. W. and D. Metcalf (1980). "*The nature and action of granulocyte-macrophage colony stimulating factors*." Blood **56**(6): 947-958.
Burmester, G. R., et al. (2014). "*Emerging cell and cytokine targets in rheumatoid arthritis*." Nat Rev Rheumatol **10**(2): 77-88.
Burmester, G. R., et al. (1983). "*The tissue architecture of synovial membranes in inflammatory and non-inflammatory joint diseases. I. The localization of the major synovial cell populations as detected by monoclonal reagents directed towards Ia and monocyte-macrophage antigens*." Rheumatol Int **3**(4): 173-181.
Burmester, G. R., et al. (2013). "*Efficacy and safety of mavrilimumab in subjects with rheumatoid arthritis*." Ann Rheum Dis **72**(9): 1445-1452.
Byrne, A. J., et al. (2015). "*Pulmonary macrophages: key players in the innate defence of the airways*." Thorax **70**(12): 1189-1196.
Cambridge, G., et al. (2003). "*Serologic changes following B lymphocyte depletion therapy for rheumatoid arthritis*." Arthritis Rheum **48**(8): 2146-2154.
Campbell, I. K., et al. (1998). "*Protection from collagen-induced arthritis in granulocyte-macrophage colony-stimulating factor-deficient mice*." J Immunol **161**(7): 3639-3644.
Campbell, I. K., et al. (2000). "*The colony-stimulating factors and collagen-induced arthritis: exacerbation of disease by M-CSF and G-CSF and requirement for endogenous M-CSF*." J Leukoc Biol **68**(1): 144-150.
Cao, Z., et al. (1996). "*TRAF6 is a signal transducer for interleukin-1*." Nature **383**(6599): 443-446.
Catrina, A. I., et al. (2014). "*Lungs, joints and immunity against citrullinated proteins in rheumatoid arthritis*." Nat Rev Rheumatol **10**(11): 645-653.

Caux, C., et al. (1996). "*CD34+ hematopoietic progenitors from human cord blood differentiate along two independent dendritic cell pathways in response to GM-CSF+TNF alpha*." J Exp Med **184**(2): 695-706.
Cecchini, M. G., et al. (1994). "*Role of colony stimulating factor-1 in the establishment and regulation of tissue macrophages during postnatal development of the mouse*." Development **120**(6): 1357-1372.
Chabaud, M., et al. (2001). "*IL-17 derived from juxta-articular bone and synovium contributes to joint degradation in rheumatoid arthritis*." Arthritis Res **3**(3): 168-177.
Chang Foreman, H. C., et al. (2012). "*Activation of interferon regulatory factor 5 by site specific phosphorylation*." PLoS One **7**(3): e33098.
Chen, B. D., et al. (1988). "*Role of granulocyte/macrophage colony-stimulating factor in the regulation of murine alveolar macrophage proliferation and differentiation*." J Immunol **141**(1): 139-144.
Cheng, T. F., et al. (2006). "*Differential activation of IFN regulatory factor (IRF)-3 and IRF-5 transcription factors during viral infection*." J Immunol **176**(12): 7462-7470.
Chiba, S., et al. (2014). "*Recognition of tumor cells by Dectin-1 orchestrates innate immune cells for anti-tumor responses*." Elife **3**: e04177.
Chien, Y. H., et al. (2014). "*gammadelta T cells: first line of defense and beyond*." Annu Rev Immunol **32**: 121-155.
Chorro, L., et al. (2009). "*Langerhans cell (LC) proliferation mediates neonatal development, homeostasis, and inflammation-associated expansion of the epidermal LC network*." J Exp Med **206**(13): 3089-3100.
Christensen, J. L., et al. (2004). "*Circulation and chemotaxis of fetal hematopoietic stem cells*." PLoS Biol **2**(3): E75.
Clark, D. N., et al. (2013). "*Four Promoters of IRF5 Respond Distinctly to Stimuli and are Affected by Autoimmune-Risk Polymorphisms*." Front Immunol **4**: 360.
Clausen, B. E., et al. (1999). "*Conditional gene targeting in macrophages and granulocytes using LysMcre mice*." Transgenic Res **8**(4): 265-277.
Coelho, F. M., et al. (2008). "*The chemokine receptors CXCR1/CXCR2 modulate antigen-induced arthritis by regulating adhesion of neutrophils to the synovial microvasculature*." Arthritis Rheum **58**(8): 2329-2337.
Colville-Nash, P. and T. Lawrence (2003). "*Air-pouch models of inflammation and modifications for the study of granuloma-mediated cartilage degradation*." Methods Mol Biol **225**: 181-189.
Courties, G., et al. (2014). "*In vivo silencing of the transcription factor IRF5 reprograms the macrophage phenotype and improves infarct healing*." J Am Coll Cardiol **63**(15): 1556-1566.
Crane, M. J., et al. (2014). "*The monocyte to macrophage transition in the murine sterile wound*." PLoS One **9**(1): e86660.
Croxford, A. L., et al. (2015). "*The Cytokine GM-CSF Drives the Inflammatory Signature of CCR2+ Monocytes and Licenses Autoimmunity*." Immunity **43**(3): 502-514.
Cui, W. and S. M. Kaech (2010). "*Generation of effector CD8+ T cells and their conversion to memory T cells*." Immunol Rev **236**: 151-166.
Cyster, J. G. (2005). "*Chemokines, sphingosine-1-phosphate, and cell migration in secondary lymphoid organs*." Annu Rev Immunol **23**: 127-159.
Dai, X. M., et al. (2002). "*Targeted disruption of the mouse colony-stimulating factor 1 receptor gene results in osteopetrosis, mononuclear phagocyte*

deficiency, increased primitive progenitor cell frequencies, and reproductive defects." Blood **99**(1): 111-120.
Dakic, A., et al. (2005). "*PU.1 regulates the commitment of adult hematopoietic progenitors and restricts granulopoiesis*." J Exp Med **201**(9): 1487-1502.
Dalmas, E., et al. (2015). "*Irf5 deficiency in macrophages promotes beneficial adipose tissue expansion and insulin sensitivity during obesity*." Nat Med **21**(6): 610-618.
Dalton, D. K., et al. (1993). "*Multiple defects of immune cell function in mice with disrupted interferon-gamma genes*." Science **259**(5102): 1739-1742.
Daneman, R., et al. (2010). "*Pericytes are required for blood-brain barrier integrity during embryogenesis*." Nature **468**(7323): 562-566.
Daniels, M. A., et al. (2006). "*Thymic selection threshold defined by compartmentalization of Ras/MAPK signalling*." Nature **444**(7120): 724-729.
Darnell, J. E., Jr., et al. (1994). "*Jak-STAT pathways and transcriptional activation in response to IFNs and other extracellular signaling proteins*." Science **264**(5164): 1415-1421.
Davies, L. C., et al. (2013). "*Tissue-resident macrophages*." Nat Immunol **14**(10): 986-995.
Davies, L. C., et al. (2013). "*Distinct bone marrow-derived and tissue-resident macrophage lineages proliferate at key stages during inflammation*." Nat Commun **4**: 1886.
Davies, L. C., et al. (2011). "*A quantifiable proliferative burst of tissue macrophages restores homeostatic macrophage populations after acute inflammation*." Eur J Immunol **41**(8): 2155-2164.
Davignon, J. L., et al. (2013). "*Targeting monocytes/macrophages in the treatment of rheumatoid arthritis*." Rheumatology (Oxford) **52**(4): 590-598.
Davoine, F. and P. Lacy (2014). "*Eosinophil cytokines, chemokines, and growth factors: emerging roles in immunity*." Front Immunol **5**: 570.
Dawidowicz, K., et al. (2011). "*The interferon regulatory factor 5 gene confers susceptibility to rheumatoid arthritis and influences its erosive phenotype*." Ann Rheum Dis **70**(1): 117-121.
De Kleer, I., et al. (2014). "*Ontogeny of myeloid cells*." Front Immunol **5**: 423.
De Lorenzi, R., et al. (2009). "*GFP-p65 knock-in mice as a tool to study NF-kappaB dynamics in vivo*." Genesis **47**(5): 323-329.
De Santa, F., et al. (2009). "*Jmjd3 contributes to the control of gene expression in LPS-activated macrophages*." EMBO J **28**(21): 3341-3352.
De Santa, F., et al. (2007). "*The histone H3 lysine-27 demethylase Jmjd3 links inflammation to inhibition of polycomb-mediated gene silencing*." Cell **130**(6): 1083-1094.
del Fresno, C., et al. (2013). "*Interferon-beta Production via Dectin-1-Syk-IRF5 Signaling in Dendritic Cells Is Crucial for Immunity to C. albicans*." Immunity **38**(6): 1176-1186.
den Haan, J. M. and G. Kraal (2012). "*Innate immune functions of macrophage subpopulations in the spleen*." J Innate Immun **4**(5-6): 437-445.
Desmedt, M., et al. (1998). "*Macrophages induce cellular immunity by activating Th1 cell responses and suppressing Th2 cell responses*." J Immunol **160**(11): 5300-5308.
Dideberg, V., et al. (2007). "*An insertion-deletion polymorphism in the interferon regulatory Factor 5 (IRF5) gene confers risk of inflammatory bowel diseases*." Hum Mol Genet **16**(24): 3008-3016.

Dieguez-Gonzalez, R., et al. (2008). "*Association of interferon regulatory factor 5 haplotypes, similar to that found in systemic lupus erythematosus, in a large subgroup of patients with rheumatoid arthritis*." Arthritis Rheum **58**(5): 1264-1274.
Dougall, W. C., et al. (1999). "*RANK is essential for osteoclast and lymph node development*." Genes Dev **13**(18): 2412-2424.
Doyle, S., et al. (2002). "*IRF3 mediates a TLR3/TLR4-specific antiviral gene program*." Immunity **17**(3): 251-263.
Draijer, C., et al. (2013). "*Characterization of macrophage phenotypes in three murine models of house-dust-mite-induced asthma*." Mediators Inflamm **2013**: 632049.
Dranoff, G., et al. (1994). "*Involvement of granulocyte-macrophage colony-stimulating factor in pulmonary homeostasis*." Science **264**(5159): 713-716.
Duffau, P., et al. (2015). "*Interferon Regulatory Factor 5 Promotes Inflammatory Arthritis*." Arthritis Rheumatol.
Dunkelberger, J. R. and W. C. Song (2010). "*Complement and its role in innate and adaptive immune responses*." Cell Research **20**(1): 34-50.
Durbin, J. E., et al. (1996). "*Targeted disruption of the mouse Stat1 gene results in compromised innate immunity to viral disease*." Cell **84**(3): 443-450.
Dutton, R. W., et al. (1998). "*T cell memory*." Annu Rev Immunol **16**: 201-223.
Eames, H. L., et al. (2015). "*Interferon regulatory factor 5 in human autoimmunity and murine models of autoimmune disease*." Transl Res **[Epub ahead of print]**.
Eames, H. L., et al. (2012). "*KAP1/TRIM28: an inhibitor of IRF5 function in inflammatory macrophages*." Immunobiology **217**(12): 1315-1324.
Eberl, G., et al. (2015). "*Innate lymphoid cells. Innate lymphoid cells: a new paradigm in immunology*." Science **348**(6237): aaa6566.
Edwards, J. C. and G. Cambridge (2001). "*Sustained improvement in rheumatoid arthritis following a protocol designed to deplete B lymphocytes*." Rheumatology (Oxford) **40**(2): 205-211.
Egan, P. J., et al. (2003). "*Suppressor of cytokine signaling-1 regulates acute inflammatory arthritis and T cell activation*." J Clin Invest **111**(6): 915-924.
Egan, P. J., et al. (2008). "*Promotion of the local differentiation of murine Th17 cells by synovial macrophages during acute inflammatory arthritis*." Arthritis Rheum **58**(12): 3720-3729.
Epelman, S., et al. (2014). "*Embryonic and adult-derived resident cardiac macrophages are maintained through distinct mechanisms at steady state and during inflammation*." Immunity **40**(1): 91-104.
Epelman, S., et al. (2014). "*Origin and functions of tissue macrophages*." Immunity **41**(1): 21-35.
Ericson, J. A., et al. (2014). "*Gene expression during the generation and activation of mouse neutrophils: implication of novel functional and regulatory pathways*." PLoS One **9**(10): e108553.
Feinberg, M. W., et al. (2007). "*The Kruppel-like factor KLF4 is a critical regulator of monocyte differentiation*." EMBO J **26**(18): 4138-4148.
Feldmann, M. (2002). "*Development of anti-TNF therapy for rheumatoid arthritis*." Nat Rev Immunol **2**(5): 364-371.
Feldmann, M., et al. (1996). "*Rheumatoid arthritis*." Cell **85**(3): 307-310.

Feng, D., et al. (2010). "*Differential requirement of histone acetylase and deacetylase activities for IRF5-mediated proinflammatory cytokine expression*." J Immunol **185**(10): 6003-6012.
Feng, D., et al. (2010). "*Genetic variants and disease-associated factors contribute to enhanced interferon regulatory factor 5 expression in blood cells of patients with systemic lupus erythematosus*." Arthritis Rheum **62**(2): 562-573.
Feng, D., et al. (2012). "*Irf5-deficient mice are protected from pristane-induced lupus via increased Th2 cytokines and altered IgG class switching*." Eur J Immunol **42**(6): 1477-1487.
Fleetwood, A. J., et al. (2007). "*Granulocyte-macrophage colony-stimulating factor (CSF) and macrophage CSF-dependent macrophage phenotypes display differences in cytokine profiles and transcription factor activities: implications for CSF blockade in inflammation*." J Immunol **178**(8): 5245-5252.
Fleming, T. J., et al. (1993). "*Selective expression of Ly-6G on myeloid lineage cells in mouse bone marrow. RB6-8C5 mAb to granulocyte-differentiation antigen (Gr-1) detects members of the Ly-6 family*." J Immunol **151**(5): 2399-2408.
Forster, R., et al. (2012). "*Lymph node homing of T cells and dendritic cells via afferent lymphatics*." Trends Immunol **33**(6): 271-280.
Ganz, T. (2012). "*Macrophages and systemic iron homeostasis*." J Innate Immun **4**(5-6): 446-453.
Garber, M., et al. (2012). "*A high-throughput chromatin immunoprecipitation approach reveals principles of dynamic gene regulation in mammals*." Mol Cell **47**(5): 810-822.
Garnier, S., et al. (2007). "*IRF5 rs2004640-T allele, the new genetic factor for systemic lupus erythematosus, is not associated with rheumatoid arthritis*." Ann Rheum Dis **66**(6): 828-831.
Gathungu, G., et al. (2012). "*A two-marker haplotype in the IRF5 gene is associated with inflammatory bowel disease in a North American cohort*." Genes Immun **13**(4): 351-355.
Gautier, E. L., et al. (2012). "*Systemic analysis of PPARgamma in mouse macrophage populations reveals marked diversity in expression with critical roles in resolution of inflammation and airway immunity*." J Immunol **189**(5): 2614-2624.
Gautier, E. L., et al. (2012). "*Gene-expression profiles and transcriptional regulatory pathways that underlie the identity and diversity of mouse tissue macrophages*." Nat Immunol **13**(11): 1118-1128.
Gautier, E. L. and L. Yvan-Charvet (2014). "*Understanding macrophage diversity at the ontogenic and transcriptomic levels*." Immunol Rev **262**(1): 85-95.
Geissmann, F., et al. (2010). "*Unravelling mononuclear phagocyte heterogeneity*." Nat Rev Immunol **10**(6): 453-460.
Geissmann, F., et al. (2003). "*Blood monocytes consist of two principal subsets with distinct migratory properties*." Immunity **19**(1): 71-82.
Geissmann, F., et al. (2010). "*Development of monocytes, macrophages, and dendritic cells*." Science **327**(5966): 656-661.
Gellert, M. (2002). "*V(D)J recombination: RAG proteins, repair factors, and regulation*." Annu Rev Biochem **71**: 101-132.
Gentek, R., et al. (2014). "*Tissue macrophage identity and self-renewal*." Immunol Rev **262**(1): 56-73.

Ghisletti, S., et al. (2010). "*Identification and Characterization of Enhancers Controlling the Inflammatory Gene Expression Program in Macrophages*." Immunity **32**(3): 317-328.
Ginhoux, F., et al. (2010). "*Fate mapping analysis reveals that adult microglia derive from primitive macrophages*." Science **330**(6005): 841-845.
Ginhoux, F. and S. Jung (2014). "*Monocytes and macrophages: developmental pathways and tissue homeostasis*." Nat Rev Immunol **14**(6): 392-404.
Gomez Perdiguero, E., et al. (2015). "*Tissue-resident macrophages originate from yolk-sac-derived erythro-myeloid progenitors*." Nature **518**(7540): 547-551.
Gonzalez, S. F., et al. (2011). "*Trafficking of B cell antigen in lymph nodes*." Annu Rev Immunol **29**: 215-233.
Goodyear, A. W., et al. (2014). "*Optimization of murine small intestine leukocyte isolation for global immune phenotype analysis*." J Immunol Methods **405**: 97-108.
Gordon, S. (2003). "*Alternative activation of macrophages*." Nat Rev Immunol **3**(1): 23-35.
Gordon, S. (2008). "*Elie Metchnikoff: father of natural immunity*." Eur J Immunol **38**(12): 3257-3264.
Gordon, S. and F. O. Martinez (2010). "*Alternative activation of macrophages: mechanism and functions*." Immunity **32**(5): 593-604.
Gordon, S., et al. (2014). "*Macrophage heterogeneity in tissues: phenotypic diversity and functions*." Immunol Rev **262**(1): 36-55.
Gosselin, D., et al. (2014). "*Environment drives selection and function of enhancers controlling tissue-specific macrophage identities*." Cell **159**(6): 1327-1340.
Graham, R. R., et al. (2006). "*A common haplotype of interferon regulatory factor 5 (IRF5) regulates splicing and expression and is associated with increased risk of systemic lupus erythematosus*." Nat Genet **38**(5): 550-555.
Gregersen, P. K., et al. (1987). "*The shared epitope hypothesis. An approach to understanding the molecular genetics of susceptibility to rheumatoid arthritis*." Arthritis Rheum **30**(11): 1205-1213.
Grespan, R., et al. (2008). "*CXCR2-specific chemokines mediate leukotriene B4-dependent recruitment of neutrophils to inflamed joints in mice with antigen-induced arthritis*." Arthritis Rheum **58**(7): 2030-2040.
Greter, M., et al. (2012). "*Stroma-derived interleukin-34 controls the development and maintenance of langerhans cells and the maintenance of microglia*." Immunity **37**(6): 1050-1060.
Griffith, J. W., et al. (2014). "*Chemokines and chemokine receptors: positioning cells for host defense and immunity*." Annu Rev Immunol **32**: 659-702.
Guilliams, M., et al. (2013). "*Alveolar macrophages develop from fetal monocytes that differentiate into long-lived cells in the first week of life via GM-CSF*." J Exp Med **210**(10): 1977-1992.
Guilliams, M., et al. (2014). "*Dendritic cells, monocytes and macrophages: a unified nomenclature based on ontogeny*." Nat Rev Immunol **14**(8): 571-578.
Guilliams, M. and L. van de Laar (2015). "*A Hitchhiker's Guide to Myeloid Cell Subsets: Practical Implementation of a Novel Mononuclear Phagocyte Classification System*." Front Immunol **6**: 406.
Haldar, M., et al. (2014). "*Heme-mediated SPI-C induction promotes monocyte differentiation into iron-recycling macrophages*." Cell **156**(6): 1223-1234.

Hamilton, J. A. (2008). "*Colony-stimulating factors in inflammation and autoimmunity*." Nat Rev Immunol **8**(7): 533-544.
Hamilton, J. A. and A. Achuthan (2013). "*Colony stimulating factors and myeloid cell biology in health and disease*." Trends Immunol **34**(2): 81-89.
Hamilton, J. A., et al. (1993). "*Regulation of macrophage colony-stimulating factor (M-CSF) production in cultured human synovial fibroblasts*." Growth Factors **9**(2): 157-165.
Haringman, J. J., et al. (2005). "*Synovial tissue macrophages: a sensitive biomarker for response to treatment in patients with rheumatoid arthritis*." Ann Rheum Dis **64**(6): 834-838.
Harrell, M. I., et al. (2008). "*Lymph node mapping in the mouse*." J Immunol Methods **332**(1-2): 170-174.
Harrington, L. E., et al. (2005). "*Interleukin 17-producing CD4+ effector T cells develop via a lineage distinct from the T helper type 1 and 2 lineages*." Nat Immunol **6**(11): 1123-1132.
Harty, J. T., et al. (2000). "*CD8+ T cell effector mechanisms in resistance to infection*." Annu Rev Immunol **18**: 275-308.
Harwood, N. E. and F. D. Batista (2010). "*Early events in B cell activation*." Annu Rev Immunol **28**: 185-210.
Hashimoto, D., et al. (2013). "*Tissue-resident macrophages self-maintain locally throughout adult life with minimal contribution from circulating monocytes*." Immunity **38**(4): 792-804.
Hashimoto, D., et al. (2011). "*Dendritic cell and macrophage heterogeneity in vivo*." Immunity **35**(3): 323-335.
Hegde, S. P., et al. (1999). "*c-Maf induces monocytic differentiation and apoptosis in bipotent myeloid progenitors*." Blood **94**(5): 1578-1589.
Heintzman, N. D., et al. (2009). "*Histone modifications at human enhancers reflect global cell-type-specific gene expression*." Nature **459**(7243): 108-112.
Heintzman, N. D., et al. (2007). "*Distinct and predictive chromatin signatures of transcriptional promoters and enhancers in the human genome*." Nat Genet **39**(3): 311-318.
Heinz, S., et al. (2010). "*Simple combinations of lineage-determining transcription factors prime cis-regulatory elements required for macrophage and B cell identities*." Mol Cell **38**(4): 576-589.
Helft, J., et al. (2015). "*GM-CSF Mouse Bone Marrow Cultures Comprise a Heterogeneous Population of CD11c(+)MHCII(+) Macrophages and Dendritic Cells*." Immunity **42**(6): 1197-1211.
Helmick, C. G., et al. (2008). "*Estimates of the prevalence of arthritis and other rheumatic conditions in the United States. Part I*." Arthritis Rheum **58**(1): 15-25.
Heng, T. S., et al. (2008). "*The Immunological Genome Project: networks of gene expression in immune cells*." Nat Immunol **9**(10): 1091-1094.
Hettinger, J., et al. (2013). "*Origin of monocytes and macrophages in a committed progenitor*." Nat Immunol **14**(8): 821-830.
Higgins, D. M., et al. (2008). "*Relative levels of M-CSF and GM-CSF influence the specific generation of macrophage populations during infection with Mycobacterium tuberculosis*." J Immunol **180**(7): 4892-4900.
Hoeffel, G., et al. (2015). "*C-Myb(+) erythro-myeloid progenitor-derived fetal monocytes give rise to adult tissue-resident macrophages*." Immunity **42**(4): 665-678.

Hoeffel, G., et al. (2012). "*Adult Langerhans cells derive predominantly from embryonic fetal liver monocytes with a minor contribution of yolk sac-derived macrophages*." J Exp Med **209**(6): 1167-1181.
Holmdahl, R., et al. (1989). "*Collagen induced arthritis as an experimental model for rheumatoid arthritis. Immunogenetics, pathogenesis and autoimmunity*." APMIS **97**(7): 575-584.
Holtschke, T., et al. (1996). "*Immunodeficiency and chronic myelogenous leukemia-like syndrome in mice with a targeted mutation of the ICSBP gene*." Cell **87**(2): 307-317.
Honda, K. and T. Taniguchi (2006). "*IRFs: master regulators of signalling by Toll-like receptors and cytosolic pattern-recognition receptors*." Nat Rev Immunol **6**(9): 644-658.
Hu, G. D., et al. (2005). "*Signaling through IFN regulatory factor-5 sensitizes p53-deficient tumors to DNA damage-induced apoptosis and cell death*." Cancer Research **65**(16): 7403-7412.
Hu, X. and L. B. Ivashkiv (2009). "*Cross-regulation of signaling pathways by interferon-gamma: implications for immune responses and autoimmune diseases*." Immunity **31**(4): 539-550.
Hume, D. A. (2008). "*Macrophages as APC and the dendritic cell myth*." J Immunol **181**(9): 5829-5835.
Hume, D. A. (2011). "*Applications of myeloid-specific promoters in transgenic mice support in vivo imaging and functional genomics but do not support the concept of distinct macrophage and dendritic cell lineages or roles in immunity*." J Leukoc Biol **89**(4): 525-538.
Hussell, T. and T. J. Bell (2014). "*Alveolar macrophages: plasticity in a tissue-specific context*." Nat Rev Immunol **14**(2): 81-93.
Ikushima, H., et al. (2013). "*The IRF family transcription factors at the interface of innate and adaptive immune responses*." Cold Spring Harb Symp Quant Biol **78**: 105-116.
Inaba, K., et al. (1992). "*Generation of large numbers of dendritic cells from mouse bone marrow cultures supplemented with granulocyte/macrophage colony-stimulating factor*." J Exp Med **176**(6): 1693-1702.
Ingersoll, M. A., et al. (2010). "*Comparison of gene expression profiles between human and mouse monocyte subsets*." Blood **115**(3): e10-19.
Inglis, J. J., et al. (2007). "*Collagen-induced arthritis in C57BL/6 mice is associated with a robust and sustained T-cell response to type II collagen*." Arthritis Res Ther **9**(5): R113.
Italiani, P., et al. (2014). "*Transcriptomic profiling of the development of the inflammatory response in human monocytes in vitro*." PLoS One **9**(2): e87680.
Ivanov, II, et al. (2006). "*The orphan nuclear receptor RORgammat directs the differentiation program of proinflammatory IL-17+ T helper cells*." Cell **126**(6): 1121-1133.
Jakubzick, C., et al. (2008). "*Lymph-migrating, tissue-derived dendritic cells are minor constituents within steady-state lymph nodes*." J Exp Med **205**(12): 2839-2850.
Jakubzick, C., et al. (2013). "*Minimal differentiation of classical monocytes as they survey steady-state tissues and transport antigen to lymph nodes*." Immunity **39**(3): 599-610.
Jenkins, S. J. and D. A. Hume (2014). "*Homeostasis in the mononuclear phagocyte system*." Trends Immunol **35**(8): 358-367.

Jenkins, S. J., et al. (2011). "*Local macrophage proliferation, rather than recruitment from the blood, is a signature of TH2 inflammation*." Science **332**(6035): 1284-1288.
Jensen, P. E. (2007). "*Recent advances in antigen processing and presentation*." Nat Immunol **8**(10): 1041-1048.
Josefowicz, S. Z. and A. Rudensky (2009). "*Control of regulatory T cell lineage commitment and maintenance*." Immunity **30**(5): 616-625.
Jung, S., et al. (2000). "*Analysis of fractalkine receptor CX(3)CR1 function by targeted deletion and green fluorescent protein reporter gene insertion*." Mol Cell Biol **20**(11): 4106-4114.
Kanayama, Y., et al. (1989). "*Possible involvement of interferon alfa in the pathogenesis of fever in systemic lupus erythematosus*." Ann Rheum Dis **48**(10): 861-863.
Kaplan, M. J. (2013). "*Role of neutrophils in systemic autoimmune diseases*." Arthritis Res Ther **15**(5): 219.
Kapsenberg, M. L. (2003). "*Dendritic-cell control of pathogen-driven T-cell polarization*." Nat Rev Immunol **3**(12): 984-993.
Karasuyama, H., et al. (2011). "*Nonredundant roles of basophils in immunity*." Annu Rev Immunol **29**: 45-69.
Kennedy, A., et al. (2011). "*Macrophages in synovial inflammation*." Front Immunol **2**: 52.
Khandpur, R., et al. (2013). "*NETs are a source of citrullinated autoantigens and stimulate inflammatory responses in rheumatoid arthritis*." Sci Transl Med **5**(178): 178ra140.
Kieusseian, A., et al. (2012). "*Immature hematopoietic stem cells undergo maturation in the fetal liver*." Development **139**(19): 3521-3530.
Kim, S., et al. (2014). "*Characterizing the genetic basis of innate immune response in TLR4-activated human monocytes*." Nat Commun **5**: 5236.
Klareskog, L., et al. (2006). "*A new model for an etiology of rheumatoid arthritis: smoking may trigger HLA-DR (shared epitope)-restricted immune reactions to autoantigens modified by citrullination*." Arthritis Rheum **54**(1): 38-46.
Klein, L., et al. (2009). "*Antigen presentation in the thymus for positive selection and central tolerance induction*." Nat Rev Immunol **9**(12): 833-844.
Koch, U. and F. Radtke (2011). "*Mechanisms of T cell development and transformation*." Annu Rev Cell Dev Biol **27**: 539-562.
Kohyama, M., et al. (2009). "*Role for Spi-C in the development of red pulp macrophages and splenic iron homeostasis*." Nature **457**(7227): 318-321.
Kolaczkowska, E. and P. Kubes (2013). "*Neutrophil recruitment and function in health and inflammation*." Nat Rev Immunol **13**(3): 159-175.
Kopf, M., et al. (2015). "*The development and function of lung-resident macrophages and dendritic cells*." Nat Immunol **16**(1): 36-44.
Kouzarides, T. (2007). "*Chromatin modifications and their function*." Cell **128**(4): 693-705.
Kozyrev, S. V. and M. E. Alarcon-Riquelme (2007). "*The genetics and biology of Irf5-mediated signaling in lupus*." Autoimmunity **40**(8): 591-601.
Krausgruber, T., et al. (2011). "*IRF5 promotes inflammatory macrophage polarization and T(H)1-T(H)17 responses*." Nat Immunol **12**(3): 231-238.
Krausgruber, T., et al. (2010). "*IRF5 is required for late-phase TNF secretion by human dendritic cells*." Blood **115**(22): 4421-4430.

Kumaravelu, P., et al. (2002). "*Quantitative developmental anatomy of definitive haematopoietic stem cells/long-term repopulating units (HSC/RUs): role of the aorta-gonad-mesonephros (AGM) region and the yolk sac in colonisation of the mouse embryonic liver*." Development **129**(21): 4891-4899.
Lam, J., et al. (2000). "*TNF-alpha induces osteoclastogenesis by direct stimulation of macrophages exposed to permissive levels of RANK ligand*." J Clin Invest **106**(12): 1481-1488.
Lanier, L. L. (2005). "*NK cell recognition*." Annu Rev Immunol **23**: 225-274.
Laslo, P., et al. (2006). "*Multilineage transcriptional priming and determination of alternate hematopoietic cell fates*." Cell **126**(4): 755-766.
Lavin, Y., et al. (2014). "*Tissue-resident macrophage enhancer landscapes are shaped by the local microenvironment*." Cell **159**(6): 1312-1326.
Lawlor, K. E., et al. (2001). "*Molecular and cellular mediators of interleukin-1-dependent acute inflammatory arthritis*." Arthritis Rheum **44**(2): 442-450.
Lawrence, T. and G. Natoli (2011). "*Transcriptional regulation of macrophage polarization: enabling diversity with identity*." Nat Rev Immunol **11**(11): 750-761.
Lazzari, E., et al. (2014). "*TRIpartite motif 21 (TRIM21) differentially regulates the stability of interferon regulatory factor 5 (IRF5) isoforms*." PLoS One **9**(8): e103609.
Lee, J., et al. (2015). "*Restricted dendritic cell and monocyte progenitors in human cord blood and bone marrow*." J Exp Med **212**(3): 385-399.
Lee, M. N., et al. (2014). "*Common genetic variants modulate pathogen-sensing responses in human dendritic cells*." Science **343**(6175): 1246980.
Lee, P. Y., et al. (2008). "*TLR7-dependent and FcgammaR-independent production of type I interferon in experimental mouse lupus*." J Exp Med **205**(13): 2995-3006.
Lemos, H. P., et al. (2009). "*Prostaglandin mediates IL-23/IL-17-induced neutrophil migration in inflammation by inhibiting IL-12 and IFNgamma production*." Proc Natl Acad Sci U S A **106**(14): 5954-5959.
Leuschner, F., et al. (2012). "*Rapid monocyte kinetics in acute myocardial infarction are sustained by extramedullary monocytopoiesis*." J Exp Med **209**(1): 123-137.
Li, Q., et al. (2008). "*Interferon regulatory factors IRF5 and IRF7 inhibit growth and induce senescence in immortal Li-Fraumeni fibroblasts*." Mol Cancer Res **6**(5): 770-784.
Lien, C., et al. (2010). "*Critical role of IRF-5 in regulation of B-cell differentiation*." Proc Natl Acad Sci U S A **107**(10): 4664-4668.
Lin, H., et al. (2008). "*Discovery of a cytokine and its receptor by functional screening of the extracellular proteome*." Science **320**(5877): 807-811.
Lin, R., et al. (2005). "*A CRM1-dependent nuclear export pathway is involved in the regulation of IRF-5 subcellular localization*." J Biol Chem **280**(4): 3088-3095.
Linsley, P. S., et al. (1990). "*T-cell antigen CD28 mediates adhesion with B cells by interacting with activation antigen B7/BB-1*." Proc Natl Acad Sci U S A **87**(13): 5031-5035.
Liu, Z. and A. Davidson (2012). "*Taming lupus-a new understanding of pathogenesis is leading to clinical advances*." Nature Medicine **18**(6): 871-882.
Lu, G., et al. (2015). "*Myeloid cell-derived inducible nitric oxide synthase suppresses M1 macrophage polarization*." Nat Commun **6**: 6676.
Lubberts, E. (2015). "*The IL-23-IL-17 axis in inflammatory arthritis*." Nat Rev Rheumatol **11**(7): 415-429.

Lyons, R., et al. (2005). "*Effective use of autoantibody tests in the diagnosis of systemic autoimmune disease*." Ann N Y Acad Sci **1050**: 217-228.
MacMicking, J., et al. (1997). "*Nitric oxide and macrophage function*." Annu Rev Immunol **15**: 323-350.
Maloy, K. J. and F. Powrie (2011). "*Intestinal homeostasis and its breakdown in inflammatory bowel disease*." Nature **474**(7351): 298-306.
Mancl, M. E., et al. (2005). "*Two discrete promoters regulate the alternatively spliced human interferon regulatory factor-5 isoforms. Multiple isoforms with distinct cell type-specific expression, localization, regulation, and function*." J Biol Chem **280**(22): 21078-21090.
Martinez, F. O. and S. Gordon (2014). "*The M1 and M2 paradigm of macrophage activation: time for reassessment*." F1000Prime Rep **6**: 13.
Martinez, F. O., et al. (2009). "*Alternative activation of macrophages: an immunologic functional perspective*." Annu Rev Immunol **27**: 451-483.
Masuda, T., et al. (2014). "*Transcription factor IRF5 drives P2X4R+-reactive microglia gating neuropathic pain*." Nat Commun **5**: 3771.
Matute-Bello, G., et al. (2008). "*Animal models of acute lung injury*." Am J Physiol Lung Cell Mol Physiol **295**(3): L379-399.
Matzinger, P. (2002). "*The danger model: a renewed sense of self*." Science **296**(5566): 301-305.
McGarry, M. P. and C. C. Stewart (1991). "*Murine eosinophil granulocytes bind the murine macrophage-monocyte specific monoclonal antibody F4/80*." J Leukoc Biol **50**(5): 471-478.
McHeyzer-Williams, L. J. and M. G. McHeyzer-Williams (2005). "*Antigen-specific memory B cell development*." Annu Rev Immunol **23**: 487-513.
McInnes, I. B. and G. Schett (2007). "*Cytokines in the pathogenesis of rheumatoid arthritis*." Nat Rev Immunol **7**(6): 429-442.
McInnes, I. B. and G. Schett (2011). "*The pathogenesis of rheumatoid arthritis*." N Engl J Med **365**(23): 2205-2219.
McKenna, H. J., et al. (2000). "*Mice lacking flt3 ligand have deficient hematopoiesis affecting hematopoietic progenitor cells, dendritic cells, and natural killer cells*." Blood **95**(11): 3489-3497.
McLean, C. Y., et al. (2010). "*GREAT improves functional interpretation of cis-regulatory regions*." Nat Biotechnol **28**(5): 495-501.
McNamee, K., et al. (2015). "*Animal models of rheumatoid arthritis: How informative are they?*" Eur J Pharmacol **759**: 278-286.
Mebius, R. E. and G. Kraal (2005). "*Structure and function of the spleen*." Nat Rev Immunol **5**(8): 606-616.
Medzhitov, R. and C. A. Janeway, Jr. (1997). "*Innate immunity: impact on the adaptive immune response*." Curr Opin Immunol **9**(1): 4-9.
Medzhitov, R. and C. A. Janeway, Jr. (2002). "*Decoding the patterns of self and nonself by the innate immune system*." Science **296**(5566): 298-300.
Medzhitov, R., et al. (1997). "*A human homologue of the Drosophila Toll protein signals activation of adaptive immunity*." Nature **388**(6640): 394-397.
Merad, M., et al. (2013). "*The dendritic cell lineage: ontogeny and function of dendritic cells and their subsets in the steady state and the inflamed setting*." Annu Rev Immunol **31**: 563-604.
Meraz, M. A., et al. (1996). "*Targeted disruption of the Stat1 gene in mice reveals unexpected physiologic specificity in the JAK-STAT signaling pathway*." Cell **84**(3): 431-442.

Metlay, J. P., et al. (1990). "*The distinct leukocyte integrins of mouse spleen dendritic cells as identified with new hamster monoclonal antibodies*." J Exp Med **171**(5): 1753-1771.
Mewar, D. and A. G. Wilson (2006). "*Autoantibodies in rheumatoid arthritis: a review*." Biomed Pharmacother **60**(10): 648-655.
Mildner, A. and S. Jung (2014). "*Development and function of dendritic cell subsets*." Immunity **40**(5): 642-656.
Mills, C. D., et al. (2000). "*M-1/M-2 macrophages and the Th1/Th2 paradigm*." J Immunol **164**(12): 6166-6173.
Miossec, P. and J. K. Kolls (2012). "*Targeting IL-17 and TH17 cells in chronic inflammation*." Nat Rev Drug Discov **11**(10): 763-776.
Misharin, A. V., et al. (2014). "*Nonclassical Ly6C(-) monocytes drive the development of inflammatory arthritis in mice*." Cell Rep **9**(2): 591-604.
Misharin, A. V., et al. (2013). "*Flow cytometric analysis of macrophages and dendritic cell subsets in the mouse lung*." Am J Respir Cell Mol Biol **49**(4): 503-510.
Mitchell, A. J., et al. (2010). "*Technical advance: autofluorescence as a tool for myeloid cell analysis*." J Leukoc Biol **88**(3): 597-603.
Mohr, W., et al. (1981). "*Polymorphonuclear granulocytes in rheumatic tissue destruction. III. an electron microscopic study of PMNs at the pannus-cartilage junction in rheumatoid arthritis*." Ann Rheum Dis **40**(4): 396-399.
Monach, P. A., et al. (2008). "*The K/BxN arthritis model*." Curr Protoc Immunol **Chapter 15**: Unit 15 22.
Moon, T. C., et al. (2010). "*Advances in mast cell biology: new understanding of heterogeneity and function*." Mucosal Immunology **3**(2): 111-128.
Moore, M. A. and D. Metcalf (1970). "*Ontogeny of the haemopoietic system: yolk sac origin of in vivo and in vitro colony forming cells in the developing mouse embryo*." Br J Haematol **18**(3): 279-296.
Mori, T., et al. (2002). "*Identification of the interferon regulatory factor 5 gene (IRF-5) as a direct target for p53*." Oncogene **21**(18): 2914-2918.
Morrison, S. J. and D. T. Scadden (2014). "*The bone marrow niche for haematopoietic stem cells*." Nature **505**(7483): 327-334.
Mosmann, T. R. and R. L. Coffman (1989). "*TH1 and TH2 cells: different patterns of lymphokine secretion lead to different functional properties*." Annu Rev Immunol **7**: 145-173.
Mosser, D. M. and J. P. Edwards (2008). "*Exploring the full spectrum of macrophage activation*." Nat Rev Immunol **8**(12): 958-969.
Motwani, M. P. and D. W. Gilroy (2015). "*Macrophage development and polarization in chronic inflammation*." Semin Immunol **27**(4): 257-266.
Mucenski, M. L., et al. (1991). "*A functional c-myb gene is required for normal murine fetal hepatic hematopoiesis*." Cell **65**(4): 677-689.
Mueller, S. N., et al. (2013). "*Memory T cell subsets, migration patterns, and tissue residence*." Annu Rev Immunol **31**: 137-161.
Mulherin, D., et al. (1996). "*Synovial tissue macrophage populations and articular damage in rheumatoid arthritis*." Arthritis Rheum **39**(1): 115-124.
Murphy, C. A., et al. (2003). "*Divergent pro- and antiinflammatory roles for IL-23 and IL-12 in joint autoimmune inflammation*." J Exp Med **198**(12): 1951-1957.
Murray, P. J., et al. (2014). "*Macrophage activation and polarization: nomenclature and experimental guidelines*." Immunity **41**(1): 14-20.

Murray, P. J. and T. A. Wynn (2011). "*Protective and pathogenic functions of macrophage subsets*." Nat Rev Immunol **11**(11): 723-737.
Mylonas, K. J., et al. (2009). "*Alternatively activated macrophages elicited by helminth infection can be reprogrammed to enable microbial killing*." J Immunol **182**(5): 3084-3094.
Naik, S. H., et al. (2013). "*Diverse and heritable lineage imprinting of early haematopoietic progenitors*." Nature **496**(7444): 229-232.
Nanki, T., et al. (2004). "*Inhibition of fractalkine ameliorates murine collagen-induced arthritis*." J Immunol **173**(11): 7010-7016.
Nathan, C. and A. Ding (2010). "*Nonresolving inflammation*." Cell **140**(6): 871-882.
Nathan, C. F., et al. (1983). "*Identification of interferon-gamma as the lymphokine that activates human macrophage oxidative metabolism and antimicrobial activity*." J Exp Med **158**(3): 670-689.
Natoli, G. (2010). "*Maintaining cell identity through global control of genomic organization*." Immunity **33**(1): 12-24.
Negishi, H., et al. (2005). "*Negative regulation of Toll-like-receptor signaling by IRF-4*." Proc Natl Acad Sci U S A **102**(44): 15989-15994.
Nerlov, C. and T. Graf (1998). "*PU.1 induces myeloid lineage commitment in multipotent hematopoietic progenitors*." Genes Dev **12**(15): 2403-2412.
Neumann, E., et al. (2010). "*Rheumatoid arthritis progression mediated by activated synovial fibroblasts*." Trends Mol Med **16**(10): 458-468.
Nguyen, H. Q., et al. (1993). "*The zinc finger transcription factor Egr-1 is essential for and restricts differentiation along the macrophage lineage*." Cell **72**(2): 197-209.
Niewold, T. B., et al. (2008). "*Association of the IRF5 risk haplotype with high serum interferon-alpha activity in systemic lupus erythematosus patients*." Arthritis Rheum **58**(8): 2481-2487.
Nistala, K., et al. (2010). "*Th17 plasticity in human autoimmune arthritis is driven by the inflammatory environment*." Proc Natl Acad Sci U S A **107**(33): 14751-14756.
Nitta, N., et al. (2007). "*Quantitative analysis of eosinophil chemotaxis tracked using a novel optical device -- TAXIScan*." J Immunol Methods **320**(1-2): 155-163.
Nussenzweig, M. C., et al. (1981). "*Studies of the cell surface of mouse dendritic cells and other leukocytes*." J Exp Med **154**(1): 168-187.
Nutt, S. L., et al. (2015). "*The generation of antibody-secreting plasma cells*." Nat Rev Immunol **15**(3): 160-171.
O'Shea, J. J. and W. E. Paul (2010). "*Mechanisms underlying lineage commitment and plasticity of helper CD4+ T cells*." Science **327**(5969): 1098-1102.
Odegaard, J. I., et al. (2007). "*Macrophage-specific PPARgamma controls alternative activation and improves insulin resistance*." Nature **447**(7148): 1116-1120.
Ohl, L., et al. (2004). "*CCR7 governs skin dendritic cell migration under inflammatory and steady-state conditions*." Immunity **21**(2): 279-288.
Ohmori, Y. and T. A. Hamilton (1997). "*IL-4-induced STAT6 suppresses IFN-gamma-stimulated STAT1-dependent transcription in mouse macrophages*." J Immunol **159**(11): 5474-5482.

Okuda, T., et al. (1996). "*AML1, the target of multiple chromosomal translocations in human leukemia, is essential for normal fetal liver hematopoiesis*." Cell **84**(2): 321-330.
Olson, M. C., et al. (1995). "*PU. 1 is not essential for early myeloid gene expression but is required for terminal myeloid differentiation*." Immunity **3**(6): 703-714.
Pancer, Z. and M. D. Cooper (2006). "*The evolution of adaptive immunity*." Annual Review of Immunology **24**: 497-518.
Parsey, M. V., et al. (1998). "*Neutrophils are major contributors to intraparenchymal lung IL-1 beta expression after hemorrhage and endotoxemia*." J Immunol **160**(2): 1007-1013.
Passegue, E., et al. (2004). "*JunB deficiency leads to a myeloproliferative disorder arising from hematopoietic stem cells*." Cell **119**(3): 431-443.
Paun, A., et al. (2011). "*Critical role of IRF-5 in the development of T helper 1 responses to Leishmania donovani infection*." PLoS Pathog **7**(1): e1001246.
Paun, A., et al. (2008). "*Functional characterization of murine interferon regulatory factor 5 (IRF-5) and its role in the innate antiviral response*." J Biol Chem **283**(21): 14295-14308.
Pierer, M., et al. (2011). "*Toll-like receptor 4 is involved in inflammatory and joint destructive pathways in collagen-induced arthritis in DBA1J mice*." PLoS One **6**(8): e23539.
Pimenta, E. M., et al. (2015). "*IRF5 is a novel regulator of CXCL13 expression in breast cancer that regulates CXCR5 (+) B- and T-cell trafficking to tumor-conditioned media*." Immunol Cell Biol **93**(5): 486-499.
Plantinga, M., et al. (2013). "*Conventional and monocyte-derived CD11b(+) dendritic cells initiate and maintain T helper 2 cell-mediated immunity to house dust mite allergen*." Immunity **38**(2): 322-335.
Pollard, J. W. (2009). "*Trophic macrophages in development and disease*." Nat Rev Immunol **9**(4): 259-270.
Poltorak, A., et al. (1998). "*Defective LPS signaling in C3H/HeJ and C57BL/10ScCr mice: mutations in Tlr4 gene*." Science **282**(5396): 2085-2088.
Purtha, W. E., et al. (2012). "*Spontaneous mutation of the Dock2 gene in Irf5-/- mice complicates interpretation of type I interferon production and antibody responses*." Proc Natl Acad Sci U S A **109**(15): E898-904.
Raes, G., et al. (2005). "*Macrophage galactose-type C-type lectins as novel markers for alternatively activated macrophages elicited by parasitic infections and allergic airway inflammation*." J Leukoc Biol **77**(3): 321-327.
Redlich, K. and J. S. Smolen (2012). "*Inflammatory bone loss: pathogenesis and therapeutic intervention*." Nat Rev Drug Discov **11**(3): 234-250.
Reis e Sousa, C. (2006). "*Dendritic cells in a mature age*." Nat Rev Immunol **6**(6): 476-483.
Reizis, B., et al. (2011). "*Plasmacytoid dendritic cells: recent progress and open questions*." Annu Rev Immunol **29**: 163-183.
Ren, J., et al. (2014). "*IKKbeta is an IRF5 kinase that instigates inflammation*." Proc Natl Acad Sci U S A **111**(49): 17438-17443.
Reth, M. and J. Wienands (1997). "*Initiation and processing of signals from the B cell antigen receptor*." Annu Rev Immunol **15**: 453-479.
Richez, C., et al. (2010). "*IFN regulatory factor 5 is required for disease development in the FcgammaRIIB-/-Yaa and FcgammaRIIB-/- mouse models of systemic lupus erythematosus*." J Immunol **184**(2): 796-806.

Rider, P., et al. (2011). "*IL-1alpha and IL-1beta recruit different myeloid cells and promote different stages of sterile inflammation*." J Immunol **187**(9): 4835-4843.
Robinson, J. T., et al. (2011). "*Integrative genomics viewer*." Nat Biotechnol **29**(1): 24-26.
Rodero, M. P., et al. (2015). "*Immune surveillance of the lung by migrating tissue monocytes*." Elife **4**.
Rosas, M., et al. (2008). "*The induction of inflammation by dectin-1 in vivo is dependent on myeloid cell programming and the progression of phagocytosis*." J Immunol **181**(5): 3549-3557.
Rosenbauer, F. and D. G. Tenen (2007). "*Transcription factors in myeloid development: balancing differentiation with transformation*." Nat Rev Immunol **7**(2): 105-117.
Rossol, M., et al. (2012). "*The CD14(bright) CD16+ monocyte subset is expanded in rheumatoid arthritis and promotes expansion of the Th17 cell population*." Arthritis Rheum **64**(3): 671-677.
Rueda, B., et al. (2006). "*Analysis of IRF5 gene functional polymorphisms in rheumatoid arthritis*." Arthritis Rheum **54**(12): 3815-3819.
Ruth, J. H., et al. (2001). "*Fractalkine, a novel chemokine in rheumatoid arthritis and in rat adjuvant-induced arthritis*." Arthritis Rheum **44**(7): 1568-1581.
Ryzhakov, G., et al. (2015). "*Activation and function of interferon regulatory factor 5*." J Interferon Cytokine Res **35**(2): 71-78.
Sakaguchi, S., et al. (2008). "*Regulatory T cells and immune tolerance*." Cell **133**(5): 775-787.
Sakamoto, H., et al. (1998). "*A Janus kinase inhibitor, JAB, is an interferon-gamma-inducible gene and confers resistance to interferons*." Blood **92**(5): 1668-1676.
Saliba, D. G., et al. (2014). "*IRF5:RelA interaction targets inflammatory genes in macrophages*." Cell Rep **8**(5): 1308-1317.
Sallusto, F. and A. Lanzavecchia (1994). "*Efficient presentation of soluble antigen by cultured human dendritic cells is maintained by granulocyte/macrophage colony-stimulating factor plus interleukin 4 and downregulated by tumor necrosis factor alpha*." J Exp Med **179**(4): 1109-1118.
Sarma, J. V. and P. A. Ward (2011). "*The complement system*." Cell and Tissue Research **343**(1): 227-235.
Sasmono, R. T., et al. (2003). "*A macrophage colony-stimulating factor receptor-green fluorescent protein transgene is expressed throughout the mononuclear phagocyte system of the mouse*." Blood **101**(3): 1155-1163.
Satoh, T., et al. (2010). "*The Jmjd3-Irf4 axis regulates M2 macrophage polarization and host responses against helminth infection*." Nat Immunol **11**(10): 936-944.
Satpathy, A. T., et al. (2012). "*Zbtb46 expression distinguishes classical dendritic cells and their committed progenitors from other immune lineages*." J Exp Med **209**(6): 1135-1152.
Savitsky, D. A., et al. (2010). "*Contribution of IRF5 in B cells to the development of murine SLE-like disease through its transcriptional control of the IgG2a locus*." Proc Natl Acad Sci U S A **107**(22): 10154-10159.
Schiwon, M., et al. (2014). "*Crosstalk between sentinel and helper macrophages permits neutrophil migration into infected uroepithelium*." Cell **156**(3): 456-468.

Schlitzer, A. and F. Ginhoux (2013). "*DNGR-ing the dendritic cell lineage*." EMBO Rep **14**(10): 850-851.
Schlitzer, A., et al. (2013). "*IRF4 transcription factor-dependent CD11b+ dendritic cells in human and mouse control mucosal IL-17 cytokine responses*." Immunity **38**(5): 970-983.
Schlitzer, A., et al. (2015). "*Identification of cDC1- and cDC2-committed DC progenitors reveals early lineage priming at the common DC progenitor stage in the bone marrow*." Nat Immunol **16**(7): 718-728.
Schneider, C., et al. (2014). "*Induction of the nuclear receptor PPAR-gamma by the cytokine GM-CSF is critical for the differentiation of fetal monocytes into alveolar macrophages*." Nat Immunol **15**(11): 1026-1037.
Schoenemeyer, A., et al. (2005). "*The interferon regulatory factor, IRF5, is a central mediator of toll-like receptor 7 signaling*." J Biol Chem **280**(17): 17005-17012.
Schraml, B. U., et al. (2013). "*Genetic tracing via DNGR-1 expression history defines dendritic cells as a hematopoietic lineage*." Cell **154**(4): 843-858.
Schulz, C., et al. (2012). "*A lineage of myeloid cells independent of Myb and hematopoietic stem cells*." Science **336**(6077): 86-90.
Scott, D. L., et al. (2010). "*Rheumatoid arthritis*." Lancet **376**(9746): 1094-1108.
Seitz, M., et al. (1994). "*Constitutive mRNA and protein production of macrophage colony-stimulating factor but not of other cytokines by synovial fibroblasts from rheumatoid arthritis and osteoarthritis patients*." Br J Rheumatol **33**(7): 613-619.
Serafini, N., et al. (2015). "*Transcriptional regulation of innate lymphoid cell fate*." Nat Rev Immunol **15**(7): 415-428.
Serbina, N. V., et al. (2008). "*Monocyte-mediated defense against microbial pathogens*." Annu Rev Immunol **26**: 421-452.
Serbina, N. V. and E. G. Pamer (2006). "*Monocyte emigration from bone marrow during bacterial infection requires signals mediated by chemokine receptor CCR2*." Nat Immunol **7**(3): 311-317.
Serbina, N. V., et al. (2003). "*TNF/iNOS-producing dendritic cells mediate innate immune defense against bacterial infection*." Immunity **19**(1): 59-70.
Shen, H., et al. (2010). "*Gender-dependent expression of murine Irf5 gene: implications for sex bias in autoimmunity*." J Mol Cell Biol **2**(5): 284-290.
Sheng, J., et al. (2015). "*Most Tissue-Resident Macrophages Except Microglia Are Derived from Fetal Hematopoietic Stem Cells*." Immunity **43**(2): 382-393.
Shi, C. and E. G. Pamer (2011). "*Monocyte recruitment during infection and inflammation*." Nat Rev Immunol **11**(11): 762-774.
Shibata, Y., et al. (2001). "*GM-CSF regulates alveolar macrophage differentiation and innate immunity in the lung through PU.1*." Immunity **15**(4): 557-567.
Shigeyama, Y., et al. (2000). "*Expression of osteoclast differentiation factor in rheumatoid arthritis*." Arthritis Rheum **43**(11): 2523-2530.
Sieweke, M. H. and J. E. Allen (2013). "*Beyond stem cells: self-renewal of differentiated macrophages*." Science **342**(6161): 1242974.
Sims, N. A. and J. H. Gooi (2008). "*Bone remodeling: Multiple cellular interactions required for coupling of bone formation and resorption*." Semin Cell Dev Biol **19**(5): 444-451.

Sindrilaru, A., et al. (2011). "*An unrestrained proinflammatory M1 macrophage population induced by iron impairs wound healing in humans and mice*." J Clin Invest **121**(3): 985-997.
Smeets, T. J., et al. (2001). "*Analysis of the cell infiltrate and expression of matrix metalloproteinases and granzyme B in paired synovial biopsy specimens from the cartilage-pannus junction in patients with RA*." Ann Rheum Dis **60**(6): 561-565.
Smolen, J. S. and D. Aletaha (2015). "*Rheumatoid arthritis therapy reappraisal: strategies, opportunities and challenges*." Nat Rev Rheumatol **11**(5): 276-289.
Soler Palacios, B., et al. (2015). "*Macrophages from the synovium of active rheumatoid arthritis exhibit an activin A-dependent pro-inflammatory profile*." J Pathol **235**(3): 515-526.
Spits, H. and J. P. Di Santo (2011). "*The expanding family of innate lymphoid cells: regulators and effectors of immunity and tissue remodeling*." Nat Immunol **12**(1): 21-27.
Stahl, E. A., et al. (2010). "*Genome-wide association study meta-analysis identifies seven new rheumatoid arthritis risk loci*." Nat Genet **42**(6): 508-514.
Stanley, E. R. (1997). "*Murine bone marrow-derived macrophages*." Methods Mol Biol **75**: 301-304.
Starr, T. K., et al. (2003). "*Positive and negative selection of T cells*." Annu Rev Immunol **21**: 139-176.
Stein, M., et al. (1992). "*Interleukin 4 potently enhances murine macrophage mannose receptor activity: a marker of alternative immunologic macrophage activation*." J Exp Med **176**(1): 287-292.
Steinman, R. M. and Z. A. Cohn (1973). "*Identification of a novel cell type in peripheral lymphoid organs of mice. I. Morphology, quantitation, tissue distribution*." J Exp Med **137**(5): 1142-1162.
Steinman, R. M., et al. (1979). "*Identification of a novel cell type in peripheral lymphoid organs of mice. V. Purification of spleen dendritic cells, new surface markers, and maintenance in vitro*." J Exp Med **149**(1): 1-16.
Stolt, P., et al. (2003). "*Quantification of the influence of cigarette smoking on rheumatoid arthritis: results from a population based case-control study, using incident cases*." Ann Rheum Dis **62**(9): 835-841.
Stone, R. C., et al. (2013). "*RNA-Seq for enrichment and analysis of IRF5 transcript expression in SLE*." PLoS One **8**(1): e54487.
Stone, R. C., et al. (2012). "*Interferon regulatory factor 5 activation in monocytes of systemic lupus erythematosus patients is triggered by circulating autoantigens independent of type I interferons*." Arthritis Rheum **64**(3): 788-798.
Stout, R. D., et al. (2005). "*Macrophages sequentially change their functional phenotype in response to changes in microenvironmental influences*." J Immunol **175**(1): 342-349.
Swirski, F. K., et al. (2009). "*Identification of splenic reservoir monocytes and their deployment to inflammatory sites*." Science **325**(5940): 612-616.
Szabo, S. J., et al. (2000). "*A novel transcription factor, T-bet, directs Th1 lineage commitment*." Cell **100**(6): 655-669.
Tada, Y., et al. (2011). "*Interferon regulatory factor 5 is critical for the development of lupus in MRL/lpr mice*." Arthritis Rheum **63**(3): 738-748.
Tak, P. P. and B. Bresnihan (2000). "*The pathogenesis and prevention of joint damage in rheumatoid arthritis: advances from synovial biopsy and tissue analysis*." Arthritis Rheum **43**(12): 2619-2633.

Takahashi, K., et al. (1989). "*Differentiation, maturation, and proliferation of macrophages in the mouse yolk sac: a light-microscopic, enzyme-cytochemical, immunohistochemical, and ultrastructural study*." J Leukoc Biol **45**(2): 87-96.
Takaoka, A., et al. (2005). "*Integral role of IRF-5 in the gene induction programme activated by Toll-like receptors*." Nature **434**(7030): 243-249.
Takeda, K., et al. (1996). "*Essential role of Stat6 in IL-4 signalling*." Nature **380**(6575): 627-630.
Takeuchi, O. and S. Akira (2010). "*Pattern recognition receptors and inflammation*." Cell **140**(6): 805-820.
Tamoutounour, S., et al. (2013). "*Origins and functional specialization of macrophages and of conventional and monocyte-derived dendritic cells in mouse skin*." Immunity **39**(5): 925-938.
Tamoutounour, S., et al. (2012). "*CD64 distinguishes macrophages from dendritic cells in the gut and reveals the Th1-inducing role of mesenteric lymph node macrophages during colitis*." Eur J Immunol **42**(12): 3150-3166.
Tamura, T., et al. (2000). "*ICSBP directs bipotential myeloid progenitor cells to differentiate into mature macrophages*." Immunity **13**(2): 155-165.
Tamura, T., et al. (2008). "*The IRF family transcription factors in immunity and oncogenesis*." Annu Rev Immunol **26**: 535-584.
Tavian, M. and B. Peault (2005). "*Embryonic development of the human hematopoietic system*." Int J Dev Biol **49**(2-3): 243-250.
Tecchio, C., et al. (2014). "*Neutrophil-derived cytokines: facts beyond expression*." Front Immunol **5**: 508.
Trapnell, B. C. and J. A. Whitsett (2002). "*Gm-CSF regulates pulmonary surfactant homeostasis and alveolar macrophage-mediated innate host defense*." Annu Rev Physiol **64**: 775-802.
Turvey, S. E. and D. H. Broide (2010). "*Innate immunity*." Journal of Allergy and Clinical Immunology **125**(2): S24-S32.
van de Laar, L., et al. (2012). "*Regulation of dendritic cell development by GM-CSF: molecular control and implications for immune homeostasis and therapy*." Blood **119**(15): 3383-3393.
van den Berg, W. B., et al. (2007). "*Murine antigen-induced arthritis*." Methods Mol Med **136**: 243-253.
van Furth, R. and Z. A. Cohn (1968). "*The origin and kinetics of mononuclear phagocytes*." J Exp Med **128**(3): 415-435.
van Furth, R., et al. (1972). "*The mononuclear phagocyte system: a new classification of macrophages, monocytes, and their precursor cells*." Bull World Health Organ **46**(6): 845-852.
Van Lent, P. L., et al. (1998). "*Local removal of phagocytic synovial lining cells by clodronate-liposomes decreases cartilage destruction during collagen type II arthritis*." Ann Rheum Dis **57**(7): 408-413.
van Venrooij, W. J., et al. (2011). "*Anti-CCP antibodies: the past, the present and the future*." Nat Rev Rheumatol **7**(7): 391-398.
Vantourout, P. and A. Hayday (2013). "*Six-of-the-best: unique contributions of gammadelta T cells to immunology*." Nat Rev Immunol **13**(2): 88-100.
Varinou, L., et al. (2003). "*Phosphorylation of the Stat1 transactivation domain is required for full-fledged IFN-gamma-dependent innate immunity*." Immunity **19**(6): 793-802.

Verreck, F. A., et al. (2004). "*Human IL-23-producing type 1 macrophages promote but IL-10-producing type 2 macrophages subvert immunity to (myco)bacteria*." Proc Natl Acad Sci U S A **101**(13): 4560-4565.
Verreck, F. A., et al. (2006). "*Phenotypic and functional profiling of human proinflammatory type-1 and anti-inflammatory type-2 macrophages in response to microbial antigens and IFN-gamma- and CD40L-mediated costimulation*." J Leukoc Biol **79**(2): 285-293.
Vyas, J. M., et al. (2008). "*The known unknowns of antigen processing and presentation*." Nat Rev Immunol **8**(8): 607-618.
Wang, C., et al. (2012). "*Evidence of association between interferon regulatory factor 5 gene polymorphisms and asthma*." Gene **504**(2): 220-225.
Wang, Y., et al. (2012). "*IL-34 is a tissue-restricted ligand of CSF1R required for the development of Langerhans cells and microglia*." Nat Immunol **13**(8): 753-760.
Wardemann, H., et al. (2003). "*Predominant autoantibody production by early human B cell precursors*." Science **301**(5638): 1374-1377.
Warnatsch, A., et al. (2015). "*Inflammation. Neutrophil extracellular traps license macrophages for cytokine production in atherosclerosis*." Science **349**(6245): 316-320.
Willemze, A., et al. (2012). "*The influence of ACPA status and characteristics on the course of RA*." Nat Rev Rheumatol **8**(3): 144-152.
Wipke, B. T. and P. M. Allen (2001). "*Essential role of neutrophils in the initiation and progression of a murine model of rheumatoid arthritis*." J Immunol **167**(3): 1601-1608.
Witmer-Pack, M. D., et al. (1993). "*Identification of macrophages and dendritic cells in the osteopetrotic (op/op) mouse*." J Cell Sci **104 (Pt 4)**: 1021-1029.
Wittkowski, H., et al. (2007). "*Effects of intra-articular corticosteroids and anti-TNF therapy on neutrophil activation in rheumatoid arthritis*." Ann Rheum Dis **66**(8): 1020-1025.
Wright, H. L., et al. (2014). "*The multifactorial role of neutrophils in rheumatoid arthritis*." Nat Rev Rheumatol **10**(10): 593-601.
Wynn, T. A., et al. (2013). "*Macrophage biology in development, homeostasis and disease*." Nature **496**(7446): 445-455.
Xu, W. D., et al. (2013). "*Interferon regulatory factor 5 and autoimmune lupus*." Expert Rev Mol Med **15**: e6.
Xu, Y., et al. (2012). "*Pleiotropic IFN-dependent and -independent effects of IRF5 on the pathogenesis of experimental lupus*." J Immunol **188**(8): 4113-4121.
Xue, J., et al. (2014). "*Transcriptome-based network analysis reveals a spectrum model of human macrophage activation*." Immunity **40**(2): 274-288.
Yamamoto, M., et al. (2003). "*Role of adaptor TRIF in the MyD88-independent toll-like receptor signaling pathway*." Science **301**(5633): 640-643.
Yanagihara, S., et al. (1998). "*EBI1/CCR7 is a new member of dendritic cell chemokine receptor that is up-regulated upon maturation*." J Immunol **161**(6): 3096-3102.
Yanai, H., et al. (2007). "*Role of IFN regulatory factor 5 transcription factor in antiviral immunity and tumor suppression*." Proc Natl Acad Sci U S A **104**(9): 3402-3407.
Yang, L., et al. (2012). "*Monocytes from Irf5-/- mice have an intrinsic defect in their response to pristane-induced lupus*." J Immunol **189**(7): 3741-3750.

Yasuda, K., et al. (2013). "*Phenotype and function of B cells and dendritic cells from interferon regulatory factor 5-deficient mice with and without a mutation in DOCK2*." Int Immunol **25**(5): 295-306.
Yasuda, K., et al. (2014). "*Interferon regulatory factor-5 deficiency ameliorates disease severity in the MRL/lpr mouse model of lupus in the absence of a mutation in DOCK2*." PLoS One **9**(7): e103478.
Yipp, B. G., et al. (2012). "*Infection-induced NETosis is a dynamic process involving neutrophil multitasking in vivo*." Nat Med **18**(9): 1386-1393.
Yona, S. and S. Gordon (2015). "*From the Reticuloendothelial to Mononuclear Phagocyte System - The Unaccounted Years*." Front Immunol **6**: 328.
Yona, S., et al. (2013). "*Fate mapping reveals origins and dynamics of monocytes and tissue macrophages under homeostasis*." Immunity **38**(1): 79-91.
Yoshida, H., et al. (1990). "*The murine mutation osteopetrosis is in the coding region of the macrophage colony stimulating factor gene*." Nature **345**(6274): 442-444.
Zeisel, A., et al. (2015). "*Brain structure. Cell types in the mouse cortex and hippocampus revealed by single-cell RNA-seq*." Science **347**(6226): 1138-1142.
Zheng, W. and R. A. Flavell (1997). "*The transcription factor GATA-3 is necessary and sufficient for Th2 cytokine gene expression in CD4 T cells*." Cell **89**(4): 587-596.
Zhu, J., et al. (2010). "*Differentiation of effector CD4 T cell populations (*)*." Annu Rev Immunol **28**: 445-489.
Zhu, W., et al. (2015). "*Anti-Citrullinated Protein Antibodies Induce Macrophage Subset Disequilibrium in RA Patients*." Inflammation.
Ziegler-Heitbrock, L., et al. (2010). "*Nomenclature of monocytes and dendritic cells in blood*." Blood **116**(16): e74-80.
Zinkernagel, R. M. (1974). "*Restriction by H-2 gene complex of transfer of cell-mediated immunity to Listeria monocytogenes*." Nature **251**(5472): 230-233.

8. Supplement

The following two first author publications resulted from the data presented in this thesis, as outlined in the declaration, and can be found at the end of this thesis:

Weiss M*, Byrne AJ*, Blazek K, Saliba DG, Pease JE, Perocheau D, Feldmann M, Udalova IA. IRF5 controls both acute and chronic inflammation. *Proceedings of the National Academy of Sciences of the United States of America*, 2015 Sep 1;112(35):11001-6.

*these authors contributed to the work equally

Weiss M, Blazek K, Byrne AJ, Perocheau DP, Udalova IA. IRF5 is a specific marker of inflammatory macrophages *in vivo*. *Mediators of Inflammation*, 2013; 2013:245804.

In addition, I contributed (either experimentally or by analysing data) to the following manuscripts which can be found online:

Blazek K, Eames HL, **Weiss M**, Byrne AJ, Perocheau D, Pease JE, Doyle S, McCann F, Williams RO, Udalova IA. IFN-λ resolves inflammation via suppression of neutrophil infiltration and IL-1β production. *The Journal of Experimental Medicine*, 2015 Jun 1;212(6):845-53.

Saliba DG, Heger A, Eames HL, Oikonomopoulos S, Teixeira A, Blazek K, Androulidaki A, Wong D, Goh FG, **Weiss M**, Byrne A, Pasparakis M, Ragoussis

J, Udalova IA. IRF5:RelA Interaction Targets Inflammatory Genes in Macrophages. *Cell Reports*, 2014 Sep 11;8(5):1308-17.

Sundlisaeter E, Edelmann RJ, Hol J, Sponheim J, Küchler AM, **Weiss M**, Udalova IA, Midwood KS, Kasprzycka M, Haraldsen G. The alarmin IL-33 is a notch target in quiescent endothelial cells. *The American Journal of Pathology*, 2012 Sep;181(3):1099-111.

8.1. Supplementary Data

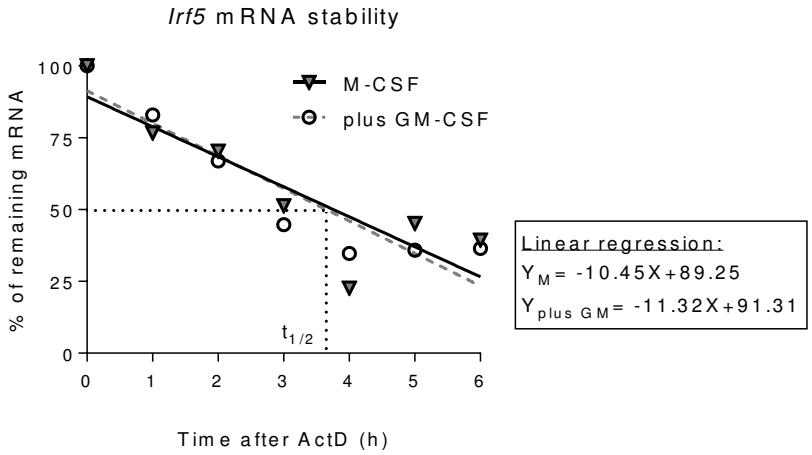

Supplementary Figure S8.1. GM-CSF does not affect *Irf5* mRNA stability.

Bone marrow derived cells were differentiated using GM-CSF (20 ng/ml) or M-CSF (100 ng/ml) as described previously. 20 ng/ml of GM-CSF were added to M-CSF macrophages at the final day of differentiation as additional stimulus. Actinomycin D (ActD) was added 6 h after stimulation with GM-CSF to inhibit synthesis of new *Irf5* mRNA production at its peak. RNA was collected up to 6 h following ActD treatment and analysed by qPCR. Transcript levels are expressed as a percentage of *Irf5* mRNA remaining compared to 6 h treatment with GM-CSF before ActD. Data was analysed using linear regression analysis, n=1.

IRF5 controls both acute and chronic inflammation

Miriam Weiss[a,1], Adam J. Byrne[a,b,1], Katrina Blazek[a], David G. Saliba[a], James E. Pease[b], Dany Perocheau[a], Marc Feldmann[a,2], and Irina A. Udalova[a,2]

[a]Kennedy Institute of Rheumatology, University of Oxford, Oxford OX3 7FY, United Kingdom; and [b]National Heart and Lung Institute, Imperial College, London SW7 2AZ, United Kingdom

Contributed by Marc Feldmann, July 25, 2015 (sent for review March 30, 2015)

Whereas the importance of macrophages in chronic inflammatory diseases is well recognized, there is an increasing awareness that neutrophils may also play an important role. In addition to the well-documented heterogeneity of macrophage phenotypes and functions, neutrophils also show remarkable phenotypic diversity among tissues. Understanding the molecular pathways that control this heterogeneity should provide abundant scope for the generation of more specific and effective therapeutics. We have shown that the transcription factor IFN regulatory factor 5 (IRF5) polarizes macrophages toward an inflammatory phenotype. IRF5 is also expressed in other myeloid cells, including neutrophils, where it was linked to neutrophil function. In this study we explored the role of IRF5 in models of acute inflammation, including antigen-induced inflammatory arthritis and lung injury, both involving an extensive influx of neutrophils. Mice lacking IRF5 accumulate far fewer neutrophils at the site of inflammation due to the reduced levels of chemokines important for neutrophil recruitment, such as the chemokine (C-X-C motif) ligand 1. Furthermore we found that neutrophils express little IRF5 in the joints and that their migratory properties are not affected by the IRF5 deficiency. These studies extend prior ones suggesting that inhibiting IRF5 might be useful for chronic macrophage-induced inflammation and suggest that IRF5 blockade would ameliorate more acute forms of inflammation, including lung injury.

macrophages | neutrophils | IRF5 | acute inflammation | arthritis

Myeloid cells are critical components of host defense. Macrophages (MPHs) and neutrophils are the two major types of myeloid cells involved in inflammatory disease, such as rheumatoid arthritis (RA), which is a chronic degenerative disease characterized by joint inflammation and bone destruction affecting up to 1% of the population (1). The molecular pathogenesis of RA has been extensively studied, and some aspects have been understood. Excess TNF is pathogenic, as witnessed by the extensive use of TNF inhibitors, which in 2014 were the world's best-selling medicines. Most of the TNF in RA is produced by synovial macrophages. The increase in the number of sublining macrophages is an early hallmark of active rheumatic disease (2), with augmented numbers of macrophages being a prominent feature of inflammatory lesions (3). The degree of synovial macrophage infiltration correlates with the degree of joint erosion (4), and their depletion from inflamed tissue has a profound therapeutic benefit (5). Neutrophils also play an important but less understood role in RA pathogenesis (6). The potential importance of neutrophils is suggested not only by their abundance, e.g., in synovial fluid of RA patients and within the pannus in patients with active RA (7, 8), but also by the neutrophil formation of extracellular traps (NETs), which can provide a source of destructive enzymes as well as autoantigens (9).

In recent years there has been a growing understanding of the heterogeneity of macrophages (10, 11) and, more recently, awareness that neutrophils may also form distinct subsets (12, 13). The exact nature of the myeloid cells in various inflammatory diseases is thus a topic of major interest, as it will not only provide clues about pathogenesis, but also contribute toward more effective therapeutics. In a mouse model of sterile inflammatory arthritis (K/BxN serum transfer induced arthritis) modeling only the effector part of the disease, nonclassical (Ly6C$^-$) monocytes enter the joint and differentiate into classical inflammatory macrophages that drive joint pathology (14). During resolution, macrophages are "alternatively activated" and promote resolution and repair. The situation in models of RA, which involve induction as well as effector phases, or more importantly, in human RA, is not yet clear.

We have documented the importance of the transcription factor IFN regulatory factor 5 (IRF5) in defining the classical inflammatory phenotype of macrophages (15, 16). IRF5 has also recently been reported to be expressed in neutrophils, specifically in neutrophils from synovial fluid of arthritic mice (13). Therefore, here we test the role of IRF5-expressing cells in antigen-induced arthritis (AIA), and document the importance of IRF5 in neutrophil joint accumulation. We find that neutrophils express little IRF5 while in the joints and that their migratory properties are not affected by the IRF5 deficiency. However, we observed a significant reduction in secretion of a major neutrophil chemoattractant, the chemokine (C-X-C motif) receptor 2 (CXCR2) binding chemokine (C-X-C motif) ligand (CXCL) 1. Neutrophil-dependent acute lung injury is also markedly reduced in the IRF5-deficient mice, indicating the importance of IRF5 in neutrophil recruitment beyond the joints. These results also document that IRF5 blockade would have a major impact on inflammation by altering both macrophage phenotypes and neutrophil recruitment, and hence defining IRF5 as a very interesting potential therapeutic target.

Results

IRF5 Ablation Limits Neutrophil Influx in the Inflamed Joint. The murine model of antigen-induced arthritis relies on s.c. immunization with methylated BSA (mBSA) plus complete Freund's

Significance

Many of the world's major chronic diseases are driven by inflammation. The most abundant inflammatory cells in these diseases are myeloid cells, such as macrophages and neutrophils. Both cell types show remarkable phenotypic diversity among tissues. Defining molecular factors that control this diversity provides abundant scope for the generation of more specific and effective therapeutics, as the lack of specificity of the current most widely used antiinflammatory approaches, such as glucocorticoids and nonsteroidal antiinflammatory molecules, leads to widespread problems if used long term, even at relatively low doses. In this study we demonstrate that a transcription factor called IFN regulatory factor 5 controls macrophage and neutrophil aspects of inflammation, and thus its blockade might be an effective therapeutic strategy for multiple indications.

Author contributions: I.A.U. designed research; M.W., A.J.B., K.B., D.G.S., J.E.P., and D.P. performed research; M.W., A.J.B., D.G.S., and I.A.U. analyzed data; and M.W., M.F., and I.A.U. wrote the paper.

The authors declare no conflict of interest.

[1]M.W. and A.J.B. contributed equally to this work.

[2]To whom correspondence may be addressed. Email: irina.udalova@kennedy.ox.ac.uk or marc.feldmann@kennedy.ox.ac.uk.

This article contains supporting information online at www.pnas.org/lookup/suppl/doi:10.1073/pnas.1506254112/-/DCSupplemental.

adjuvant (CFA), followed by intraarticular injection of mBSA into the knee joint (17). The model is characterized by infiltration of polymorphonuclear and mononuclear cells, pannus formation, and erosion of bone and cartilage (17), and is Th17 dependent (18). We have previously reported that synovial macrophages from the AIA-affected joints are characterized by high levels of IRF5 (16). Here, we aimed to determine the role that IRF5 plays in synovial physiology and function in both naïve joints and during inflammatory arthritis. IRF5 deficient mice ($IRF5^{-/-}$) and their littermate wild-type controls (WT) were immunized with mBSA in CFA and 7 d later, knees were either challenged with mBSA or PBS control (Fig. S1*A*). Knee swelling of WT mice was induced rapidly and peaked at day 2, after which time swelling decreased. $IRF5^{-/-}$ mice showed significantly less swelling at day 2 in comparison with WT controls (Fig. 1*A*). Reduced swelling corresponded to a decreased number of cells recovered from excised knee joints at that point (Fig. 1*B*). Knee pathology at day 2 was further assessed histologically for the degree of inflammatory infiltrate into the synovium and joint cavity, synovial capsule and synovial membrane thickness and bone erosion, respectively (Fig. S1*B*). IRF5 knockout mice displayed a significantly lower synovial membrane thickening score in the mBSA-challenged knees than WT mice (Fig. 1*C*). Consistent with resolved knee swelling at the later stages, we observed reduced synovial membrane thickening at day 7 (Fig. S1*B*).

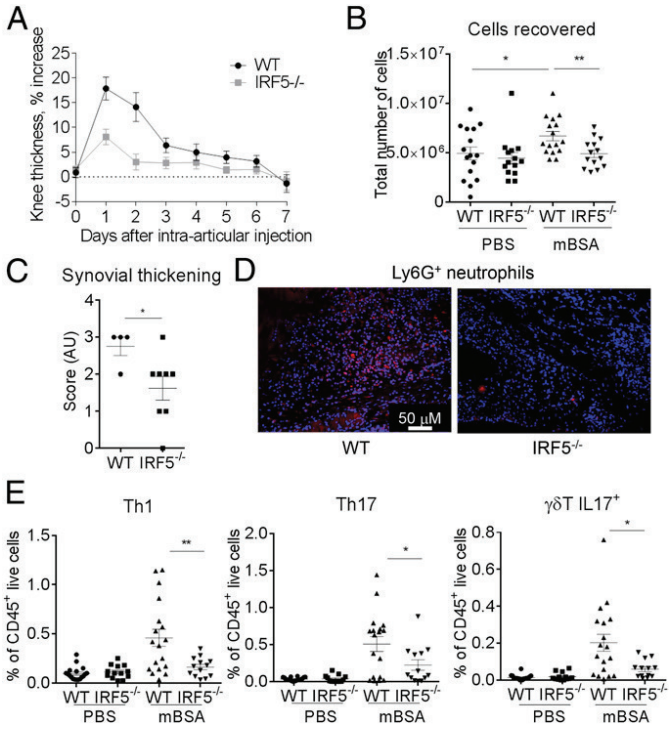

Fig. 1. IRF5 ablation limits neutrophil influx in the inflamed knee. (*A*) Comparison of knee swelling between inflamed knees of the $IRF5^{-/-}$ and WT animals, expressed as a percentage of swelling of the mBSA-challenged knee compared with the PBS knee. (*B*) Total number of cells recovered from excised knee joints of the $IRF5^{-/-}$ and WT animals at day 2 of the AIA. (*C*) Synovial thickness of inflamed knees at day 2 post intraarticular injection of mBSA based on examination of histology slides (Fig. S1*B*). (*D*) $Ly6G^+$ cells detected within the synovial capsule of inflamed knees in the $IRF5^{-/-}$ and WT animals, analyzed by immunohistochemical staining and confocal microscopy. Cell nuclei are marked by DAPI staining in blue and $Ly6G^+$ cells are shown in red. Compare 52 ± 17 and 14 ± 3 $Ly6G^+$ cells per field for WT and $IRF5^{-/-}$ ($P = 0.0045$). (*E*) Number of Th1, Th17, and γδ T $IL17^+$ cells in the joints of mice at day 7 of AIA, expressed as a percentage of live $CD45^+$ cells. Data show the mean and SEM derived from 10 to 20 mice from three to four independent AIA experiments. Each dot represents an individual mouse. Statistical analysis was performed by one-tailed Mann–Whitney *u* test. $*P < 0.05$; $**P < 0.01$; $***P < 0.001$.

The observed difference in the number of leukocytes recovered from mBSA-challenged knees at day 2 compared with the PBS controls (Fig. 1*B*) was mirrored by the increase in myeloid cell numbers, i.e., $CD11b^+F4/80^{hi}CD64^{hi}$ macrophages, $CD11b^+F4/80^{dim}$ monocytes, $CD11b^+F4/80^+CD11c^+$ dendritic cells (DCs), and neutrophils (Fig. S1*C*). There was no change in the number of $CD11b^-F4/80^-CD11c^+$ dendritic cells (Fig. S1*C*). Due to the likelihood of substantial influx into the neutrophil pool from the bone marrow (BM) when harvesting knees, we used pro-IL1β as a marker for activated neutrophils (19) and focused on synovial-activated neutrophils $CD11b^+F4/80^-Ly6G^+$pro-$IL1\beta^+$. The number of synovial-activated neutrophils was significantly reduced in inflamed knees of $IRF5^{-/-}$ mice (Fig. S1*C*), whereas the numbers of synovial monocytes, macrophages, and DCs were unaffected (Fig. S1*C*). This was confirmed by immunohistochemical staining of slides for $Ly6G^+$ cells and cell counting, which demonstrated a clear reduction in synovial neutrophil infiltrate in the $IRF5^{-/-}$ animals (Fig. 1*D*). Neutrophils are thus the only myeloid cells, whose influx or propagation depends on IRF5 during early stages of AIA.

IL-17 produced by $CD4^+$ (Th17) cells or γδ T cells plays an important role in the pathogenesis of AIA (18). Thus, we analyzed the number of IL-17 producing Th17 and γδ T cells in the joints of mice at days 2 and 7 of the disease. Minimal $CD4^+$ and no γδ T-cell populations were detected at day 2, whereas by day 7, the T-cell response in WT mBSA knees was increased compared with day 2 (Fig. S2*A*). However, in $IRF5^{-/-}$ animals the T-cell response at day 7 was significantly reduced, affecting both Th17 and γδ T $IL17^+$ cells, as well as IFNγ-producing Th1 cells (Fig. 1*E*). We also observed a reduction in the levels of IFNγ and IL-17A mRNA and of cytokines facilitating generation of Th1/Th17 cells, e.g., IL-1β, IL-6, IL-12p40, and IL-23p19 (Fig. S2*B*).

To assess a potential effect of IRF5 deficiency on the immunization process preceding the intraarticular challenge, inguinal lymph nodes were harvested 7 d after immunization. Lymph node cell suspensions were stimulated with α-CD3 or mBSA for 48 h and T-cell proliferation was measured. Both stimulations resulted in a significant increase in lymphocyte proliferation, including proliferation of $CD4^+$ and $CD8^+$ T cells, but proliferative responses were unaffected by IRF5 deficiency (Fig. S2*C*). As B cells appear to play a critical role in arthritis pathogenesis (20), and express variable levels of IRF5, we examined B-cell numbers and function during the immunization of the $IRF5^{-/-}$ animals. No $CD19^+$ B cells were detected in the joint, whereas the number of $CD19^+$ B cells in the blood, spleen, and lymph node remained unaffected (Fig. S2*D*). Total B-cell (IgG1 and IgG2a) responses in the serum were assessed at day 2 of AIA and revealed no significant change for IgG1 and a reduction in the levels of IgG2a (Fig. S2*E*). This is in agreement with the previously documented role for IRF5 in the control of the *IgG2a* locus (21).

Taken together, the deficiency limits the neutrophil influx into the inflamed joint in the early stages of arthritis and leads to a reduction in the Th1/Th17 and γδT $IL-17^+$ cells in the joint at the later stages.

Synovial Macrophages in the Naïve and Inflamed Knee. The phenotype and origin of macrophages in the knee joint in the steady state or during inflammatory arthritis are not known. Recent work by Misharin et al. demonstrated that the ankle synovial lining of naïve mice consists of a heterogeneous population of macrophages, with the majority being true tissue-resident cells ($CD11b^+CD11c^{int}F4/80^+CD64^+MHCII^-$) and about a fifth originating from bone marrow ($CD11b^+CD11c^{int}F4/80^+CD64^+MHCII^+$) (14). Applying a similar gating strategy (*SI Appendix*, *FACS Gating Strategy and Representative Plots*) we demonstrate that the total number of $CD11b^+F4/80^+CD64^+$ macrophages in both ankle and

knee is reduced in IRF5$^{-/-}$ mice (Fig. S3*A*). The reduction seemed to be mainly due to the effect on the number of MHCII^{+} macrophages (Fig. 2*A*) that display the highest level of IRF5 expression within macrophage populations (Fig. 2*B*). Of interest, we find a higher representation of MHCII^{+} macrophages in the knee than in the ankle (Fig. 2*A*), whereas MHCII^{-} macrophages in the ankle express higher levels of IRF5 than their counterparts in the knee (Fig. 2*B*). These data highlight differences between the two joints in naïve animals.

To elucidate the source of macrophages infiltrating the knee in response to mBSA challenge, AIA was performed using C-C chemokine receptor 2 deficient mice (CCR2$^{-/-}$), which lack CCR2 expression on classical Ly6C^{+} monocytes essential for their trafficking (22). The influx of CD11b^{+}F4/80^{dim} monocytes and CD11b^{+}F4/80^{hi} macrophages was almost completely abolished in the mBSA-challenged joints of CCR2$^{-/-}$ mice (Fig. 2*C*). Ly6C was expressed on 80–90% of monocytes and macrophages in the knee joints of immunized mice, with 50–60% of those being Ly6C^{hi} (Fig. S3*B*). This finding represents a drastic increase in the amount of Ly6C^{hi} cells compared with steady-state joints without intraarticular antigen challenge. A total of 60% of macrophages in PBS-treated knees and 90% of macrophages in the mBSA-challenged knees were CD64^{hi} (Fig. S3*C*). IRF5 deficiency did not affect monocyte, macrophage, or DC infiltrate into the mBSA-challenged knee (Fig. S1*B*), but expression of CD64 (Fc gamma receptor 1) on macrophages was reduced (Fig. S3*D*). Consistent with our previously reported observations (15), we observed a shift toward an alternatively activated macrophage phenotype in the IRF5$^{-/-}$ animals, with a lower number of macrophages expressing MHC II and higher numbers expressing CD206 (Fig. 2*E*).

Taken together, these data suggest that in the antigen-driven arthritis model, Ly6C^{+} circulating monocytes are preferentially recruited into the inflamed joint and give rise to Ly6C^{+} inflammatory macrophages. The presence of IRF5 appears to be important for differentiation of monocytes into CD64^{+} macrophages and for the establishment of the MHCII^{+} inflammatory macrophage phenotype in the arthritic joint.

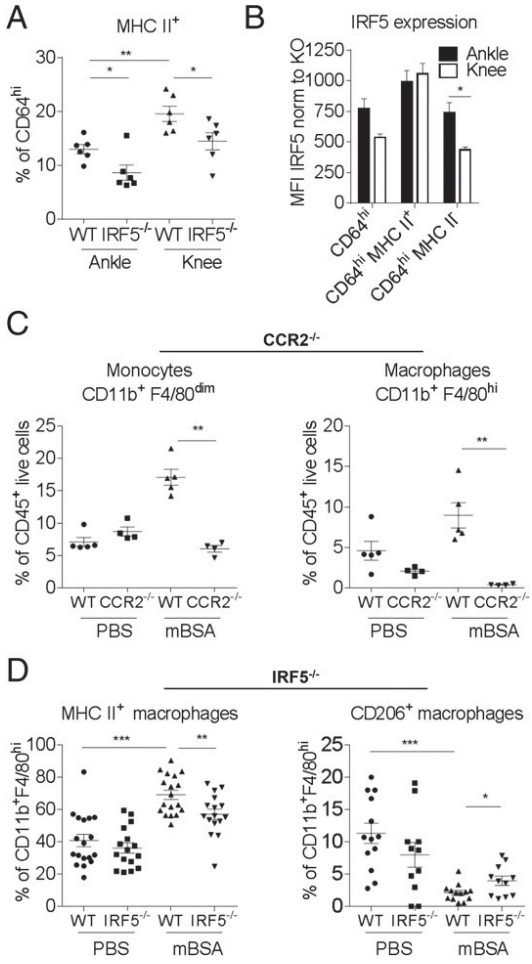

Fig. 2. Characterization of synovial macrophages in naïve knees and during AIA. (*A*) Number of tissue resident MHCII^{+} macrophages in both ankle and knee joints of naïve IRF5$^{-/-}$ mice and WT controls. (*B*) IRF5 expression within tissue resident macrophage populations defined by mean fluorescence intensity (MFI) and normalized to MFI of IRF5-deficient animals. Data shown are the mean and SEM derived from 6 mice from a representative experiment. Statistical analysis was performed by two-way ANOVA with Bonferroni's correction for multiple comparisons. *$P < 0.05$. (*C*) Number of CD11b^{+} F4/80^{dim} monocytes and CD11b^{+}F4/80^{hi} macrophages in the mBSA-challenged knees or PBS controls of CCR2$^{-/-}$ and WT mice, expressed as a percentage of live CD45^{+} cells. (*D*) Number of MHCII^{+} or CD206^{+} macrophages in the mBSA-challenged knees or PBS controls of IRF5$^{-/-}$ and WT animals, expressed as a percentage of CD11b^{+}F4/80^{hi} cells. Data shown are mean and SEM derived from 4–7 mice from a representative AIA experiment (*A* and *C*) or 10–20 mice from three to four independent AIA experiments (*C* and *D*). Each dot represents an individual mouse. Statistical analysis was performed by one-tailed Mann–Whitney *u* test. *$P < 0.05$; **$P < 0.01$; ***$P < 0.001$.

IRF5 Controls Neutrophil Influx via Regulation of Chemokine Production Such as CXCL1. Because the recruitment of neutrophils into the knees of IRF5$^{-/-}$ animals was significantly reduced, we set out to examine whether neutrophils themselves were affected by the loss of IRF5. Firstly, we measured the levels of IRF5 expression in neutrophils in WT mice and found them to be significantly lower compared with monocytes and macrophages in the knee (Fig. 3*A*). Secondly, we examined the migratory capacity of neutrophils toward the neutrophil chemoattractant CXCL2 using the EZ-Taxiscan system, which allows visualization of cell migration in shallow, linear gradients and provides real-time analysis of neutrophil movement (23). Neutrophils were isolated from the air pouch, created on the dorsal surface of the mice and injected with zymosan (24) (Fig. S4*A*). Approximately 80% of the recovered cells after injection of 100 μg of zymosan were CD11b^{+}Ly6G^{+} neutrophils. The Euclidean distance that neutrophils covered when migrating toward the attractant was comparable in WT and IRF5$^{-/-}$ cells (Fig. 3*B* and Fig. S4*B*). Notably, basal neutrophil movement, in the absence of any chemoattractant, was not affected either. Hence, we conclude that lack of IRF5 does not affect the intrinsic capacities of neutrophils to migrate toward a chemokine. To assess whether secretion of neutrophil attracting chemokines was altered in IRF5$^{-/-}$ mice, we analyzed levels of known neutrophil chemoattractants, such as CXCL1, CXCL2, CXCL10, chemokine (C-C motif) ligand (CCL) 3, CCL4, CCL5, in the supernatants of synovial leukocytes isolated from mBSA-treated knees, by Luminex analysis. We found that the levels of CXCL1 were significantly affected by the loss of IRF5 (Fig. 3*C*).

Next, we examined whether the reduction in neutrophil influx in IRF5$^{-/-}$ mice was confined to inflammation in the joint. We considered a model of acute lung injury, which is characterized by a high influx of neutrophils into the challenged lung (25). IRF5$^{-/-}$ and WT mice were administered LPS intranasally at 1 mg/kg body weight and culled 24 h later (Fig. S4*C*). IRF5$^{-/-}$ mice showed significantly less cellular infiltrate in bronchoalveolar lavage fluid (BAL) and more specifically displayed a significant reduction in the number of neutrophils recruited into the lung 24 h post challenge (Fig. 3*D*). The number of other infiltrating myeloid cells such as monocytes and macrophages were not affected in the lung, but the levels of secreted CXCL1 were also significantly reduced once again (Fig. 3*E*).

In summary, the recruitment of neutrophils to the sites of inflammation is severely affected in the absence of IRF5, due to the deficient production of neutrophil chemoattractants.

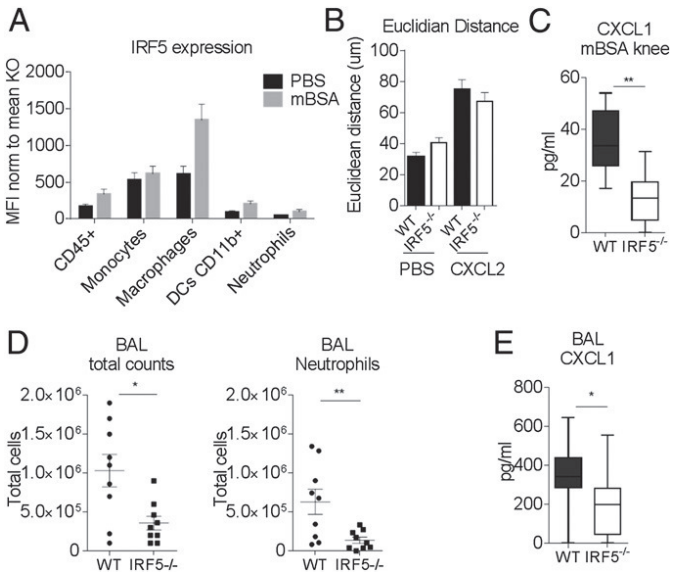

Fig. 3. Neutrophil recruitment in IRF5$^{-/-}$ mice is limited due to the decrease in CXCL1 secretion. (*A*) IRF5 expression within cell populations of the inflamed knee defined by MFI. Data shown are the mean and SEM derived from 10–20 mice from three to four independent AIA experiments. (*B*) The tracks of air pouch neutrophilic infiltrate in an EZ-Taxiscan migrating toward CXCL2 (Fig. S4*B*) were analyzed to show the Euclidean distance each cell traveled in a 45-min time period. Data shown are the average and SEM of three independent experiments each including 9–20 movies per treatment. (*C*) Levels of CXCL1 in the supernatants of the synovial leukocytes isolated from the mBSA-treated knees. Data are shown as mean with 95% confidence interval from 6 mice from a representative AIA experiment. (*D*) Number of infiltrating cells and neutrophils in bronchoalveolar lavage fluid (BAL) of the IRF5$^{-/-}$ and WT mice challenged with LPS intranasally. Each dot represents an individual mouse. (*E*) Levels of CXCL1 in BAL of LPS-challenged animals. Data are shown as mean with 95% confidence interval from 9–10 mice from two independent experiments. Statistical analysis was performed by one-tailed Mann–Whitney *u* test. *$P < 0.05$; **$P < 0.01$.

IRF5 Orchestrates Expression of Chemokines in Bone-Marrow–Derived Macrophages. To investigate whether IRF5 is recruited to the chemokine gene control regions and whether the expression of chemokine genes in general is affected by the lack of IRF5, we used GM-CSF mouse bone marrow cultures, which represented a mix of macrophages and dendritic cells (GM-BM-DC/MPHs) (Fig. S4*D*) (26), both expressing similar levels of IRF5 (Fig. S4*E*). IRF5 ChIP-Seq datasets were generated in WT and IRF5$^{-/-}$ GM-BM-DC/MPHs and were stimulated with LPS for up to 4 h, as previously described (27). After filtering out false positive IRF5 binding peaks detected in IRF5$^{-/-}$ GM-BM-DC/MPHs, 2,538 bona fide binding peaks were mapped to gene promoter regions (up to 10 kb upstream and 0.5 kb of the transcription start site). The defined genes with IRF5 binding sites in their promoters were then subjected to gene ontology analysis, which produced the following categories of molecular functions: cytokine activity, cytokine receptor binding, chemokine activity, chemokine receptor binding (Hyper false discovery rate q-value <10–10^{10}). Chemokines whose promoters were targeted by IRF5 in GM-BM-DC/MPHs stimulated by LPS for 2 h included CXCL1, CXCL2, CXCL10, CXCL16, CCL3, CCL4, CCL5, CCL6, CCL9, CCL11, CCL12, CCL17, and CCL22 (Fig. 4*A* and Fig. S5*A*).

We next examined mRNA expression of eight selected chemokines from the list in IRF5$^{-/-}$ and WT GM-BM-DC/MPHs stimulated with LPS for 1 and 4 h using quantitative RT-PCR. Expression of five of them, such as CXCL1, CXCL2, CXCL10, CCL3, and CCL4, was significantly reduced in IRF5$^{-/-}$ macrophages (Fig. 4*B* and Fig. S5*B*). In addition, expression of two other chemokines known to be important for neutrophil trafficking, CXCL3 and CXCL5, was also significantly reduced (Fig. S5*B*). Moreover, we have previously shown that the expression of both IL-1α and IL-1β, which are potent chemoattractants for myeloid cells (28), is also under IRF5 control in GM-BM-DC/MPHs (27).

Hence, the combined global profiling of IRF5-bound sites and gene expression analysis in macrophages/DCs deficient in IRF5 have highlighted the direct role for IRF5 in transcriptional regulation of key chemokine genes and specifically, those involved in neutrophil trafficking.

Discussion

Neutrophil recruitment to the sites of infection has long been considered to be a key event in microbial clearance through their release of toxic molecules, including reactive oxygen species and also of cytokines and chemokines, which subsequently orchestrate the course of inflammation. Consequently, their removal from the site of inflammation is vital for maintaining host health. Here, we demonstrate that deficiency in transcription factor IRF5, which has been previously shown to modulate macrophage phenotype, also significantly reduces neutrophil trafficking to the sites of inflammation in various tissues. We unravel a systemic role for IRF5 in regulating chemokine gene expression in macrophages, including the expression of major neutrophil chemoattractants. Moreover, we discover that IRF5 is critical for the establishment of the MHCII^{+} phenotype in both steady-state macrophages of the knee joint and in monocyte-derived macrophages during antigen-induced arthritis.

Heterogeneity of tissue macrophages has been extensively analyzed in the last few years, with possible coexisting mechanisms of macrophage development from recruited blood monocytes and local self-renewal of tissue-resident macrophages, such as Kupffer cells, lung, peritoneal, and splenic macrophages, being described (11). However, the origin of synovial macrophages remained elusive until recently. Recent work by Misharin et al. using a series of elegant chimera experiments demonstrated that the synovial lining in the naïve mouse ankle joint contains a heterogeneous population of macrophages, with the majority being true tissue-resident cells (MHCII^{-}) but about a fifth originating from the bone marrow (MHCII^{+}) (14). Of interest, expression of CX3CR1 was mainly confined to MHCII^{-} synovial macrophages, further suggesting that these cells originate prenatally. We have extended the characterization of synovial macrophages by demonstrating that in both ankle and knee joints, the population of MHCII^{+} macrophages is severely compromised in IRF5-deficient animals (Fig. 2). We also noted some differences between macrophage populations in the two joints analyzed. First, there appears to be a higher representation

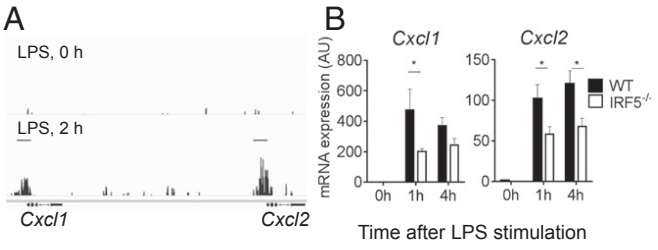

Fig. 4. IRF5 controls chemokine network. (*A*) Representative UCSC (University of California, Santa Cruz) genome browser tracks in the *Cxcl1*/*Cxcl2* loci for IRF5 binding peaks in unstimulated (LPS, 0 h) or LPS-stimulated (LPS, 2 h) GM-BM-DC/MPHs. (*B*) mRNA expression of selected chemokines in IRF5$^{-/-}$ and WT GM-BM-DC/MPHs stimulated with LPS for 0, 1, and 4 h using quantitative RT-PCR. Data shown are the mean and SEM derived from three mice from a representative experiment. Statistical analysis was performed by two-way ANOVA with Bonferroni's correction for multiple comparisons. *$P < 0.05$; **$P < 0.01$.

of MHCII^{+} macrophages in the knee than in the ankle. Second, MHCII^{-} macrophages in the ankle express higher levels of IRF5 than those in the knee. Further detailed analysis, such as fate mapping, will be necessary to ultimately determine the origin of synovial macrophage populations in the knee.

In the K/BxN model of sterile inflammatory arthritis, circulating nonclassical (Ly6C^{-}) blood monocytes are recruited to the joint and differentiate into classically activated inflammatory macrophages, driving joint pathology (14). In contrast, we find that in the AIA model, the majority of the infiltrating monocytes were Ly6C^{int} or Ly6C^{hi}. Moreover, their recruitment was almost completely abolished in the mBSA-challenged joints of CCR2$^{-/-}$ mice that are deficient in circulating Ly6C^{+} monocytes (Fig. 2*C*). Thus, despite somewhat similar joint pathologies and large neutrophil influxes manifested at early stages, the two models clearly differ in the types of circulating monocytes recruited to the joint and hence in their pathogenesis. As demonstrated by a clear shift in Ly6C expression between the naïve and PBS control knees (Fig. 2*D*), the immunization with CFA composed of inactivated and dried mycobacteria is likely to predispose to preferential recruitment of classical monocytes to the site of inflammation. Of significance, in patients with RA, it is the intermediate CD14^{++}CD16^{+} (corresponding to Ly6C^{int} in mouse) blood monocytes that appear to be significantly increased in patients with RA, whereas nonclassical CD14^{+}CD16^{++} (Ly6C^{-} in mouse) remained the same (29).

Mice lacking IRF5 demonstrate a shift toward type-2 immune response in a diet-induced model of obesity (30) and a pristane-induced model of lupus (31). In addition, in the pristine-induced lupus model, IRF5$^{-/-}$ monocytes show reduced migration and reduced expression of CCR2 and CXCR4 into the peritoneal cavity (32). However, this difference is not observed in the bone marrow, and monocytes egress normally into circulation. Moreover, the influx of Ly6C^{hi} monocytes into the peritoneal cavity upon thioglycollate stimulation remains unaffected. Thus, the observed effect on monocyte migration and receptor expression appears to be specific to pristane injection rather than a general property of monocytes lacking IRF5. Our own data show that the influx of monocytes remains unaffected, both in the knee and in the lung (Fig. S1*C*).

Blocking neutrophil influx into the joints, either with Ly6G antibodies or by interfering with neutrophil migration e.g., by using a CXCR1/CXCR2 allosteric inhibitor, has been demonstrated to significantly reduce arthritis development in different mouse models of the disease, including AIA (33). Moreover, blockade of CXCL1, a CXCR2 ligand, with antibodies, led to a reduced number of neutrophils in the joint cavity of AIA mice (34), mimicking the effect of the IRF5 deletion observed in this study.

Macrophages, neutrophils, and epithelial cells can all secrete CXCL1 and promote neutrophil entry. However, in the inflamed arthritic knee, macrophages express the highest levels of IRF5, exceeding the IRF5 level detected in neutrophils by more than 10-fold [compare mean fluorescence intensity (MFI) of 1,344 ± 214 and 95 ± 33, $P < 0.0001$]. IRF5 expression was not detected in CD45 negative cells (used as a proxy for epithelial cells) of the knee. Moreover, no difference in the secretion of CXCL1 was observed between WT and IRF5$^{-/-}$ bone-marrow–derived neutrophils in response to a range of toll-like receptor agonists (13). We observe a significantly lower mRNA expression of CXCL1 by BM–derived DC/macrophages stimulated with LPS (Fig. 4). Taken together these data suggest that it is macrophage-specific production of CXCL1 and possibly other chemokines not detected by our assay or not tested that is likely to be affected most by the lack of IRF5. Our preliminary data using myeloid deleters, *LysM-cre* mice crossed with *Irf5*$^{flox/flox}$ mice, indicate that reduction of IRF5 expression in macrophages is responsible for the observed decrease in CXCL1 secretion. In future studies, we plan to further test this hypothesis by generating more specific ablations of IRF5 in macrophages and neutrophils.

Neutrophils display marked abnormalities in phenotype and function in autoimmune diseases, including RA, systemic vasculitis, and systemic lupus erythematosus (35), complementing macrophage alterations. In these conditions, neutrophils may play a central role in the initiation and perpetuation of aberrant immune responses and organ damage. Here we show that inhibition of IRF5 activity leads to reduction in neutrophil influx at the sites of acute inflammation. Thus, in addition to the previously suggested and recently confirmed role of IRF5 in balancing the arms of Th1/Th17 and Th2 adoptive immune responses (15, 30, 36), IRF5 also plays a direct role in controlling the innate immune responses leading to host tissue damage. These results augment the evidence suggesting that IRF5 blockade might be an effective therapeutic target. How to block IRF5 may not be easy, as transcription factors are often considered "nondruggable," but perhaps other steps, such as the regulation of IRF5 activation by modifying enzymes might be more tractable. Such therapeutics would likely be useful in a very wide spectrum of diseases.

Materials and Methods

Mice. IRF5$^{-/-}$ mice were bred on a C57BL/6 background and their generation has been described previously (37). As a recent study identified a spontaneous mutation in some colonies of IRF5$^{-/-}$ mice, experimental animals were genotyped for a mutation in Dock2 (38); all mice used in this study were determined to be free of this homozygous mutation. CCR2$^{-/-}$ mice (B6.129S4-Ccr2tm1Ifc/J, JAX stock number 004999) were also bred on a C57BL/6 background. The experimental animal procedures used in this work were approved by the Kennedy Institute of Rheumatology Ethics Committee and the United Kingdom Home Office.

Antigen-Induced Arthritis. We induced arthritis as described previously (17, 18). At 9 or 14 d, the mice were killed and the knee joints were excised and subjected to clinical and histological analyses. Spleen, blood, and inguinal lymph nodes were harvested occasionally in addition to knee joints. Single cells of knee, mediastinal lymph nodes, blood, or spleen were subjected to flow cytometry analysis. For further details, see *SI Materials and Methods*.

Acute Lung Injury. Following short anesthesia with isofluorane, mice were administered LPS at a dose of 1 mg/kg body weight intranasally. Mice were killed 24 h after the challenge, bronchoalveolar lavage was performed, and lavage fluid was collected. Afterward, the whole lung was harvested and both were used for further analyses.

Air Pouch. Mice were anesthetized with isofluorane and 3 mL of air was injected s.c. to create a dorsal air pouch with a top-up of air 3 d later. At 6 d after the creation of the air pouch, mice were challenged with 100 μg zymosan (Sigma) injected directly into the pouch. Animals were killed 4 h later and infiltrating cells were harvested from the air pouch.

In Vitro Bone-Marrow–Derived DC/Macrophages. Bone marrow progenitors were differentiated into DC/macrophage cultures in vitro in the presence of recombinant murine GM-CSF (20 ng/mL; Preprotech). For further details, see *SI Materials and Methods*.

Cytokine Detection. Secreted cytokines in the cell supernatants and BAL were quantified using the Luminex bead-based assay (R&D Systems) following manufacturer's instructions. Measurements were performed using a Luminex 100 analyzer (Luminex).

Neutrophil Migration. For real-time analysis of migrating neutrophils, a 12-channel TAXIScan (23) was used with a 5-μm chip according to the manufacturer's protocol (Effector Cell Institute). Sequential image data were generated from individual jpegs processed with ImageJ (National Institutes of Health), equipped with the manual tracking and chemotaxis tool plugins (Ibidi). Euclidean distances refer to the total Euclidean distance traveled by individual cells in a particular experiment.

Cell Proliferation Assay. Inguinal lymph nodes were harvested from immunized mice and cell suspensions were plated at 200,000–300,000 cells per well. Cells were stimulated with either α-CD3 (clone 145–2C11), mBSA antigen (50 μg/mL), or media alone (naïve) for 48 h at 37 °C. To determine proliferation, replicating DNA was stained using an EdU kit according to the manufacturer's protocol (Life Technologies). Briefly, EdU was added 2 h

before the end of stimulation. Extracellular staining and flow cytometry were performed as described in *SI Materials and Methods*.

RNA Extraction and Quantitative Real-Time RT-PCR. Total RNA was extracted from joints of mice or in vitro differentiated macrophages with an RNeasy Mini kit according to the manufacturer's instructions (Qiagen) and cDNA was synthesized from total RNA with a High Capacity cDNA Reverse Transcription kit (Life Technologies). Gene expression was measured by the change-in-threshold (ΔΔCT) method based on real-time PCR in an ABI 7900HT or ViiA7 with TaqMan primer sets (Life Technologies).

Statistical Analyses. Statistical analysis was carried out with GraphPad v6.0 (GraphPad Software) using two-way ANOVA with Bonferroni's correction (multiple comparisons) or Mann–Whitney tests (comparisons between two groups).

ACKNOWLEDGMENTS. We thank Fiona McCann and Kay McNamee for help with animal models. This work was supported by the Kennedy Institute Trustees Research Fund (M.W. and K.B.), American Asthma Foundation Early Excellence Award AAF 11-0105 (to I.A.U. and A.J.B.) and MRC Project Grant MR/J001899/1 (to I.A.U. and D.G.S.).

1. Helmick CG, et al.; National Arthritis Data Workgroup (2008) Estimates of the prevalence of arthritis and other rheumatic conditions in the United States. Part I. *Arthritis Rheum* 58(1):15–25.
2. Tak PP, Bresnihan B (2000) The pathogenesis and prevention of joint damage in rheumatoid arthritis: Advances from synovial biopsy and tissue analysis. *Arthritis Rheum* 43(12):2619–2633.
3. Smeets TJ, et al. (2001) Analysis of the cell infiltrate and expression of matrix metalloproteinases and granzyme B in paired synovial biopsy specimens from the cartilage-pannus junction in patients with RA. *Ann Rheum Dis* 60(6):561–565.
4. Mulherin D, Fitzgerald O, Bresnihan B (1996) Synovial tissue macrophage populations and articular damage in rheumatoid arthritis. *Arthritis Rheum* 39(1):115–124.
5. Barrera P, et al. (2000) Synovial macrophage depletion with clodronate-containing liposomes in rheumatoid arthritis. *Arthritis Rheum* 43(9):1951–1959.
6. Wright HL, Moots RJ, Edwards SW (2014) The multifactorial role of neutrophils in rheumatoid arthritis. *Nat Rev Rheumatol* 10(10):593–601.
7. Mohr W, Westerhellweg H, Wessinghage D (1981) Polymorphonuclear granulocytes in rheumatic tissue destruction. III. an electron microscopic study of PMNs at the pannus-cartilage junction in rheumatoid arthritis. *Ann Rheum Dis* 40(4):396–399.
8. Wittkowski H, et al. (2007) Effects of intra-articular corticosteroids and anti-TNF therapy on neutrophil activation in rheumatoid arthritis. *Ann Rheum Dis* 66(8): 1020–1025.
9. Khandpur R, et al. (2013) NETs are a source of citrullinated autoantigens and stimulate inflammatory responses in rheumatoid arthritis. *Sci Transl Med* 5(178):178ra40.
10. Murray PJ, et al. (2014) Macrophage activation and polarization: Nomenclature and experimental guidelines. *Immunity* 41(1):14–20.
11. Sieweke MH, Allen JE (2013) Beyond stem cells: Self-renewal of differentiated macrophages. *Science* 342(6161):1242974.
12. Becher B, et al. (2014) High-dimensional analysis of the murine myeloid cell system. *Nat Immunol* 15(12):1181–1189.
13. Ericson JA, et al.; ImmGen Consortium (2014) Gene expression during the generation and activation of mouse neutrophils: Implication of novel functional and regulatory pathways. *PLoS One* 9(10):e108553.
14. Misharin AV, et al. (2014) Nonclassical Ly6C(-) monocytes drive the development of inflammatory arthritis in mice. *Cell Reports* 9(2):591–604.
15. Krausgruber T, et al. (2011) IRF5 promotes inflammatory macrophage polarization and TH1-TH17 responses. *Nat Immunol* 12(3):231–238.
16. Weiss M, Blazek K, Byrne AJ, Perocheau DP, Udalova IA (2013) IRF5 is a specific marker of inflammatory macrophages in vivo. *Mediators Inflamm* 2013:245804.
17. Asquith DL, Miller AM, McInnes IB, Liew FY (2009) Animal models of rheumatoid arthritis. *Eur J Immunol* 39(8):2040–2044.
18. Egan PJ, van Nieuwenhuijze A, Campbell IK, Wicks IP (2008) Promotion of the local differentiation of murine Th17 cells by synovial macrophages during acute inflammatory arthritis. *Arthritis Rheum* 58(12):3720–3729.
19. Parsey MV, Tuder RM, Abraham E (1998) Neutrophils are major contributors to intraparenchymal lung IL-1 beta expression after hemorrhage and endotoxemia. *J Immunol* 160(2):1007–1013.
20. Dorner T, Lipsky PE (2014) B cells: Depletion or functional modulation in rheumatic diseases. *Curr Opin Rheumatol* 26(2):228–236.
21. Savitsky DA, Yanai H, Tamura T, Taniguchi T, Honda K (2010) Contribution of IRF5 in B cells to the development of murine SLE-like disease through its transcriptional control of the IgG2a locus. *Proc Natl Acad Sci USA* 107(22):10154–10159.
22. Boring L, et al. (1997) Impaired monocyte migration and reduced type 1 (Th1) cytokine responses in C-C chemokine receptor 2 knockout mice. *J Clin Invest* 100(10): 2552–2561.
23. Nitta N, Tsuchiya T, Yamauchi A, Tamatani T, Kanegasaki S (2007) Quantitative analysis of eosinophil chemotaxis tracked using a novel optical device: TAXIScan. *J Immunol Methods* 320(1-2):155–163.
24. Colville-Nash P, Lawrence T (2003) Air-pouch models of inflammation and modifications for the study of granuloma-mediated cartilage degradation. *Methods Mol Biol* 225:181–189.
25. Matute-Bello G, Frevert CW, Martin TR (2008) Animal models of acute lung injury. *Am J Physiol Lung Cell Mol Physiol* 295(3):L379–L399.
26. Helft J, et al. (2015) GM-CSF mouse bone marrow cultures comprise a heterogeneous population of CD11c(+)MHCII(+) macrophages and dendritic cells. *Immunity* 42(6): 1197–1211.
27. Saliba DG, et al. (2014) IRF5:RelA interaction targets inflammatory genes in macrophages. *Cell Reports* 8(5):1308–1317.
28. Rider P, et al. (2011) IL-1α and IL-1β recruit different myeloid cells and promote different stages of sterile inflammation. *J Immunol* 187(9):4835–4843.
29. Rossol M, Kraus S, Pierer M, Baerwald C, Wagner U (2012) The CD14(bright) CD16+ monocyte subset is expanded in rheumatoid arthritis and promotes expansion of the Th17 cell population. *Arthritis Rheum* 64(3):671–677.
30. Dalmas E, et al. (2015) Irf5 deficiency in macrophages promotes beneficial adipose tissue expansion and insulin sensitivity during obesity. *Nat Med* 21(6):610–618.
31. Xu Y, et al. (2012) Pleiotropic IFN-dependent and -independent effects of IRF5 on the pathogenesis of experimental lupus. *J Immunol* 188(8):4113–4121.
32. Yang L, Feng D, Bi X, Stone RC, Barnes BJ (2012) Monocytes from Irf5-/- mice have an intrinsic defect in their response to pristane-induced lupus. *J Immunol* 189(7): 3741–3750.
33. Coelho FM, et al. (2008) The chemokine receptors CXCR1/CXCR2 modulate antigen-induced arthritis by regulating adhesion of neutrophils to the synovial microvasculature. *Arthritis Rheum* 58(8):2329–2337.
34. Grespan R, et al. (2008) CXCR2-specific chemokines mediate leukotriene B4-dependent recruitment of neutrophils to inflamed joints in mice with antigen-induced arthritis. *Arthritis Rheum* 58(7):2030–2040.
35. Kaplan MJ (2013) Role of neutrophils in systemic autoimmune diseases. *Arthritis Res Ther* 15(5):219.
36. Feng D, et al. (2012) Irf5-deficient mice are protected from pristane-induced lupus via increased Th2 cytokines and altered IgG class switching. *Eur J Immunol* 42(6): 1477–1487.
37. Takaoka A, et al. (2005) Integral role of IRF-5 in the gene induction programme activated by Toll-like receptors. *Nature* 434(7030):243–249.
38. Purtha WE, Swiecki M, Colonna M, Diamond MS, Bhattacharya D (2012) Spontaneous mutation of the Dock2 gene in Irf5$^{-/-}$ mice complicates interpretation of type I interferon production and antibody responses. *Proc Natl Acad Sci USA* 109(15): E898–E904.

Supporting Information

Weiss et al. 10.1073/pnas.1506254112

SI Materials and Methods

Antigen-Induced Arthritis. We induced arthritis as described previously (18, 19). Briefly, at day 0, mice were sedated using inhaled isofluorane anesthesia and subsequently immunized with 100 μg of mBSA (Sigma) emulsified in 100 μL of complete Freund's adjuvant (BD Difco), administered s.c. at the base of the tail. At day 7, we induced arthritis by means of an intraarticular injection of mBSA (200 μg in 10 μL of sterile PBS), or PBS alone using a sterile 33-gauge microcannula, in sedated animals. At 9 or 14 d, the mice were killed and the knee joints were excised. Spleen, blood, and inguinal lymph nodes were harvested occasionally in addition to knee joints.

Clinical and Histological Methods. Arthritic knees were fixed in 10% (vol/vol) buffered formalin. Knees were decalcified in 10% (vol/vol) EDTA and dehydrated before embedding in paraffin wax. Coronal sections were stained with hematoxylin and eosin. Joints were scored in a blinded manner for degree of joint space infiltrate, bone erosion, and synovial thickening. The inflammation score was based on joint space infiltrate. For immunohistochemical analysis, paraffin-embedded sections were stained with APC-conjugated Ly6G (clone 1A8; Biolegend) or isotype control and positive cells were viewed under fluorescence microscopy. Total cells/nuclei in the same section were stained with 4′-6-diamidino-2-phenylindole (DAPI, ProLong Gold; Life Technologies). IgG1 and IgG2a paired antibodies (R&D Systems) were used to measure serum antibody levels by ELISA.

Flow Cytometry. Single cell suspensions of knees, mediastinal lymph nodes, blood, or spleen were suspended in FACS buffer (0.5% BSA, 0.02 N sodium azide in PBS, pH 7.4). To distinguish between live and dead cells, we used a viability dye (Life Technologies), followed by staining with antibodies against CD45 (clone 30-F11), CD11b (clone M1/70), F4/80 (clone BM8), Ly6C (clone AL-21), Ly6G/GR-1 (clone RB6-8C5), GR-1 (clone 1A8-Ly6g), CD64 (clone X54-5/7.1), CD11c (clone N418), MHCII (clone M5/114.15.2), CD206 (clone C068C2), CD19 (eBio1 D3), CD4 (clone RM4-5), and γδ TCR (clone eBioGL3). For intracellular FACS staining, cell suspensions were stimulated with a mixture of PMA (Merck), ionomycin (Merck), and Brefeldin A (Sigma) for T-cell cytokines and with LPS (Alexis Biochemicals), Brefeldin A, and Monensin (BD) for myeloid-derived cytokines. Following extracellular staining as above, cells were fixed and permeabilized using the Foxp3 staining set (eBioscience) followed by staining with pro-IL1β (clone NJTEN3), IL17a (clone eBio17B7), and IFNγ (clone XMG1.2) antibodies. FACS analysis was performed using a FACS Canto II or Fortessa X-20 (BD), and the data were analyzed with FlowJo software, version 7.6 (Treestar).

In Vitro Bone-Marrow–Derived DC/Macrophages. To generate in vitro differentiated DC/macrophages, bone marrow progenitors from wild-type and knockout mice were cultured in RPMI-1640 medium with L-glutamine (PAA Laboratories) supplemented with 10% (vol/vol) FCS, 1% penicillin/streptomycin, 0.01% 2-mercaptoethanol, and with recombinant murine GM-CSF (20 ng/mL; Preprotech). On day 3 of culture, fresh medium with 20 ng/mL GM-CSF was added to the plates. On day 6, half of the medium was removed from each plate and spun down. Cell pellets were then resuspended in fresh medium containing GM-CSF and added back to the culture plate. After 8 d, adherent and nonadherent cells were harvested, washed with PBS, replated, and then stimulated with LPS (100 ng/mL; Alexis Biochemicals).

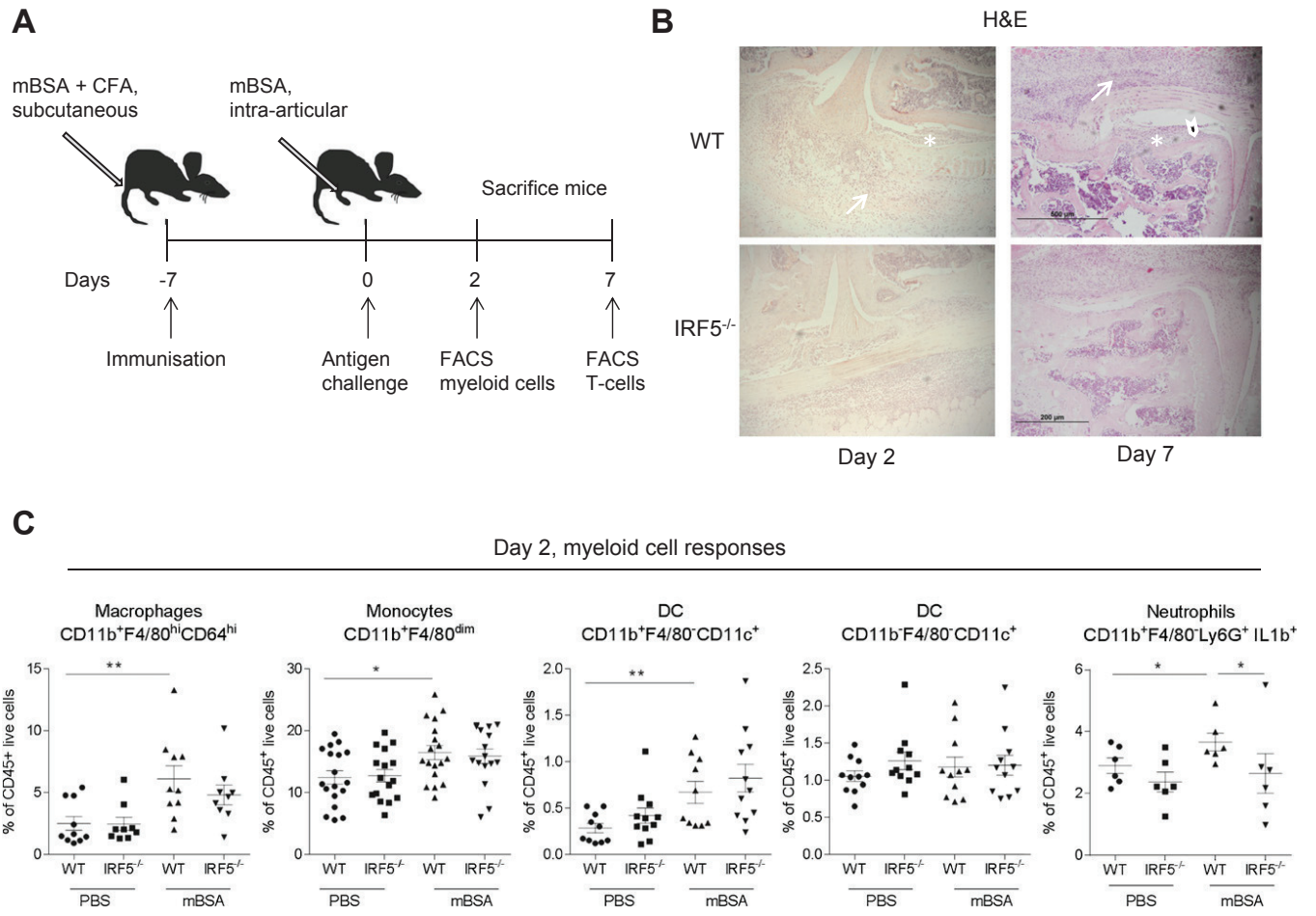

Fig. S1. AIA model in IRF5$^{-/-}$ mice, innate immune responses. (*A*) Schematic diagram showing treatment and harvest time points in the antigen-induced arthritis model. (*B*) Representative images of the knee showing areas of bone erosion (arrowhead), synovial thickening (asterisk), and leukocyte infiltration into joint space (arrows). (*C*) Total number of macrophages, monocytes, DCs, and pro-IL-1β^{+} neutrophils recovered from excised knee joints of IRF5$^{-/-}$ and WT animals at day 2 of AIA, expressed as a percentage of live CD45^{+} cells. Data shown are the mean and SEM derived from 10–20 mice from three to four independent AIA experiments. Each dot represents an individual mouse. Statistical analysis was performed by one-tailed Mann–Whitney *u* test. **P* < 0.05; ***P* < 0.01.

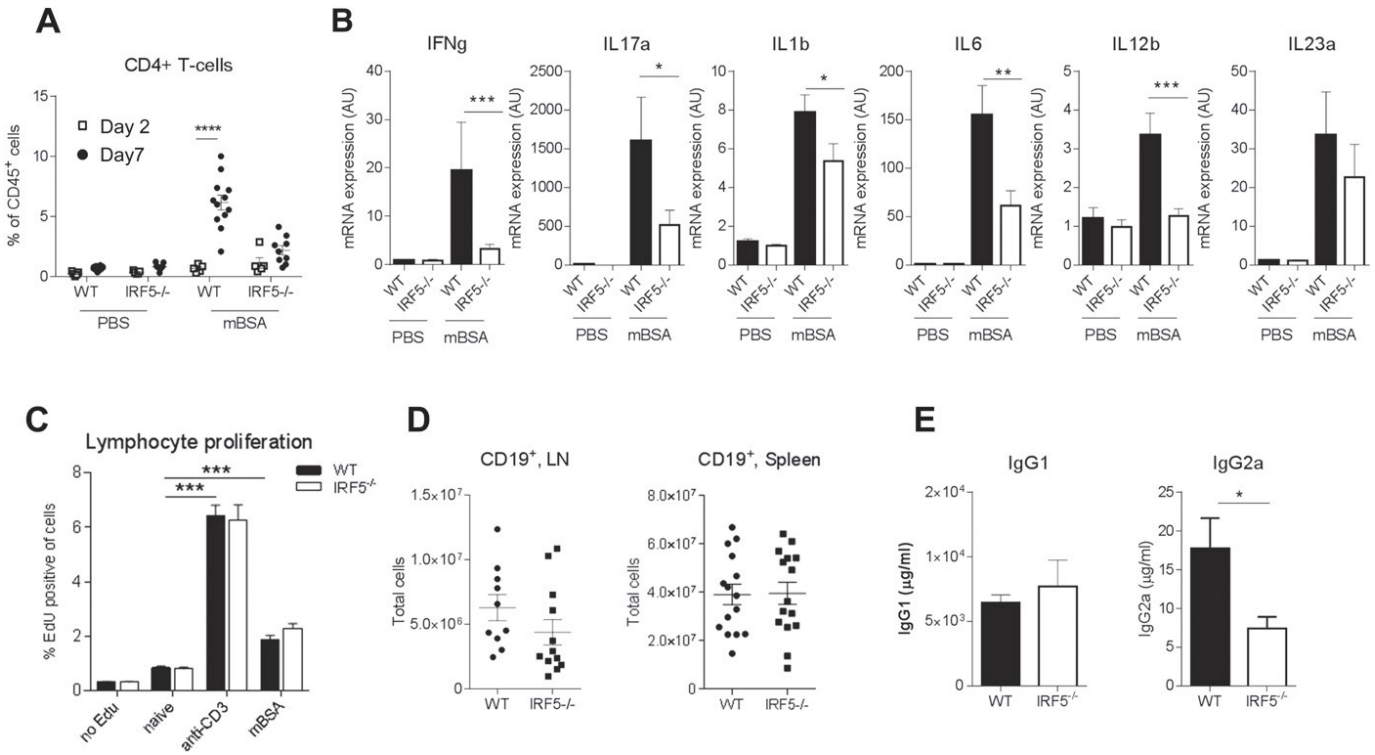

Fig. S2. AIA model in IRF5$^{-/-}$ mice, adaptive immune responses. (*A*) IRF5 WT and KO were immunized with mBSA and challenged with mBSA or PBS control 7 d later. Knees were excised on day 2 or 7 of disease and analyzed using flow cytometry. Cell suspensions obtained from knees were stained for CD45^{+} live and CD4 expression to identify CD4^{+} T cells. Statistical analysis performed by two-way ANOVA and Bonferroni's multiple comparison. (*B*) IL17, IFN-γ, IL-1β, IL-6, IL-12p40, and IL-23p19 mRNA in whole joint extracts from arthritic mice at day 2 of AIA. Data shown are the mean and SEM derived from 10–20 mice from three to four independent AIA experiments. (*C*) Proliferation of lymphocytes after 48-h stimulation with αCD3 or mBSA. The data are mean and SEM derived from six independent lymphocyte cultures from lymph nodes (LNs) of IRF5$^{-/-}$ and WT arthritic mice. Statistical analysis was performed by one-tailed paired *t* test. (*D*) Total number of B cells in the lymph nodes and spleen. The data are mean and SEM derived from 10 to 15 independent cell preparations from LNs and spleens of the IRF5$^{-/-}$ and WT immunized mice. Each dot represents an individual mouse. (*E*) Levels of total IgG1 and IgG2a in the serum. The data are mean and SEM using 3–5 mice treated from a representative AIA experiment. Statistical analysis was performed by two-tailed unpaired *t* test. *$P < 0.05$; **$P < 0.01$; ***$P < 0.001$; ****$P \leq 0.0001$.

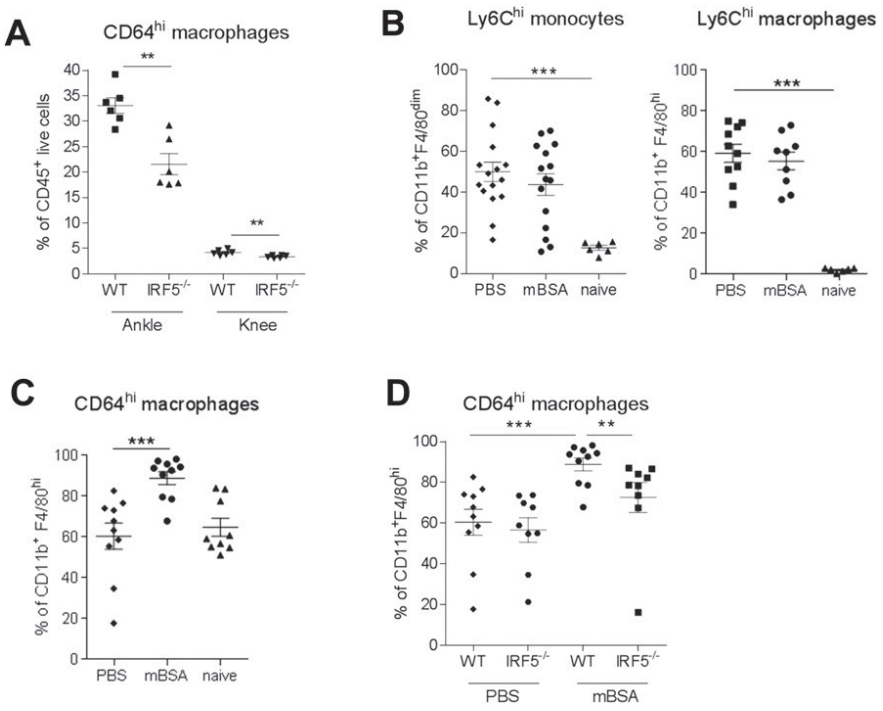

Fig. S3. Characterization of synovial macrophages. (*A*) Number of tissue resident CD64^{hi} macrophages in both the ankles and knees of naïve IRF5$^{-/-}$ mice and WT controls. Data shown are mean and SEM derived from 4 to 7 mice from a representative experiment. (*B*) Number of Ly6C^{hi} monocytes and macrophages, expressed as a percentage of CD11b^{+}F4/80^{dim} and CD11b^{+}F4/80^{hi} cells, respectively. (*C*) Number of CD64^{hi} macrophages, expressed as a percentage of CD11b^{+} F4/80^{dim} and CD11b^{+}F4/80^{hi} cells, respectively. (*D*) Number of CD64^{hi} macrophages in the mBSA-challenged knees or PBS controls of IRF5$^{-/-}$ and WT animals, expressed as a percentage of CD11b^{+}F4/80^{hi} cells. Data shown are mean and SEM derived from 10 to 11 mice from two to three independent AIA experiments. Each dot represents an individual mouse. Statistical analysis was performed by one-tailed Mann–Whitney *u* test. **P* < 0.05; ***P* < 0.01; ****P* < 0.001.

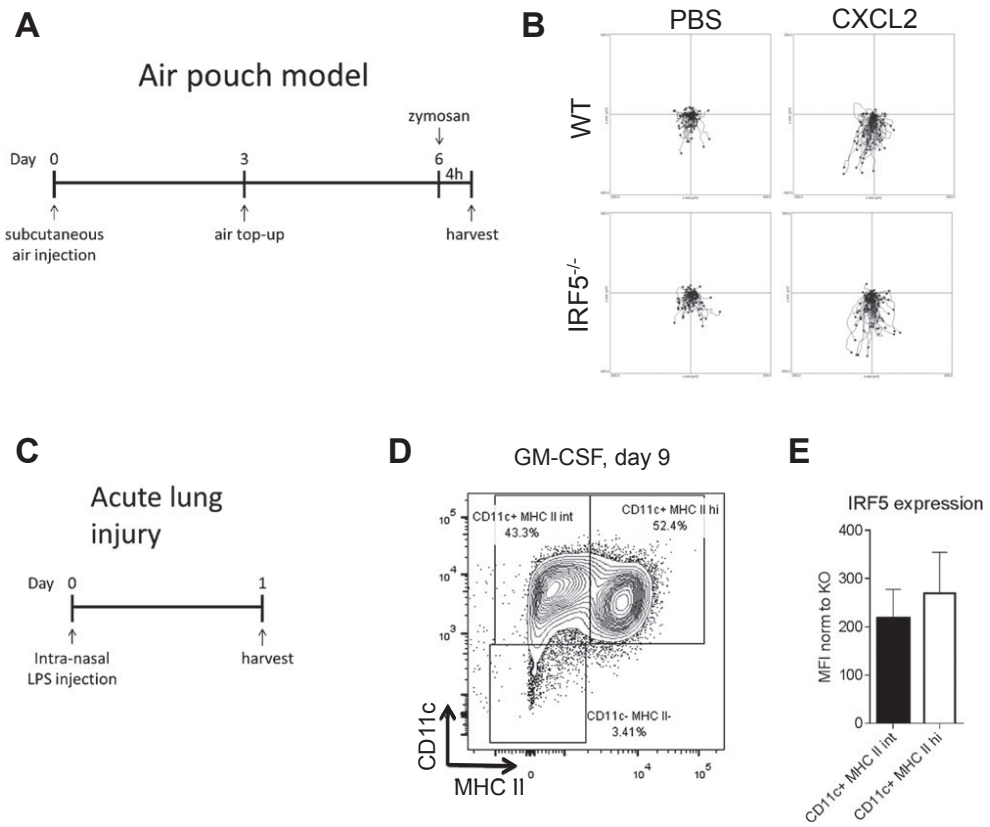

Fig. S4. Models of air pouch and acute lung injury and GM-CSF bone marrow cultures. (*A*) Schematic time line of the air pouch model showing s.c. air injections and challenge with zymosan. (*B*) Center-zeroed tracks of air pouch neutrophilic infiltrate in an EZ-Taxiscan migrating toward CXCL2. (Scale in μm.) (*C*) Schematic diagram showing treatment and harvest time points in the acute lung inflammation model. (*D*) Bone marrow progenitors were differentiated with GM-CSF for 9 d before samples were taken for flow cytometry. Cells were stained for the surface markers CD11b, CD11c, and MHCII. The depicted population was first gated by size and for CD11b expression. The plot is representative of $n = 3$. (*E*) Intracellular IRF5 staining in GM-CSF bone marrow cultures was quantified using MFI normalized to IRF5 KO. Error bars represent the SE for $n = 3$.

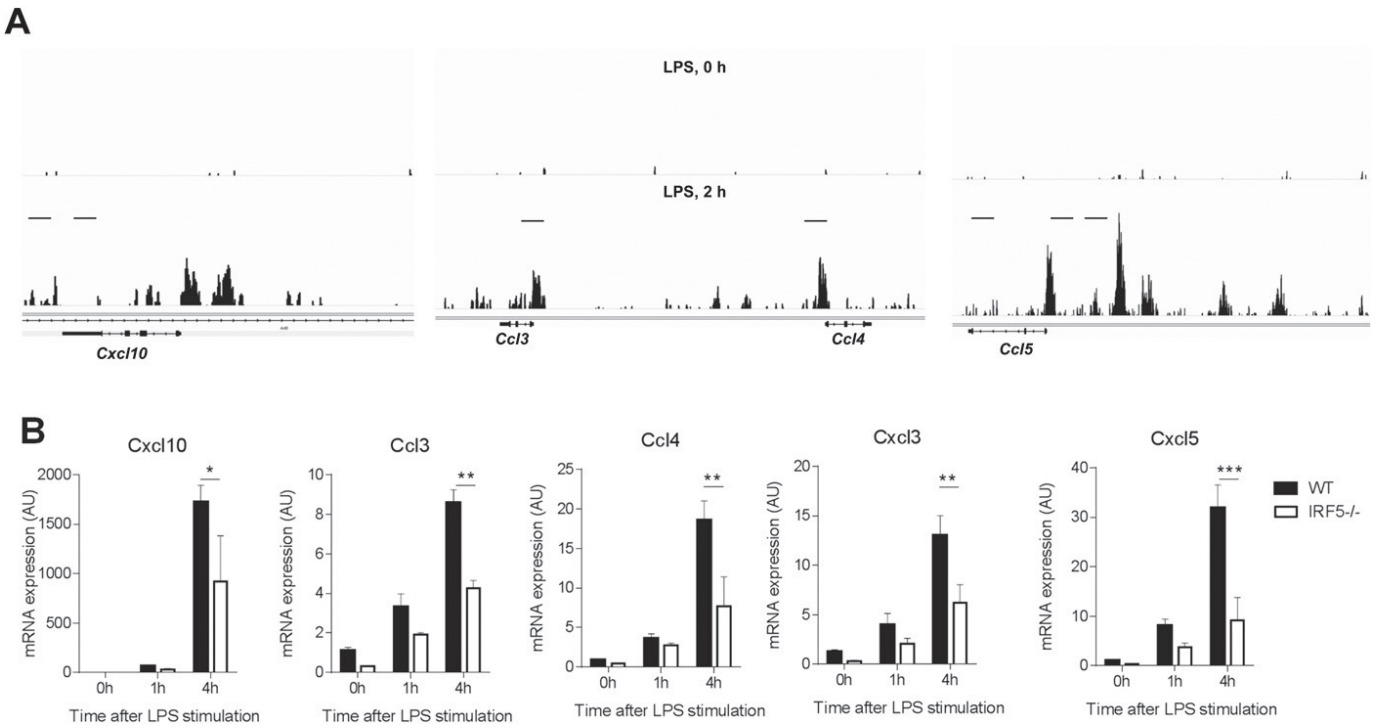

Fig. S5. IRF5 controls chemokine network. (*A*) Representative UCSC (University of California, Santa Cruz) genome browser tracks in the *Cxcl10*, *Ccl3*, *Ccl4*, and *Ccl5* loci for IRF5 binding peaks in unstimulated (LPS, 0 h) or LPS-stimulated (LPS, 2 h) GM-bone-marrow–derived macrophages/DCs (GM-BM-DC/MPHs). (*B*) CXCL10, CCL3, CCL4, CXCL3, and CXCL5 mRNA expression in the IRF5$^{-/-}$ and WT GM-BM-DC/MPHs stimulated with LPS for 0, 1, and 4 h using quantitative RT-PCR. Data shown are the mean and SEM derived from three mice from a representative experiment. Statistical analysis was performed by two-way ANOVA with Bonferroni's correction for multiple comparisons. *$P < 0.05$; **$P < 0.01$. Data shown are mean and SEM derived from five to six mice from a representative AIA experiment. Each dot represents an individual mouse. Statistical analysis was performed by one-tailed Mann–Whitney *u* test. **$P < 0.01$; ***$P < 0.001$.

Other Supporting Information Files

SI Appendix (PDF)

Hindawi Publishing Corporation
Mediators of Inflammation
Volume 2013, Article ID 245804, 9 pages
http://dx.doi.org/10.1155/2013/245804

Research Article

IRF5 Is a Specific Marker of Inflammatory Macrophages *In Vivo*

Miriam Weiss,[1] Katrina Blazek,[1] Adam J. Byrne,[1,2] Dany P. Perocheau,[1] and Irina A. Udalova[1]

[1] *Kennedy Institute of Rheumatology, University of Oxford, Roosevelt Drive, Headington, Oxford OX3 7FY, UK*
[2] *Leukocyte Biology Section, National Heart and Lung Institute, Sir Alexander Fleming Building, Faculty of Medicine, Imperial College, South Kensington, London SW7 2AZ, UK*

Correspondence should be addressed to Miriam Weiss; miriam.weiss@stx.ox.ac.uk
and Irina A. Udalova; irina.udalova@kennedy.ox.ac.uk

Received 31 August 2013; Revised 29 November 2013; Accepted 30 November 2013

Academic Editor: Salahuddin Ahmed

Copyright © 2013 Miriam Weiss et al. This is an open access article distributed under the Creative Commons Attribution License, which permits unrestricted use, distribution, and reproduction in any medium, provided the original work is properly cited.

Macrophages are an integral part of the innate immune system and key players in pathogen clearance and tissue remodelling. Both functions are accomplished by a pivotal network of different macrophage subtypes, including proinflammatory M1 and anti-inflammatory M2 macrophages. Previously, our laboratory identified the transcription factor interferon regulatory factor 5 (IRF5) as the master regulator of the M1 macrophage polarisation. IRF5 was found to be highly expressed in human M1 compared to M2 macrophages. Furthermore, IRF5 dictates the expression of proinflammatory genes such as *IL12b* and *IL23a* whilst repressing anti-inflammatory genes like *IL10*. Here we show that murine bone marrow derived macrophages differentiated *in vitro* with GM-CSF are also characterised by high levels of IRF5 mRNA and protein and express proinflammatory cytokines upon LPS stimulation. These macrophages display characteristic expression of M1-marker MHC II but lack the M2-marker CD206. Significantly, we develop intracellular staining of IRF5- expressing macrophages and utilise it to recapitulate the *in vitro* results in an *in vivo* model of antigen-induced arthritis, emphasising their physiological relevance. Thus, we establish the species-invariant role of IRF5 in controlling the inflammatory macrophage phenotype both *in vitro* and in *in vivo*.

1. Introduction

Macrophages are immune cells involved in recognition of pathogenic stimuli and the initiation and resolution of inflammation. They can adapt to various different environmental signals giving rise to several subtypes with distinct functions [1]. These subtypes can be classified as M1 (classically activated) and M2 (alternatively activated) macrophages. In addition, there are several phenotypes associated with M2 macrophages, for example, M2-like or tumour associated macrophages [2]. M1 macrophages secrete high levels of IL-12 and IL-23 but low levels of IL-10, whereas M2 macrophages secrete low levels of IL-12 and IL-23 but high levels of IL-10 [3].

Several reports have described the *in vitro* differentiation of lineage-defined macrophages. In general, these methods utilise M-CSF (macrophage colony stimulating factor; CSF-1) to differentiate bone marrow derived progenitors, followed by priming with various stimuli. Addition of interferon-γ followed by lipopolysaccharide (LPS) stimulation has been used to acquire M1 macrophages whereas addition of IL-4 or IL-13 without LPS yields M2 macrophages [3]. Another established method uses GM-CSF (granulocyte/macrophage colony stimulating factor) in order to generate M1 macrophages or alternatively M-CSF treatment for M2 differentiation, usually followed by LPS challenge for both subtypes [4, 5]. In the physiological situation, M-CSF is detected in low steady state levels whereas GM-CSF has been shown to be increased upon stimulation with inflammatory stimuli, such as IL-1, TNF, or LPS [6, 7].

Macrophages are also known to play a key role in autoimmune diseases such as rheumatoid arthritis (RA), a degenerative disease characterised by joint inflammation and bone destruction [8]. At the site of inflammation, macrophages are present in high numbers and it has been found that depletion ameliorates disease severity [9–11]. More

specifically, M1 macrophages contribute to RA pathogenesis by secreting proinflammatory cytokines and thereby taking part in the Th1/Th17 response [12, 13].

Distinct macrophage subtypes are not only characterised by their differences in cytokine release but also display differential expression of key transcription factors. Recently, we identified the transcription factor interferon regulatory factor 5 (IRF5) as the major regulator of proinflammatory M1 macrophage polarisation [14]. IRF5 directly induces the expression of proinflammatory cytokines such as IL-6, IL-12b, and IL-23a whilst repressing transcription of anti-inflammatory cytokines such as IL-10 [14, 15]. IRF5 is involved in various inflammatory processes such as the type I interferon response to virus infection and pathogen recognition receptor signalling [16]. Upon viral infection, IRF5 is phosphorylated and thereby translocated to the nucleus where it binds to the regulatory regions of its target genes [17]. Nonviral stimulation of toll-like receptors (TLR) including TLR4, 7, and 9 also leads to activation of IRF5 [16]. Moreover, polymorphisms in the *IRF5* gene have been found to associate with RA [18, 19].

Despite the major role IRF5 plays in macrophage activation, it has rarely been used to track inflammatory macrophages in disease. In this study, we aim to characterise murine macrophages and IRF5 expression in both *in vitro* and *in vivo* models of inflammation. We therefore used the murine model of antigen-induced arthritis (AIA) in which mice are immunised with methylated BSA (mBSA) prior to intra-articular injection of mBSA in one knee, leading to localised inflammation and a Th17 response [20, 21]. First, we analysed *in vitro* differentiated macrophages regarding their IRF5 expression, LPS response, and surface receptor expression. We then used flow cytometry to label intracellular IRF5 in both the *in vitro* macrophages and those derived from the affected knee of the AIA mouse model.

2. Material and Methods

2.1. Animals and Antigen-Induced Arthritis. For this study wild type mice were bred on a C57Bl/6 background. The experimental animal procedures used in this work were approved by the Kennedy Institute of Rheumatology Ethics Committee and the UK Home Office.

We induced arthritis as described previously; briefly, at day zero, mice were sedated using inhaled isoflurane anaesthesia and subsequently immunised with 100 μg of mBSA emulsified in 0.2 mL of complete Freund's adjuvant, administered intra-dermally at the base of the tail. At day seven, we induced arthritis by means of an intraarticular injection of mBSA (200 μg in 10 μL of sterile PBS), or PBS alone using a sterile 33-gauge microcannula, in sedated animals. At day nine, the mice were sacrificed and the knee joints were excised.

2.2. In Vitro Differentiation of Macrophages. For the generation of *in vitro* differentiated macrophages, bone marrow from wild type mice was cultured in RPMI-1640 medium with L-glutamine (PAA Laboratories) supplemented with 10% FCS, 1% penicillin/streptomycin, 0.01% 2-mercaptoethanol, and with either recombinant murine GM-CSF (20 ng/mL; Peprotech) or recombinant human M-CSF (100 ng/mL; Peprotech). After eight days, adherent cells were washed with PBS and replated, then stimulated with LPS (100 ng/mL; Alexis Biochemicals).

2.3. RNA Extraction and Quantitative Real-Time PCR. Total RNA was extracted using RNeasy Mini Kit (Qiagen) as per the manufacturer's instructions. Contaminating genomic DNA was removed from RNA samples using the RNase-Free DNase Set (Qiagen). Total RNA was reverse-transcribed into cDNA using the High Capacity cDNA Reverse Transcription Kit (Life Technologies) as per the manufacturer's instructions. Real-time PCR reactions were performed on an ABI 7900HT (Life Technologies) with TaqMan primer sets for murine *Fizz1*, *iNOS*, *Il10*, *Il12b*, *Il23a*, *Irf5*, and *Hprt* (Life Technologies) and gene expression was analysed using the change-in-threshold $\Delta\Delta$Ct-method.

2.4. Western Blot. For protein isolation, cells were harvested with Versene (EDTA) 0.02% (Lonza). Pellets were resuspended with macrophage lysis buffer (20 mM Tris pH 8, 300 mM NaCl, 1% NP40, and 10% glycerol) containing freshly added protease inhibitors (Roche). Samples were incubated on ice for 30 min before cellular debris was removed by centrifugation for 15 min, at 13,000 rpm/4°C. Lysates were transferred into new tubes and stored at −80°C. To determine the protein concentration of whole cell lysates a BCA test (Thermo Scientific) was performed according to the manufacturer's instructions.

5–7 μg of total protein were resolved by Novex Tris-glycine gel (Life Technologies), transferred onto a PVDF membrane (GE Healthcare) by wet western blotting, and subjected to incubation with rabbit anti-IRF5 (Abcam) or mouse anti β-actin (Sigma), followed by detection with horseradish-peroxidase- (HRP-) conjugated secondary antibodies and chemiluminescent substrate solution ECL (GE Healthcare).

2.5. Enzyme Linked Immunosorbent Assay (ELISA). Supernatants of stimulated cells were transferred into tubes, centrifuged for 5 min at 3,300 rpm, and stored at −20°C until needed. Cytokine secretion was quantified for murine IL-10 (eBioscience), IL-12p70 (eBioscience), and IL-23 (eBioscience) according to the manufacturer's instructions. Absorbance was read at 450 nm by a spectrophotometric ELISA plate reader (Labsystems Multiscan Biochromic) and analysed using Ascent Labsystems software. All samples were analysed in triplicate in a volume of 50 μL.

2.6. Flow Cytometry. Single cell suspensions of *in vitro* differentiated macrophages and knees were washed with FACS buffer (1% BSA, 0.01% sodium azide in PBS, and pH 7.4) and stained with the following antibodies: APC conjugated anti-CD206 antibody (BioLegend), APC-Cy7 conjugated anti-CD11b antibody (BD Biosciences), PE conjugated anti-MCH II [I-A/I-E] antibody (BD Biosciences), PerCP

conjugated anti-CD45 antibody (BD Biosciences), and PE-Cy7 conjugated anti-F4/80 (eBioscience). For intracellular FACS staining, cells were fixed with fixation/permeabilisation solution (eBioscience) and washed with permeabilisation buffer (eBioscience). Samples were then stained with rabbit anti-IRF5 antibody (Abcam) followed by secondary staining with goat anti-rabbit Alexa Fluor 488 (Life Technologies). FACS analysis was performed using a FACS Canto II (BD Biosciences), and the data were analysed with Flow Jo software, version 7.6 (Treestar).

2.7. Statistical Analyses. Statistical analysis was performed using GraphPad v5.0 (GraphPad Software) using two-way ANOVA (with Bonferroni's multiple comparisons) or unpaired one-tailed Mann-Whitney *U* tests (comparisons between two groups). *P* values less than 0.05 were considered significant.

3. Results and Discussion

3.1. High Levels of IRF5 Expression in Murine GM-CSF Differentiated Bone Marrow Derived Macrophages. In order to assess the expression of IRF5 *in vitro*, bone marrow derived macrophages were differentiated with either GM-CSF or M-CSF (GM-BMDM and M-BMDM, resp.). After nine days of differentiation, macrophages were challenged with LPS for 0 h, 1 h, 4 h, 8 h, and 24 h and analysed for mRNA and protein levels of IRF5.

In unstimulated murine cells, IRF5 levels were considerably higher in GM-CSF differentiated compared to M-CSF differentiated macrophages (Figure 1(a)). Interestingly, this expression pattern is also exhibited by their unstimulated human macrophage counterparts, with significantly higher IRF5 expression in GM-CSF *in vitro* differentiated human macrophages compared to those differentiated with M-CSF [14].

Upon LPS stimulation, IRF5 mRNA and protein expression were induced in M-CSF differentiated murine cells and further induced in GM-CSF differentiated murine cells. *Irf5* mRNA levels increased between 4 and 8 h but protein levels were already higher after 1 h of poststimulation (Figure 1(a)) we therefore hypothesised that the LPS-induced production of IRF5 was most likely due to a combination of two factors: (1) increased mRNA levels and (2) protein stabilisation, possibly related to activation by phosphorylation or ubiquitination [22, 23]. IRF5 has been shown to be essential for the proinflammatory phenotype of human monocyte derived GM-CSF macrophages upon LPS stimulation. However, mRNA and protein levels in human M-CSF derived macrophages are not further induced upon LPS stimulation, suggesting some species-specific or cell source-specific differences in LPS-regulated IRF5 production.

3.2. Distinct Cytokine Expression Profiles of M-CSF and GM-CSF Derived BMDMs. Next, to determine the inflammatory properties of *in vitro* differentiated murine macrophages, expression and secretion of the cytokines IL-10, IL-12, and IL-23 were analysed.

As expected, each macrophage subtype was found to display differential behaviour to LPS stimulation regarding their cytokine expression (Figures 1(b) and 1(c)). Transcription and secretion of the anti-inflammatory cytokine IL-10 were elevated in M-CSF differentiated macrophages compared to GM-CSF treated cells. LPS stimulation of M-BMDMs resulted in increased IL-10 expression on both transcript and protein level. At 24 h, *Il10* mRNA returned to an almost basal level, whereas protein secretion remained high. IL-10 protein secretion was significantly higher following 8 h LPS stimulation in M-BMDMs whereas GM-BMDMs only showed basal IL-10 expression.

Proinflammatory cytokines IL-12 and IL-23 were found to be expressed at much higher levels in GM-CSF derived macrophages whereas M-BMDMs show only minimal expression of proinflammatory cytokines, although with similar kinetics of expression as in GM-BMDMs (Figure S1A in Supplementary Material available online at http://dx.doi.org/10.1155/2013/245804). The differences in cytokine expression were statistically significant on both the transcript and protein levels. *Il12b* mRNA was induced upon LPS stimulation in GM-BMDMs, with the highest levels observed 8 h after stimulation. Secretion of IL12p70 was increased from 4 h of stimulation onwards. Although M-BMDMs expressed low levels of *Il23a* mRNA following 1 h of stimulation, they did not secrete heterodimeric IL-23 protein at any time point. In GM-BMDMs *Il23a* mRNA expression peaked following 1 h of LPS stimulation, while IL-23 protein secretion extended to 24 h after LPS stimulation.

We also noted that IRF5 levels increased in M-BMDMs upon LPS stimulation but did not result in significant induction of proinflammatory cytokines. Thus, we hypothesised that this could be due to a lower functional activity of IRF5 in M-BMDMs, as IRF5 protein is subject to posttranslational modifications such as phosphorylation and ubiquitination [22–24]. However, the status of posttranslational modifications for IRF5 in LPS stimulated macrophages is yet to be determined. Furthermore, the availability of activating cofactors potentially required for IRF5 mediated induction of proinflammatory cytokines might be different in M-BMDMs compared to GM-BMDMs.

Thus, consistent with its proposed role as a master regulator of the M1 macrophage phenotype and in accordance with data for human *in vitro* differentiated macrophages [14], GM-CSF differentiated BMDMs express high levels of IRF5 and produce IL-12 as well as IL-23 following stimulation with LPS, whereas M-CSF differentiated BMDMs express lower levels of IRF5 and produce IL-10. These data confirm the study of Fleetwood et al. [4] that suggested that GM-CSF and M-CSF induce a distinct M1 or M2 BMDM phenotype, respectively.

3.3. Specific Intracellular IRF5 Staining of M-CSF and GM-CSF Derived BMDMs. In order to establish intracellular IRF5 staining, expression was measured by fluorescence activated cell sorting (FACS) of unstimulated and LPS stimulated GM- and M-BMDMs at day nine of differentiation. Known cell surface receptor markers of M1 and M2 macrophages,

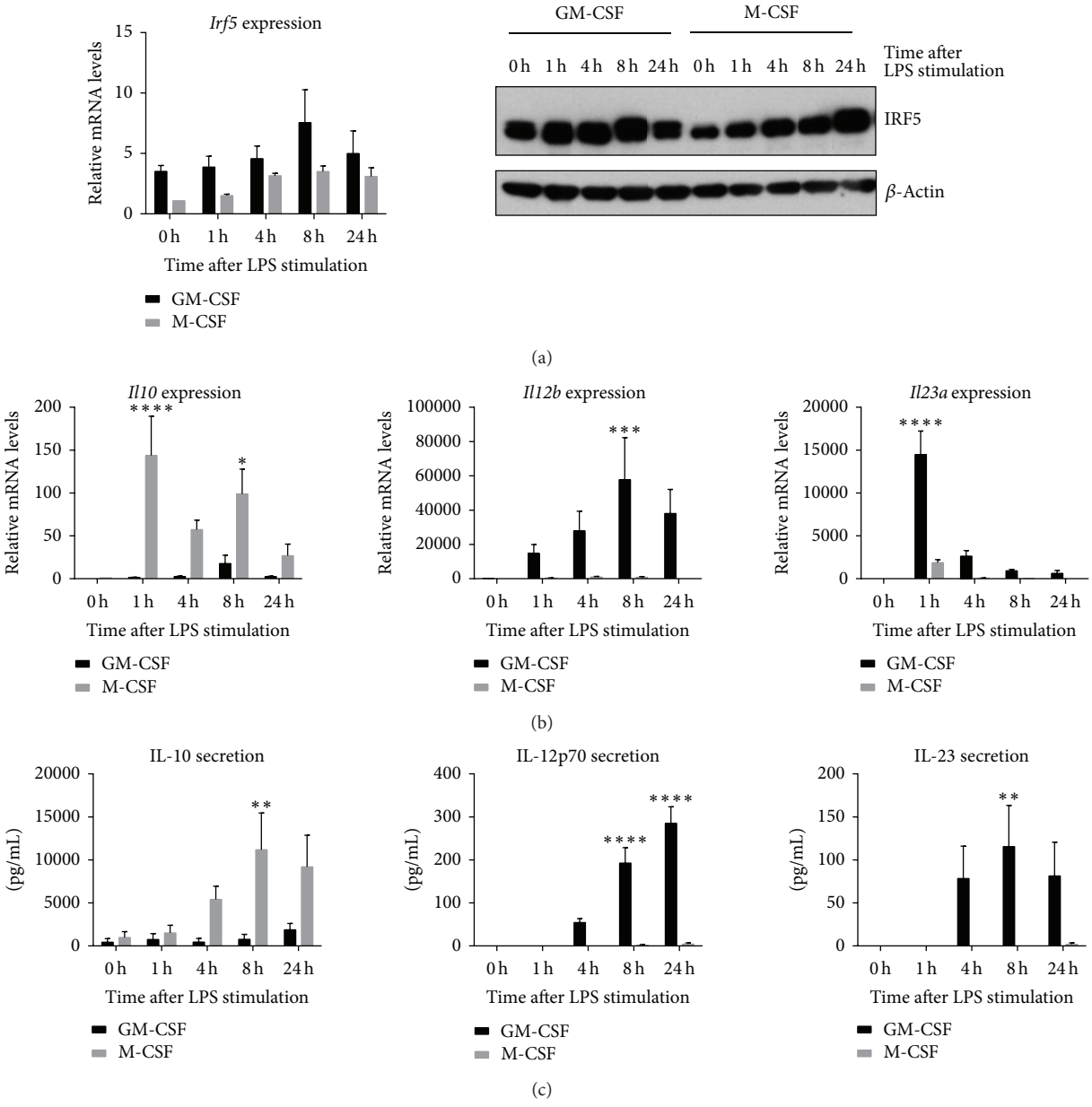

Figure 1: IRF5 levels and cytokine response of *in vitro* differentiated macrophages. BMDMs were differentiated with GM-CSF (20 ng/mL) or M-CSF (100 ng/mL) for eight days. All cells were challenged with LPS for the indicated time periods. (a) Transcript levels were measured with real-time PCR. Error bars represent the standard error for $n = 6$. Protein levels of IRF5 and β-actin were determined by western blot. Experiment is representative for three independent experiments. (b) and (c) At each time point RNA (top panel) and supernatants (bottom panel) were collected. Error bars represent the standard error for $n = 5$. Statistical analysis was performed by 2-way ANOVA and Bonferroni's multiple comparison. $^{*}P \leq 0.05$; $^{**}P \leq 0.01$; $^{***}P \leq 0.001$; $^{****}P \leq 0.0001$.

MHCII, and CD206 (mannose receptor), respectively, as well as the pan macrophage marker F4/80 were used as controls for specificity of IRF5 staining.

Around 70% of the M-CSF derived macrophages were F4/80^{high} and CD206^{high} (Figure 2(a)). GM-CSF differentiated macrophages on the other hand were generally F4/80^{low} and only 1-2% of them expressed CD206. Although F4/80 is reported to be highly expressed on all tissue macrophages, GM-CSF derived cells only showed a low percentage of F4/80+ cells. This could be because GM-CSF can also induce differentiation into DCs, effectively leading to generation of DC-like macrophages [25]. Conversely, 80% of unstimulated GM-CSF derived BMDMs expressed MHC II, whereas in CD206 positive M2 macrophages only 10% of cells exhibit expression of this marker (Figure 2(b)). A similar distribution was observed for IRF5, where over 70% of unstimulated GM-BMDMs were IRF5+ compared to only 5% of unstimulated M-BMDMs. In summary, most unstimulated M-BMDMs display the M2 marker CD206 and F4/80 whereas GM-BMDMs lack the latter but express M1 markers MHC II and

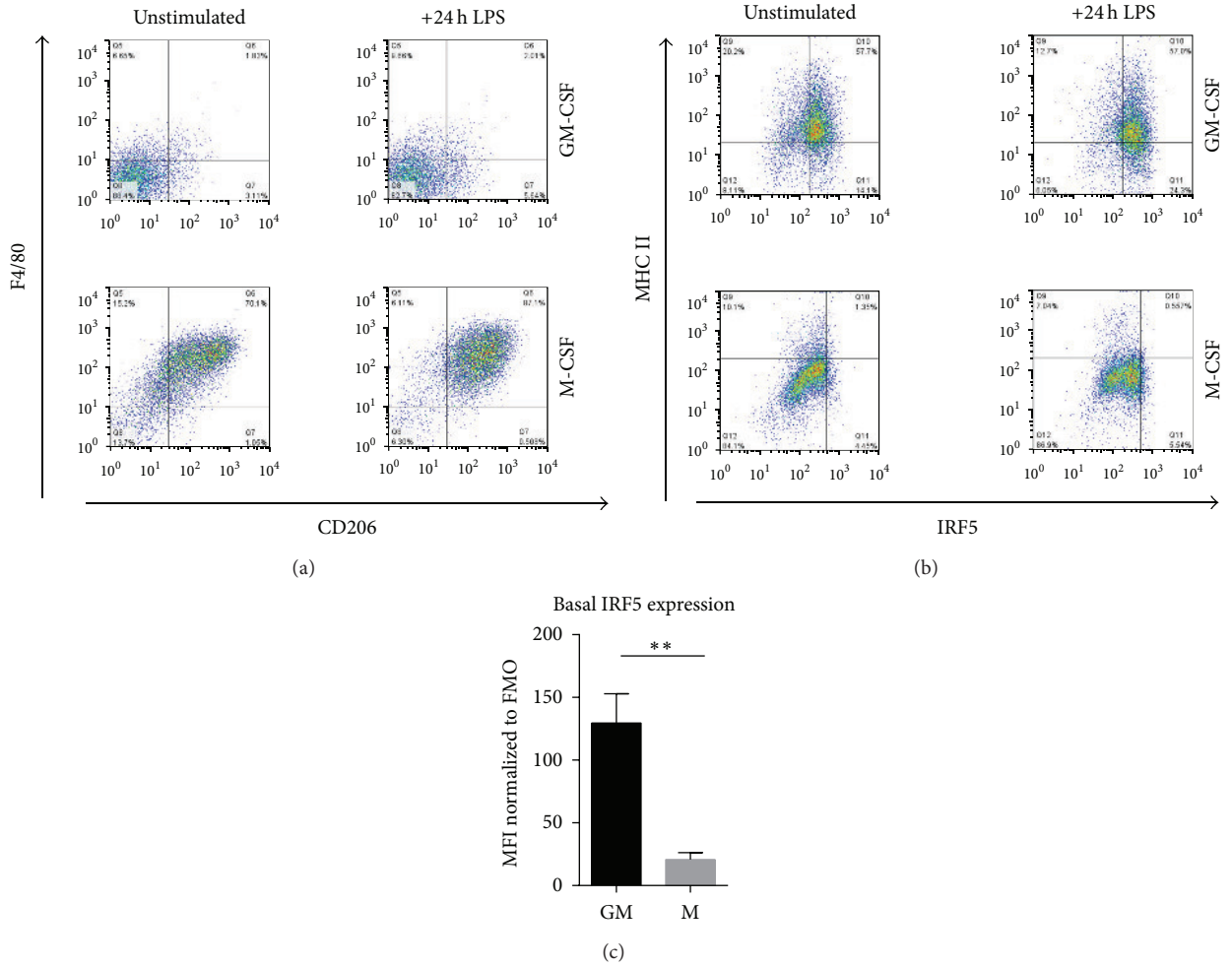

FIGURE 2: Surface receptor expression of polarised macrophages and intracellular IRF5 staining. Macrophages were *in vitro* differentiated with GM-CSF or M-CSF for eight days and then stimulated with LPS for 24 h. FACS samples were collected before and after stimulation. (a) and (b) Samples were stained for the expression of F4/80, CD206, MHC II, and IRF5. (c) Macrophages were stained for intracellular IRF5 and staining in unstimulated cells was quantified by mean fluorescence intensity (MFI). Error bars represent the standard error for $n = 6$. Statistical analysis was performed by one-tailed Mann-Whitney U test. $^{**}P \leq 0.01$.

IRF5. Basal IRF5 levels in unstimulated cells were quantified using mean fluorescence intensity (MFI) (Figure 2(c)). The MFI for IRF5 in GM-CSF derived macrophages was found to be sixfold higher than in M-CSF differentiated macrophages. The quantified differences in the IRF5 levels were further confirmed by the analysis of IRF5 mRNA and protein levels in these samples (Figure S1B).

LPS stimulation only minimally increased expression of F4/80 and CD206 in GM-BMDMs, whilst in M-BMDMs the percentage of $F4/80^{high}$ $CD206^{high}$ cells increased to almost 90%. MHC II expression decreased after 24 h of LPS stimulation in both cell types, consistent with the previous reports indicating that LPS does not induce expression of MHC II in macrophages [26–28]. Of significance, the population of $IRF5^{+}$ cells increased to over 80% in LPS-stimulated GM-BMDMs but remained unchanged in M-BMDMs contrary to the observed increase in IRF5 protein levels detected by Western Blot analysis (Figure 1(a)). Although the same antibody is used for both techniques, in a Western Blot, proteins are denatured, whereas in FACS proteins are in a native configuration. It is possible that in M-BMDMs native IRF5 protein is in a conformation that does not allow its recognition by this antibody unless denatured. The structure of proteins can be affected by posttranslational modifications such as phosphorylation or ubiquitination which also dictate protein activity. As highlighted above, the manner in which IRF5 is modified in stimulated macrophages is the subject of ongoing research.

Thus, we have developed intracellular IRF5 staining and demonstrated that M1 macrophages have a higher percentage of IRF5+ cells than M2 macrophages. It is worth noting though that FACS staining for IRF5 in macrophages is challenging due to relatively high background from secondary antibodies and macrophage autofluorescence. A reporter IRF5 mouse strain, similar to the described RelA-GFP knock-in [29], would further facilitate analysis of IRF5 expression

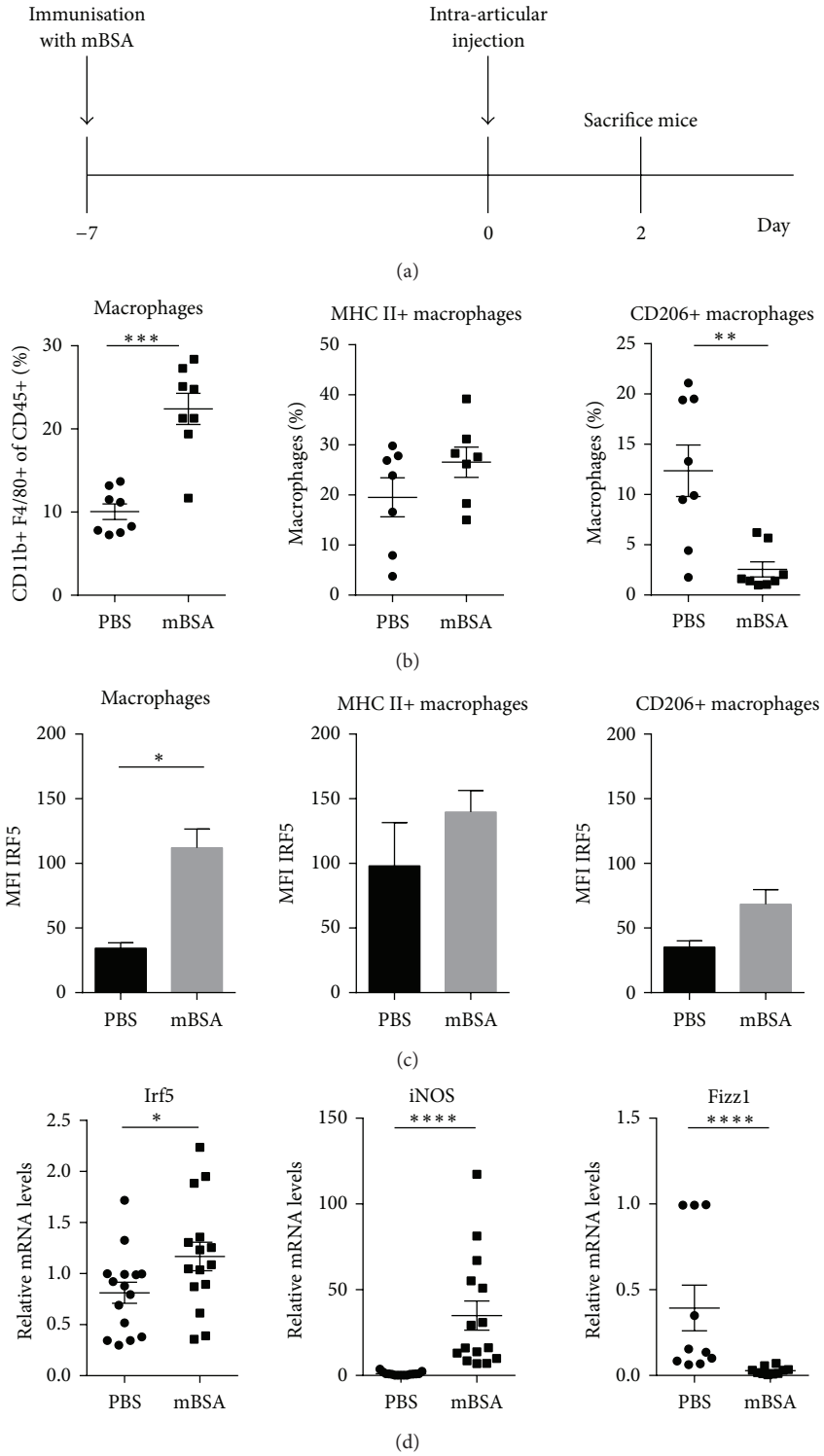

Figure 3: Macrophage populations and IRF5 expression at the site of inflammation in a mouse model of arthritis. Mice were immunised with mBSA in complete Freud's adjuvant prior to intra-articular injection of mBSA or PBS. Knees were collected at day two of disease. (a) Schematic of the experimental set-up for antigen-induced arthritis. (b) Samples from three independent experiments were stained for flow cytometry with antibodies against CD45, CD11b, F4/80, CD206, and MHC II. (c) IRF5 FACS staining was quantified calculating the mean fluorescence intensity in knees of three wild type mice. (d) Total RNA was isolated from knees of three independent experiments and analysed by real-time PCR for expression of Irf5, iNOS, and Fizz1. Statistical analysis was performed throughout by one-tailed Mann-Whitney U test. $^{*}P \leq 0.05$; $^{**}P \leq 0.01$; $^{***}P \leq 0.001$; $^{****}P \leq 0.0001$.

in macrophage populations and possibly other cell types in *in vivo* models. In addition, it would be helpful in the analysis of the intracellular localisation of IRF5 in response to stimulation.

3.4. IRF5 Expressing Macrophages at the Site of Inflammation in an Experimental Model of Arthritis. Finally, we utilised a murine model of antigen-induced arthritis to explore the possibility of using IRF5 as a marker of inflammatory macrophages in a disease setting. Mice were immunised with mBSA and after seven days arthritis was induced by intra-articular injection of mBSA (affected knee) or PBS (control knee) (Figure 3(a)). Affected knees and control knees were harvested two days after injection and subjected to FACS analysis. In addition, RNA was isolated from knees to study mRNA levels of *Irf5* and macrophage markers at the site of inflammation. The chosen markers were *iNOS* and *Fizz1* for M1 and M2 macrophages, respectively [30, 31].

Macrophages were defined as CD45+, CD11b+, and F4/80+ cells. Within this population, we identified proinflammatory (MHC II+ CD206−) and anti-inflammatory (MHC II-CD206+) macrophage subsets. The percentage of total macrophage populations, as well as the proinflammatory macrophage subset, was significantly increased in inflamed knees compared to control knees (Figure 3(b)). In contrast, the percentage of CD206+ macrophages was found to be significantly reduced after antigen challenge. These results also demonstrate that there are a large number of macrophages which do not fit either category. This probably reflects the extent of macrophage plasticity and the wide spectrum of *in vivo* macrophage subtypes [32]. This especially holds true in a disease setting where incoming macrophages might be at different stages of polarisation and where the inflammatory environment can be constantly changing.

Quantification of IRF5 FACS staining in macrophages demonstrated that increased IRF5 expression can be detected in affected knees (Figure 3(c)). When IRF5 levels were assessed in each macrophage population individually, it was observed that proinflammatory macrophages express relatively high levels of IRF5. CD206+ macrophages express less IRF5 but also show a minor increase in inflamed knees, suggesting that the remaining CD206+ macrophages at the site of inflammation express more IRF5 than they did prior to challenge. The *in vivo* data confirm the findings in *in vitro* differentiated macrophages that proinflammatory macrophages do express higher levels of IRF5 than CD206+ macrophages.

Analysis of whole knee RNA extracts supported these observations and demonstrated that *Irf5* transcript levels are significantly augmented in affected knees (Figure 3(d)). Expression of the M1 marker *iNOS* was significantly higher in mBSA injected knees whereas *Fizz1* expression is diminished. Taken together, these results indicate that there is an increasing amount of proinflammatory macrophages at the site of inflammation which correlates with an increase in IRF5 mRNA and protein. We therefore conclude that IRF5 is an appropriate marker for detection of inflammatory macrophages in this arthritis disease model. However, it has to be kept in mind that although IRF5 levels within macrophage populations increase, this may not necessarily translate into elevated protein activity since the phosphorylation status and cellular localisation are not taken into account. It has been shown that IRF5 undergoes posttranslational modifications and is regulated by phosphorylation and ubiquitination [22–24]. However, the role of IRF5 activation in the context of disease has not been studied extensively and further research will be required to elucidate this [33].

Recently, IRF5 was used as an indicator for M1 macrophage infiltrate in house dust mite induced asthma animal models [34]. Although this study did not describe the phenotype of the IRF5 expressing macrophages in detail, it demonstrated that IRF5 can potentially be used as a marker in a different disease setting and tissue. This is particularly important since IRF5 associates not only with RA but also with several other autoimmune diseases such as inflammatory bowel disease, asthma, and systemic lupus erythematosus [35–38].

It has recently become clear that in addition to macrophages derived from infiltrating monocytes generated in bone marrow, tissue-resident macrophages of different origin may also play a crucial role in inflammation [39, 40]. Moreover, transcriptional profiling of macrophages from different origins demonstrated heterogeneity of macrophage populations and revealed tissue-specific transcriptional signatures [32]. This suggests that identification of subset specific transcription factors is needed to tease out the contribution of different macrophage subtypes in inflammatory processes, especially in disease-related chronic inflammation or autoimmunity that so far received less attention [41]. We hypothesise that IRF5 could play a critical role in tracking inflammatory macrophages in various inflammatory diseases.

4. Conclusions

To conclude, this study clearly demonstrates that IRF5 is highly expressed in murine proinflammatory macrophages and may be utilised as a reliable marker for macrophages at sites of inflammation. Murine GM-BMDMs express IRF5 and proinflammatory cytokines *in vitro* when challenged with LPS. We show that it is possible to label intracellular IRF5 in these proinflammatory macrophages, as well as in macrophages in an inflamed knee during the progression of an experimental mouse model of antigen-induced arthritis. Thus, this study describes a useful method for tracking proinflammatory macrophages and demonstrates its feasibility in a murine disease model.

References

[1] D. M. Mosser and J. P. Edwards, "Exploring the full spectrum of macrophage activation," *Nature Reviews Immunology*, vol. 8, no. 12, pp. 958–969, 2008.

[2] S. K. Biswas and A. Mantovani, "Macrophage plasticity and interaction with lymphocyte subsets: cancer as a paradigm," *Nature Immunology*, vol. 11, no. 10, pp. 889–896, 2010.

[3] S. Gordon, "Alternative activation of macrophages," *Nature Reviews Immunology*, vol. 3, no. 1, pp. 23–35, 2003.

[4] A. J. Fleetwood, T. Lawrence, J. A. Hamilton, and A. D. Cook, "Granulocyte-macrophage colony-stimulating factor (CSF) and macrophage CSF-dependent macrophage phenotypes display differences in cytokine profiles and transcription factor activities: implications for CSF blockade in inflammation," *Journal of Immunology*, vol. 178, no. 8, pp. 5245–5252, 2007.

[5] F. A. W. Verreck, T. de Boer, D. M. L. Langenberg et al., "Human IL-23-producing type 1 macrophages promote but IL-10-producing type 2 macrophages subvert immunity to (myco)bacteria," *Proceedings of the National Academy of Sciences of the United States of America*, vol. 101, no. 13, pp. 4560–4565, 2004.

[6] J. A. Hamilton, "Colony-stimulating factors in inflammation and autoimmunity," *Nature Reviews Immunology*, vol. 8, no. 7, pp. 533–544, 2008.

[7] F. A. W. Verreck, T. de Boer, D. M. L. Langenberg, L. van der Zanden, and T. H. M. Ottenhoff, "Phenotypic and functional profiling of human proinflammatory type-1 and anti-inflammatory type-2 macrophages in response to microbial antigens and IFN-γ- and CD40L-mediated costimulation," *Journal of Leukocyte Biology*, vol. 79, no. 2, pp. 285–293, 2006.

[8] A. Kennedy, U. Fearon, D. J. Veale, and C. Godson, "Macrophages in synovial inflammation," *Frontiers in Immunology*, vol. 2, article 52, 2011.

[9] T. J. M. Smeets, M. C. Kraan, S. Galjaard, P. P. Youssef, M. D. Smith, and P. P. Tak, "Analysis of the cell infiltrate and expression of matrix metalloproteinases and granzyme B in paired synovial biopsy specimens from the cartilage-pannus junction in patients with RA," *Annals of the Rheumatic Diseases*, vol. 60, no. 6, pp. 561–565, 2001.

[10] P. Barrera, "Synovial macrophage depletion with clodronate-containing liposomes in rheumatoid arthritis," *Arthritis & Rheumatism*, vol. 43, no. 9, pp. 1951–1959, 2000.

[11] P. L. E. M. van Lent, A. E. M. Holthuysen, N. van Rooijen, L. B. A. van de Putte, and W. B. van den Berg, "Local removal of phagocytic synovial lining cells by clodronate- liposomes decreases cartilage destruction during collagen type II arthritis," *Annals of the Rheumatic Diseases*, vol. 57, no. 7, pp. 408–413, 1998.

[12] K. Nistala, S. Adams, H. Cambrook et al., "Th17 plasticity in human autoimmune arthritis is driven by the inflammatory environment," *Proceedings of the National Academy of Sciences of the United States of America*, vol. 107, no. 33, pp. 14751–14756, 2010.

[13] M. Chabaud, E. Lubberts, L. Joosten, W. van den Berg, and P. Miossec, "IL-17 derived from juxta-articular bone and synovium contributes to joint degradation in rheumatoid arthritis," *Arthritis Research*, vol. 3, no. 3, pp. 168–177, 2001.

[14] T. Krausgruber, K. Blazek, T. Smallie et al., "IRF5 promotes inflammatory macrophage polarization and TH1-TH17 responses," *Nature Immunology*, vol. 12, no. 3, pp. 231–238, 2011.

[15] A. Takaoka, H. Yanai, S. Kondo et al., "Integral role of IRF-5 in the gene induction programme activated by Toll-like receptors," *Nature*, vol. 434, no. 7030, pp. 243–249, 2005.

[16] K. Honda and T. Taniguchi, "IRFs: master regulators of signalling by Toll-like receptors and cytosolic pattern-recognition receptors," *Nature Reviews Immunology*, vol. 6, no. 9, pp. 644–658, 2006.

[17] B. J. Barnes, P. A. Moore, and P. M. Pitha, "Virus-specific activation of a novel Interferon Regulatory Factor, IRF-5, results in the induction of distinct interferon α genes," *Journal of Biological Chemistry*, vol. 276, no. 26, pp. 23382–23390, 2001.

[18] E. A. Stahl, S. Raychaudhuri, E. F. Remmers et al., "Genome-wide association study meta-analysis identifies seven new rheumatoid arthritis risk loci," *Nature Genetics*, vol. 42, no. 6, pp. 508–514, 2010.

[19] K. Dawidowicz, Y. Allanore, M. Guedj et al., "The Interferon Regulatory Factor 5 gene confers susceptibility to rheumatoid arthritis and influences its erosive phenotype," *Annals of the Rheumatic Diseases*, vol. 70, no. 1, pp. 117–121, 2011.

[20] D. L. Asquith, A. M. Miller, I. B. McInnes, and F. Y. Liew, "Animal models of rheumatoid arthritis," *European Journal of Immunology*, vol. 39, no. 8, pp. 2040–2044, 2009.

[21] P. J. Egan, A. van Nieuwenhuijze, I. K. Campbell, and I. P. Wicks, "Promotion of the local differentiation of murine Th17 cells by synovial macrophages during acute inflammatory arthritis," *Arthritis and Rheumatism*, vol. 58, no. 12, pp. 3720–3729, 2008.

[22] M. Y. Balkhi, K. A. Fitzgerald, and P. M. Pitha, "Functional regulation of MyD88-activated Interferon regulatory factor 5 by K63-linked polyubiquitination," *Molecular and Cellular Biology*, vol. 28, no. 24, pp. 7296–7308, 2008.

[23] H. C. C. Foreman, S. van Scoy, T. F. Cheng, and N. C. Reich, "Activation of interferon regulatory factor 5 by site specific phosphorylation," *PLoS ONE*, vol. 7, no. 3, Article ID e33098, 2012.

[24] M. Y. Balkhi, K. A. Fitzgerald, and P. M. Pitha, "IKKα negatively regulates IRF-5 function in a MyD88-TRAF6 pathway," *Cellular Signalling*, vol. 22, no. 1, pp. 117–127, 2010.

[25] K. Inaba, M. Inaba, N. Romani et al., "Generation of large numbers of dendritic cells from mouse bone marrow cultures supplemented with granulocyte/macrophage colony-stimulating factor," *Journal of Experimental Medicine*, vol. 176, no. 6, pp. 1693–1702, 1992.

[26] A. Celada, M. J. Klemsz, and R. A. Maki, "Interferon-γ activates multiple pathways to regulate the expression of the genes for major histocompatibility class II I-Aβ, tumor necrosis factor and complement component C3 in mouse macrophages," *European Journal of Immunology*, vol. 19, no. 6, pp. 1103–1109, 1989.

[27] M. Rescigno, S. Citterio, C. Thèry et al., "Bacteria-induced neobiosynthesis, stabilization, and surface expression of functional class I molecules in mouse dendritic cells," *Proceedings of the National Academy of Sciences of the United States of America*, vol. 95, no. 9, pp. 5229–5234, 1998.

[28] S. C. Sicher, G. W. Chung, M. A. Vazquez, and C. Y. Lu, "Augmentation or inhibition of IFN-γ-induced MHC class II expression by lipopolysaccharides: the roles of TNF-α and nitric oxide, and the importance of the sequence of signaling," *Journal of Immunology*, vol. 155, no. 12, pp. 5826–5834, 1995.

[29] R. de Lorenzi, R. Gareus, S. Fengler, and M. Pasparakis, "GFP-p65 knock-in mice as a tool to study NF-κB dynamics *in vivo*," *Genesis*, vol. 47, no. 5, pp. 323–329, 2009.

[30] J. MacMicking, Q. W. Xie, and C. Nathan, "Nitric oxide and macrophage function," *Annual Review of Immunology*, vol. 15, pp. 323–350, 1997.

[31] S. Gordon and F. O. Martinez, "Alternative activation of macrophages: mechanism and functions," *Immunity*, vol. 32, no. 5, pp. 593–604, 2010.

[32] E. L. Gautier, "Gene-expression profiles and transcriptional regulatory pathways that underlie the identity and diversity of mouse tissue macrophages," *Nature Immunology*, vol. 13, no. 11, pp. 1118–1128, 2012.

[33] R. C. Stone, D. Feng, J. Deng et al., "Interferon Regulatory Factor 5 activation in monocytes of systemic lupus erythematosus

patients is triggered by circulating autoantigens independent of type i interferons," *Arthritis and Rheumatism*, vol. 64, no. 3, pp. 788–798, 2012.

[34] C. Draijer, P. Robbe, C. E. Boorsma, M. N. Hylkema, and B. N. Melgert, "Characterization of macrophage phenotypes in three murine models of house-dust-mite-induced asthma," *Mediators of Inflammation*, vol. 2013, Article ID 632049, 10 pages, 2013.

[35] V. Dideberg, G. Kristjansdottir, L. Milani et al., "An insertion-deletion polymorphism in the interferon regulatory factor 5 (IRF5) gene confers risk of inflammatory bowel diseases," *Human Molecular Genetics*, vol. 16, no. 24, pp. 3008–3016, 2007.

[36] G. Gathungu, C. K. Zhang, W. Zhang, and J. H. Cho, "A two-marker haplotype in the IRF5 gene is associated with inflammatory bowel disease in a North American cohort," *Genes and Immunity*, vol. 13, no. 4, pp. 351–355, 2012.

[37] C. Wang, M. J. Rose-Zerilli, G. H. Koppelman et al., "Evidence of association between Interferon Regulatory Factor 5 gene polymorphisms and asthma," *Gene*, vol. 504, no. 2, pp. 220–225, 2012.

[38] W. D. Xu, H. F. Pan, Y. Xu, and D. Q. Ye, "Interferon regulatory factor 5 and autoimmune lupus," *Expert Reviews in Molecular Medicine*, vol. 15, article e6, 2013.

[39] L. C. Davies, M. Rosas, S. J. Jenkins et al., "Distinct bone marrow-derived and tissue-resident macrophage lineages proliferate at key stages during inflammation," *Nature Communications*, vol. 4, article 1886, 2013.

[40] S. J. Jenkins, D. Ruckerl, P. C. Cook et al., "Local macrophage proliferation, rather than recruitment from the blood, is a signature of TH2 inflammation," *Science*, vol. 332, no. 6035, pp. 1284–1288, 2011.

[41] L. C. Davies, S. J. Jenkins, J. E. Allen, and P. R. Taylor, "Tissue-resident macrophages," *Nature Immunology*, vol. 14, no. 10, pp. 986–995, 2013.